Missouri University of Science and Technology
Scholars' Mine

CCFSS Library (1939 - present)

Wei-Wen Yu Cold-Formed Steel Library

01 May 1990

Design of automotive structural components using high strength sheet steels effect of strain rate on material properties of sheet steels and structural strengths of cold-formed steel members

Maher Kassar

Wei-Wen Yu
Missouri University of Science and Technology, wwy4@mst.edu

Follow this and additional works at: https://scholarsmine.mst.edu/ccfss-library

 Part of the Structural Engineering Commons

Recommended Citation

Kassar, Maher and Yu, Wei-Wen, "Design of automotive structural components using high strength sheet steels effect of strain rate on material properties of sheet steels and structural strengths of cold-formed steel members" (1990). *CCFSS Library (1939 - present)*. 145.
https://scholarsmine.mst.edu/ccfss-library/145

This Technical Report is brought to you for free and open access by Scholars' Mine. It has been accepted for inclusion in CCFSS Library (1939 - present) by an authorized administrator of Scholars' Mine. This work is protected by U. S. Copyright Law. Unauthorized use including reproduction for redistribution requires the permission of the copyright holder. For more information, please contact scholarsmine@mst.edu.

Civil Engineering Study 90-2
Structural Series

Fourteenth Progress Report

DESIGN OF AUTOMOTIVE STRUCTURAL COMPONENTS USING HIGH STRENGTH SHEET STEELS

EFFECT OF STRAIN RATE ON MATERIAL PROPERTIES OF SHEET STEELS AND STRUCTURAL STRENGTHS OF COLD-FORMED STEEL MEMBERS

by

Maher Kassar
Research Assistant

Wei-Wen Yu
Project Director

A Research Project Sponsored by the American Iron and Steel Institute

May 1990

Department of Civil Engineering
University of Missouri-Rolla
Rolla, Missouri

PREFACE

This report is based on a dissertation presented to the Faculty of the Graduate School of the University of Missouri-Rolla (UMR) in partial fulfillment of the requirements for the degree of Doctor of Philosophy in Civil Engineering.

The technical guidance provided by members of the AISI Task Force on Automotive Structural Design, the AISI Automotive Applications Committee Design Panel, and the AISI staff is gratefully acknowledged. These members are: Messrs. S. J. Errera (Chairman), J. Borchelt, R. Cary, F. L. Cheng, A. M. Davies, J. D. Grozier, C. Haddad, A. L. Johnson, C. M. Kim, K. H. Lin, J. N. Macadam, H. Mahmood, D. Malen, J. G. Schroth, P. G. Schurter, T. N. Seel, and M. T. Vecchio.

All materials used in the experimental study were donated by LTV Steel Company, Inland Steel Company, and National Steel Corporation.

Appreciation is also expressed to Messrs. J. Bradshaw, F. Senter, and J. Tucker, staff of the Department of Civil Engineering, and to Messrs. K. Hass, A. Johnston, and R. Haselhorst, former staff of the Department of Civil Engineering, for their technical support. The assistance given by Mr. C. L. Pan in the preparation and performance of the tests is greatly appreciated.

ABSTRACT

In structural design, the material properties of steels and the strengths of cold-formed steel members are affected by strain rate. Two subjects were investigated experimentally and analytically in this study. They are 1) effect of strain rate on mechanical properties of sheet steels in tension and compression, and 2) structural strengths of stub columns and beams subjected to dynamic loads.

Three sheet steels with nominal yield strengths ranging from 35 to 100 ksi were studied under different strain rates. A total of 124 tensile coupons and 54 compressive coupons were tested in this phase of study. The structural strengths of 37 stub columns and 30 beam specimens fabricated from 35XF sheet steel were investigated in the second phase of this study under different strain rates. The results showed that the material properties as well as the strengths of the structural members increased with the strain rate. The amount of increase was found to be dependent on the material yield strengths and the strain rates used in the tests.

The effective width approach included in the current AISI Automotive Steel Design Manual was utilized for the evaluation of member strengths using static and dynamic yield stresses corresponding to the strain rates used in the tests. Good agreement was achieved between the predicted and tested member strengths when using the dynamic yield stresses in the comparison.

TABLE OF CONTENTS

	Page
PREFACE	ii
ABSTRACT	iii
LIST OF ILLUSTRATIONS	x
LIST OF TABLES	xix
I. INTRODUCTION	1
A. GENERAL	1
B. PURPOSE OF INVESTIGATION	2
C. SCOPE OF INVESTIGATION	3
II. REVIEW OF LITERATURE	5
A. GENERAL	5
B. MATERIALS	5
1. Mechanical Properties of Sheet Steel	6
a. Engineering Stress-Strain Curves	6
b. True Stress-Strain Curves	13
2. Strain Rate	15
a. Strain-Rate Dynamic Testing	15
b. Effect of Strain Rate on Mechanical Properties	19
i) Structural Steels and High Strength Steels	19
ii) Stainless Steels	42
iii) Aluminum	42
c. Strain-Rate History Effect	55

TABLE OF CONTENTS (Cont'd)

	Page
C. STRUCTURAL MEMBERS	66
1. Structural Behavior of Compression Elements Under Static Loads	66
a. Elastic Local Buckling of Flat Compression Elements	66
i) Stiffened Elements	67
ii) Unstiffened Elements	69
b. Inelastic Buckling of Flat Compression Elements	72
c. Post-Buckling Behavior of Flat Compression Elements	73
d. Development of Effective Width Formulas	77
2. Response of Structural Members to Dynamic Loads	84
a. Flexural Members	85
b. Columns	96
III. EXPERIMENTAL PROGRAM	106
A. GENERAL	106
B. MATERIAL PROPERTIES	106
1. Materials	106
2. Uniaxial Tests	106
a. Tension Tests	108
i) ASTM Specifications	108
ii) Specimens	108
iii) Equipment	108
iv) Procedure	117

TABLE OF CONTENTS (Cont'd)

	Page
b. Compression Tests	119
i) ASTM Specifications	119
ii) Specimens	124
iii) Equipment	124
iv) Procedure	129
3. Tensile Test Results	132
a. Stress-Strain Curves	132
b. Mechanical Properties	139
i) Yield Strength or Yield Point, F_y	139
ii) Ultimate Tensile Strength, F_u	152
iii) Ductility	152
4. Compressive Test Results	152
a. Stress-Strain Curves	152
b. Mechanical Properties	156
i) Proportional Limit, F_{pr}	156
ii) Yield Strength or Yield Point, F_y	166
C. STRUCTURAL MEMBERS	168
1. Material Properties	172
2. Beam Tests for Stiffened Elements	172
a. Specimens	172
b. Strain Measurements	179
c. Instrumentation and Test Procedure	183
d. Test Results	186

TABLE OF CONTENTS (Cont'd)

	Page
3. Stub Column Tests for Stiffened Elements	188
a. Specimens	188
b. Strain Measurements	193
c. Instrumentation and Test Procedure	196
d. Test Results	199
4. Beam Tests for Unstiffened Elements	206
a. Specimens	206
b. Strain Measurements	206
c. Instrumentation and Test Procedure	209
d. Test Results	213
5. Stub Column Tests for Unstiffened Elements	213
a. Specimens	213
b. Strain Measurements	222
c. Instrumentation and Test Procedure	223
d. Test Results	223
IV. EVALUATION OF EXPERIMENTAL DATA	232
A. GENERAL	232
B. EVALUATION OF MATERIAL TEST DATA	233
1. Mechanical Properties	233
a. Proportional Limit, F_{pr}	233
b. Yield Strength or Yield Point, F_y	233
c. Ultimate Tensile Strength, F_u	236

TABLE OF CONTENTS (Cont'd)

	Page
2. Strain Rate Sensitivity	237
3. Prediction of Yield Strength for High Strain Rates.	240
C. EVALUATION OF STRUCTURAL MEMBER EXPERIMENTAL DATA	247
1. Beam Tests for the Study of Stiffened Elements	247
a. Critical Local Buckling Strength	247
b. Ultimate Flexural Strength	251
i) Yield Flexural Strength	251
ii) Inelastic Reserve Capacity	255
2. Stub Column Tests for the Study of Stiffened Elements	267
a. Critical Local Buckling Load	269
b. Ultimate Axial Load	271
3. Beam Tests for the Study of Unstiffened Elements	279
a. Critical Local Buckling Strength	279
b. Ultimate Flexural Strength	283
4. Stub Column Tests for the Study of Unstiffened Elements	291
a. Critical Local Buckling Load	291
b. Ultimate Axial Load	293
5. Deflection of Beam Specimens	302
V. CONCLUSIONS	311
A. GENERAL	311
B. MATERIALS	311
C. STRUCTURAL MEMBERS	312

TABLE OF CONTENTS (Cont'd)

Page

BIBLIOGRAPHY..... 314

APPENDIX - NOTATION..... 325

LIST OF ILLUSTRATIONS

Figure		Page
2.1	Stress-Strain Curves of Carbon Steel Sheets[12]	7
2.2	Determination of Yield Point for Gradual-Yielding Steel[12]	9
2.3	Effects of Strain Hardening and Strain Aging on Stress-Strain Characteristics[12]	9
2.4	Influence of Bauschinger Effect[12]	12
2.5	Comparison of Engineering and True Stress-Strain Curves[12]	12
2.6	Effect of Strain Rate on Stress-Strain Curve for Structural Steel[36]	20
2.7	True Yield Stresses at Various Strains Versus Strain Rate for a Low-Carbon Steel at Room Temperature[39]	20
2.8	True Yield Stresses at Various Strains Versus Strain Rate for a Low-Carbon Steel at 200° C [39]	23
2.9	True Yield Stresses at Various Strains Versus Strain Rate for a Low-Carbon Steel at 400° C [39]	23
2.10	True Yield Stresses at Various Strains Versus Strain Rate for a Low-Carbon Steel at 600° C [39]	24
2.11	Strain-Rate Changes During Tensile Test, Four Strain Rates Shown Are 10^{-1}, 10^{-2}, 10^{-3}, and 10^{-4} sec^{-1} (Ref. 42)	24
2.12	Relationship Between Flow Stress and Natural Strain for Low-Carbon Steels[44]	29
2.13	Relationship Between Flow Stress and Natural Strain for Medium-Carbon Steels[44]	30
2.14	Relationship Between Flow Stress and Natural Strain for High-Carbon Steels[44]	31
2.15	Effect of Strain Rate at -50°, 75°,and 600° F on the Yield and Tensile Strengths of USS COR-TEN Steel[46]	33
2.16	Effect of Strain Rate at -50°, 75°,and 600° F on the Yield and Tensile Strengths of USS TRI-TEN Steel[46]	34

LIST OF ILLUSTRATIONS (Cont'd)

Figure		Page
2.17	Effect of Strain Rate on Mechanical Properties of a HSLA Steel[41]	36
2.18	Effect of Crosshead Speed on Yield Behavior and Tensile Strength[47]	37
2.19	Stress-Strain Curves for SA-106 Carbon Steel Pipe[48]	37
2.20	The Variation of the Strain Rate Sensitivity (m-value) with Strain Rate[49]	39
2.21	Stress-Strain Curves for High Strength Steel at Varying Strain Rate[50]	39
2.22	Dynamic Stress-Strain Curves for AISI Type 304 Stainless Steel[52]	43
2.23	Dynamic Stress-Strain Diagram of AISI Type 304L Stainless Steel[52]	43
2.24	Dynamic Stress-Strain Diagram of AISI Type 347 Stainless Steel[52]	44
2.25	The Ambient-Temperature Yield Stress of Annealed Type 21-6-9 Stainless Steel as a Function of Strain Rate[53]	44
2.26	Analysis of the Uniaxial Stress, Strain, and Strain Rate Data for Aluminum 1060-O[54]	45
2.27	Dynamic Yield Stress (Minus the Static Yield Stress) Versus Strain Rate for Steel[55]	46
2.28	Dynamic Yield Stress (Minus the Static Yield Stress) Versus Strain Rate for Aluminum[55]	46
2.29	Effect of Strain Rate on the Stress Required to Compress Aluminum to 40% Reduction at Various Temperatures[43]	48
2.30	Stress-Strain Curves for 1100-0 Aluminum in Tension and Compression[57]	53
2.31	Stress-Strain Curves for 6061-T6 Aluminum in Compression at Several Strain Rates[57]	54
2.32	Strain and Strain-Rate Dependence of the Flow Stress of High-Purity Aluminum[58]	56

LIST OF ILLUSTRATIONS (Cont'd)

Figure		Page
2.33	Strain and Strain-Rate Dependence of the Flow Stress of Aluminum 1060-O[58]	56
2.34	Strain and Strain-Rate Dependence of the Flow Stress of Aluminum 1100-O[58]	56
2.35	Compression Tests on Aluminums 7075-T6 and 6061-T6[60]	57
2.36	Strain-Rate Sensitivity of Aluminum Alloys[33]	57
2.37	Cyclic Static-Dynamic-Static Loading for Aluminum[59]	59
2.38	Cyclic Dynamic-Static-Dynamic Loading for Aluminum[59]	59
2.39	Cyclic Dynamic Loading for Aluminum[59]	60
2.40	Effect of Alteration of Strain Rate Upon Flow Stress (Static-Dynamic)[62]	62
2.41	Effect of Alteration of Strain Rate Upon Flow Stress (Dynamic-Static)[62]	62
2.42	Results of Constant and Incremental Strain-Rate Tests on 1020 Hot Rolled Steel (HRS)[64]	64
2.43	Results of Constant and Incremental Strain-Rate Tests on 1080 Cold Rolled Steel (CRS)[64]	64
2.44	Tensile True Stress-True Strain Curves at Ambient Temperature for Monotonic Loading to Fracture at a Strain Rate of 0.004 sec^{-1} (Curve A) and 500 sec^{-1} (Curve B), and for Quasi Prestraining Followed by Dynamic Reloading to Fracture[61].	65
2.45	Structural Members with Stiffened and Unstiffened Elements[26]	68
2.46	Rectangular Plate Simply Supported on Four Edges and Under Uniform Compression Stress[117]	70
2.47	Buckling Coefficients for Flat Rectangular Stiffened Plates[117]	70
2.48	Rectangular Plate Simply Supported on Three Edges and Under Uniform Compression Stress[117]	71
2.49	Buckling Coefficients for Flat Rectangular Unstiffened Plates[117]	71

LIST OF ILLUSTRATIONS (Cont'd)

Figure		Page
2.50	Strut and Bar Grid Model Simply Supported Along Its Edges and Subjected to End Loading[26]	75
2.51	Consecutive Stages of Stress Distribution in Stiffened Compression Elements[26]	75
2.52	Effective Design Width of a Stiffened Compression Element[26]	78
2.53	Effective Design Width of an Unstiffened Compression Element[26]	78
2.54	Recorded Load Time Pulse[89]	88
2.55	Yield Stresses vs. Time to Yield[89]	89
2.56	Variation of Upper and Lower Yield Moments with Strain Rate at Surface of Specimen[99]	92
2.57	Peak Displacement Versus Impulse	97
2.58	Deflection of Mid-Point of Column[106]	99
2.59	Variation of First Maximum Stress (Solid Curve) and Mean Post-Buckling Stress (Broken Curve) with Compression Rate,[110] for Column with t/D= 0.067	101
3.1	Location of Tension and Compression Coupons[12]	109
3.2	Nominal Dimensions of Tension Coupons Used for 100XF, 50XF, and 35XF[12]	110
3.3	Material Test System (MTS) 880 Used for Tension Tests	112
3.4	Test Setup Showing the Attachment of Extensometer	114
3.5	MTS 880 Automated Test System and Software Overview	115
3.6	MTS 880 Test Controller Servo Control Loop	116
3.7	Typical Function Generator Ramp Waveform	120
3.8	Strain-Time Curve for 100XF-LT-1,(Virgin Material)	121
3.9	Strain-Time Curve for 100XF-LT-3,(Virgin Material)	122

LIST OF ILLUSTRATIONS (Cont'd)

Figure		Page
3.10	Strain-Time Curve for 50XF-LT-7,(Virgin Material).....	123
3.11	Nominal Dimensions of Compression Coupons Used for All Sheet Steels.....	125
3.12	MTS Load Frame, MTS Controller, CAMAC Data Acquisition System, and Data General Graphic Display Terminal Used for Compression Tests.....	127
3.13	Compression Subpress, Jig, Compressometer, and Test Specimen Used for Compression Tests.....	128
3.14	Assembly of Compression Subpress, Jig, and Compressometer (Back View).....	131
3.15	Stress-Strain Curves for 100XF-LT-1, 100XF-LT-4, and 100XF-LT-6,(Virgin Material).....	133
3.16	Stress-Strain Curves for 50XF-LT-1, 50XF-LT-4, and 50XF-LT-9,(Virgin Material).....	134
3.17	Stress-Strain Curves for 35XF-LT-1, 35XF-LT-4, and 35XF-LT-9,(Virgin Material).....	135
3.18	Stress-Strain Curves for 50XF-LT Steel at Strain Rate of 0.0001 in./in./sec.....	136
3.19	Stress-Strain Curves for 50XF-LT Steel at Strain Rate of 0.01 in./in./sec.....	137
3.20	Stress-Strain Curves for 50XF-LT Steel at Strain Rate of 1.0 in./in./sec.....	138
3.21	Stress-Strain Curves for 100XF-LC Steel Under Different Strain Rates.....	153
3.22	Stress-Strain Curves for 50XF-LC Steel Under Different Strain Rates.....	154
3.23	Stress-Strain Curves for 35XF-LC Steel Under Different Strain Rates.....	155
3.24	Stress-Strain Curve for Determination of Mechanical Properties of 35XF-TC-4.....	167
3.25	Configurations of Test Specimens for Members Having Stiffened Compression Flanges.....	169

LIST OF ILLUSTRATIONS (Cont'd)

Figure		Page
3.26	Configurations of Test Specimens for Members Having Unstiffened Compression Flanges	170
3.27	Hat Sections Used for Beam Tests	178
3.28	Locations of Strain Gages on Hat Sections	181
3.29	Modified Strain Reversal Method Used to Determine the Critical Buckling Load	182
3.30	Test Setup for Beams with a Stiffened Flange	184
3.31	End View for the Hat Beam Test Setup	185
3.32	Typical Failure of Hat Beams with a Stiffened Flange	189
3.33	Typical Plot of Load vs. Location of Neutral Axis for Beams with a Stiffened Flange (Specimen 3A0A)	190
3.34	Typical Plot of Strain vs. Time for Hat Beams with a Stiffened Flange (Strain Gage # 5 for Specimen 3A1A)	191
3.35	Load-Strain Curves of Strain Gages # 1 and 2 Installed at the Center of the Stiffened Flange (Specimen 3C0A)	192
3.36	Cross Sections of Box-Shaped Stub Columns Used for the Study of Stiffened Elements	194
3.37	Locations of Strain Gages at Midheight of Box-Shaped Stub Columns	194
3.38	Locations of Strain Gages along the Specimen Length for Box-Shaped Stub Column Having Large w/t Ratio	197
3.39	Test Setup of Stub Columns with Stiffened Flanges (Specimen 1B3B)	198
3.40	Failure of Stub Columns with Stiffened Flanges (Front View)	200
3.41	Typical Plot of Strain vs. Time for Stub Columns with Stiffened Flanges (Strain Gage # 3 for Specimen 1A3B)	201
3.42	Load-Strain Curves of Strain Gages # 5 and 6 Installed at the Center of a Stiffened Flange (Specimen 1C1B)	202

LIST OF ILLUSTRATIONS (Cont'd)

Figure		Page
3.43	Load-Displacement Curves for Stub-Column Specimens 1A1A, 1A2A, and 1A3A	203
3.44	Load-Displacement Curves for Stub-Column Specimens 1B1A, 1B2A, and 1B3A	204
3.45	Load-Displacement Curves for Stub-Column Specimens 1C1A, 1C2A, and 1C3A	205
3.46	Cross Sections of Channel Beams Used for the Study of Unstiffened Elements	207
3.47	Locations of Strain Gages at Midspan Section of Channel Beams	210
3.48	Test Setup for Channel Beams with Unstiffened Flanges	211
3.49	Photograph of Test Setup for Channel Beams with Unstiffened Flanges	212
3.50	Typical Failure of Channel Beams with Unstiffened Flanges.	214
3.51	Typical Plot of Strain vs. Time for Channel Beams with Unstiffened Flanges (Strain Gage # 3 for Specimen 4C2B)	215
3.52	Load-Strain Curves of Strain Gages # 1 and 2 Installed at the Tip of an Unstiffened Flange (Spec. 4C2A)	216
3.53	Load-Displacement Curves for Channel Beam Specimens 4A0A, 4A1A, and 4A2A	217
3.54	Load-Displacement Curves for Channel Beam Specimens 4B0A, 4B1A, and 4B2A	218
3.55	Load-Displacement Curves for Channel Beam Specimens 4C0A, 4C1A, and 4C2A	219
3.56	Cross Sections of I-Shaped Stub Columns	220
3.57	Locations of Strain Gages at Midheight of I-Shaped Stub Columns	220
3.58	Test Setup of Stub Columns with Unstiffened Flanges	224
3.59	Typical Failure of Stub Columns with Unstiffened Flanges	225

LIST OF ILLUSTRATIONS (Cont'd)

Figure		Page
3.60	Typical Plot of Strain vs. Time for Stub Columns with Unstiffened Flanges (Strain Gage # 3 for Specimen 2B3A)...	226
3.61	Load-Strain Curves of Strain Gages # 1 and 2 Installed at the Tip of an Unstiffened Flange (Spec. 2C0A).....	227
3.62	Load-Displacement Curves for I-Shaped Stub Columns 2A1A, 2A2A, and 2A3A.....	228
3.63	Load-Displacement Curves for I-Shaped Stub Columns 2B1A, 2B2A, and 2B3A.....	229
3.64	Load-Displacement Curves for I-Shaped Stub Columns 2C0A,2C1A, 2C2A, and 2C3A.....	230
4.1	Tensile Yield Stress vs. Logarithmic Strain-Rate Curve for 100XF-LT, (Virgin Material).....	241
4.2	Compressive Yield Stress vs. Logarithmic Strain-Rate Curve for 100XF-LC, (Virgin Material).....	242
4.3	Tensile Yield Stress vs. Logarithmic Strain-Rate Curve for 50XF-LT, (Virgin Material).....	243
4.4	Compressive Yield Stress vs. Logarithmic Strain-Rate Curve for 50XF-LC, (Virgin Material).....	244
4.5	Tensile Yield Stress vs. Logarithmic Strain-Rate Curve for 35XF-LT, (Virgin Material).....	245
4.6	Compressive Yield Stress vs. Logarithmic Strain-Rate Curve for 35XF-LC, (Virgin Material).....	246
4.7	Stress Distribution in Sections with Yielded Tension Flanges at Ultimate Moments[26].....	256
4.8	Moment-Displacement Curve for Hat-Beam Specimen 3B0A.....	262
4.9	Moment-Displacement Curve for Hat-Beam Specimen 3B1A.....	263
4.10	Moment-Displacement Curve for Hat-Beam Specimen 3B2B.....	264
4.11	Stress Distribution in Tested Hat Sections.....	265

LIST OF ILLUSTRATIONS (Cont'd)

Figure		Page
4.12	Ratios of Dynamic to Static Average Ultimate Moments vs. Logarithmic Strain Rate for Hat-Beam Specimens.....	268
4.13	Load-Displacement Curve for Box-Shaped Stub Column Specimen 1B1A.....	275
4.14	Load-Displacement Curve for Box-Shaped Stub Column Specimen 1B2B.....	276
4.15	Load-Displacement Curve for Box-Shaped Stub Column Specimen 1B3A.....	277
4.16	Ratios of Dynamic to Static Average Ultimate Loads vs. Logarithmic Strain Rate for Box-Shaped Stub Columns.....	280
4.17	Moment-Displacement Curve for Channel Beam Specimen 4B0A..	287
4.18	Moment-Displacement Curve for Channel Beam Specimen 4B1B..	288
4.19	Moment-Displacement Curve for Channel Beam Specimen 4B2B..	289
4.20	Ratios of Dynamic to Static Average Ultimate Moments vs. Logarithmic Strain Rate for Channel Beam Specimens.....	292
4.21	Load-Displacement Curve for I-Shaped Stub Column Specimen 2B1A.....	298
4.22	Load-Displacement Curve for I-Shaped Stub Column Specimen 2B2B.....	299
4.23	Load-Displacement Curve for I-Shaped Stub Column Specimen 2B3A.....	300
4.24	Ratios of Dynamic to Static Average Ultimate Loads vs. Logarithmic Strain Rate for I-Shaped Stub Columns.....	303
4.25	Schematic Diagram for Beam Specimen Showing Midspan Deflection.....	304
4.26	Typical Moment-Deflection Curve for Hat-Beam Specimens, Specimen 3C1B.....	308
4.27	Typical Moment-Deflection Curve for Channel Beam Specimens, Specimen 4C0A.....	310

LIST OF TABLES

Table		Page
2.1	Dynamic Aspects of Mechanical Testing[32]	16
2.2	Experimental Techniques for High Strain Rate Testing[34]	18
2.3	Values of Strain Rate Sensitivity Exponent, m, and Constant C of Yield Strength of the Tested Materials[41]	18
2.4	Effect of Strain Rate and Temperature on the Stress Required to Compress Steel[43]	27
2.5	Values of C for Steels Using Equation (2.13)[43]	28
2.6	Values of m for Steels Using Equation (2.13)[43]	28
2.7	Standard Strain Rate Sensitivity and New Strain Rate Parameters[49]	40
2.8	Strain Rate Sensitivity for Different Microstructures Determined by Strain Rate Jump Tests at 6.7×10^{-5} sec^{-1}, 6.7×10^{-4} sec^{-1}, and 6.7×10^{-3} sec^{-1} (Ref. 51)	40
2.9	Effect of Strain Rate and Temperature on the Stress Required to Compress Aluminum[43]	49
2.10	Values of C for Aluminums Using Equation (2.13)[43]	50
2.11	Values of m for Aluminums Using Equation (2.13)[43]	50
2.12	Results of Compression Tests on Commercially Pure Aluminum at Constant Strain Rates Based on Equation (2.17)[56]	51
2.13	α and β Values of Equation 2.48 for the Calculation of Dynamic Correction Factor for Thin-Walled Steel Columns with Various Cross-Sections	105
3.1	Chemical Compositions of the Sheet Steels Used	107
3.2	Classification of the MTS Extensometer	107
3.3	Number of Performed Tensile Coupon Tests	111
3.4	MTS Transducer Ranges and the Corresponding Load, Strain, or Displacement Values	118
3.5	Function Generator Ramp Time and the Corresponding Strain Rate (Tensile Tests)	118

LIST OF TABLES (Cont'd)

Table		Page
3.6	Number of Performed Compressive Coupon Tests.....	126
3.7	Classification of the MTS Compressometer.....	130
3.8	Function Generator Ramp Time and the Corresponding Strain Rate (Compressive Tests).....	130
3.9	Tested Mechanical Properties of 100XF Sheet Steel, Virgin Material.....	140
3.10	Tested Mechanical Properties of 50XF Sheet Steel, Virgin Material.....	141
3.11	Tested Mechanical Properties of 50XF Sheet Steel, 2% Cold Stretched, Non-Aged Material.....	142
3.12	Tested Mechanical Properties of 50XF Sheet Steel, 8% Cold Stretched, Non-Aged Material.....	142
3.13	Tested Mechanical Properties of 50XF Sheet Steel, 2% Cold Stretched, Aged Material.....	143
3.14	Tested Mechanical Properties of 50XF Sheet Steel, 8% Cold Stretched, Aged Material.....	143
3.15	Tested Mechanical Properties of 35XF Sheet Steel, Virgin Material.....	144
3.16	Tested Mechanical Properties of 35XF Sheet Steel, 2% Cold Stretched, Non-Aged Material.....	145
3.17	Tested Mechanical Properties of 35XF Sheet Steel, 8% Cold Stretched, Non-Aged Material.....	145
3.18	Tested Mechanical Properties of 35XF Sheet Steel, 2% Cold Stretched, Aged Material.....	146
3.19	Tested Mechanical Properties of 35XF Sheet Steel, 8% Cold Stretched, Aged Material.....	146
3.20	Average Tested Mechanical Properties of 100XF Sheet Steel, Longitudinal Tension, Virgin Material.....	147
3.21	Average Tested Mechanical Properties of 100XF Sheet Steel, Transverse Tension, Virgin Material.....	147

LIST OF TABLES (Cont'd)

Table		Page
3.22	Average Tested Mechanical Properties of 50XF Sheet Steel, Longitudinal Tension	148
3.23	Average Tested Mechanical Properties of 50XF Sheet Steel, Transverse Tension	149
3.24	Average Tested Mechanical Properties of 35XF Sheet Steel, Longitudinal Tension	150
3.25	Average Tested Mechanical Properties of 35XF Sheet Steel, Transverse Tension	151
3.26	Tested Mechanical Properties of 100XF Sheet Steel, Longitudinal Compression	157
3.27	Tested Mechanical Properties of 100XF Sheet Steel Transverse Compression	158
3.28	Tested Mechanical Properties of 50XF Sheet Steel Longitudinal Compression	159
3.29	Tested Mechanical Properties of 50XF Sheet Steel Transverse Compression	160
3.30	Tested Mechanical Properties of 35XF Sheet Steel Longitudinal Compression	161
3.31	Tested Mechanical Properties of 35XF Sheet Steel Transverse Compression	162
3.32	Average Tested Mechanical Properties of 100XF Sheet Steel Longitudinal Compression	163
3.33	Average Tested Mechanical Properties of 100XF Sheet Steel Transverse Compression	163
3.34	Average Tested Mechanical Properties of 50XF Sheet Steel Longitudinal Compression	164
3.35	Average Tested Mechanical Properties of 50XF Sheet Steel Transverse Compression	164
3.36	Average Tested Mechanical Properties of 35XF Sheet Steel Longitudinal Compression	165

LIST OF TABLES (Cont'd)

Table		Page
3.37	Average Tested Mechanical Properties of 35XF Sheet Steel Transverse Compression	165
3.38	Designation of Test Specimens Used in This Study	171
3.39	Number of Performed Stub Column Tests, Box Sections Having Stiffened Compression Elements	173
3.40	Number of Performed Stub Column Tests, I-Sections Having Unstiffened Compression Elements	174
3.41	Number of Performed Beam Tests, Hat Sections Having Stiffened Compression Flanges	175
3.42	Number of Performed Beam Tests, Channel Sections Having Unstiffened Compression Flanges	176
3.43	Average Mechanical Properties of 35XF Sheet Steel used in the Experimental Study Under Different Strain Rates	177
3.44	Dimensions of Beam Specimens with Stiffened Flanges Fabricated from 35XF Sheet Steel	180
3.45	The CAMAC Frequencies and the Corresponding Sampling Rates	187
3.46	Dimensions of Stub Columns with Stiffened Flanges Fabricated from 35XF Sheet Steel	195
3.47	Dimensions of Beam Specimens with Unstiffened Flanges Fabricated from 35XF Sheet Steel	208
3.48	Dimensions of Stub Columns with Unstiffened Flanges Fabricated from 35XF Sheet Steel	221
4.1	Ratios of Dynamic to Static Mechanical Properties for Three Sheet Steels Based on Tables 3.20 to 3.25	234
4.2	Ratios of Dynamic to Static Compressive Yield Stresses for Three Sheet Steels Based on Tables 3.32 to 3.36	235
4.3	Values of Strain Rate Sensitivities m for Three Sheet Steels Based on the Changes of the Yield Stresses at Different Strain Rates, (Tensile Coupon Tests)	238

LIST OF TABLES (Cont'd)

Table		Page
4.4	Values of Strain Rate Sensitivities m for Three Sheet Steels Based on the Changes of the Yield Stresses at Different Strain Rates, (Compressive Coupon Tests).....	239
4.5	Comparison of Computed and Tested Critical Buckling Moments, Beam Specimens with a Stiffened Flange (Based on k=4.0), (35XF Sheet Steel).....	250
4.6(a)	Comparison of Computed and Tested Yield Moments, Beam Specimens with a Stiffened Flange, (35XF Sheet Steel) (Based on Static Yield Stress).....	253
4.6(b)	Comparison of Computed and Tested Yield Moments, Beam Specimens with a Stiffened Flange, (35XF Sheet Steel) (Based on Dynamic Yield Stress).....	254
4.7(a)	Comparison of Computed and Tested Failure Moments Based on the Effective Width Formulas in the 1986 AISI Automotive Steel Design Manual for Beam Specimens with a Stiffened Flange, (35XF Sheet Steel) (Based on Static Yield Stress).....	259
4.7(b)	Comparison of Computed and Tested Failure Moments Based on the Effective Width Formulas in the 1986 AISI Automotive Steel Design Manual for Beam Specimens with a Stiffened Flange, (35XF Sheet Steel) (Based on Dynamic Yield Stress).....	260
4.8	Average Tested Ultimate Moments for Hat-Beam Specimens with a Stiffened Flange, (35XF Sheet Steel)...	266
4.9	Average Ultimate Moment Ratios for Hat-Beam Specimens Having Stiffened Flanges, (35XF Sheet Steel)...	266
4.10	Comparison of Computed and Tested Critical Buckling Loads, Stub Columns with Stiffened Flanges (Based on k=4.0), (35XF Sheet Steel).....	270
4.11(a)	Comparison of Computed and Tested Failure Loads Based on the Effective Width Formulas in the 1986 AISI Automotive Steel Design Manual for Stub Columns with Stiffened Flanges, (35XF Sheet Steel) (Based on Static Yield Stress).....	272

LIST OF TABLES (Cont'd)

Table		Page
4.11(b)	Comparison of Computed and Tested Failure Loads Based on the Effective Width Formulas in the 1986 AISI Automotive Steel Design Manual for Stub Columns with Stiffened Flanges, (35XF Sheet Steel) (Based on Dynamic Yield Stress).....	273
4.12	Average Tested Failure Loads for Stub Column Specimens with Stiffened Flanges, (35XF Sheet Steel).....	278
4.13	Ratios of Average Ultimate Loads for Stub Column Specimens Having Stiffened Flanges (35XF Sheet Steel).....	278
4.14	Comparison of Computed and Tested Critical Buckling Moments, Beam Specimens with Unstiffened Flanges (Based on k=0.43), (35XF Sheet Steel).....	282
4.15(a)	Comparison of Computed and Tested Ultimate Moments, Beam Specimens with Unstiffened Flanges, (35XF Sheet Steel) (Based on Static Yield Stress).....	284
4.15(b)	Comparison of Computed and Tested Ultimate Moments, Beam Specimens with Unstiffened Flanges, (35XF Sheet Steel) (Based on Dynamic Yield Stress).....	285
4.16	Average Tested Failure Moments for Channel Beam Specimens with Unstiffened Flanges, (35XF Sheet Steel)	290
4.17	Ratios of Average Ultimate Moments for Channel Beam Specimens Having Unstiffened Flanges, (35XF Sheet Steel)..	290
4.18	Comparison of Computed and Tested Critical Buckling Loads, Stub Columns with Unstiffened Flanges (Based on k=0.43), (35XF Sheet Steel).....	294
4.19(a)	Comparison of Computed and Tested Failure Loads Based on the Effective Width Formulas in the 1986 AISI Automotive Steel Design Manual for Stub Columns with Unstiffened Flanges, (35XF Sheet Steel) (Based on Static Yield Stress).....	296
4.19(b)	Comparison of Computed and Tested Failure Loads Based on the Effective Width Formulas in the 1986 AISI Automotive Steel Design Manual for Stub Columns with Unstiffened Flanges, (35XF Sheet Steel) (Based on Dynamic Yield Stress).....	297

LIST OF TABLES (Cont'd)

Table		Page
4.20	Average Tested Failure Loads for I-Shaped Stub Column Specimens with Unstiffened Flanges, (35XF Sheet Steel)..	301
4.21	Ratios of Ultimate Loads for I-Shaped Stub Column Specimens Having Unstiffened Flanges, (35XF Sheet Steel)	301
4.22	Deflections under Service Moments Based on Effective Sections for Hat-Beam Specimens with Stiffened Flanges, (35XF Sheet Steel).....	305
4.23	Deflections under Service Moments Based on Effective Sections for Channel Beam Specimens with Unstiffened Flanges, (35XF Sheet Steel).....	306

I. INTRODUCTION

A. GENERAL

During recent years, automotive manufacturers have produced lighter vehicles for the purpose of achieving fuel economy. To accomplish the construction of such automobiles, high strength sheet steels with various yield strengths up to 190 ksi have been used for auto parts and structural components.[1-9]

In order to provide some technical assistance for the design of such high strength steels, the first edition of the "Guide for Preliminary Design of Sheet Steel Automotive Structural Components" was issued by American Iron and Steel Institute (AISI) in February 1981.[10] In view of the fact that the design information contained in this document can be used only for sheet steels with yield strengths of up to 80 ksi, a research project has been conducted at the University of Missouri-Rolla (UMR) since 1982 to study the structural strength of automotive components using high strength sheet steels. In the first phase of the UMR program, typical mechanical properties and representative stress-strain curves were established by a series of static tests for different grades of sheet steels with yield strengths ranging from 49 to 164 ksi. The second phase of the UMR project was directed toward the web crippling strength of beam webs and the strength of members consisting of flat and curved elements. The research findings were presented in ten progress reports.[11-20] In addition, the effective design widths of high strength cold-formed steel members were also

investigated.[21] Some of the research results were used in the first edition of the AISI Automotive Steel Design Manual published in 1986.[22] This manual brings together material properties, product design, and manufacturing information to make the most effective use of sheet steels with yield strengths of up to 140 ksi.

Because the previous UMR studies were limited only to the tests subject to static loads and it is well known that the yield strength, tensile strength, and the stress-strain relationship of sheet steels as well as the strengths of structural members are affected by the rate of strain used for the tests, additional research work was conducted at the University of Missouri-Rolla since May, 1988. The research findings were presented in three progress reports[23-25] and are summarized in this thesis.

B. PURPOSE OF INVESTIGATION

The main purpose of this investigation was to study the effect of strain rate on mechanical properties of sheet steels and on the strengths of steel beams and stub columns fabricated from 35XF sheet steel. Because the current effective width formulas used to predict the ultimate strengths of stiffened and unstiffened elements were derived from the results of static tests, the primary goals of this study were to determine the adequacy of these effective width formulas for the design of structural members subjected to dynamic loads.

C. SCOPE OF INVESTIGATION

This study was primarily involved with the experimental determination of the dynamic material properties of three selected sheet steels with nominal yield strengths ranging from 35 to 100 ksi under different strain rates. The strain rates ranged from 0.0001 to 1.0 in./in./sec. All tests were performed at UMR's Engineering Research Laboratory by using the new MTS 880 Test System. The test data developed from the material coupon tests were used for the evaluation of stub column and beam tests, for which the specimens were fabricated from 35XF sheet steel and were tested under different strain rates. Both the stub columns and beams consisted of stiffened and unstiffened compression elements. In the current experimental investigation, a limited range of width-to-thickness ratios was covered for both stiffened and unstiffened elements. The ranges of w/t ratios were from 26.92 to 76.64 for stiffened elements, and from 8.93 to 20.87 for unstiffened elements.

As an initial step of this investigation, numerous publications and research reports related to the effect of strain rate on mechanical properties of sheet steels and on the structural strengths of axial and flexural steel memebers were reviewed in detail. Chapter II contains a summary of the review of literature.

In Chapter III, the experimental study of the dynamic mechanical properties of the selected sheet steels and the structural behavior of cold-formed steel members consisting of stiffened and unstiffened elements tested under different strain rates are presented. Details

of test specimens, test procedure, and test results are presented in this chapter.

The material and structural member test results are evaluated in Chapter IV. Comparisons of the predicted and tested structural member loads are also provided in this chapter. Finally, the research findings are summarized in Chapter V.

II. REVIEW OF LITERATURE

A. GENERAL

In the early portion of the study, many publications and research papers concerning effect of strain rate on the strengths of materials and structural members were reviewed. Section II.B includes a review of mechanical properties of sheet steels. In this section a summary of other research findings related to the effect of strain rate on mechanical properties of metals in tension and compression is presented.

The available literature on the effective width design formulas for stiffened and unstiffened compression elements under static loads is described in Section II.C. This section also includes the effect of strain rate and dynamic loads on structural strengths of flexural and axially loaded members.

B. MATERIALS

The mechanical properties of sheet steels are reviewd in Section II.B.1 with an emphasis on engineering and true stress-strain curves. The effect of strain rate on tensile and compressive mechanical properties of steel, stainless steel and aluminum is presented in Section II.B.2.

1. Mechanical Properties of Sheet Steel.

a. Engineering Stress-Strain Curves. The stress-strain curve is the relationship between the stress and the corresponding strain. For engineering stress-strain curves, the stress , f , is measured by the load, P , divided by the original, unreduced area, A_o , of the specimen, i.e.

$$f = P / A_o \tag{2.1}$$

The engineering strain, ϵ , is the difference between the original, unreduced gage length, ℓ_o , and the deformed length, ℓ , divided by the original length, i.e.

$$\epsilon = (\ell - \ell_o) / (\ell_o) \tag{2.2}$$

For high strength sheet steels, the two basic types of engineering stress-strain (f-ϵ) curves are gradual and sharp yielding as shown in Figure 2.1[26]. The classification of the f-ϵ curve is based on the yielding behavior of the steel. As a general rule, hot-rolled sheet steels tend to be sharp yielding (Figure 2.1(a)) while those sheet steels that are cold-rolled or cold reduced in thickness are gradual yielding (Figure 2.1(b)).

Sharp yielding steels typically exhibit an upper and lower yield point (points A and B in Figure 2.1(a), respectively). Because the upper yield point is much more sensitive to strain rate, specimen alignment, and shape of the tested cross-section than the lower yield point, the lower yield point is customarily used to represent the yield stress of sharp yielding sheet steels subject to static loading[27,28].

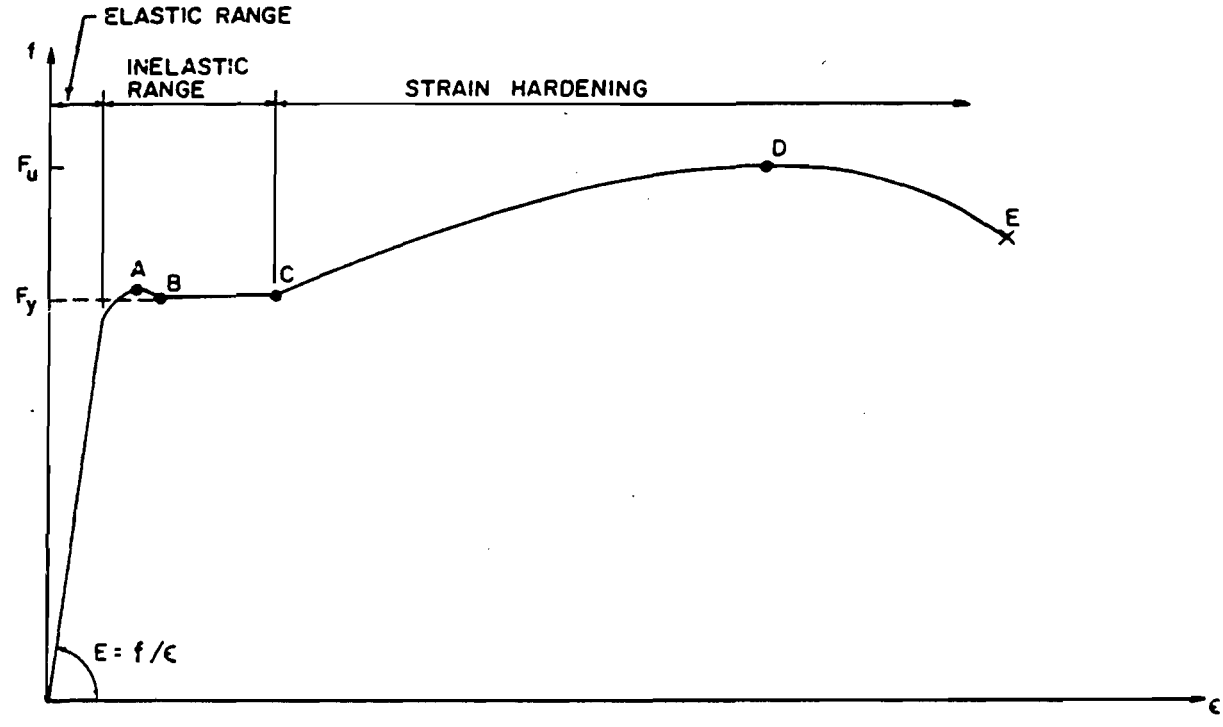

(a) SHARP-YIELDING STEEL

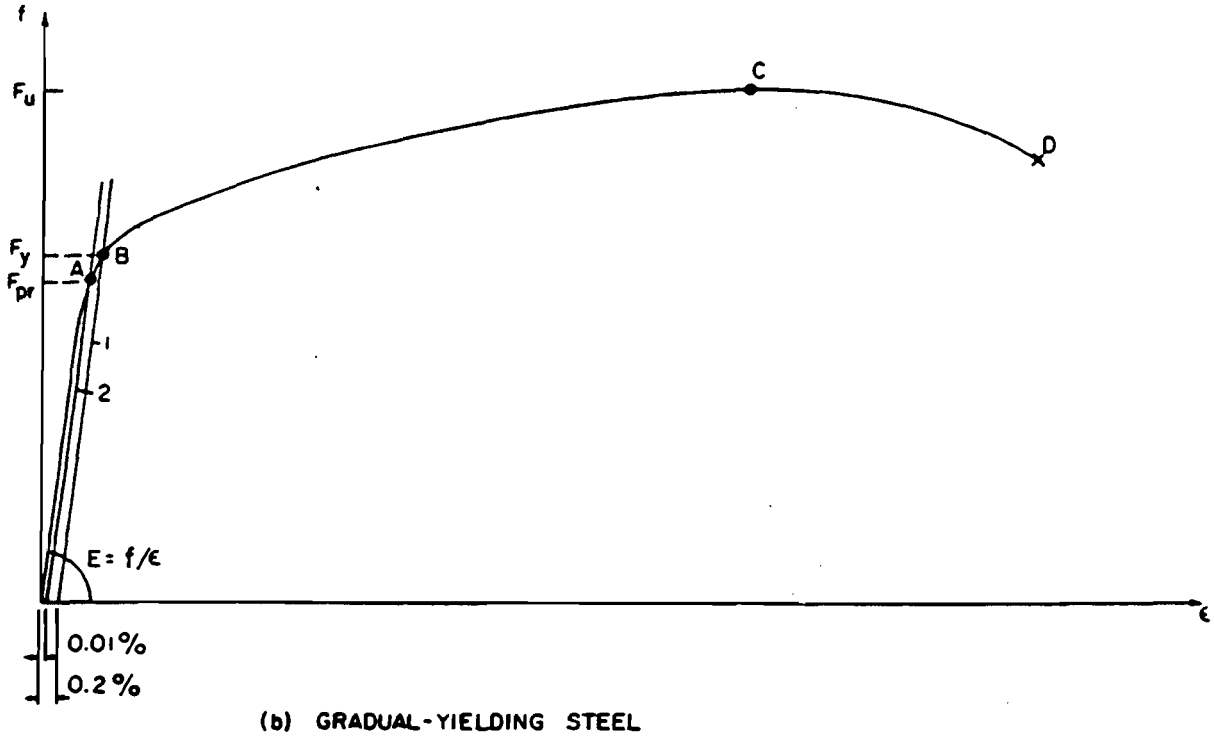

(b) GRADUAL-YIELDING STEEL

Fig. 2.1 Stress-Strain Curves of Carbon Steel Sheets[12]

In view of the fact that gradual yielding steels do not have such an obvious yield point, their yield strength is defined by either an offset method or the strain-under-load method as described in ASTM Standard A370. The offset method consists of drawing a straight line parallel to the initial linear portion of the f-ϵ curve at a given strain offset. For this study, an offset of 0.2 percent strain was chosen. Using this method, the intersection of the straight line and the f-ϵ curve defines the yield strength as shown in Figure 2.2(a)[26]. The strain-under-load method defines the yield point as the stress corresponding to some fixed value of strain. The strain usually chosen is 0.5 percent as shown in Figure 2.2(b)[26].

The slope of the linear portion of the f-ϵ diagram is known as the modulus of elasticity, E . The point beyond which the f-ϵ curve becomes nonlinear is called the proportional limit (point A in Figure 2.1(b)). For sheet steels, whether they are gradual or sharp yielding, the proportional limit may be determined by the 0.01 percent offset method in exactly the same manner that the yield stress was defined for gradual yielding sheet steels, except that the offset is now only 0.01 percent.

Once the specimen is strained beyond the yield point, the load carrying capacity of the steel continues to increase slightly in spite of the fact that the cross-sectional area of the specimen is continually decreasing. Since engineering stress is calculated based on the original area, there must be some other phenomenon occuring that causes the increase in load carrying capacity. This phenomenon is commonly referred to as work hardening or strain hardening and may be explained by dislocation theory[27]. The rate of strain hardening is high at the onset

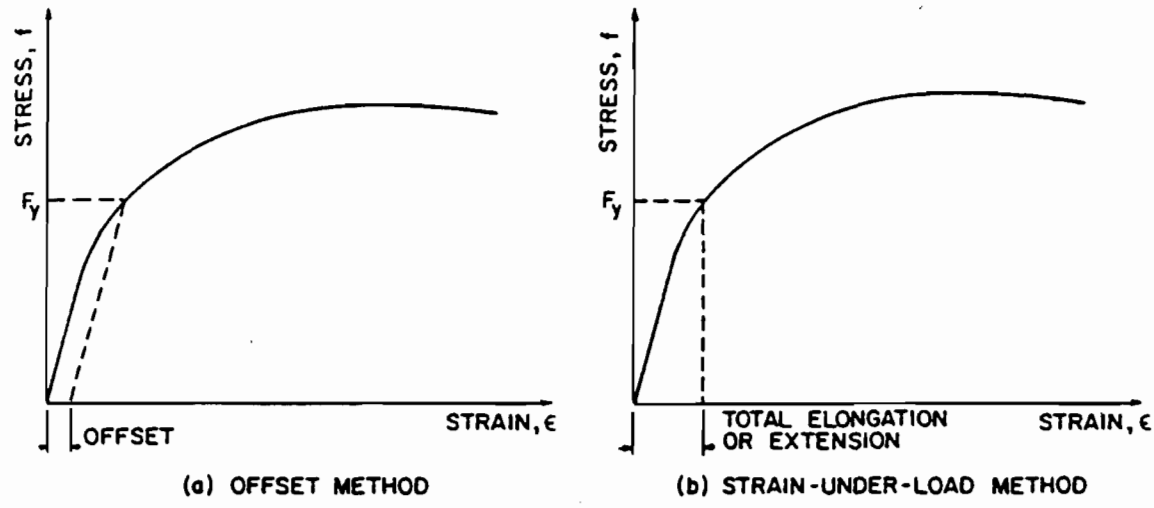

Fig. 2.2 Determination of Yield Point for Gradual-Yielding Steel[12]

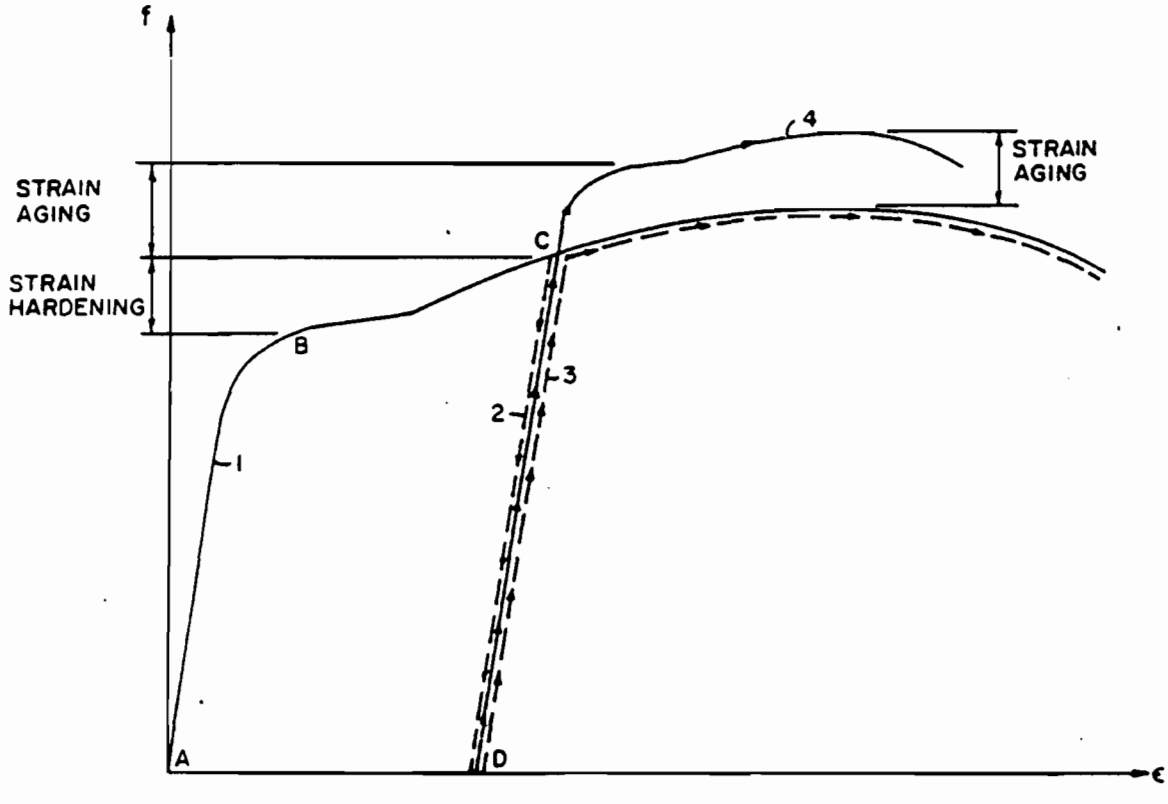

Fig. 2.3 Effects of Strain Hardening and Strain Aging on Stress-Strain Characteristics[12]

of yielding. However, as the strain is increased, the amount of strain hardening decreases to the point where it can no longer offset the continuous reduction of specimen area. At that point the maximum possible stress or ultimate strength, F_u , is reached in the steel. Further elongation of the tensile specimen results in localized straining of a small portion of the gage length known as necking[29]. The necked region continues to decrease in area at a faster pace than the strain hardening, which results in a decrease in the total load that the specimen can withstand. This unloading results in all areas of the specimen, other than the necked region, being unloaded back into the elastic range while the stress in the necked area continues to increase until fracture[27].

A material property that is dependent on the strain that a material can withstand up until fracture is ductility. Ductility is commonly defined by two methods. They are

a) total elongation (percent) = $100*(\ell_f - \ell_o)/\ell_o$, and (2.3)

b) reduction in area (percent) = $100*(A_o - A_f)/A_o$ (2.4)

In the above equations, the f subscripts denote the values at fracture . Although standard values are usually used for ℓ_o and A_o, it is important to realize that either method of measuring ductility will give varying results if non-standard values of ℓ_o and A_o are used[27].

Another important material property yet to be discussed is the capability of a material to absorb energy without fracture. Energy absorption is especially important in the design of structures such as automobile components, highway guard rails, and machinery guards[30]. For a particular material the energy absorption is given by the area under the stress-strain curve from zero loading to fracture. Therefore the

amount of absorption depends not only on the yield and ultimate strength but on the total elongation of the material as well.

Figure 2.3[26] illustrates the effect on the stress-strain curve of stressing a given sheet steel beyond the yield stress and then removing the load before failure. As shown by curve 2 of Figure 2.3, if the load is removed at point C along the stress-strain curve, then the unloading path follows a line very nearly the slope of the elastic portion of the stress-strain diagram. The elastic strain, ϵ_e , recovered upon unloading from point C is equal to the stress at C, f_c , divided by the modulus of elasticity, E, or $\epsilon_e = f_c/E$. The permanent set or plastic strain, ϵ_p , is represented by the line AD. Curve 3 represents the stress-strain curve if reloading occurs immediately and Curve 4 if reloading occurs after strain aging. It can be seen that, if the material is immediately reloaded (Curve 3), strain hardening produces an increase in apparent yield strength and a decrease in ductility as compared to the virgin material. If reloading occurs after a period of time, a phenomenon known as strain aging occurs (Curve 4) which results in an even higher value of yield stress and tensile strength; however, the ductility decreases even more.

If the reloading from point D is opposite the original loading (e.g. compression instead of tension) as shown in Figure 2.4[30], the new value of the yield point G might be lower than the original yield point B. Also, if this load is reversed so that the load is now in the original direction, the yield point H may be lower than the original yield point B. This effect was observed by Johann Bauschinger, of Germany, in 1886 and is commonly referred to as the Bauschinger Effect [30].

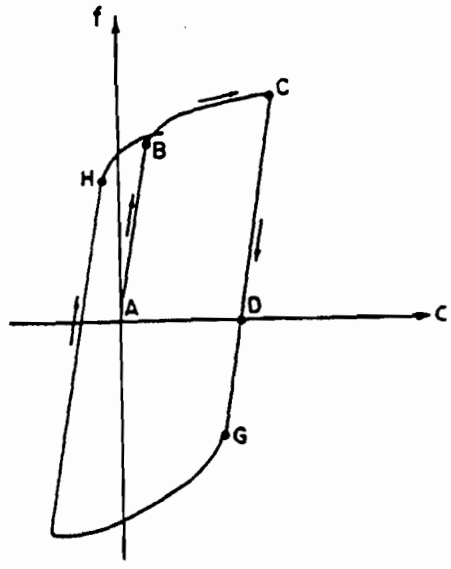

Fig. 2.4 Influence of Bauschinger Effect[12]

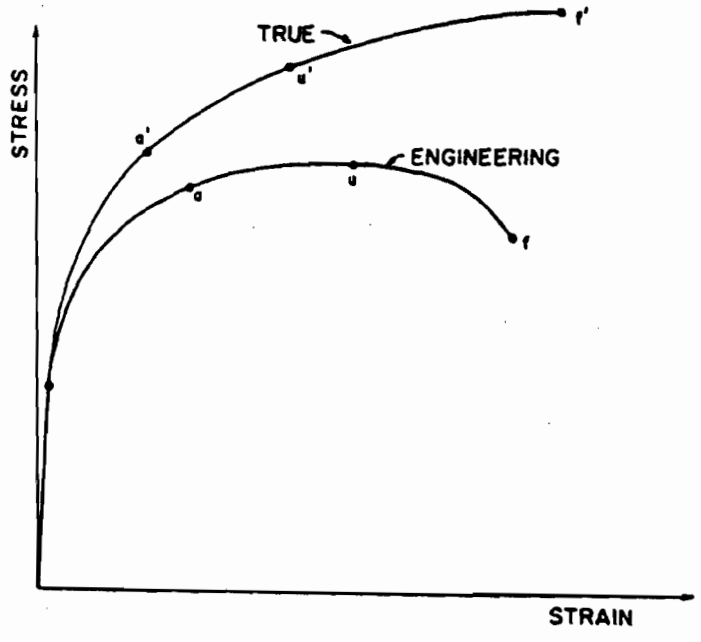

Fig. 2.5 Comparison of Engineering and True Stress-Strain Curves[12]

b. <u>True Stress-Strain Curves</u>. The exact or true stress, σ, in a tensile test is equal to the load, P, divided by the actual area, A, as follows:

$$\sigma = P / A \qquad (2.5)$$

As the load increases and thus the cross-sectional area decreases, the corresponding true stress will be greater than the engineering stress computed for the same loading. Since there is no appreciable change in area in the elastic range, the true and engineering stresses are practically identical. However, as the stress reaches the inelastic range, the strain increases and thus the area decreases much more for a given stress increase than in the elastic range. Therefore, the difference between true and engineering stresses become apparent in the inelastic range as can be seen in Figure 2.5[27]. By comparing the shape of the true and engineering stress-strain diagrams in the inelastic range, it can be seen that the difference between the two curves continually increases with increasing strain. It is also interesting to note that the true stress steadily increases up to fracture. This type of continuous increase of the σ-ϵ curve seems much more logical than the engineering curve because it is difficult to imagine the stress actually decreasing in a material that is tested from zero load to fracture.

The true stress and strain may be related to the engineering stress and strain by assuming constancy of volume of the specimen. In other words, the initial volume, $A_o \ell_o$, should be equal to the instantaneous volume, $A\ell$. Thus

$$A_o \ell_o = A \ell \qquad (2.6)$$

$$A = A_o \ell_o / \ell = A_o (\ell_o / (\ell_o (1+\epsilon))$$

$$A = A_o/(1+\epsilon) \tag{2.7}$$

Therefore the true stress, σ, may be given as

$$\sigma = P/A = P\,(1+\epsilon)/\,A_o = f(1+\epsilon) \tag{2.8}$$

The true or natural strain, ϵ', can be determined from the differential increment of strain, $d\epsilon'$, as

$$d\epsilon' = d\ell/\ell \tag{2.9}$$

where ℓ is the actual length to which $d\ell$ is added. The total unit elongation becomes

$$\epsilon' = \int_{\ell_0}^{\ell} \frac{d\ell}{\ell} = \ln\left(\frac{\ell}{\ell_0}\right) = \ln\,(1+\epsilon) \tag{2.10}$$

Equations 2.8 and 2.10 obviously may be used in converting from engineering stress and strain to true stress and strain[28]. After necking, the above equations are not valid. Since the length changes within the gage length are now localized in the necked region, the engineering strain, which assumes a uniform strain over the gage length, cannot be used to calculate the true stress and natural strain. An alternate method for computing the true stress in the necked region is described by Hosford and Caddel on page 53 of Ref. 27.

From inspecting the above equations for stress and strain, it can be seen that for very small strains, such as those occuring in the elastic range, the engineering and true stresses and strains will be practically the same. Therefore, for properties such as yield stress and modulus of elasticity, the engineering values should be sufficiently accurate. However, for studies using stress-strain data in the plastic range, "the

true stress and strain are more meaningful than engineering stress and strain[27]."

2. Strain Rate. Strain rate ($\dot{\epsilon}$) is the rate of change of strain (ϵ) with respect to time (t) :

$$\dot{\epsilon} = d\epsilon / dt \qquad (2.11)$$

where ϵ can be either the engineering or the true strain. For a constant strain rate experiment, the strain rate is simply the total strain divided by the duration of the test[31] :

$$\dot{\epsilon} = \epsilon / t \qquad (2.12)$$

The unit of strain rate is the inverse of time sec^{-1}.

For the design of economical and safer cars, understanding of the effects of impact loading, controlled crash and energy absorption on automobile components is essential. Since these design considerations involve dynamic loading, the effects of strain rates on the mechanical properties of the sheet steels must be known in order for the engineer to design a safe and efficient vehicle and moreover to reduce the need for conducting expensive full-scale dynamic testing[1].

a. Strain Rate Dynamic Testing. Some considerations in strain rate dynamic testing have been summarized by Lindholm[32] as shown in Table 2.1[32]. At strain rates of the order of 10^{-6} to 10^{-5} sec^{-1} the creep behavior of a material is the primary consideration, usually at elevated temperature for metals, for which the creep-type laws are used to describe the mechanical behavior[33]. At a higher strain rate, in the range of 10^{-4} to 10^{-3} sec^{-1}, the uniaxial tension, compression, or quasistatic

Table 2.1 Dynamic Aspects of Mechanical Testing[32]

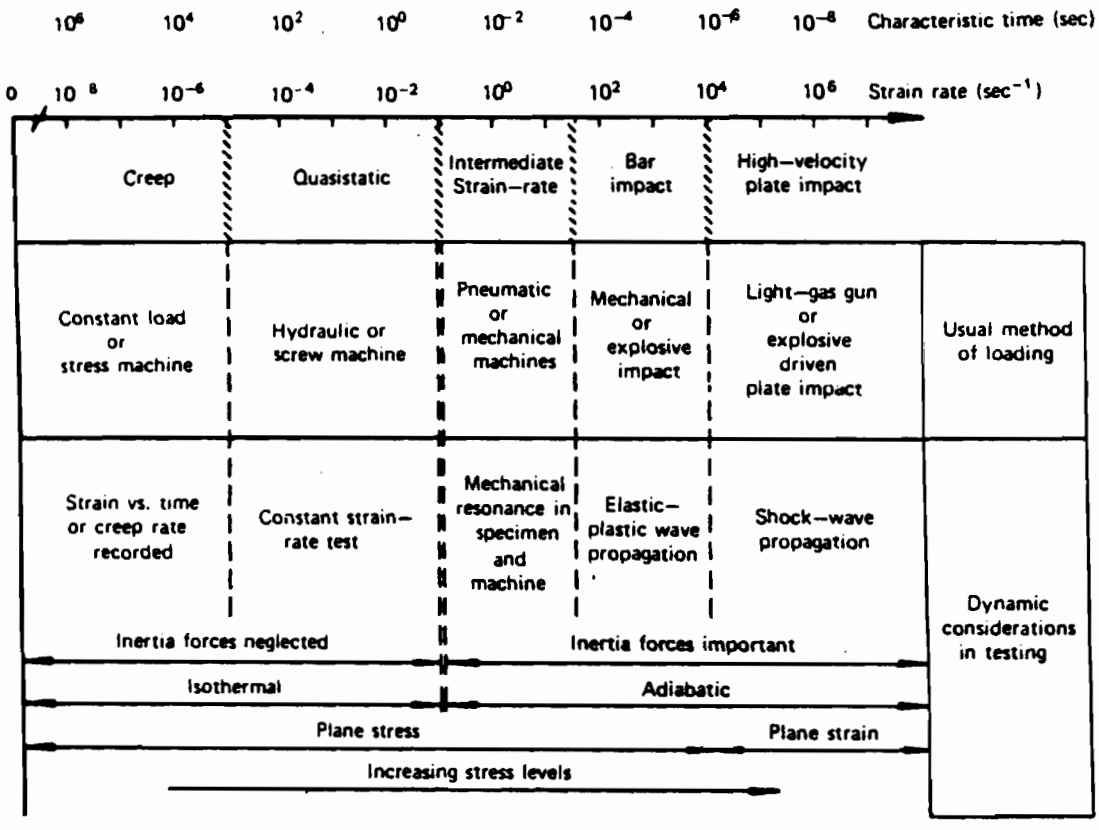

stress-strain curve obtained from constant strain-rate test is used to describe the material behavior. Although the quasistatic stress-strain curve is often treated as an inherent property of a material, it is a valid description of the material only at the strain rate at which the test was conducted. When higher strain rates are encountered, the stress-strain relationships may change, and alternate testing techniques have to be employed. Constant strain-rate tests can be performed with specialized testing apparatus at strain rates up to approximately 10^4 sec^{-1}. The range of strain rates from 10^{-1} to 10^2 sec^{-1} is generally referred to as the intermediate or medium strain-rate condition. It is within this condition that strain- rate effects first become a consideration in most metals, although the magnitude of such effects may be quite small or even nonexistent in some cases[33]. Strain rates of 10^3 sec^{-1} or higher are generally treated as the range of high strain-rate response, although there are no precise definitions as to strain-rate conditions and care must be taken in evaluating the test data to note the actual strain rates rather than the terminology. It is within the high strain-rate condition that inertia and wave-propagation effects first become important in interpreting experimental data. At these high rates, care must be taken to distinguish between average values of stress and strain and local values that may be the result of one or more high-intensity stress waves propagating through a material. At the strain rate of 10^5 sec^{-1} or higher, it is generally dealing with shock waves propagating through materials that are in a state of uniaxial strain. At these very high rates and the associated very short time scale involved, thermodynamic considerations become important[33]. Table 2.2[34] shows the

Table 2.2

Experimental Techniques for High Strain Rate Testing[34]

Mode	Applicable Strain Rate, sec^{-1}	Testing Technique
Compression	≤ 0.1	Conventional load frames
	0.1 to 100	Special servohydraulic frames
	0.1 to 500	Cam plasometer and drop test
	200 to 10^4	Hopkinson pressure bar
	10^4 to 10^5	Taylor impact test
Tension	≤ 0.1	Conventional load frames
	0.1 to 100	Special servohydraulic frames
	100 to 10^4	Hopkinson pressure bar
	10^4	Expanding ring
	$\geq 10^5$	Flyer plate
Shear	≤ 0.1	Conventional shear test
	0.1 to 100	Special servohydraulic frames
	10 to 1000	Torsional impact
	100 to 10^4	Hopkinson (Kolsky) bar
	10^3 to 10^4	Double-notch shear and punch
	10^4 to 10^7	Pressure-shear plate impact

Table 2.3

Values of Strain Rate Sensitivity Exponent, m, and Constant C of Yield Strength of the Tested Materials[41]

Material	m	ln C
HRAK-AR	0.045	10.72223
HRAK-Ann+TR	0.056	10.58935
HSLA-40	0.045	10.74515
HSLA-45-1	0.035	10.94544
HSLA-45-2	0.024	10.83534
HSLA-50	0.026	10.98135
HSLA-80-1	0.020	11.36871
HSLA-80-2	0.018	11.40914

experimental techniques that are used for various strain rate conditions in compression, tension, and shear testing. Unfortunately, there are no standardized procedures for high strain rate tests. Many different machines, specimen configurations, and measuring devices have been used. This makes a comparison of the test results of different investigators difficult and often makes it impossible to compare the properties of a group of materials since the behavior of a material is quite often influenced by the experimental conditions. It is important that the true behavior be studied by different methods to isolate any excessive influence of the technique and to verify the validity of the data[35].

b. Effect of Strain Rate on Mechanical Properties. The effect of strain rate on mechanical properties varies for each material. These general trends are well known, but because the magnitude of the change in properties with strain rate is so varied for each material, no general quantitative theory exists that satisfactorily predicts the mechanical behavior of materials over a wide range[33].

For most materials, mechanical properties tend to increase at higher strain rates. The following sections discuss the effect of strain rate on mechanical properties of structural and high strength sheet steels, stainless steels, and aluminum.

i) Structural Steels and High Strength Steels. The effect of the strain rate on the mechanical behavior of mild steel has long been a subject of interest to researchers since the beginning of this century. Figure 2.6[36] shows stress-strain curves obtained from structural steels tested at various strain rates. Clearly, the yield strength of the

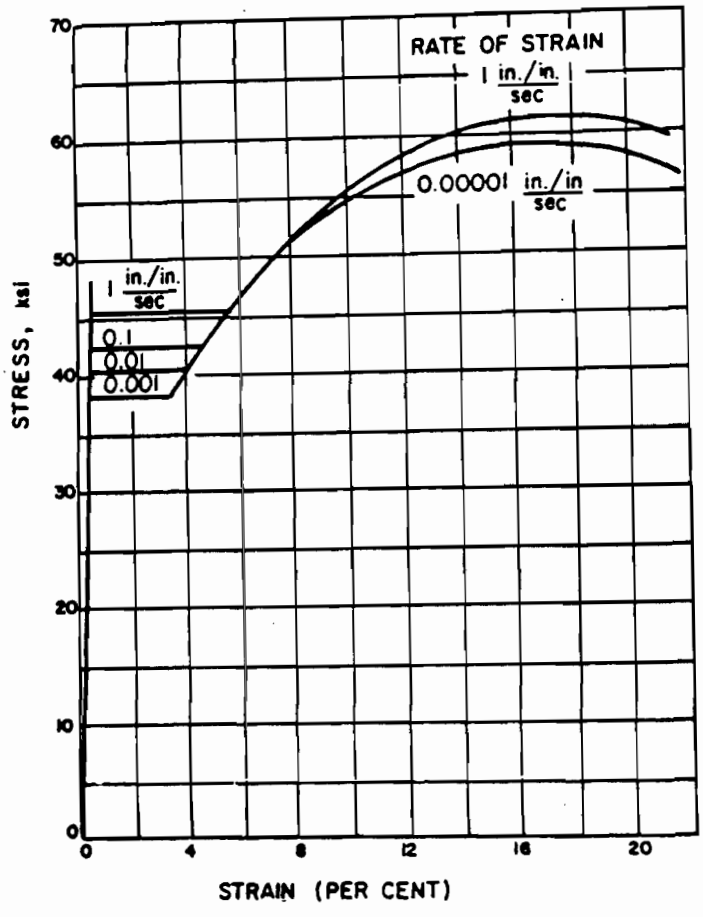

Fig. 2.6 Effect of Strain Rate on Stress-Strain Curve for Structural Steel[36]

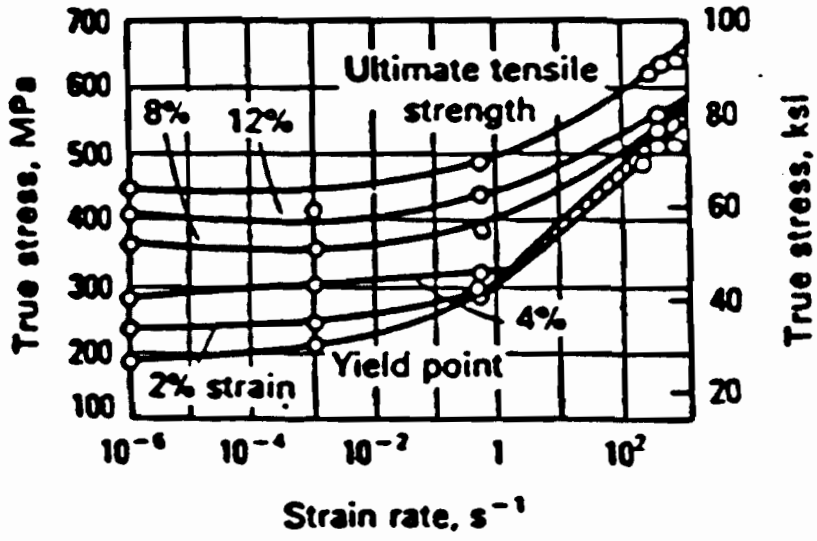

Fig. 2.7 True Yield Stresses at Various Strains Versus Strain Rate for a Low-Carbon Steel at Room Temperature[39]

material increases as the strain rate increases. This is the most consistently observed effect of strain rate on material properties.

Historically, Ludwik was the first to study the effect of the speed of streching upon the stress at which a metal yields[37]. He found a logarithmic relation between the stress at which a metal yields and the strain rate as early as 1909.

In 1925, Korber and Storp compared impact tests with ordinary static tests for various metals[37]. These tests showed a considerable increase in the yield stress in the more rapid tests.

The effect of changing the speed of deformation on various metals was studied by Prandtl and his associates in 1932[37]. Their results were in agreement with the relation found by Ludwik.

In 1937, Winlock and Leiter investigated the effect of the strain rate upon the yielding of deep-drawing sheet steel[38]. Their results showed that the yield stress and the corresponding elongation were considerably affected by the strain rate. The ultimate strength was also influenced but to a smaller extent than the yield strength.

In the 1940s, Manjoine[39] studied the relationships between strain rate, temperature, and the material properties of mild steels. Figure 2.7[39] illustrates the true yield stresses at various strains for a low-carbon steel at room temperature. It can be seen that between strain rates of 10^{-6} sec^{-1} and 10^{-3} sec^{-1} yield stress increases only by 10%. Above the strain rate of 1.0 sec^{-1}, however, the same increase of strain rate doubles the yield stress. For the data shown in Figure 2.7, at every level of strain, the flow stress increases with increasing strain rate. However, a decrease in strain-hardening rate is exhibited at higher strain

rate. The results of the combined effects of strain rate and temperature at 200°, 400°, and 600° C are shown in Figures 2.8 to 2.10[39], respectively. At the highest temperature of 600° C, yield strength increases with increasing strain-rate, but strain hardening increases (rather than decreases) with increasing strain rate. At intermediate temperatures shown in Figures 2.8 and 2.9, however, regions of negative strain rate sensitivity are visible; that is, under certain conditions of strain , strain rate, and temperature , the flow stresses of carbon steels decrease with an increase in strain rate. This is in contrast with the usual strain rate effect[40].

Based on the research findings presented in Refs. 27 and 41, the true stress in metals may be determined by the strain rate as follows:

$$\sigma = C\, \dot{\epsilon}^{m} \qquad (2.13)$$

where

σ = true stress

$\dot{\epsilon}$ = true strain rate

m = strain rate sensitivity exponent

C = material constant

In Equation (2.13), it is possible to determine the value of "m" from tensile tests by changing the strain rate suddenly and by measuring the instantaneous change in stress. This technique is illustrated in Figure 2.11[42]. By applying Equation (2.13) to two different strain rates and eliminating C, we have[42]

$$m = \ln(\sigma_2 / \sigma_1) / \ln(\dot{\epsilon}_2 / \dot{\epsilon}_1) \qquad (2.14)$$

According to Hosford and Caddel[27], the magnitude of "m" for most metals is usually between 0 and 0.03. The value of C depends on the strain rate,

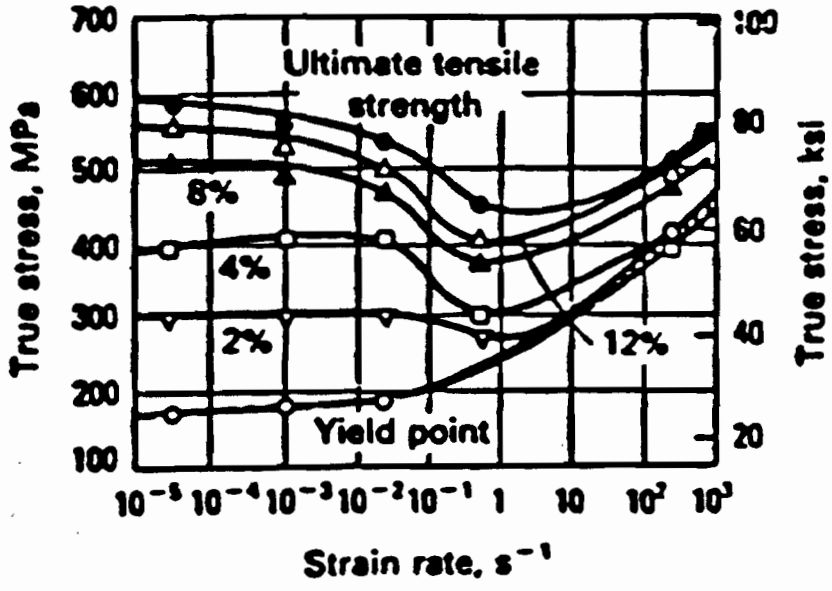

Fig. 2.8 True Yield Stresses at Various Strains Versus Strain Rate for a Low-Carbon Steel at 200°C [39]

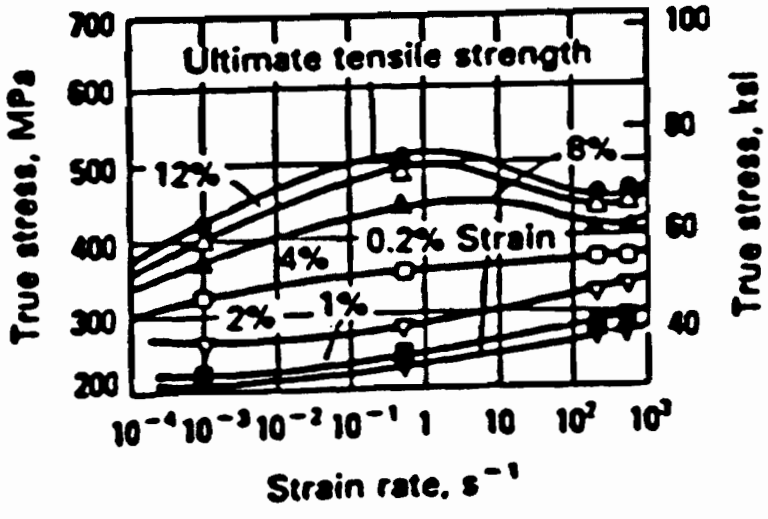

Fig. 2.9 True Yield Stresses at Various Strains Versus Strain Rate for a Low-Carbon Steel at 400°C [39]

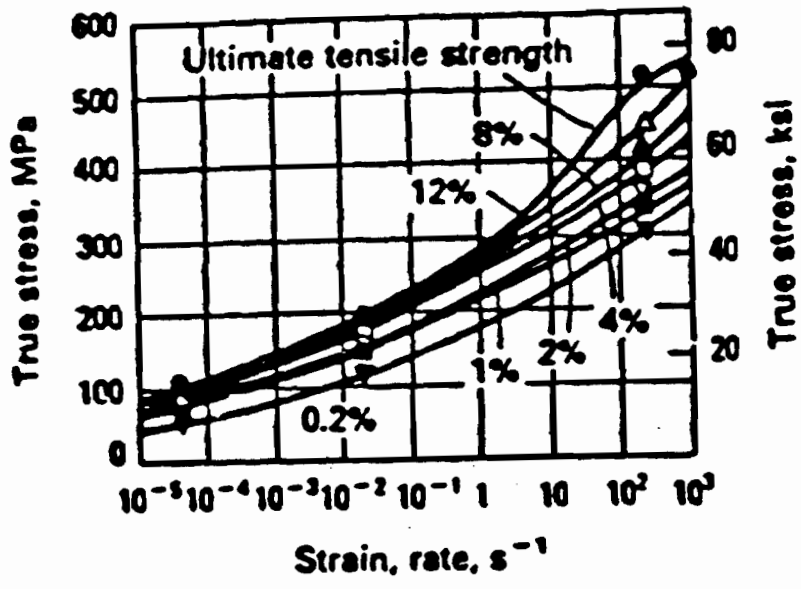

Fig. 2.10 True Yield Stresses at Various Strains Versus Strain Rate for a Low-Carbon Steel at 600°C [39]

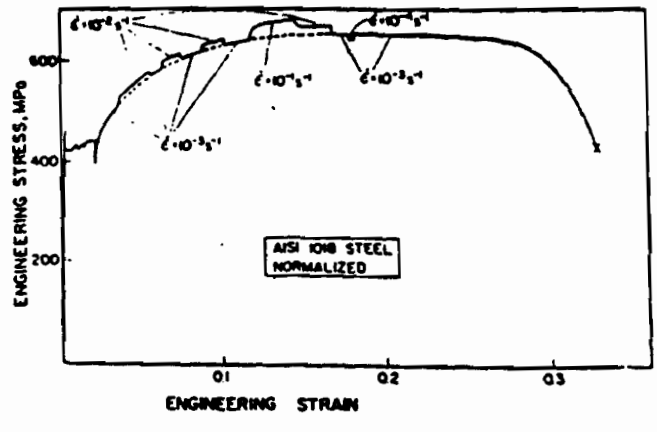

Fig. 2.11 Strain-Rate Changes During Tensile Test, Four Strain Rates Shown Are 10^{-1}, 10^{-2}, 10^{-3}, and 10^{-4} sec^{-1} (Ref.42)

temperature and the type of material[27]. For a given material, the values of C and m can be determined empirically. For example, the resulting magnitudes of C and m obtained from Chatfield and Rote's tests are listed in Table 2.3[41]. It is interesting to note from Table 2.3 that the m values range from 0.018 to 0.056, which are slightly exceeding the range of m values given by Hosford. As expected, the values of ln C (and thus C) increase as the yield strength increases. However, the m values show a steady decrease with the increasing yield strength. An analysis of the results given in Table 4 of Chatfield and Rote's report[41] seems to indicate that the increase in C is offset by the decrease in m values, such that the total increase in yield strength for a given strain rate remains approximately the same regardless of the material strength.

Another useful relationship between the true stress and strain rate is given by Hosford[27] as:

$$\sigma_2 = \sigma_1 \left(\dot{\epsilon}_2 / \dot{\epsilon}_1 \right)^m \qquad (2.15)$$

where σ_1 and σ_2 are the true stresses corresponding to strain rate $\dot{\epsilon}_1$ and $\dot{\epsilon}_2$, respectively. Therefore, if σ_1, $\dot{\epsilon}_1$ and m are known, then σ_2 can be found for any desired value of $\dot{\epsilon}_2$.

If the strain rate sensitivity of a material is known as a design parameter, the engineer may use this property to his advantage and thus a more economical design may be obtained. For example, an automotive engineer may take advantage of the increased yield point (if available) caused by the high strain rate associated with impact when he designs a part to withstand impact loading without permanent deformation[41].

In 1955, Alder and Phillips[43] studied the combined effects of strain rate and temperature on compressive mechanical properties of steel,

copper, and aluminum. The stress-strain curves were determined for these three materials at constant true strain rates in the range from 1 to 40 in./in./sec. The maximum compressive strain was 50% for temperatures ranging from 930° to 1200° C. The tests were conducted using the cam plastometer compression machine which was designed by Orwan and Los[8] in 1950. Table 2.4 presents their experimental results for steels at various strains, strain rates, and temperatures. It can be observed from this table that increase in strain rate or decrease in temperature resulted in an increase in the stress at any given compression strain. Alder and Phillips used Eq. (2.13) for the stress-strain rate relationship. The values of Eq. (2.13) constants C and m obtained from Alder and Phillips' work are given in Tables 2.5 and 2.6, respectively. It can be seen that m tends to increase while C decreases and/or the temperature increases.

In 1957, Cook[44] used the cam plastometer machine to determine the compressive yield strengths for twelve different types of steel at 900°, 1000°, 1100°, and 1200° C combined with constant strain rates of 1.5, 8, 40, and 100 in./in./sec. The experimental results obtained from this investigation for low, medium and high carbon steels are given in Figs. 2.12 through 2.14, respectively. These curves illustrate the relationships between yield strengths and natural strains for three steels tested at different temperatures and strain rates. It is observed from the results of Cook and Alder and Phillips that the yield strengths of steels increase as the strain rate increases and/or the temperature decreases. However, a noticeable feature of many of the curves of this investigation is the drop in yield strength at high strains which is contributed, as Cook concluded, to the predominance of thermal softening

Table 2.4

Effect of Strain Rate and Temperature on the Stress Required to Compress Steel[43]

Specimen Dia., mm.	Temp., °C.	Strain Rate, sec.$^{-1}$	Average Stress (10^3 lb./in.^{2}) to Compress:				
			10%	20%	30%	40%	50%
18	18	slow *	77·5	92·0	98·0	102	105
12	930	4·35	18·6	22·3	23·5	23·9	24·1
		7·4	19·0	22·9	25·1	26·4	26·2
		12·9	20·9	24·0	25·8	27·0	27·1
		23·1	21·6	25·3	27·4	28·6	29·4
12	1000	4·35	14·8	18·3	20·0	20·7	20·1
18		4·35	14·8	17·9	19·6	20·8	20·3
12		7·4	16·4	19·2	21·0	22·1	22·0
18		7·4	15·5	18·6	20·8	22·3	22·2
12		12·9	16·9	19·7	21·4	22·6	22·8
12		23·1	18·6	21·6	22·9	23·9	24·4
18	1060	4·35	12·8	15·2	16·6	17·1	16·3
		7·4	13·6	16·0	17·9	18·7	18·5
		12·9	14·5	16·9	18·6	19·9	20·2
		23·1	15·4	18·4	20·3	21·7	22·1
18	1135	4·35	11·0	12·9	13·8	13·8	13·1
		7·4	11·6	13·6	14·8	15·3	14·7
		12·9	12·4	14·5	15·8	16·7	16·9
		23·1	13·6	15·9	17·4	18·3	18·5
18	1200	4·35	9·0	10·6	11·0	10·9	10·1
		7·4	9·5	10·9	11·7	11·8	11·2
		12·9	10·2	11·6	12·5	12·7	12·5
		23·1	10·9	12·6	13·7	14·3	14·0

Table 2.5

Values of C for Steels Using Equation (2.13)[43]

Temp., °C.	Value of C for a Compression of:				
	10%	20%	30%	40%	50%
930	16·3	19·4	20·4	20·9	20·9
1000	13·0	15·6	17·3	18·0	16·9
1060	10·9	12·9	14·0	14·4	13·6
1135	9·1	10·5	11·2	11·0	9·9
1200	7·6	8·6	8·8	8·3	7·6

Table 2.6

Values of m for Steels Using Equation (2.13)[43]

Temp., °C.	Value of *m* for a Compression of:				
	10%	20%	30%	40%	50%
930	0·088	0·084	0·094	0·099	0·105
1000	0·108	0·100	0·090	0·093	0·122
1060	0·112	0·107	0·117	0·127	0·150
1135	0·123	0·129	0·138	0·159	0·198
1200	0·116	0·122	0·141	0·173	0·196

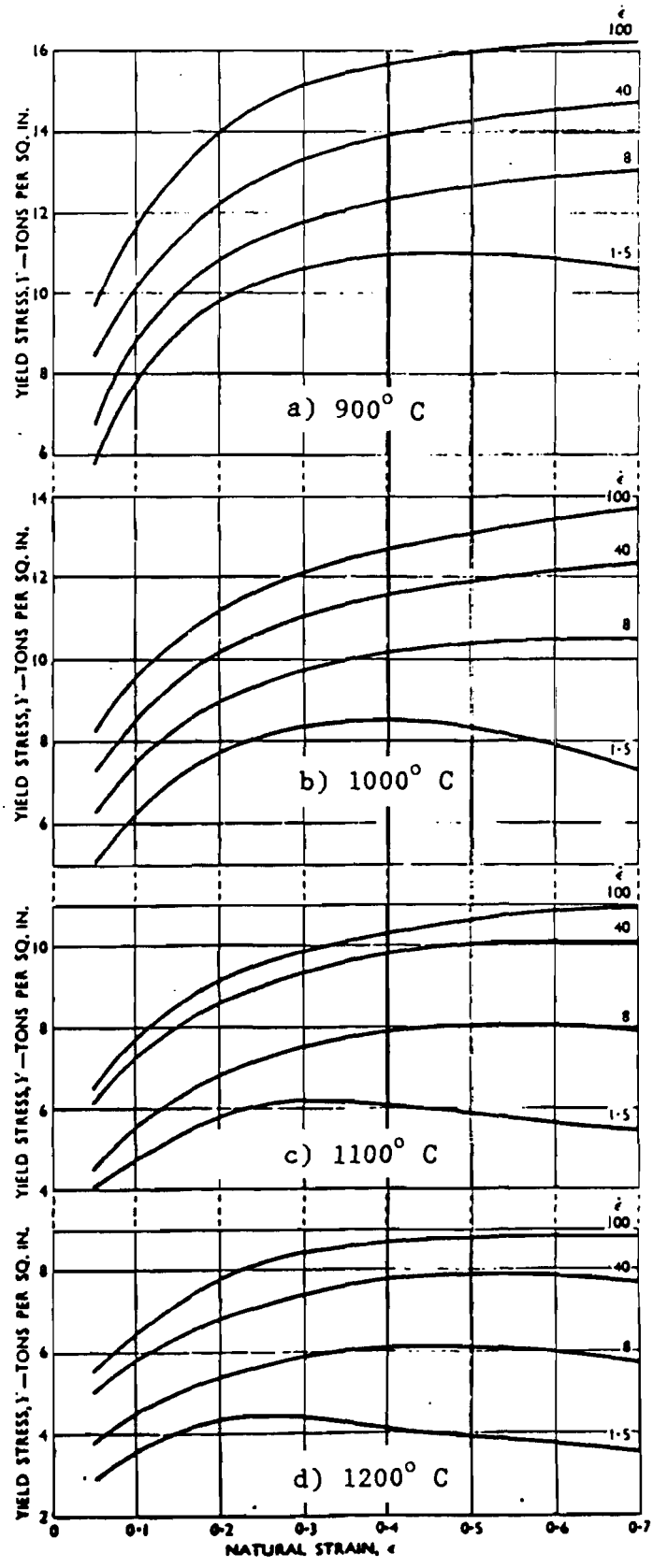

Fig. 2.12 Relationship Between Flow Stress and Natural Strain for Low-Carbon Steels[44]

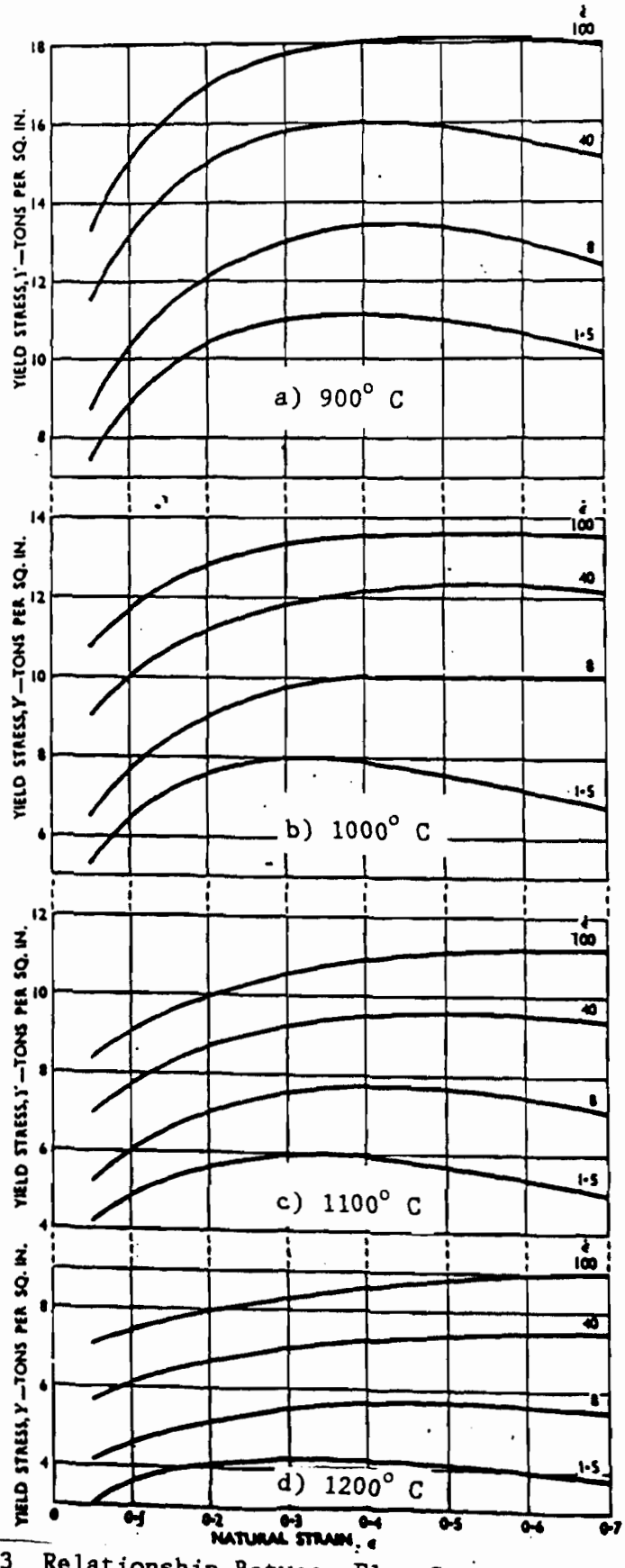

Fig. 2.13 Relationship Between Flow Stress and Natural Strain for Medium-Carbon Steels[44]

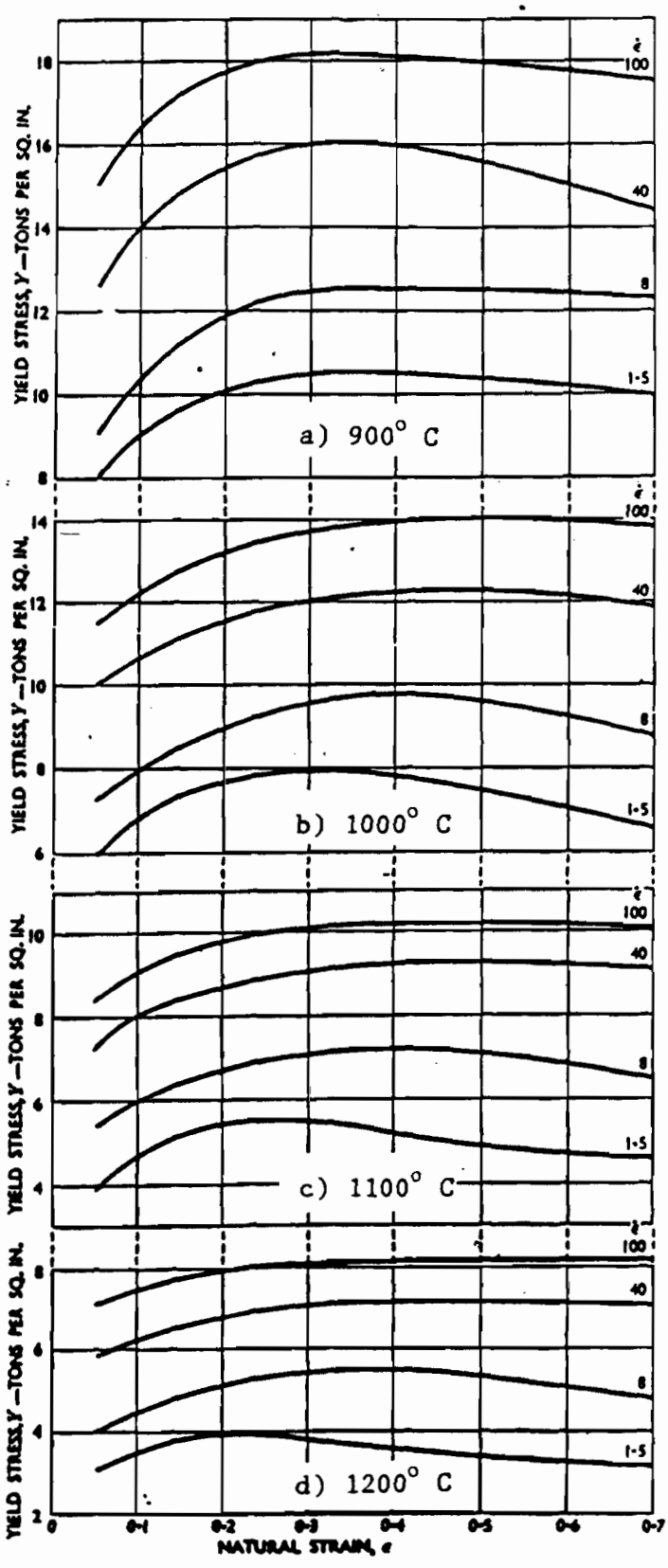

Fig. 2.14 Relationship Between Flow Stress and Natural Strain for High-Carbon Steels[44]

of the steels over strain hardening as the compression proceeds. Comparison of the three curves shown in Figs. 2.12 to 2.14 for the three carbon steels also reveals that the tendency for the stress to drop increases with the steel carbon content.

By using the Split Hopkinson method, Davies and Hunter[45] investigated in 1963 the dynamic compressive mechanical behavior of some metals including steel. The compressive loading cycles was of 30 micro-seconds duration which generated strain rates in the range of 1,000 to 10,000 in./in./sec. The results obtained from this investigation indicated that the ratio of the dynamic to static yield strength of the mild steel used is 2.6.

In 1963, United States Steel Corporation[46] conducted numerous tests on high-strength, low-alloy steels (COR-TEN and TRI-TEN) for the purpose of studying the effects of the strain rate and temperature on the tensile properties of these steels. The tests were conducted at strain rates of 3×10^{-5} in./in./sec, 5×10^{-3} in./in./sec., and 1.0 in./in./sec at temperature of -50° F, 75° F (room temperature), and 600° F. The results obtained from this investigation indicated that as the strain rate was increased at -50° F and at 75° F, the tensile strength and the 0.2 percent offset yield strength increased as shown in Figs. 2.15 and 2.16[46]. However , as the strain rate increased at 600° F, the tensile strength decreased. The ductility of the COR-TEN steel, as measured by percent elongation and reduction of area, did not appear to be strain-rate sensitive at -50° F and room temperature, but at 600° F, the reduction of area for the fastest rate was higher than that for the slowest rate.

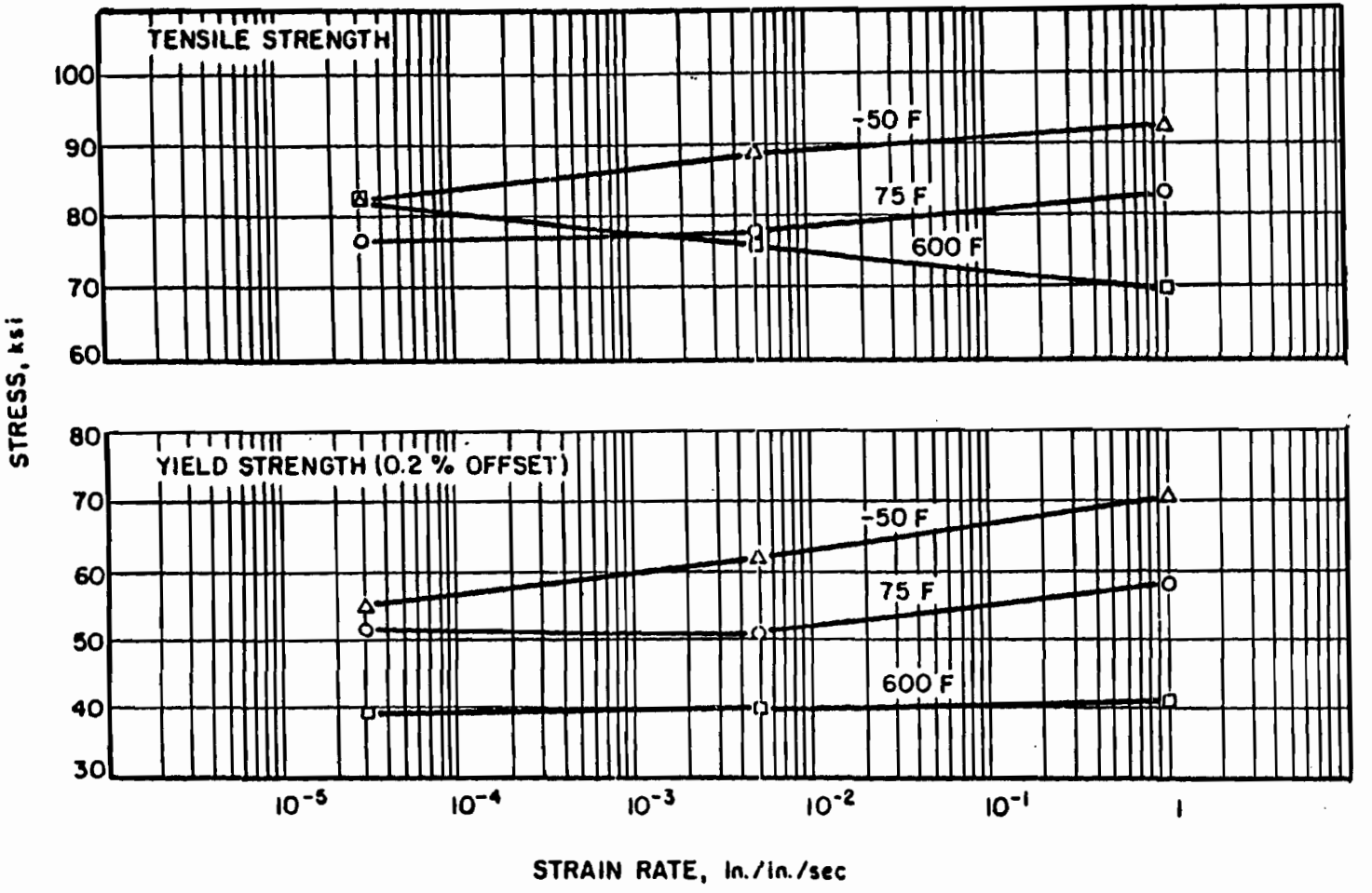

Fig. 2.15 Effect of Strain Rate at -50°, 75°, and 600° F on the Yield and Tensile Strengths of USS COR-TEN Steel[46]

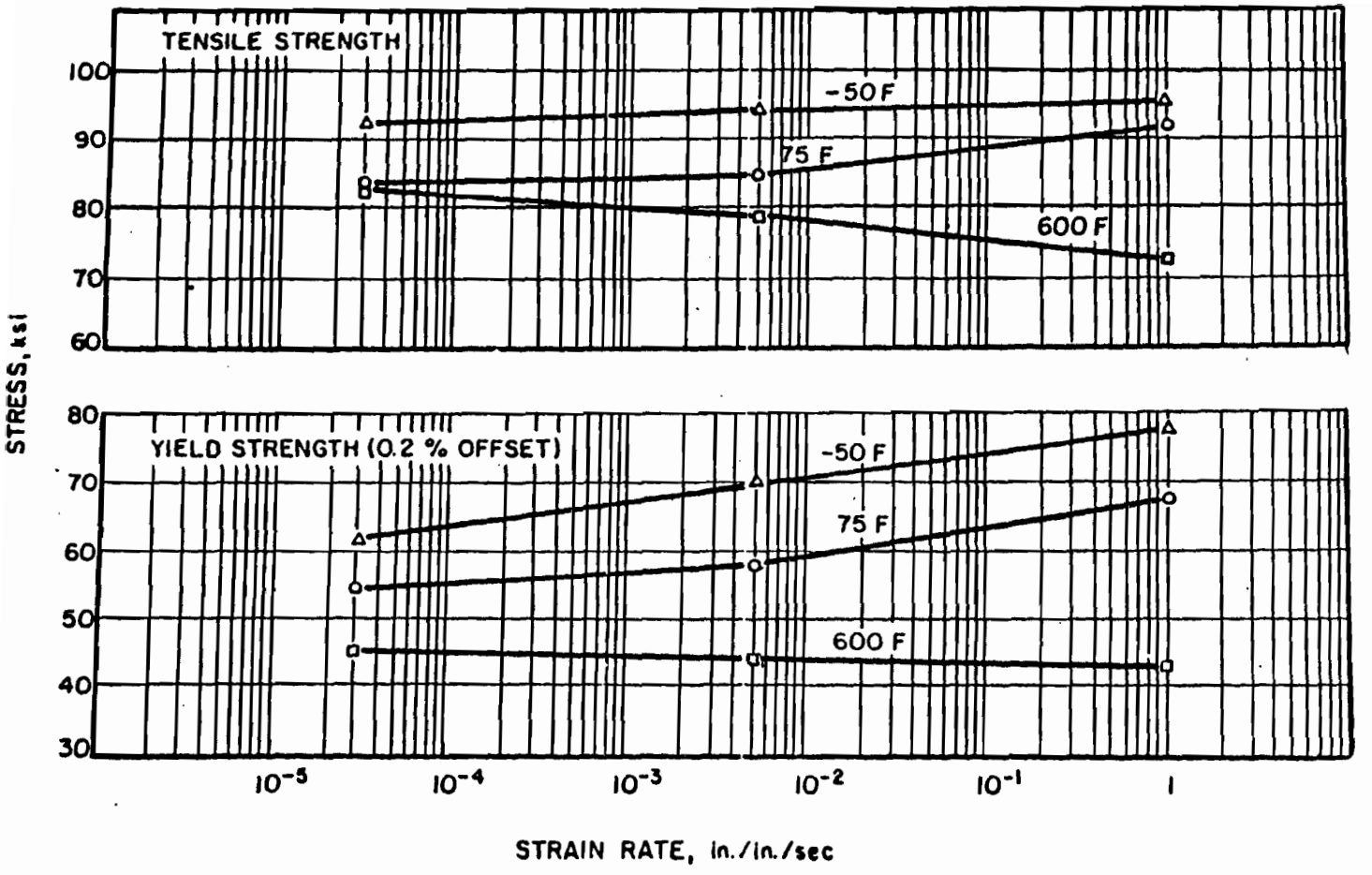

Fig. 2.16 Effect of Strain Rate at -50°, 75°, and 600° F on the Yield and Tensile Strengths of USS TRI-TEN Steel[46]

The percent elongation of the TRI-TEN steel appeared to be somewhat strain-rate dependent, decreasing slightly as the strain rate increased.

In 1974, Chatfield and Rote[41] completed a comprehensive report concerning the influence of strain rate on the mechanical properties of high strength, low alloy (HSLA) steels. In this study six different HSLA steels were tested with yield strengths ranging from 40 to 80 ksi. They also tested three different aluminum alloys for comparison with the HSLA steels. Approximate strain rates used were 0.008, 0.8, 8.0 and 80. in./in./sec. All tests were performed at room temperature. Figure 2.17[41] shows the relationship between yield and tensile strengths, uniform elongation and strain rate for a typical HSLA steel.

As can be seen from Fig. 2.17, the yield and tensile strengths both increase substantially with increasing strain rate while the uniform elongation, which is the strain at the onset of the necking, decreases slightly. This indicates that the total elongation is relatively independent of strain rate. It is, therefore, expected that the absorbed energy of the HSLA steel also increases with increasing strain rates. Such an increase in absorbed energy is obviously desirable for the automotive components.

In 1982, Watanabe[47] studied the yield behavior of low-carbon sheet steels at room temperature under the strain rates of 10^{-4} to 10^{-1} sec^{-1} using an Instron type machine. The results showed another break point of the dependence of the yield stress on the strain rate of 3×10^{-3} sec^{-1}, which is different from Manjoine's strain rate of 10^{-1} sec^{-1} as shown in Fig. 2.18[47]. This means that the dependence of yield stress, yield point elongation, and tensile strength on the strain rate in the range of high

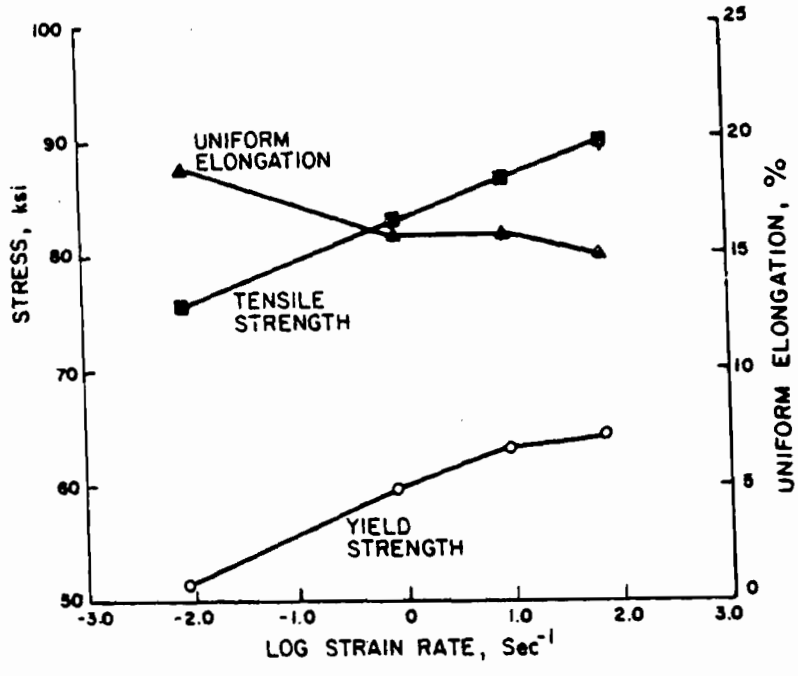

Fig. 2.17 Effect of Strain Rate on Mechanical Properties of a HSLA Steel[41]

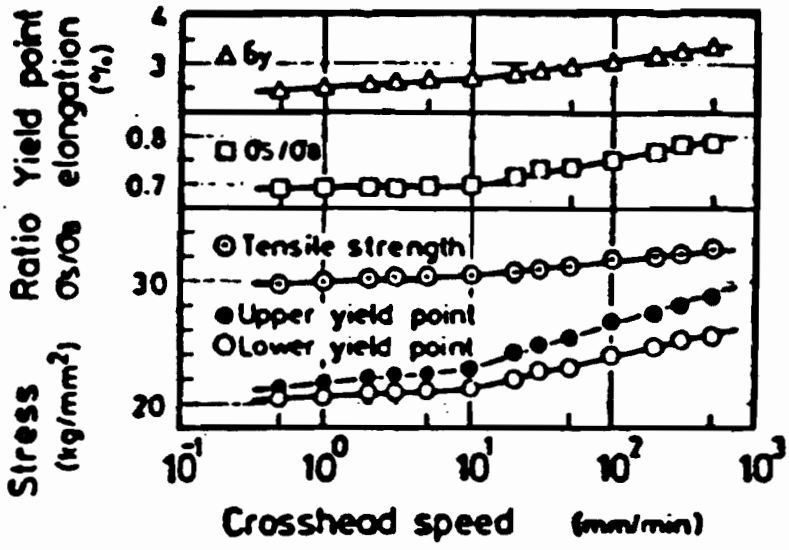

Fig. 2.18 Effect of Crosshead Speed on Yield Behavior and Tensile Strength[47]

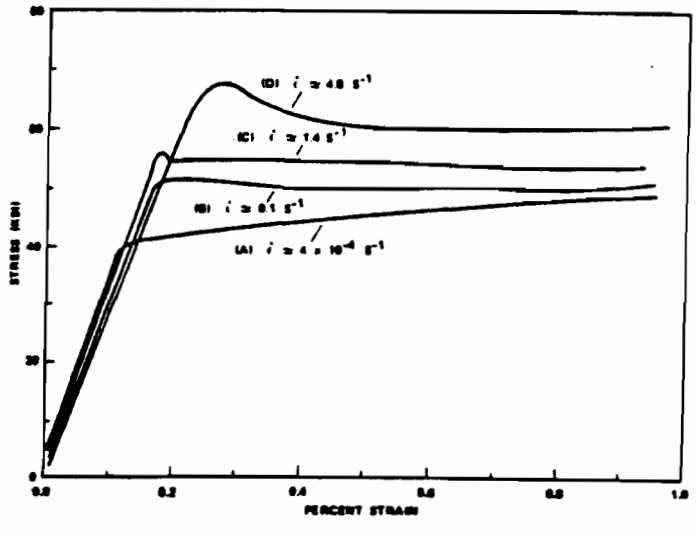

Fig. 2.19 Stress-Strain Curves for SA-106 Carbon Steel Pipe[48]

strain rate above 3 x 10^{-3} sec^{-1} is larger than that at lower strain rates. Figure 2.18 also shows that the yield stress is more sensitive to strain rate as compared with the tensile strength.

Also in 1982, Peterson, Schwabe, and Fertis[48] conducted experiments to measure the effect of strain rate on the tensile properties of SA-106 carbon steel pipe. It was observed that the increase in the strain rate from $4x10^{-4}$ to 4 sec^{-1} raised the yield strength by approximately 30 percent as illustrated in Fig. 2.19.

In 1983, Sachdev and Wagoner[49] found that the strain rate sensitivity m is strongly dependent on the strain rate for steel . This investigation included four types of steel: an interstitial free (IF) steel, a hot rolled, plain carbon steel (HR), and two high strength steels one with a ferrite-pearlite microstructure (HSLA) and the other with a ferrite-martensite (DP) microstructure. A new equation was developed to correlate the strain-rate sensitivity and the strain rate as follows[49]:

$$m = b\,\dot{\epsilon}^{a} \qquad (2.16)$$

In the above equation, a and b are constants to be determined from tests. Figure 2.20[49] shows the strain-rate sensitivity index, m, for the steels tested as a function of strain rate. The curves represent the best fits for Equation (2.16) for the steels tested under the selected strain rate range. The best fit coefficients obtained from these curves are given in Table 2.7[49] along with the m-values. Note that for each steel the strain-rate sensitivity is well-characterized by the new equation.

In 1984, Meyer[50] conducted tension tests on high strength sheet steels at strain rates between $5x10^{-4}$ sec^{-1} and $5x10^{3}$ sec^{-1}. Figure 2.21 shows the stress-strain curves of the tested steel at different strain

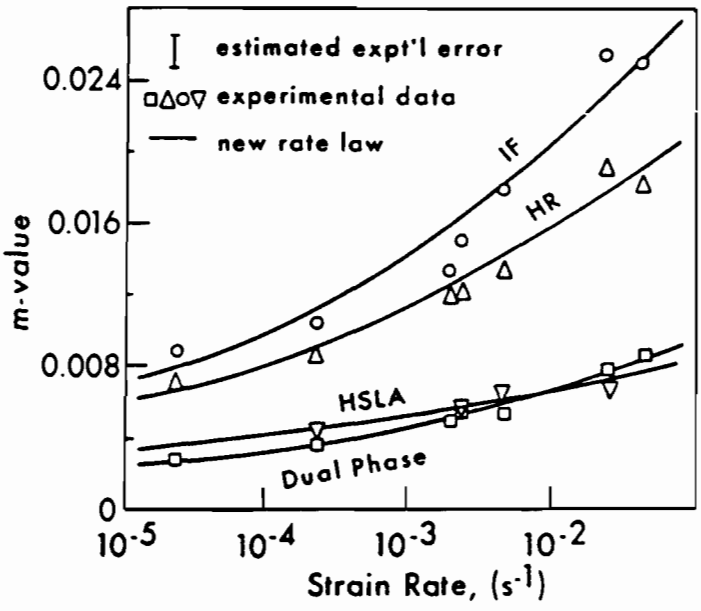

Fig. 2.20 The Variation of the Strain Rate Sensitivity (m-value) With Strain Rate[49]

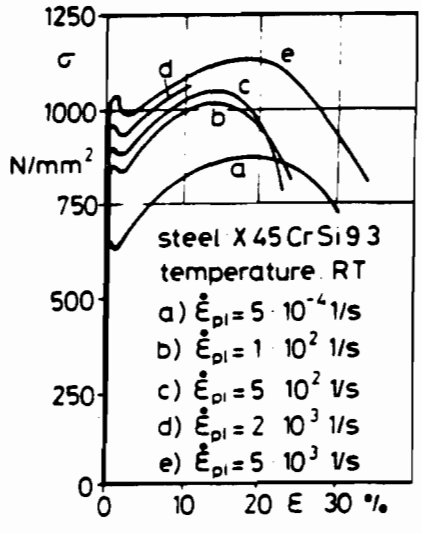

Fig. 2.21 Stress-Strain Curves for High Strength Steel at Varying Strain Rate[50]

Table 2.7

Standard Strain Rate Sensitivity

and New Strain Rate Parameters[49]

Material	m	b	a
IF	0.011	0.039	0.150
HR	0.008	0.029	0.134
HSLA	0.004	0.010	0.102
DP	0.003	0.013	0.149

Table 2.8

Strain Rate Sensitivity for Different Microstructures

Determined by Strain Rate Jump Tests at 6.7×10^{-5} sec^{-1}, 6.7×10^{-4} sec^{-1}, and 6.7×10^{-3} sec^{-1} (Ref. 51)

Microstructures	m low to intermediate strain rate	m intermediate to high strain rate
Cold-rolled	0.002	0.004
Normalized	0.002	0.004
Martensitic	0.003	0.005
Tempered martensitic	0.003	0.006
Ferrite-carbide	0.003	0.005

rates. It is observed from this figure that both yield and ultimate tensile strengths are increased with the increasing strain rate. However, the ductility decreased when the strain rate increased from 5×10^{-4} sec^{-1} to 2×10^{3} sec^{-1}. At higher strain rates above 2×10^{3} sec^{-1}, the material becomes more ductile again.

Recently, Nagorka[51] conducted an experimental investigation to observe the effect of microstructure and strain rate on the stage III strain hardening and ductility of dual-phase steels. The five types of steels included in this investigation were cold-rolled, normalized, martensitic, tempered martensitic, and ferrite-carbide. Table 2.8[51] lists the values of the strain rate sensitivity for the five steels studied. The m values were calculated for low to intermediate strain rates (6.7×10^{-5} sec^{-1} to 6.7×10^{-4} sec^{-1}) and intermediate to high strain rates (6.7×10^{-4} sec^{-1} to 6.7×10^{-3} sec^{-1}). Based on the m values given in this table, Nagorka concluded that the strain rate sensitivities of various microstructures are the same for any given strain rate and increase with increasing strain rate. These observations indicate that m is insensitive to changes in microstructures. Also, it was concluded from this study that the uniform elongation increases slightly with increasing strain rate for most of the microstructures tested, whereas post-uniform elongation increases significantly with increasing strain rate.

Another very important mechanical property is the modulus of elasticity, E. Norris, et al., state in Ref. 36 that, based on a limited number of tests on ordinary structural carbon steel, the modulus of elasticity is unaffected by strain rates.

ii) Stainless Steels. Albertini and Montagnani[52] have conducted tests on three austenitic stainless steels (AISI types 304, 304L and 347). The results of these tests are presented in Figs. 2.22 to 2.24[52], which indicate an increase in yield and ultimate strengths for all materials when the strain rate increases. However, decreases in the total elongations are exhibited.

In 1984, Hopkinson split-bar tests were performed on type 21-6-9 austenitic stainless steels from ambient temperature to 1023° K by Kassner and Breithaupt[53]. These high strain rate tests (10^2 to 10^4 sec^{-1}) were compared with lower strain rate tests (10^{-4} sec^{-1}). The results as shown in Figure 2.25[53] indicate that the strain-rate sensitivity of this type of stainless steel is not strongly dependent on the strain rate. The value of m was determined to be 0.03846 by measuring the slope of the indicated best-fit line.

iii) Aluminum. Structural aluminums were found to be less strain rate sensitive than steels. Figure 2.26[54] shows the data obtained for 1060-O aluminum. Between strain rates of 10^{-3} sec^{-1} and 10^3 sec^{-1}, the stress at 2% plastic strain increases by less than 20%. Another contrast to the behavior of steel as demonstrated in Fig. 2.26 is that strain hardening increases with increasing strain rate. Reference 55 summarizes several data sets relating to the yield stress dependence on strain rate in steel and aluminum (Figs. 2.27 and 2.28[55]). The comparison shows that for aluminum, the effect on yield stress is less significant and occurs only at extremely high strain rates. Note the difference in vertical scales in Figs. 2.27 and 2.28.

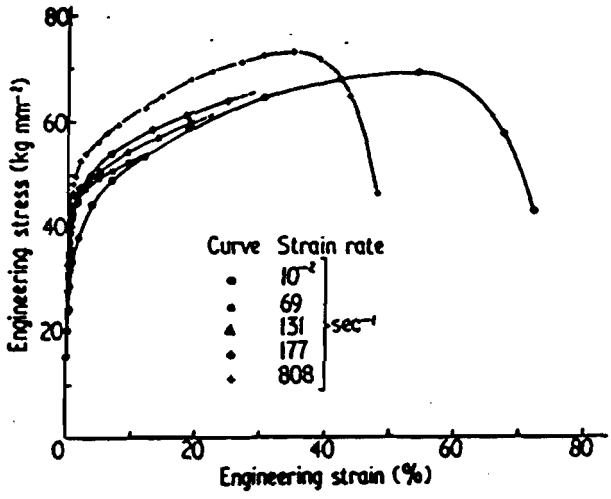

Fig. 2.22 Dynamic Stress-Strain Curves for AISI Type 304 Stainless Steel[52]

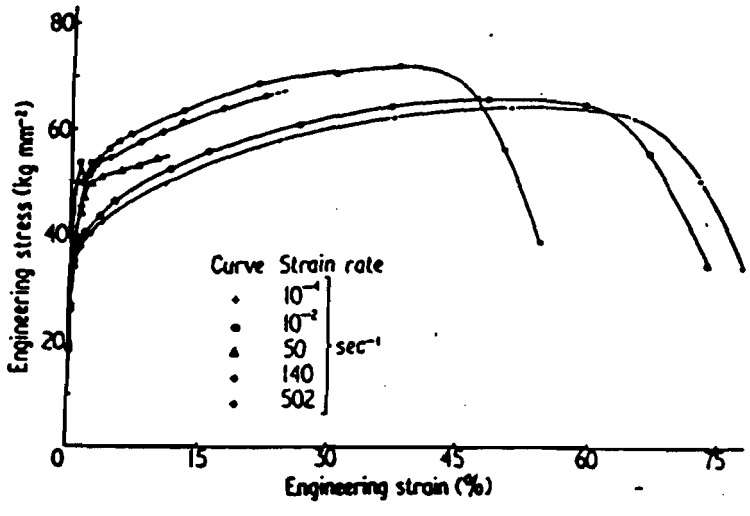

Fig. 2.23 Dynamic Stress-Strain Diagram of AISI Type 304L Stainless Steel[52]

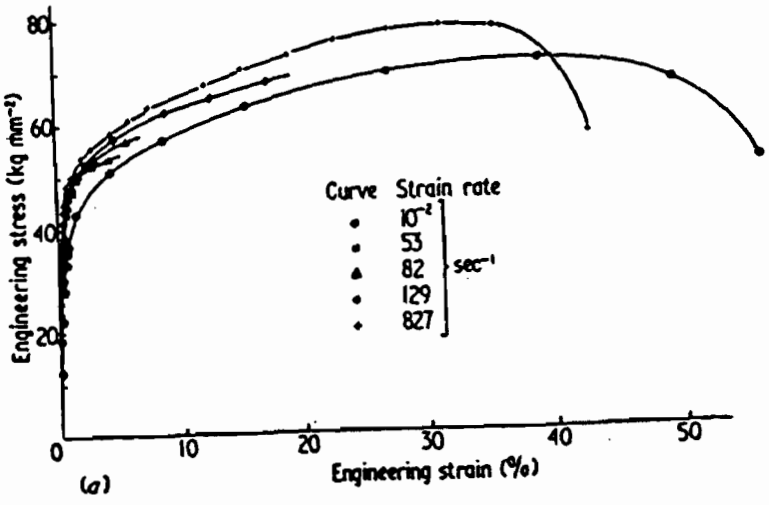

Fig. 2.24 Dynamic Stress-Strain Diagram of AISI Type 347 Stainless Steel[52]

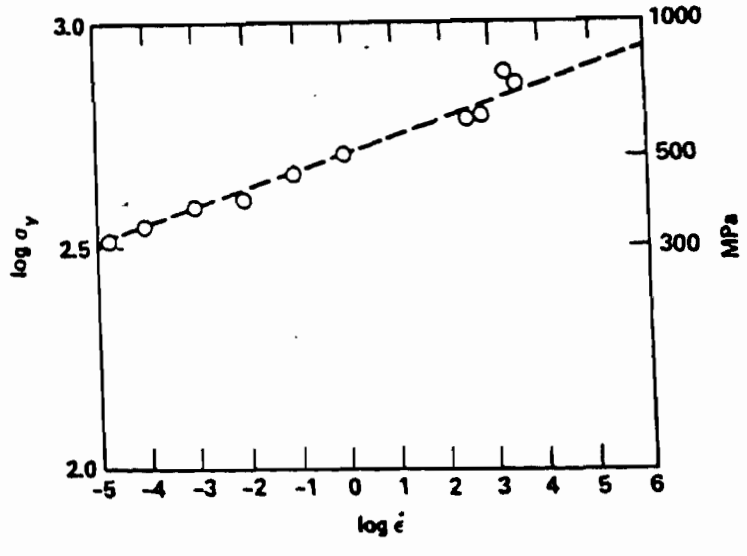

Fig. 2.25 The Ambient-Temperature Yield Stress of Anneald Type 21-6-9 Stainless Steel As a Function of Strain Rate[53]

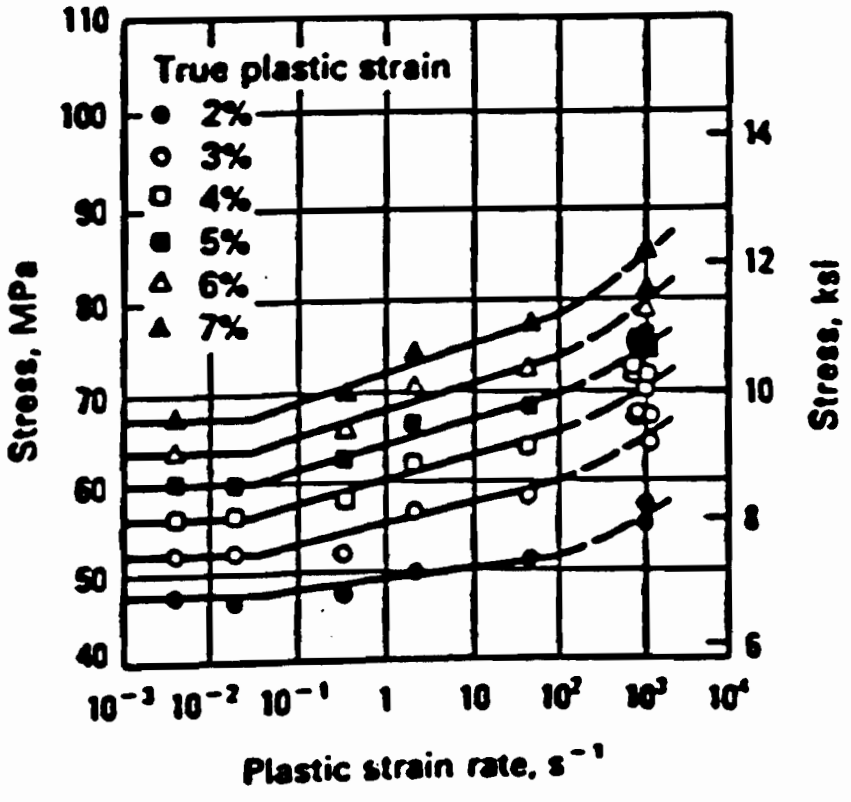

Fig. 2.26 Analysis of the Uniaxial Stress, Strain, and Strain Rate Data for Aluminum 1060-O[54]

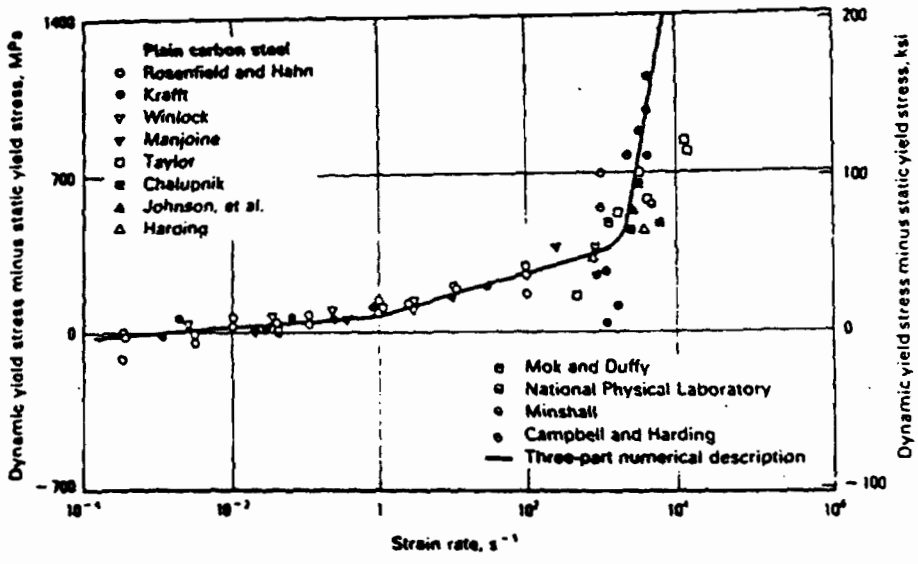

Fig. 2.27 Dynamic Yield Stress (Minus the Static Yield Stress) Versus Strain Rate for Steel[55]

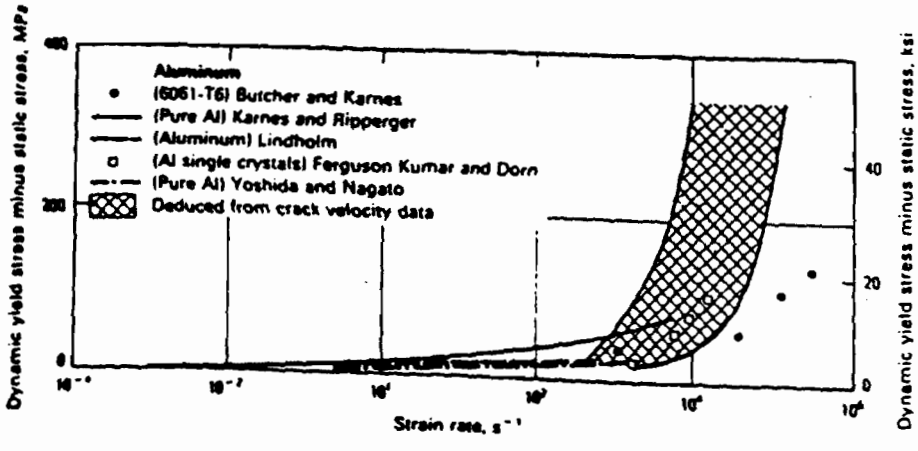

Fig. 2.28 Dynamic Yield Stress (Minus the Static Yield Stress) Versus Strain Rate for Aluminum[55]

Alder and Phillips[43] also performed compression tests on aluminum to study the combined effects of strain rate and temperature using the cam plastometer compression testing machine. The compression tests on aluminum were conducted under the strain rate range of 1 to 40 in./in./sec. combined with temperatures ranging from -190° C to 550° C. Figure 2.29 shows typical stress versus logarithmic strain rate curves at various temperatures. It is observed from this figure that the stress at a given strain increases as the strain rate increases and/or the temperature decreases. Table 2.9 presents the experimental results for aluminum. The values of C and m according to Equation 2.13 are given in Tables 2.10 and 2.11, respectively. No drop in stress was observed at high strains as in the case of steel.

Commercially pure aluminum specimens were tested by Hockett[56] in 1959 at room temperature using the cam plstometer compression testing machine at three strain rates of 0.23, 0.455, and 1.46 in./in./sec. From the measurements of load and time throughout each test, true stress versus true strain curves were plotted. These curves fit an equation of the form:

$$\sigma = A\,(1 - e^{B\epsilon}) + C\,\epsilon \qquad (2.17)$$

where σ is the true stress, ϵ is the true strain, A, B, and C are parameters determined from the tests, and e is the base of natural logarithm. The parameters A and C were found to be dependent upon temperature and strain rate, increasing with decreasing temperature and with large increases in strain rate. The parameter B was found to be essentially independent of temperature, but a large increase of strain rate produces an increase in B. Table 2.12 presents the values of the parameters A, B and C as a result of the compression tests conducted on

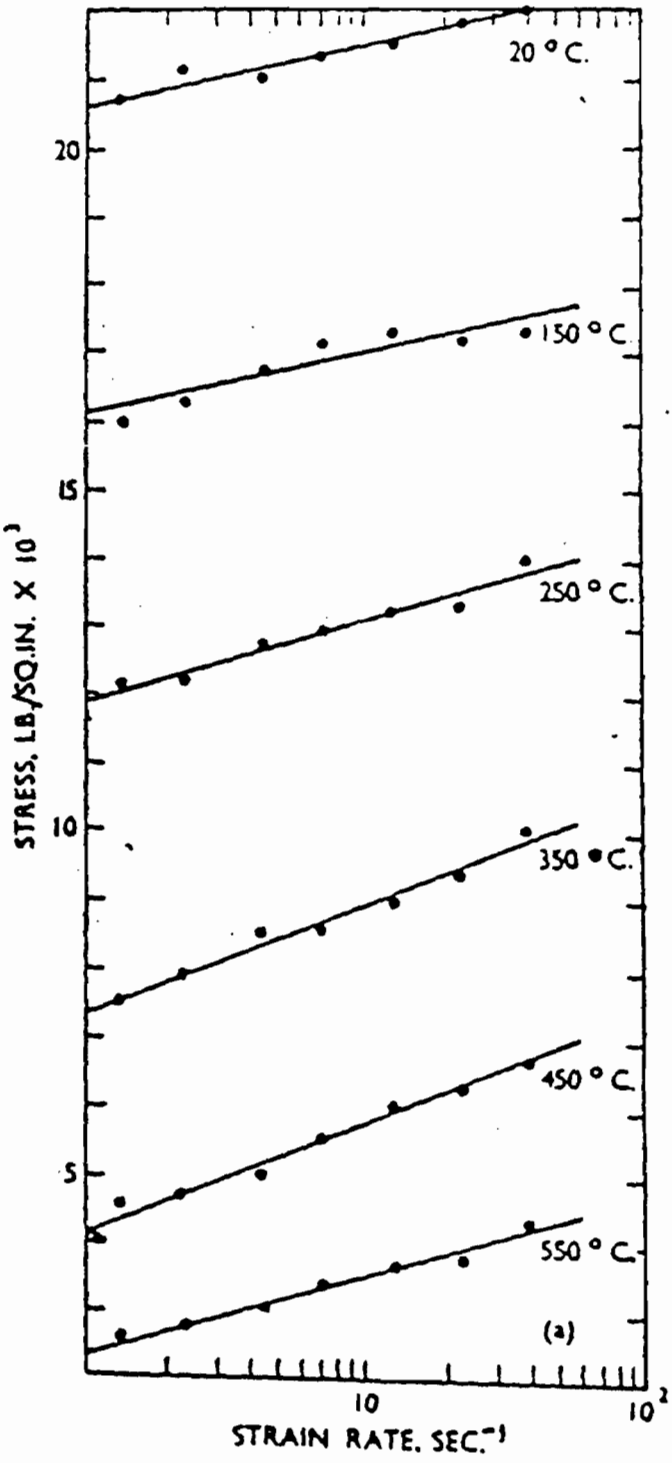

Fig. 2.29 Effect of strain rate on the Stress Required to Compress Aluminum to 40% Reduction at Various Temperatures[43]

Table 2.9

Effect of Strain Rate and Temperature on the Stress Required to Compress Aluminum [43]

Batch	Specimen Dia., mm.	Temp., °C.	Strain Rate, sec.$^{-1}$	Average Stress (10^3 lb./in.^{2}) to Compress:				
				10%	20%	30%	40%	50%
b	12	−190	4·38	28·1	34·1	33·9	32·2	31·6
b	12	−120	4·38	18·6	22·4	24·7	26·3	27·8
b	12	− 75	4·38	17·4	20·9	23·0	24·5	25·8
a	18	− 75	4·38	16·0	19·5	21·5	23·0	24·1
a	18	18	slow*	12·9	15·4	17·0	18·8	20·5
a	18		1·34	14·7	17·2	19·0	20·7	22·1
a	18		2·31	14·9	17·6	19·5	21·1	22·6
a	18		4·38	14·1	17·0	19·2	21·0	22·4
b	12		4·38	14·5	17·2	19·2	20·6	21·9
a	18		7·15	14·6	17·5	19·5	21·3	22·9
a	18		12·9	15·1	17·9	19·8	21·5	23·0
b	12		12·9	15·0	17·9	19·7	21·1	22·3
a	18		23·1	15·3	18·2	20·1	21·8	23·1
a	18		39·3	15·1	18·1	20·1	22·0	23·3
a	18	150	1·34	11·4	13·5	14·9	16·0	16·9
			2·31	11·5	13·8	15·3	16·3	17·2
			4·38	11·9	14·1	15·6	16·7	17·8
			7·15	12·0	14·2	15·7	17·1	17·9
			12·9	12·0	14·2	15·9	17·3	18·2
			23·1	12·1	14·2	15·8	17·2	18·4
			39·3	12·1	14·3	16·0	17·4	18·5
a	18	250	1·34	9·2	10·6	11·5	12·1	12·5
			2·31	9·4	10·7	11·6	12·2	12·6
			4·38	9·5	11·0	12·1	12·7	13·1
			7·15	9·6	11·1	12·1	12·9	13·1
			12·9	9·8	11·6	12·6	13·3	13·6
			23·1	9·8	11·5	12·6	13·4	13·8
a	18	350	1·34	6·3	7·0	7·3	7·5	7·5
			2·31	6·3	7·1	7·6	7·8	7·9
			4·38	6·8	7·7	8·2	8·5	8·6
			7·15†	6·7	7·6	8·2	8·6	8·7
			12·9	7·0	8·1	8·6	9·0	9·1
			23·1	7·3	8·3	9·0	9·4	9·7
			39·3	7·7	8·8	9·5	10·0	10·2

Table 2.10

Values of C for Aluminums Using Equation (2.13)[43]

Metal	Temp., °C.	Value of C for a Compression of:				
		10%	20%	30%	40%	50%
Al	18	14·6	17·1	18·9	20·6	22·0
	150	11·4	13·5	15·0	16·1	17·0
	250	9·1	10·5	11·4	11·9	12·3
	350	6·3	6·9	7·2	7·3	7·4
	450	3·9	4·3	4·5	4·4	4·3
	550	2·2	2·4	2·5	2·4	2·4

Table 2.11

Values of m for Aluminums Using Equation (2.13)[43]

Metal	Temp., °C.	Value of *m* for a Compression of:				
		10%	20%	30%	40%	50%
Al	18	0·013	0·018	0·018	0·018	0·020
	150	0·022	0·022	0·021	0·024	0·026
	250	0·026	0·031	0·035	0·041	0·041
	350	0·055	0·061	0·073	0·084	0·088
	450	0·100	0·098	0·100	0·116	0·130
	550	0·130	0·130	0·141	0·156	0·155

Table 2.12

Results of Compression Tests on Commercially Pure Aluminum at Constant Strain Rate, Based on Equation (2.17)[56]

Strain Rate, $\dot{\epsilon}$, per sec	Variance of Fit, s_f^2	Standard Deviation of Fit, s_f	First Parameter, A	Standard Deviation of A, s_A	Second Parameter, B	Standard Deviation of B, s_B	Third Parameter, C	Standard Deviation of C, s_C	Number of Points n
2.30×10^{-1}	347 103	589.2	11 303	237	−25.92	1.46	13 496	473	70
4.55×10^{-1}	2 496 161	1 579.2	11 662	637	−19.12	2.54	13 220	1 221	89
1.46	2 749 815	1 685.3	10 972	515	−22.49	2.80	15 750	1 037	124

commercially pure aluminum at constant true strain rates along with the statistical parameters which were obtained from fitting the experimental data to Equation 2.17.

Tests in compression and tension for a large number of metals under high strain rates were performed by Lindholm and Yeakley[57] in 1968. Figure 2.30 shows stress-strain curves for 1100-0 aluminum in both tension and compression at various strain rates. The lower strain rate tests were performed on a standard Instron testing machine and the rest of the tests were performed using the Split Hopkinson Pressure Bar. For the comparison between the tension and compression data, all values of stress, strain, and strain rate are true values. It has been observed from the results of many tests that for very low strain rates, the stress levels in tension and compression agree well, although the increase in flow stress with increasing strain rate differs in detail. Figure 2.31 shows a number of compression stress-strain data for 6061-T6 aluminum alloy, for which the wide variation in strain rate appears to have negligible effect on the stress levels. This is found to be true for other high-strength aluminum alloys according to Lindholm and Yeakley. As a result, the equivalence of the data obtained from the Split Hopkinson Pressure Bar with that obtained at low strain rates from an Instron machine indicates that wave propagation and inertia forces are not contributing any significant error to the measurements in the dynamic tests.

A large amount of the available data has been reviewed by Lindholm and Bessy[58]. The materials tested include several commercial aluminum alloys. The data cover strain rates from 10^{-5} to about 10^{3} sec^{-1}. The strain rate sensitivity was found to be constant over a large range of

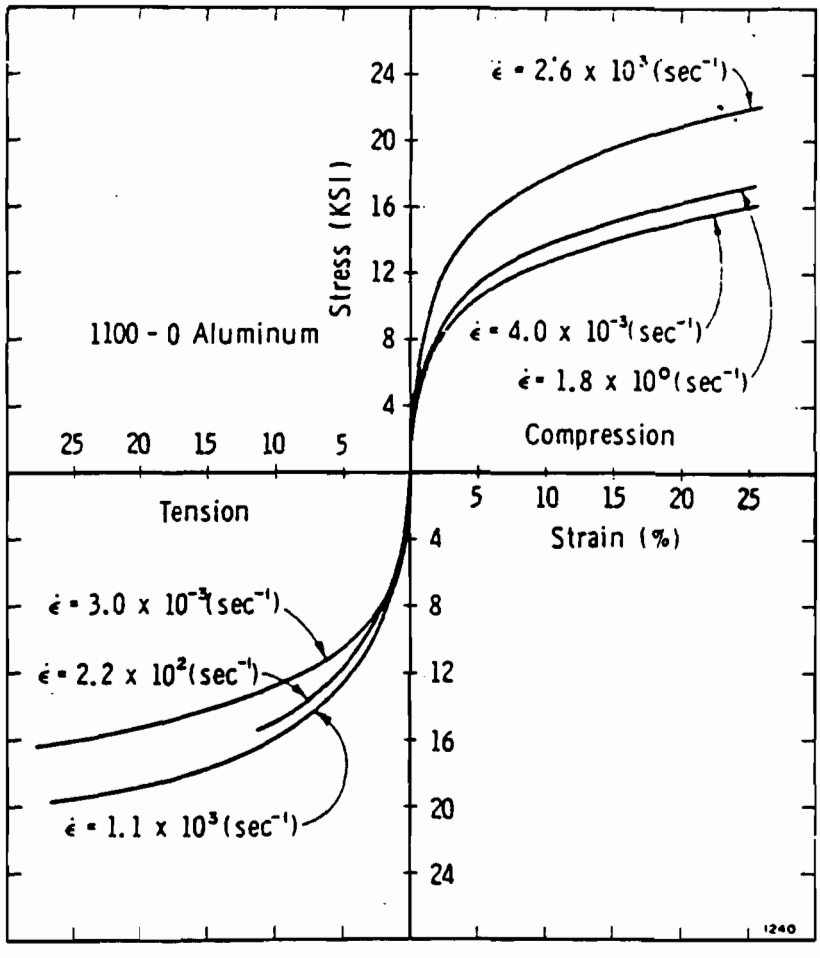

Fig. 2.30 Stress-Strain Curves for 1100-0 Aluminum in Tension and Compression[57]

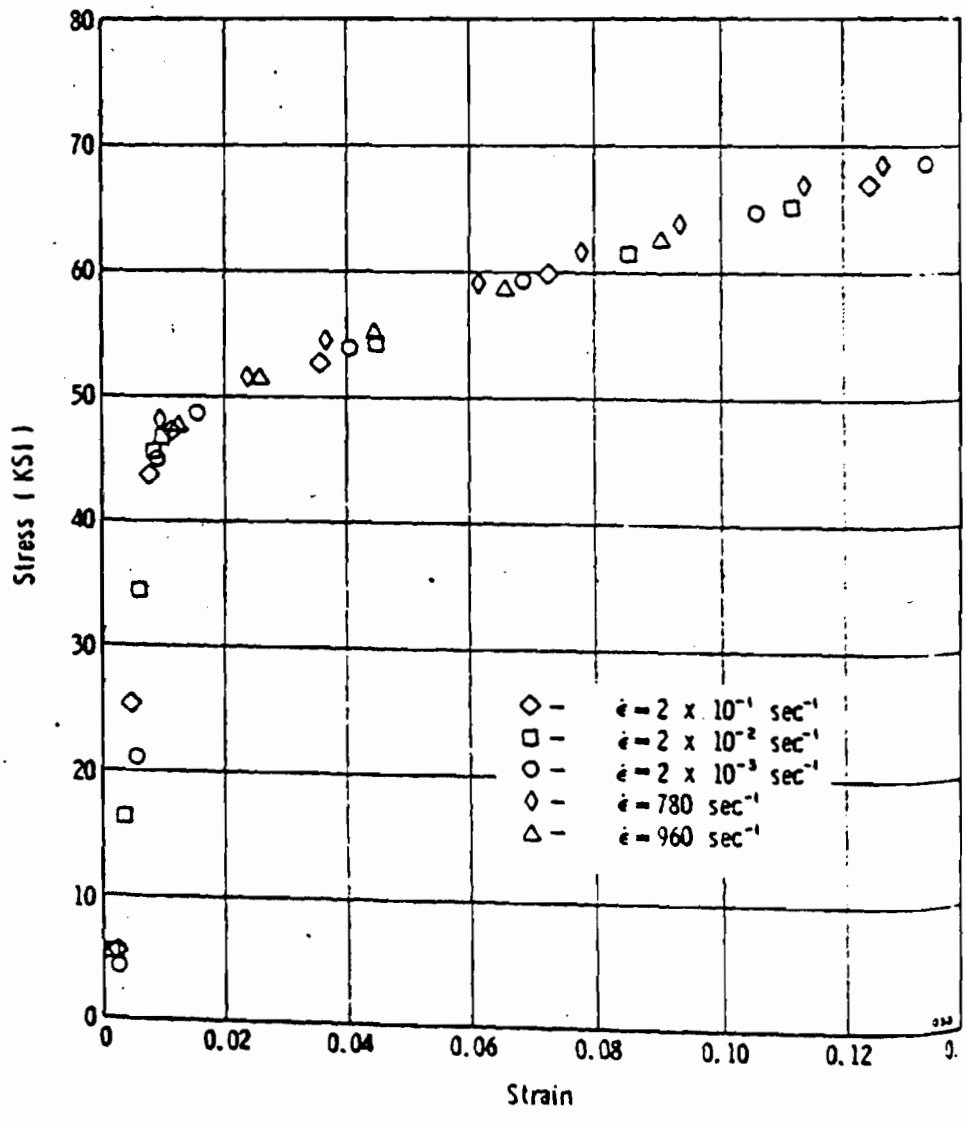

Fig. 2.31 Stress-Strain Curves for 6061-T6 Aluminum in Compression at Several Strain Rates[57]

strain rates. Figures 2.32 to 2.34[58] show the effect of plastic strain rate on the flow stress at a constant true strain and a constant temperature. In some cases, rate independent behavior is observed at low strain rates. In general, the value of m was found to increase with increasing strain rate. From these figures, it can be seen that the flow stress may be related to the strain and strain rate over the wide range of strain rates by the following equation[59]

$$\sigma = \sigma_o(\epsilon) + \sigma_1(\epsilon) \log \dot{\epsilon} \qquad (2.18)$$

where $\sigma_o(\epsilon)$ is the stress-strain relation at unit strain rate.

Green and Maiden[60] have conducted two compression tests on two types of aluminums, 6061-T6 and 7075-T6. The range of the strain rates was from 0.03 sec^{-1} to 560 sec^{-1}. Figure 2.35[60] shows the stress strain data of 7075-T6 at various strain rates. It is apparent from the results of these tests that both aluminums are not sensitive to the change in the strain rate.

Figure 2.36[33] shows a method of comparing the previous investigation data in terms of a rate-sensitivity parameter versus the static flow stress. The parameter is the increase in flow stress from a static test to a dynamic test at a given strain divided by the static flow stress and the log of the difference in strain rates. It represents the percentage increase in stress per unit of log strain rate. It is shown from this figure that the degree of rate sensitivity is increased as material strength is decreased, or as purity increases.

c. Strain-Rate History Effect. In addition to the effect of strain rate on the mechanical properties of materials, the history of

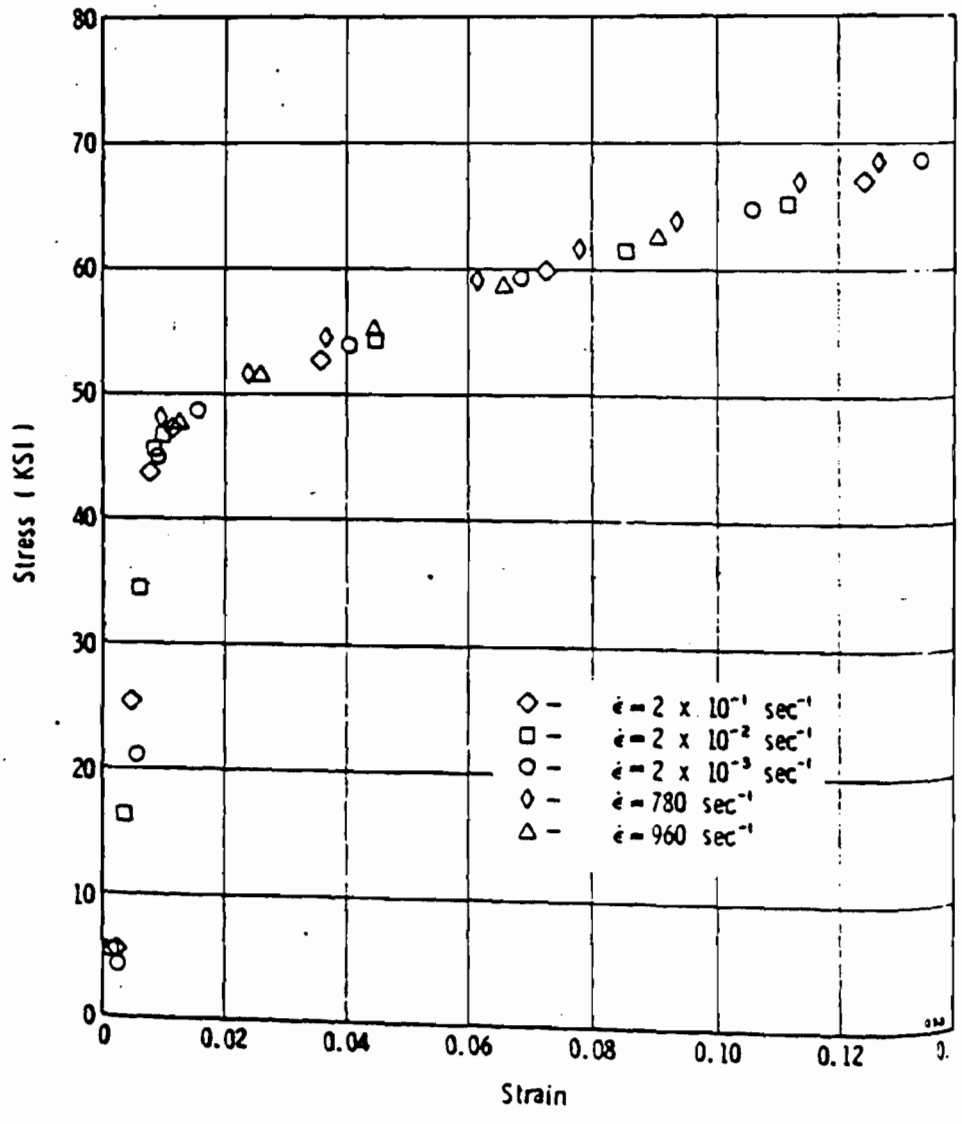

Fig. 2.31 Stress-Strain Curves for 6061-T6 Aluminum in Compression at Several Strain Rates[57]

strain rates. Figures 2.32 to 2.34[58] show the effect of plastic strain rate on the flow stress at a constant true strain and a constant temperature. In some cases, rate independent behavior is observed at low strain rates. In general, the value of m was found to increase with increasing strain rate. From these figures, it can be seen that the flow stress may be related to the strain and strain rate over the wide range of strain rates by the following equation[59]

$$\sigma = \sigma_o(\epsilon) + \sigma_1 (\epsilon) \log \dot{\epsilon} \qquad (2.18)$$

where $\sigma_o(\epsilon)$ is the stress-strain relation at unit strain rate.

Green and Maiden[60] have conducted two compression tests on two types of aluminums, 6061-T6 and 7075-T6. The range of the strain rates was from 0.03 sec^{-1} to 560 sec^{-1}. Figure 2.35[60] shows the stress strain data of 7075-T6 at various strain rates. It is apparent from the results of these tests that both aluminums are not sensitive to the change in the strain rate.

Figure 2.36[33] shows a method of comparing the previous investigation data in terms of a rate-sensitivity parameter versus the static flow stress. The parameter is the increase in flow stress from a static test to a dynamic test at a given strain divided by the static flow stress and the log of the difference in strain rates. It represents the percentage increase in stress per unit of log strain rate. It is shown from this figure that the degree of rate sensitivity is increased as material strength is decreased, or as purity increases.

c. Strain-Rate History Effect. In addition to the effect of strain rate on the mechanical properties of materials, the history of

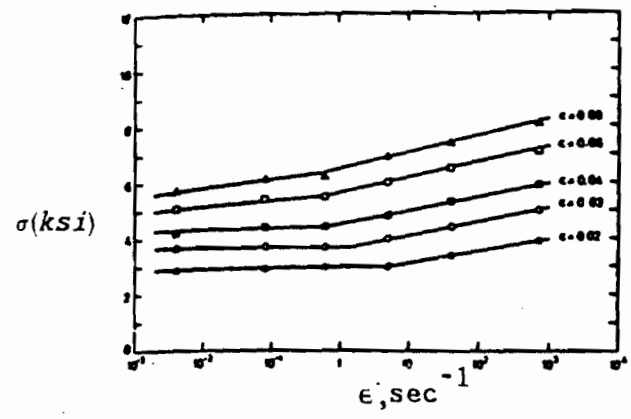

Fig. 2.32 Strain and Strain-Rate Dependence of the Flow Stress of High-Purity Aluminum[58]

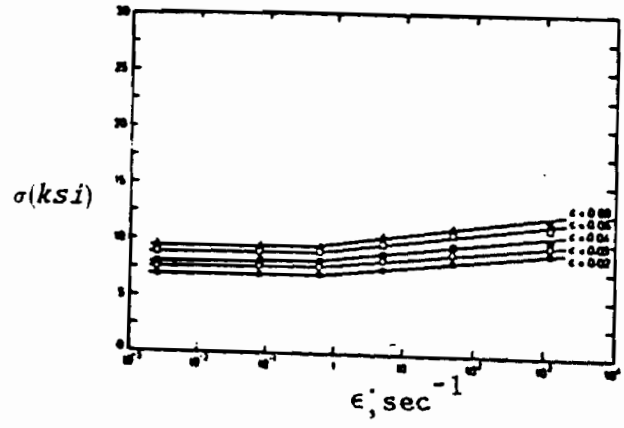

Fig. 2.33 Strain and Strain-Rate Dependence of the Flow Stress of Aluminum 1060-O[58]

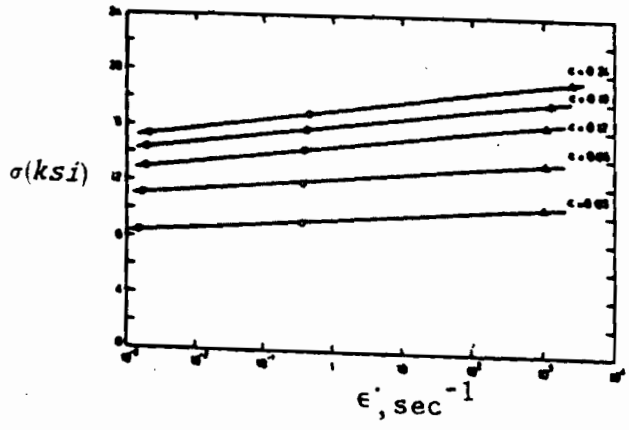

Fig. 2.34 Strain and Strain-Rate Dependence of the Flow Stress of Aluminum 1100-O[58]

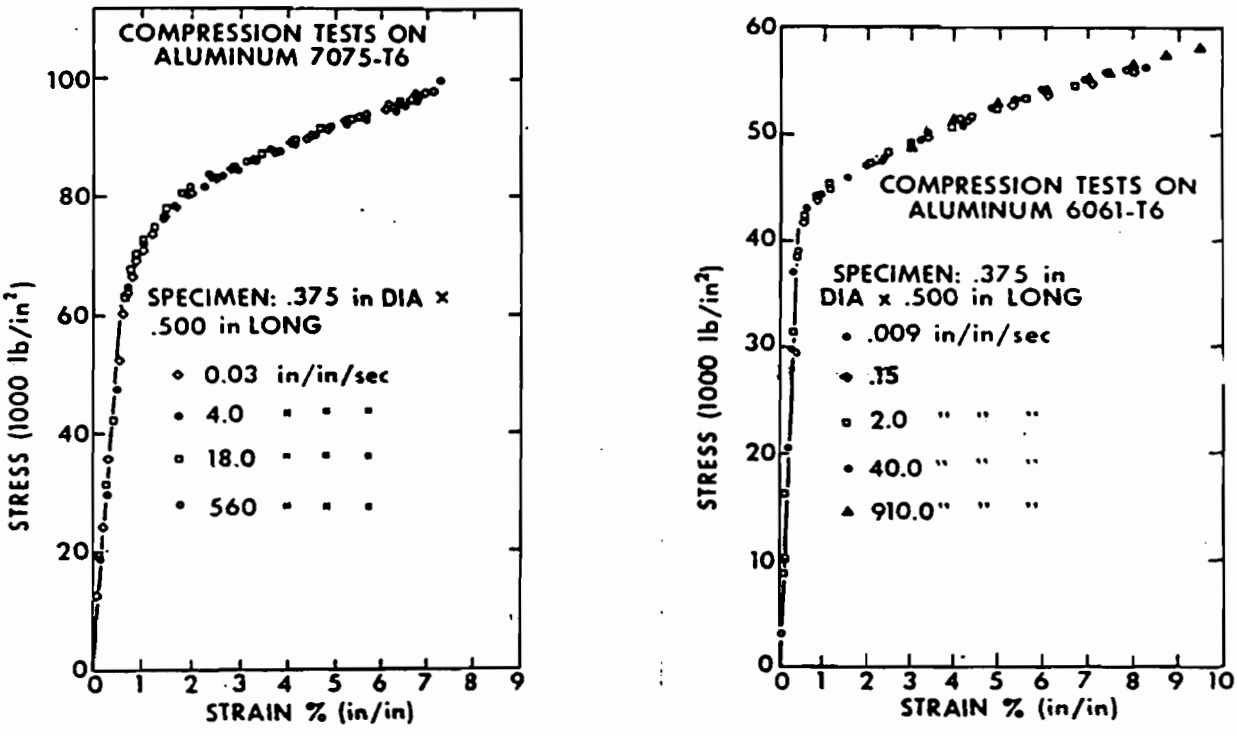

Fig. 2.35 Compression Tests on Aluminums 7075-T6 and 6061-T6[60]

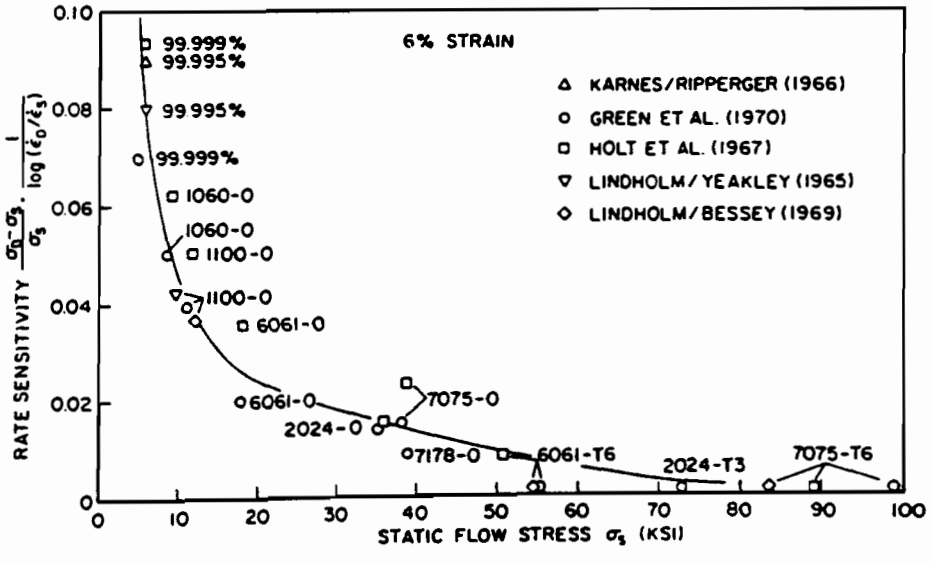

Fig. 2.36 Strain-Rate Sensitivity of Aluminum Alloys[33]

loading can affect the flow stresses at a given strain and strain rate. A number of investigators have examined the loading history to determine its contribution to the mechanical behavior characteristics. A technique that has achieved popularity over the last decade is the jump test or more properly the incremental strain-rate test, for which a specimen is subjected to a slow rate of loading followed by a very high loading rate[33].

Incremental as well as interrupted (prestrained) tests are most useful tools for the study of strain-rate history effects in metal, especially if the change in strain-rate covers several orders of magnitude, say from quasi-static to dynamic or vice versa, in order to submit the material in question to the most critical and demanding conditions[61].

The early experiments involved with dynamic strain rates and intended for a study of strain-rate history are those of Lindholm[59]. Figures 2.37 to 2.39[59] show Lindholm's results for cyclic loading of aluminum. It is evident that the stress in dynamic tests following a static pre-loading is not equal to the stress found at the same strain in all dynamic loading (as shown by the dotted line) . This difference is due to strain rate history. In addition, Lindholm wondered if the result was influenced by the dwell-time at zero load . To investigate this question he loaded a specimen dynamically to 8 percent strain, unloaded, and then reloaded dynamically . The result, as shown in Fig. 2.39, shows a history effect for a dwell-time of three minutes, while for a dwell-time of 450 micro seconds none can be seen.

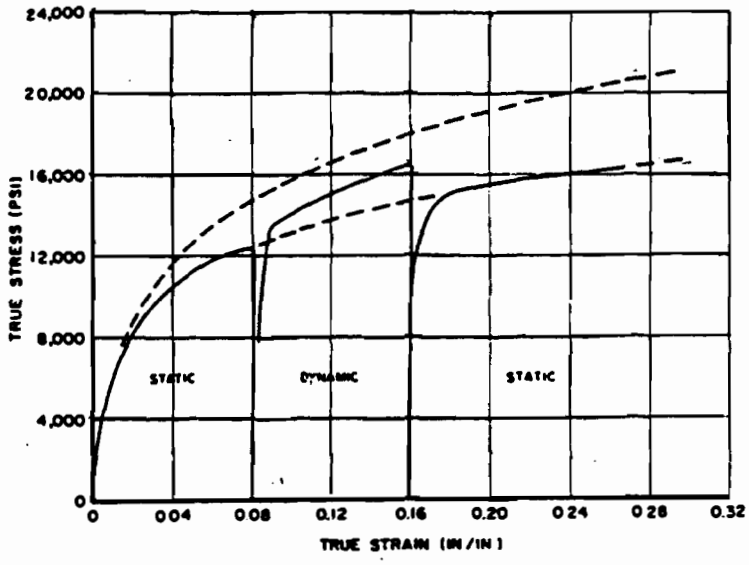

Fig. 2.37 Cyclic Static-Dynamic-Static Loading for Aluminum[59]

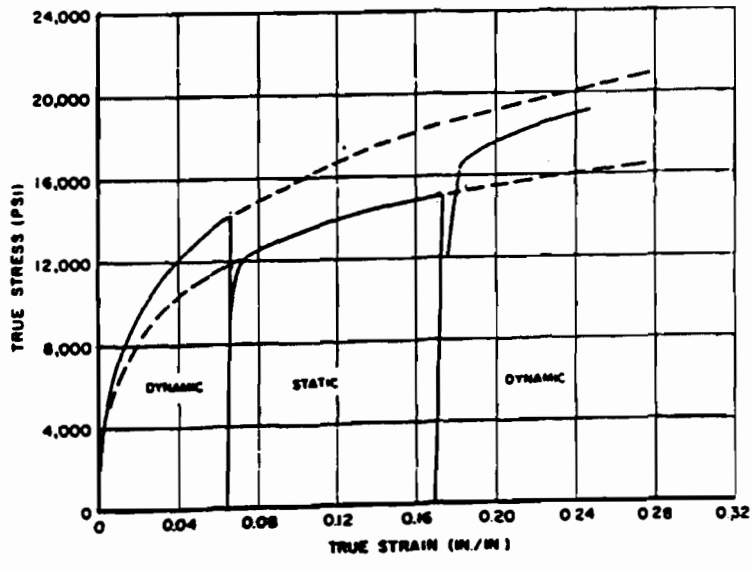

Fig. 2.38 Cyclic Dynamic-Static-Dynamic Loading for Aluminum[59]

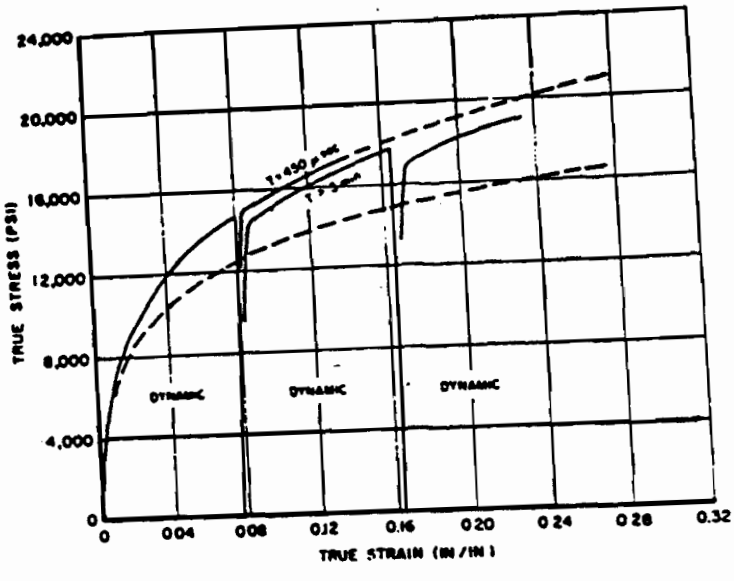

Fig. 2.39 Cyclic Dynamic Loading for Aluminum[59]

Sirakashi and Usui[62] tested three materials over a large range of temperatures. Jumps in strain rate were made from 10^{-3} sec^{-1} to four different dynamic strain rates. Figures 2.40 and 2.41[62] show the effect of alteration of strain rate upon the flow stress. In Fig. 2.40, point A_o is reached with a constant strain rate of 10^{-3} sec^{-1}. The strain rate is then changed to 10^{3} sec^{-1}. Two dotted curves in the figure are stress strain curves with a constant strain rate. It may be seen in the figure that the flow stress does not reach the value at point A_2, which lies on the dotted curves with constant strain rate of 10^{3} sec^{-1}, in spite of the alteration of strain rate. The same situation may be seen in Fig. 2.41, where the strain rate is changed from 10^{3} sec^{-1} to 10^{-3} sec^{-1} at point B_o. These results clearly show that the history of strain rate is another factor which has an effect upon the flow stress. In other words, the flow stress will be different depending upon the strain rate history, which the material has experienced, even if strain, strain rate and temperature are all the same at the moment considered. The effect of strain rate history may be attributed to the "memory" of strain rate which has been stored in the material, probably as a change in structure.

The most extensive series of jump tests is probably that of Eleiche and Campbell conducted in 1976[63]. These investigators tested copper, titanium and mild steel. The tests were performed over a range of temperatures and strains up to 60% in shear. They concluded that copper is sensitive to strain rate history, while titanium and steel are less sensitive to history, but more sensitive to direct effects of strain rate

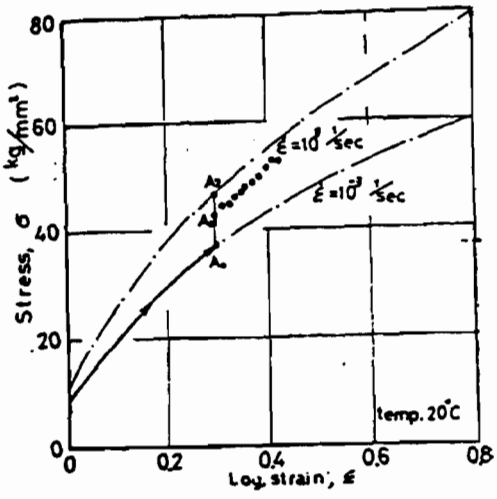

Fig. 2.40 Effect of Alteration of Strain Rate Upon Flow Stress (Static-Dynamic)[62]

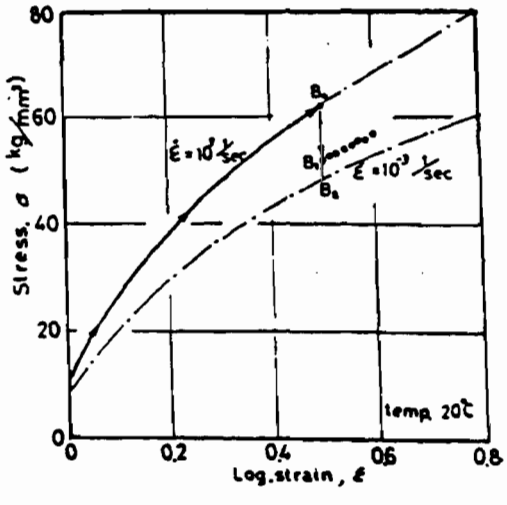

Fig. 2.41 Effect of Alteration of Strain Rate Upon Flow Stress (Dynamic-Static)[62]

Jump tests to higher strain rates using 1020 hot rolled steel and 1080 cold rolled steel were performed by Wilson et al[64] in 1979. See Figures 2.42 and 2.43[64]. Both steels, 1020 hot rolled steel, and 1080 colled rolled steel show a strong strain rate sensitivity and insensitivity to strain rate history.

A recent experimental study of the strain rate history effect on the tensile strength of AISI type 316 stainless steel using interrupted testing was conducted by Eleiche, Albertini, and Montagnani[61] in 1985. True stress-true strain curves resulting from their interrupted testing accompanied by a strain rate change from 0.004 to 500 sec^{-1} at various values of strain are presented in Fig. 2.44[61]. Also plotted are curves showing the variation of the temperature rise in each specimen during the corresponding dynamic deformation. The investigated prestrain range was from 0.0047 in./in to 0.3048 in./in. It can be seen from this figure that a well-defined yield point exists whose level is much higher than that reached in the quasi-static prestraining. For small prestrains, this yield stress level is very close to the flow stress level reached at the same strain in a test conducted entirely at the dynamic rate (curve B in Fig. 2.44). The conclusion of this study was that even though stainless steel is known to be strain-rate sensitive, it has been shown that it is insensitive to strain-rate history, within the range of strain rate covered in the tests and at ambient temperature.

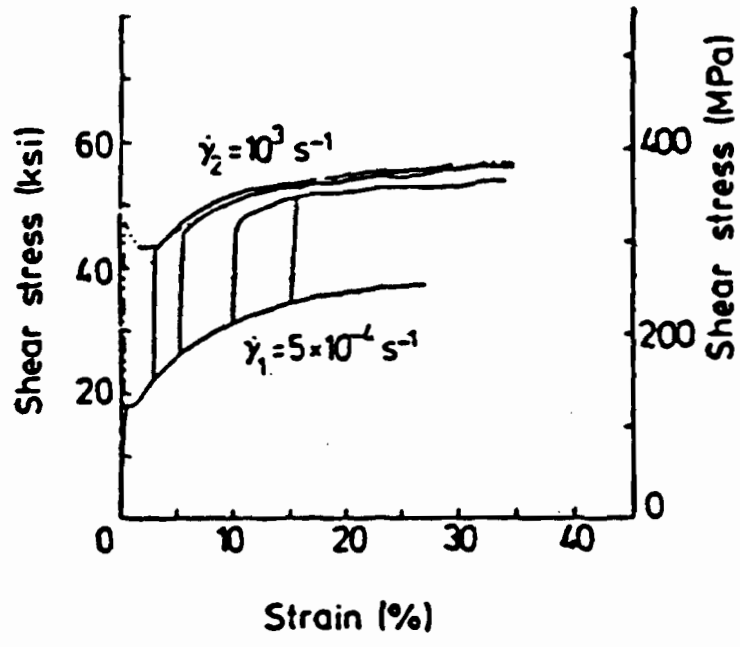

Fig. 2.42 Results of Constant and Incremental Strain-Rate Tests on 1020 Hot Rolled Steel (HRS)[64]

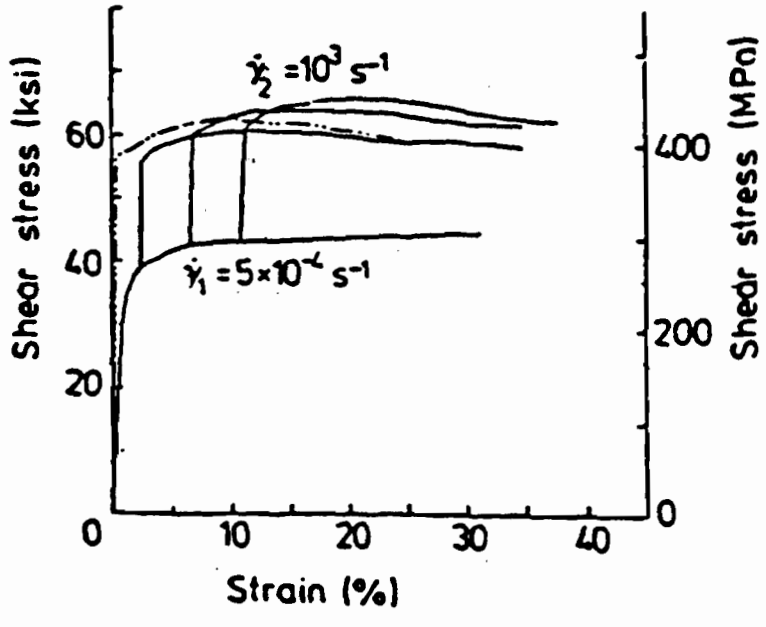

Fig. 2.43 Results of Constant and Incremental Strain-Rate Tests on 1080 Cold Rolled Steel (CRS)[64]

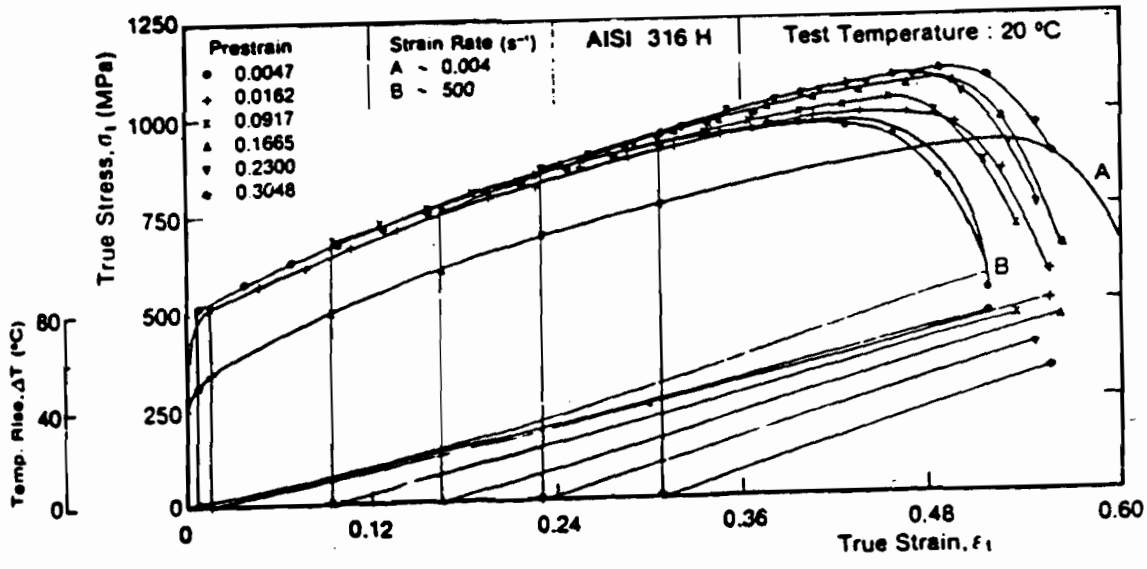

Fig. 2.44 Tensile True Stress-True Strain Curves at Ambient Temperature for Monotonic Loading to Fracture at a Strain Rate of 0.004 sec^{-1} (Curve A) and 500 sec^{-1} (Curve B), and for Quasi Static Prestraining Followed by Dynamic Reloading to Fracture[61]

C. STRUCTURAL MEMBERS

This part of the literature survey covers both theoretical and experimental work for the following two major subjects:

1. The structural behavior of stiffened and unstiffened compression elements under static loads presented in Section II.C.1.

2. The response of structural members to dynamic loads discussed in Section II.C.2 which focuses on those cases related to flexural and axially loaded members for the purpose of studying the effect of strain rate due to dynamic loads on the structural strengths of these members.

1. Structural Behavior of Compression Elements Under Static Loads. The analytical solutions of the elastic local buckling strengths of both stiffened and unstiffened compression elements are presented in Section II.C.1.a. The buckling stress in the inelastic range is discussed in Section II.C.1.b. In Section II.C.1.c, the theoretical background of the postbuckling behavior of rectangular stiffened and unstiffened compression elements is briefly reviewed. The development of effective width formulas for the prediction of the maximum strength of stiffened and unstiffened compression elements is presented in Section II.C.1.d. Also presented in this section are the effective width formulas used in the current AISI Cold Formed Steel Design Manual[65] and AISI Automotive Design Manual.[22]

a. Elastic Local Buckling of Flat Compression Elements. The elastic local buckling behavior of thin elements is governed by a differential

equation based on the small deflection theory of plates. The analytical solution for the critical buckling stress of plates is available from solving the differential equation by using the energy method.[66,67] Timoshenko[66] has presented a series of solutions of plate buckling for several different types of compression elements, considering various boundary conditions. Figure 2.45 shows different sructural members with stiffened and unstiffened compression elements.

The methods of determining the critical buckling stresses of compression elements are summarized in Sections II.C.1.a.i and II.C.1.a.ii for stiffened and unstiffened elements, respectively.

i) Stiffened Elements. The critical buckling stress of compression elements can be determined by solving the following differential equation. This equation was originally derived by Saint Venant in 1883.[68]

$$\frac{\partial^4\omega}{\partial x^4} + 2\frac{\partial^4\omega}{\partial x^2\partial y^2} + \frac{\partial^4\omega}{\partial y^4} = \frac{1}{D}\left[q + f_x t\frac{\partial^2\omega}{\partial x^2} + f_y t\frac{\partial^2\omega}{\partial y^2} + 2\tau_{xy}t\frac{\partial^2\omega}{\partial x\partial y}\right] \qquad (2.19)$$

where ω = lateral deflection of the plate

q = lateral uniform load applied to the plate

t = thickness of the plate

$D = Et^3/(12(1-\mu^2))$

E = modulus of elasticity

μ = Poisson's ratio = 0.3 for steel

f_x, f_y = stress components normal to the edges of the plate and

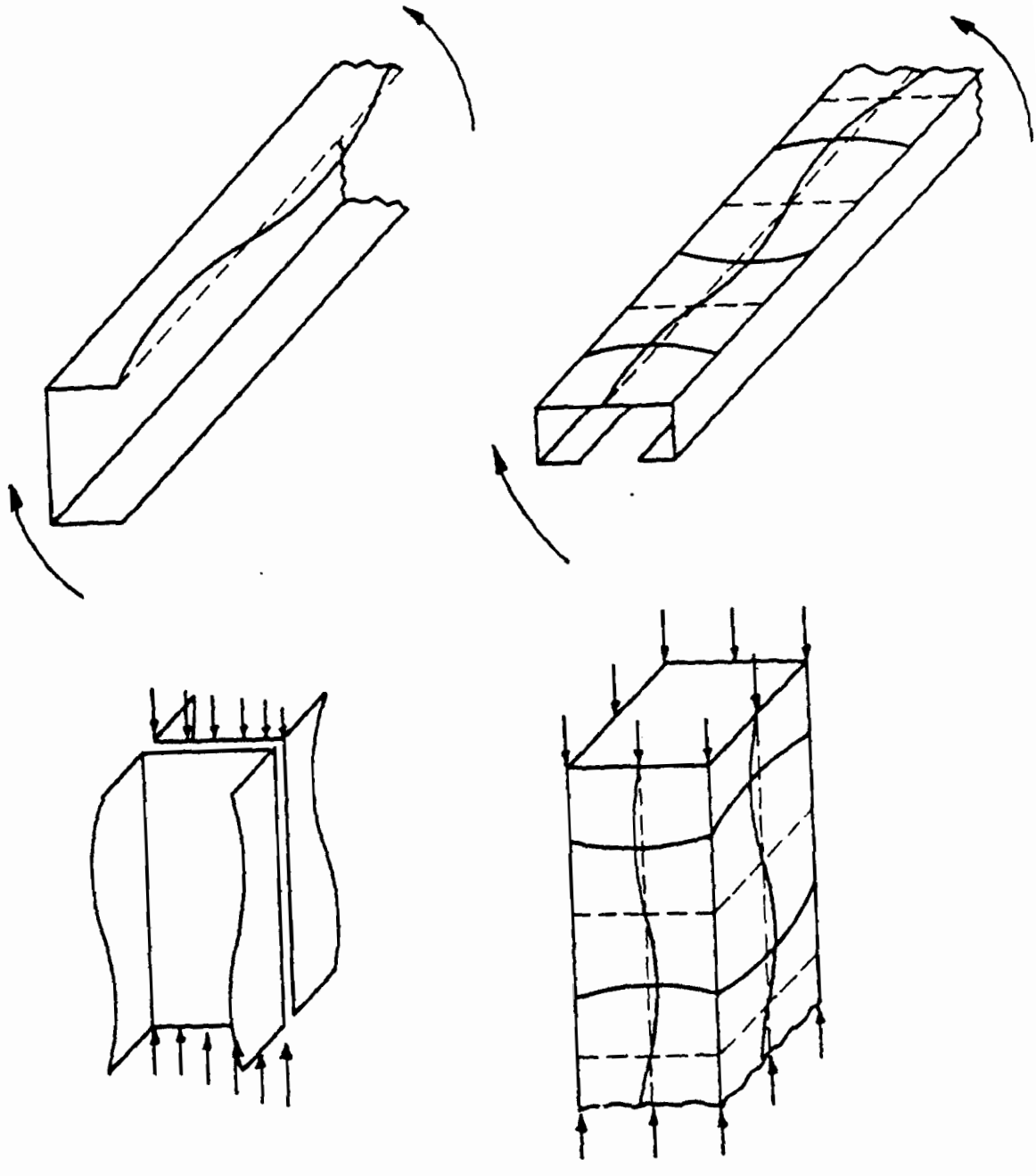

(a) Members with Unstiffened Compression Elements

(b) Members with Stiffened Compression Elements

Fig. 2.45 Structural Members with Stiffened and Unstiffened Elements[26]

lying in the x-y plane

τ_{xy} = shear stress component on the edges of the plate in the x-z and y-z plane

The solution of Eq. 2.19 for a rectangular plate simply supported on four edges, as shown in Fig. 2.46, is given in Eq. 2.20.

$$f_{cr} = \frac{k\pi^2 E}{12(1-\mu^2)(w/t)^2} \quad (2.20)$$

The value of k, as shown in Fig. 2.47, depends on the magnitude of the aspect ratio (a/w) of the plate and the number of half sine waves in the direction of compression. In Fig. 2.47, it is noted that the value of k is equal to four for a square plate and for any plate with an aspect ratio equal to an integer. In addition, for a long plate with an aspect ratio larger than four, the value of k approaches to four. Therefore, a minimum value of k equal to four is conservatively used in practical design without considering the rotational restraint along the unloaded edges.

ii) Unstiffened Elements. The same governing Equation (2.20) can also be used for unstiffened plates, as shown in Fig. 2.48, which are simply supported on three edges and the other edge free. Solving Eq. (2.20) by satisfying the unstiffened plate boundary conditions, one can obtain the following expression for the critical buckling stress of unstiffened compression elements in which the buckled plate has only one

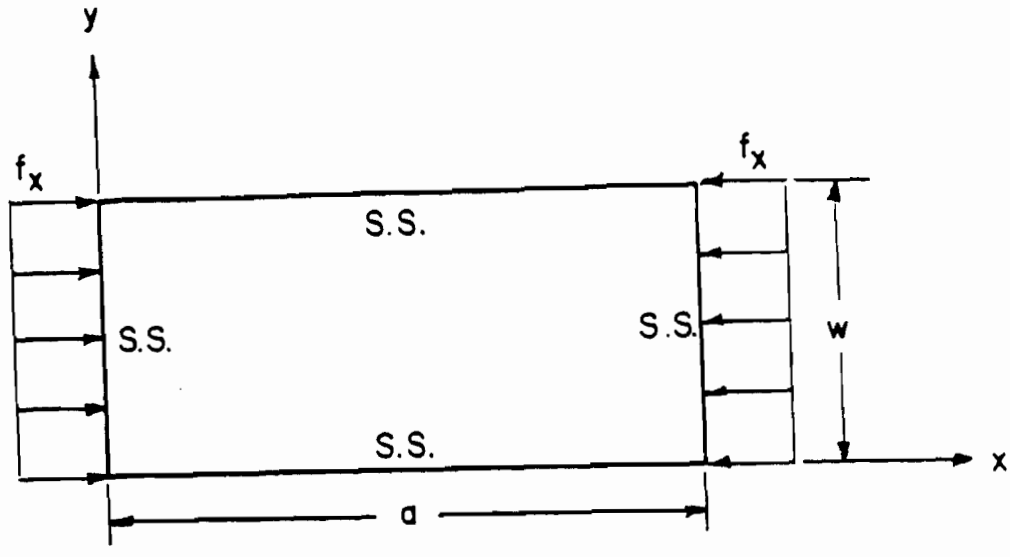

Figure 2.46 Rectangular Plate Simply Supported on Four Edges and Under Uniform Compression Stress [117]

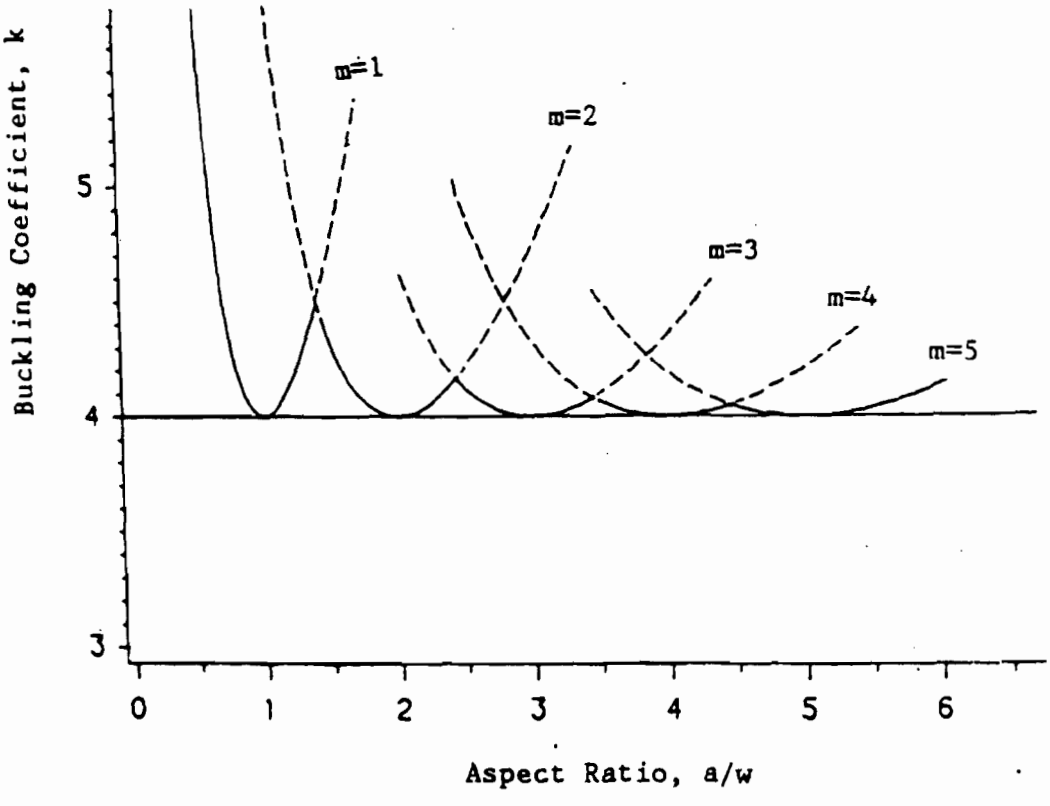

Figure 2.47 Buckling Coefficients for Flat Rectangular Stiffened Plates [117]

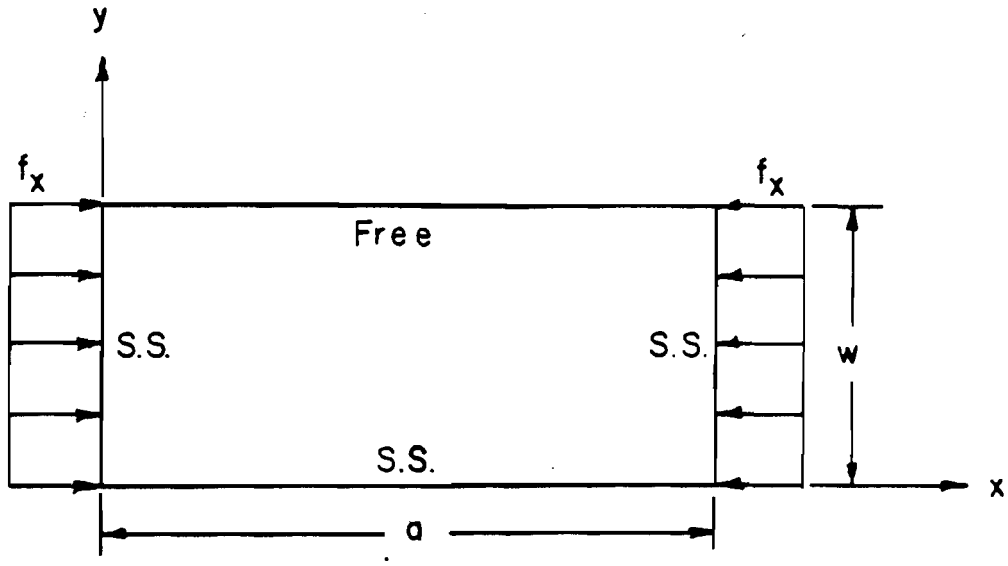

Figure 2.48 Rectangular Plate Simply Supported on Three Edges and Under Uniform Compression Stress[117]

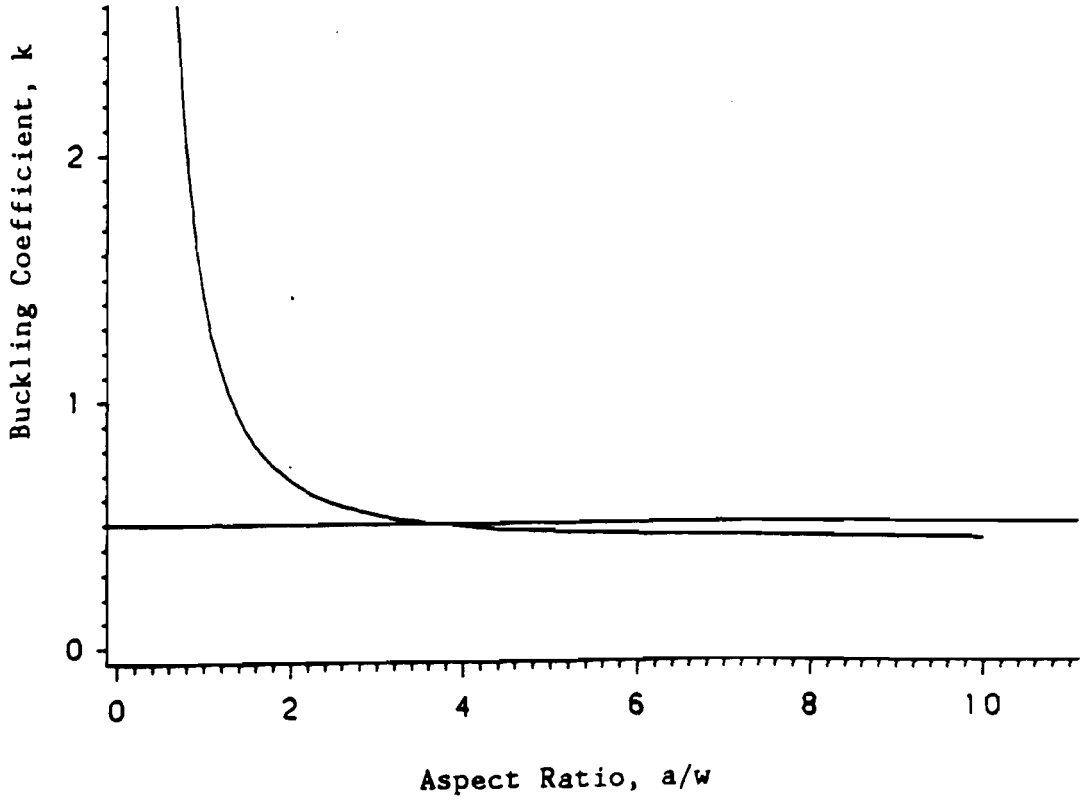

Figure 2.49 Buckling Coefficients for Flat Rectangular Unstiffened Plates[117]

half sine wave in the direction of compression regardless of the length of plate

$$f_{cr} = \frac{k\pi^2 D}{tw^2} \qquad (2.21)$$

in which k is a numerical factor depending on the magnitude of the ratio of a/w. An approximate solution based on an energy method has been presented by both Timoshenko[66] and Bulson[67]. The buckling coefficient was found to be

$$k = \left(\frac{w}{a}\right)^2 + 6\frac{1-\mu}{\pi^2} . \qquad (2.22)$$

Figure 2.49 shows the relationship between buckling coefficient and aspect ratio of the rectangular unstiffened plate. Reference 67 indicates that the approximate solution is close to the exact solution. Figure 2.49 also shows that the value of k approaches a constant value of 0.425 as the aspect ratio of the plate approaches infinity. Poisson's ratio μ is equal to 0.3.

b. Inelastic Buckling of Flat Compression Elements. A plate may buckle at a stress level beyond the proportional limit of the steel when the flat width-to-thickness (w/t) ratio is small. The plate becomes an anisotropic plate when it buckles in the inelastic range. The analytical

study of local buckling in the inelastic range is complicated because of the anisotropic nature of the material. However, analytical investigations of plates that buckled in the inelastic range have been considered by numerous researchers.[69-73] A brief discussion of plate buckling in the inelastic range is presented in this section.

In 1924, Bleich[69] extended the theory of flat plate stability into the inelastic range by considering the plate as an anisotropic type and by introducing a reduced modulus into Eq. (2.20). He assumed that the reduced modulus is effective only for strips of a plate in the direction of the compressive stress, whereas the elastic modulus remains valid for strips in the direction perpendicular to the compression stress.

The following equation for the buckling stress in the inelastic range is in terms of the elastic buckling stress $(f_{cr})_e$ and the plasticity reduction factor, η.

$$(f_{cr})_{in} = \eta (f_{cr})_e = \frac{\eta k \pi^2 E}{12(1-\mu^2)(w/t)^2} \qquad (2.23)$$

In Eq. (2.23), $\eta = \sqrt{E_t/E}$, which is the plasticity reduction factor for a simply supported plate subjected to uniform compressive stresses in one direction.

c. Post-Buckling Behavior of Flat Compression Elements. Some one-dimensional structural members, such as columns, normally fail at or

slightly below the theoretical critical buckling load. However, compression flanges of thin-walled structural members, with relatively large w/t ratios as shown in Fig. 2.45, can continue to carry increasing loads after the onset of local buckling of the compression elements. This phenomenon is well-known as the post-buckling strength of a plate.

The deflected shape of a stiffened compression element in the post-buckling range can be visualized from a grid model as shown in Fig. 2.50. The transverse bars, which are anchored at the sides of the grid, act as tie rods to support the deflection of the longitudinal struts. This means that the membrane stresses developed in the transverse direction in the real stiffened plate act as hoop stresses, which restrain the lateral displacements caused by the longitudinal load.

Because of the transverse membrane stresses and the resulting redistribution of stress occurring in the plate, additional load may be carried by the plate after the critical buckling load is reached. In a stiffened plate, the stress distribution is uniform prior to its buckling as shown in Fig. 2.51(a). After buckling, the stress distribution is nonuniform while the load continues to increase as shown in Fig. 2.51(b). The redistribution of stress will continue until the stress at the supported edges reaches the yield stress of the steel. Failure normally occurs when the edge stress reaches the yield point of the material as shown in Fig. 2.51(c).

Because the membrane stresses are developed in the transverse direction and because the deflection of the plate is usually much larger than its thickness after buckling, small deflection theory of plate

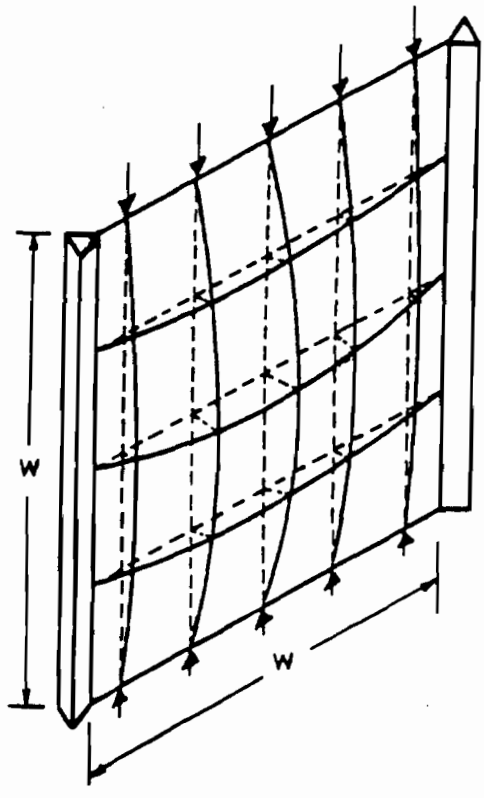

Fig. 2.50 Strut and Bar Grid Model Simply Supported Along Its Edges and Subjected to End Loading[26]

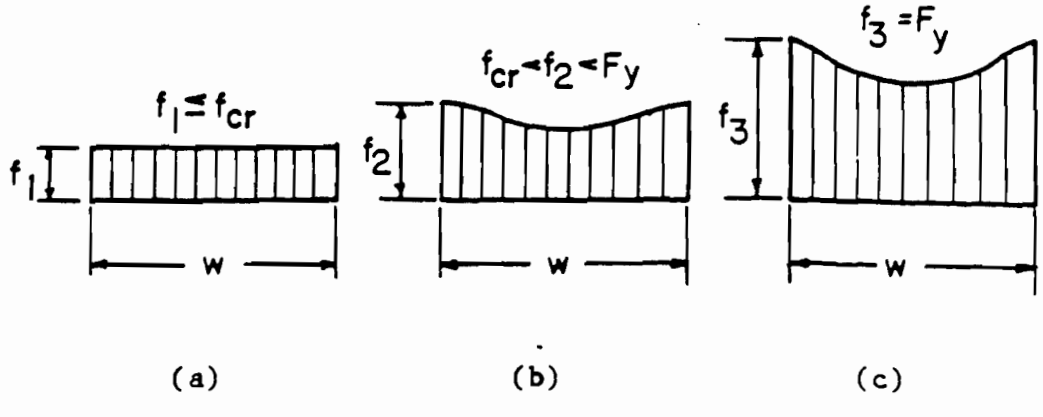

Fig. 2.51 Consecutive Stages of Stress Distribution in Stiffened Compression Elements [26]

bending, which was used to derive the critical local buckling stress of plates, can not be applied for the post-buckling range. For these reasons, the large deflection theory of plates is used for the analysis of plates in the post-buckling range.

In 1910,[74] von Karman developed large deflection equations for plates in the post-buckling range by taking the membrane stresses into account. The differential equation is given by Timoshenko in the following form:[66]

$$\frac{\partial^4 \omega}{\partial x^4} + 2\frac{\partial^4 \omega}{\partial x^2 \partial y^2} + \frac{\partial^4 \omega}{\partial y^4} = \frac{t}{D}\left[\frac{\partial^2 F}{\partial y^2}\frac{\partial^2 \omega}{\partial x^2} - 2\frac{\partial^2 F}{\partial x \partial y}\frac{\partial^2 \omega}{\partial x \partial y} + \frac{\partial^2 F}{\partial x^2}\frac{\partial^2 \omega}{\partial y^2}\right] \quad (2.24)$$

where F is a stress function. The median fiber stresses are defined as follows:

$$f_x = \frac{\partial^2 F}{\partial y^2}, \qquad f_y = \frac{\partial^2 F}{\partial x^2}, \qquad \tau_{xy} = -\frac{\partial^2 F}{\partial x \partial y} \quad (2.25)$$

This equation has been used by many researchers to study the post-buckling behavior of square plates. The exact solution for Eq. (2.24) is very difficult because this equation is a fourth order, nonlinear differential equation. Approximate solutions for the differential equation have been proposed by Schnadel,[75] Timoshenko,[66] Cox,[76] Marguerre,[77] and Levy.[78] They used the energy method and assumed

a wave form of the deflected plate to study the post-buckling behavior of the plate.

An approximate solution of the differential equation based on the large deflection theory was found to be too difficult for use in practical design because of its complexity. Therefore, the effective width design formulas are currently empirical in nature. In the past, the effective width concept has been successfully used for the prediction of post-buckling strengths of stiffened and unstiffened compression elements. The development of Winter's formulas is reviewed in the following section.

d. Development of Effective Width Formulas. In 1932,[79] von Karman introduced a concept of "Effective Width" to determine the ultimate strength of thin metal sheets in aeronautical structures. In his approach, it was assumed that the entire load is carried by two effective strips with a uniformly distributed stress equal to the edge stress, f_{max}, as shown in Fig. 2.52, instead of using the full width of the compression element with actual, nonuniform stress distribution.

To extend the use of the effective width formula for practical design of plates with small w/t ratios and for stress levels lower than the yield point, in the 1940s Winter[80-82] performed extensive tests for the compression flanges of cold-formed steel sections at Cornell University. Based on his test results, Winter derived effective width formulas for the design of both stiffened and unstiffened compression elements under uniform compression as follows:

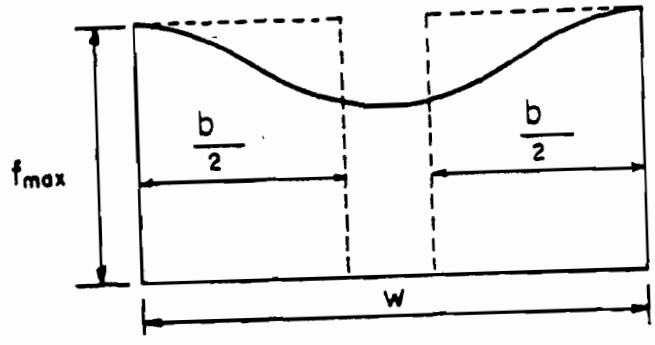

Fig. 2.52 Effective Design Width of a Stiffened Compression Element [26]

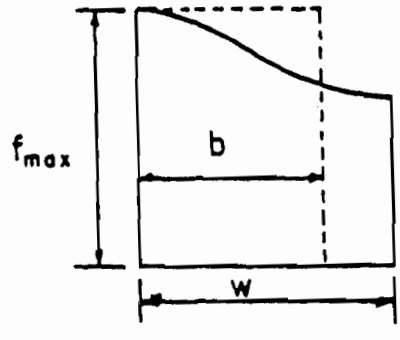

Fig. 2.53 Effective Design Width of an Unstiffened Compression Element [26]

(1) Stiffened Elements:

$$b = 1.9t\sqrt{\frac{E}{f_{max}}}\left[1 - 0.475\left(\frac{t}{w}\right)\sqrt{\frac{E}{f_{max}}}\right] \qquad (2.26)$$

or

$$b = \left[\sqrt{\frac{f_{cr}}{f_{max}}}\left(1 - 0.25\sqrt{\frac{f_{cr}}{f_{max}}}\right)\right]w \ . \qquad (2.27)$$

This equation is similar to von Karmam's equation given in Reference 77 with the addition of an empirical correction factor which accounts for the effect of initial imperfections of compression elements. The correction factor is

$$1 - 0.475\left(\frac{t}{w}\right)\sqrt{\frac{E}{f_{max}}} \ . \qquad (2.28)$$

(2) Unstiffened Elements:

$$b = 0.8t\sqrt{\frac{E}{f_{max}}}\left[1 - 0.202\left(\frac{t}{w}\right)\sqrt{\frac{E}{f_{max}}}\right] \ . \qquad (2.29)$$

The effective width of unstiffened compression elements can be calculated from Eq. (2.29), in which the post-buckling strength of unstiffened elements is considered. In this approach, the entire load is assumed to be carried by an effective strip with a uniformly distributed stress equal to the edge stress, f_{max}, as shown in Fig. 2.53, instead of using the full width of the compression element with a varying stress distribution. Additional research conducted by Kalyanaraman[83-85] at Cornell University has shown good agreement with Eq. (2.37).

It is noted that Eqs. (2.26) and (2.29) depend not only on the edge stresses but also on the w/t ratio. Because the maximum edge stress, f_{max}, was introduced for F_y, these two equations can be applied to any range of stress levels.

The effective width approach has been used for the design of stiffened compression elements since 1946, whereas the reduced allowable stress method was used for the design of unstiffened compression elements until the AISI Specification was revised in 1986.

Equation (2.26) was used for the design of cold-formed steel structural members until 1968. Based on the accumulated design experience with a restudy of original and additional test results, the following less conservative and more accurate equation was recommended for determination of the effective width, b, of stiffened compression elements

$$b = 1.9t\sqrt{\frac{E}{f_{max}}}\left[1 - 0.415\left(\frac{t}{w}\right)\sqrt{\frac{E}{f_{max}}}\right] \qquad (2.30)$$

or

$$b = \left[\sqrt{\frac{f_{cr}}{f_{max}}} \left(1 - 0.22 \sqrt{\frac{f_{cr}}{f_{max}}} \right) \right] w \ . \qquad (2.31)$$

Equation (2.30) has been used in the AISI Specification[86] since 1968 and maintained in the 1980 AISI Specification[87]. Based on the research conducted by Pekoz[88], a different format of the effective width formula, which is based on Eq. (2.31), is used in the 1986 AISI Design Manual[22]. The same effective width formula is also used in the current AISI Specification for unstiffened compression elements by specifying a different buckling coefficient.

In Sections B2.1 and B3.1 of the 1986 AISI Specification, the effective widths of stiffened and unstiffened compression elements can be determined by using the following equations:

(1) For Load Capacity Determination: The effective width b for computing the load-carrying capacity of uniformly compressed elements can be determined from the following formulas:

$$b = w \qquad \text{when} \quad \lambda \leq 0.673, \qquad (2.32)$$

$$b = \rho w \qquad \text{when} \quad \lambda > 0.673, \qquad (2.33)$$

where b = effective width of a compression element

w = flat width of a compression element

$$\rho = (1 - 0.22/\lambda)/\lambda \quad . \tag{2.34}$$

λ is a slenderness factor determined as follows:

$$\lambda = \frac{1.052}{\sqrt{k}} \left(\frac{w}{t}\right)\left(\sqrt{\frac{f}{E}}\right) \tag{2.35}$$

where f = the edge stress

E = modulus of elasticity, 29500 ksi

k = plate buckling coefficient

= 4 for stiffened elements supported by a web on each longitudinal edge

= 0.43 for unstiffened elements supported by a web on a longitudinal edge and free on the other.

(2) For Deflection Determination: The effective widths b_d in computing deflections shall be determined from the following formulas:

$$b_d = w \qquad \text{when} \qquad \lambda \leq 0.673, \tag{2.36}$$

$$b_d = \rho w \qquad \text{when} \qquad \lambda > 0.673, \tag{2.37}$$

where w = flat width of a compression element

ρ = reduction factor determined by either of the following two procedures:

(1) Procedure I.

A low estimate of the effective width may be obtained from Eqs. (2.34) and (2.35) where f_d is substituted for f and defined as the computed compressive stress in the element being considered (calculations are based on the effective section at the load for which deflections are determined).

(2) Procedure II.

For stiffened elements supported by a web on each longitudinal edge an improved estimate of the effective width can be obtained by calculating ρ as follows:

$$\rho = 1 \qquad \text{when} \quad \lambda \leq 0.673 \qquad (2.38)$$

$$\rho = (1.358 - 0.461/\lambda)/\lambda \qquad \text{when} \quad 0.673 < \lambda < \lambda_c \qquad (2.39)$$

$$\rho = (0.41 + 0.59\sqrt{F_y/f} - 0.22/\lambda)/\lambda \qquad \text{when} \quad \lambda \geq \lambda_c \qquad (2.40)$$

where $$\lambda_c = 0.256 + 0.328(w/t)(\sqrt{F_y/E}). \qquad (2.41)$$

and λ is as defined by Eq. (2.35) except that f_d is substituted for f.

For the uniformly compressed unstiffened elements, the effective widths used in computing deflections shall be determined in accordance with Procedure I except that f_d is substituted for f.

Based on the extensive research work sponsored by the American Iron and Steel Institute, the effective width approach was extended in the 1986 AISI Specification for the design of beam webs and stiffened elements with stress gradient, perforated elements, and elements with edge stiffeners or intermediate stiffeners. Detailed information on the effective width formulas used for these types of elements can be found in Ref. 65.

The effective width formulas (Eq. 2.32 through 2.35) are also presented in Sections 3.1.2.1(a) and (b) of the AISI Automotive Steel Design Manual[22] for steels with yield strengths up to 80 ksi. These equations calculate the effective widths of fully stiffened and unstiffened compression elements based on the effective width formulas used in the 1986 AISI Specification. Also included in these sections are the effective width formulas for steels with yield strengths higher than 80 ksi (84 to 153 ksi) based on the recent research conducted by Pan at University of Missouri-Rolla in 1988.[21] In addition, Sections 3.1.2.3 and 3.1.2.4 of the Automotive Design Manual discuss the effective width formulas for sections having 1) curved plate elements, and 2) curved and straight plate elements, respectively. The latter formulas were based on Parks and Yu's research findings.[19]

2. Response of Structural Members to Dynamic Loads. It has been a general practice for the structural designer to increase the live load for the effect of dynamic loading and to assume that the properties of the material he employs are unaffected by the nature of the loading.

Developments in several separate fields has reached a point where proper analysis of structural behavior under impact overload conditions could take place. The understanding of material properties under static and dynamic loading has been developed to the stage where dynamic stress-strain curves can be produced for common engineering materials. The instrumentation used in the dynamic tests has been developed to a degree that accurate studies can be made of high speed effects without the introduction of significant errors from the instrumentation itself. The digital computers provide a facility for studying systems too tedious or intractable to attempt by manual means.[89]

In this section, some of the developments used in the past research for the response of structures to dynamic overloads are reviewed. Particular attention has been directed to those items related to beams, and columns.

a. Flexural Members. Flexural members subject to impact loading have been the subject of investigation, especially during the last three decades. In this section, some of these investigations will be summarized in chronological order.

In 1958, Parkes[90] studied encastre beams with impact loading applied transversely at any point on their span. One of the main objectives of his work was to evaluate the effect of material strain-rate sensitivity on the accuracy of the analysis. Test specimens were fabricated from mild steel, brass and duralumin. It was found that mild steel is the most sensitive to strain-rate as compared with the other two materials. The

correlation between theoretical and experimental results can be improved with taking the strain-rate sensitivity into account.

A developement of an analysis to determine the response of a simply-supported beam subject to a concentrated impact load at midspan was presented by Ezra[91] in 1958. He was actually attempting to develop a theory for comparison with the test results of Duwez and Clark.[92] His mathematical model allows the use of full-plastic moment, taking account of yield stress as affected by the strain-rate. The theoretical values show increasingly better agreements with the test results as the impact speed of the test increases. This indicates that the strain-rate sensitivity is a significant factor for the tests.

For small-scale cantilever beams with tip mass, two series of tests were performed by Bodner and Symonds[93] in 1962. In the first series, the base of the cantilever was impacted against a solid support, and in the second the tip mass was loaded either by an explosive charge, or being hit by a rifle bullet. Two materials were used for the specimens. They were mild steel and a less strain-rate sensitive aluminum alloy. Theoretical results were initially obtained from the use of a simple "rigid-plastic" theory. Comparisons between these results and the test results showed that any discrepancies between the two results were sensibly independent of the angle of rotation of the hinge at the fixed support. It was concluded that strain-rate sensitivity was the only significant factor causing error, as all other factors would be dependent on the rotation angle at the fixed support. To check this conclusion, an analysis including strain-rate effects gave good agreements with the

test results. An important point, that the authors made, is that the use of an overall percentage increase of yield atress may lead to errors in some situations.

In 1963, Rawlings[94] reported on an experimental investigation of strain-rate effects on yield loads for beam tests. He tested a series of simply supported mild-steel beams using a two-point loading system so that a plastic hinge could be formed in the central portion of the beam. All loads were applied by large falling masses. The force pulse applied to the beam was measured at the lever by electric-resistance strain-gages. Repeated tests were performed on beam specimens to investigate the behavior under different cycles of stress. Original specimens showed a marked upper yield peak for short duration, and a major amount of lower yield bending for long duration as shown in Fig. 2.54. The results for the relationship between lower yield value and the time taken to yield obtained from beam tests (Fig. 2.55) showed good agreement with the relationship obtained from material tests. The author concluded that the full plastic moment is independent of the method of loading.

Using the experimental results of Parkes, Ting[95] developed in 1965 a formula for cantilever beams loaded dynamically on the basis of rigid-plastic theory, which took into account large geometric changes. His results compare very favorably with Parkes' experimental results. He concluded that not all of the errors between the theory and experimental results can be attributed to strain-rate effects, as had been previously assumed. Ting was concerned primarily with the high-speed, low-mass loading causing travelling hinges. For high-mass, low-speed loading,

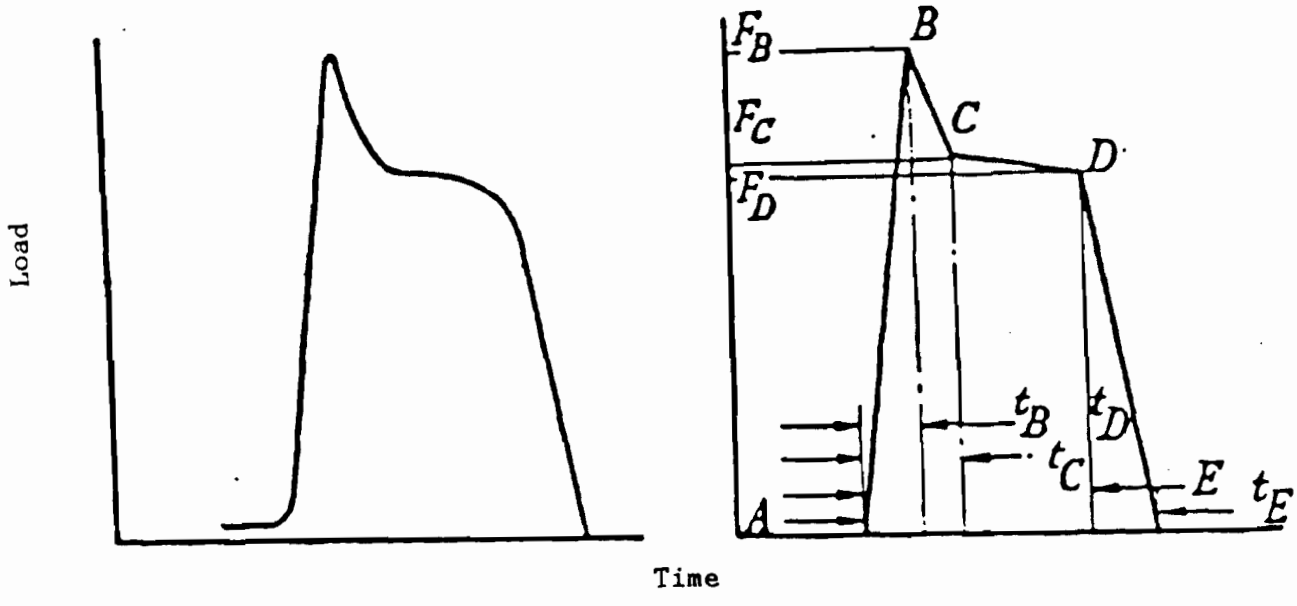

a) Typical Pulse

b) Assumed Shape

Fig. 2.54 Recorded Load Time Pulse[89]

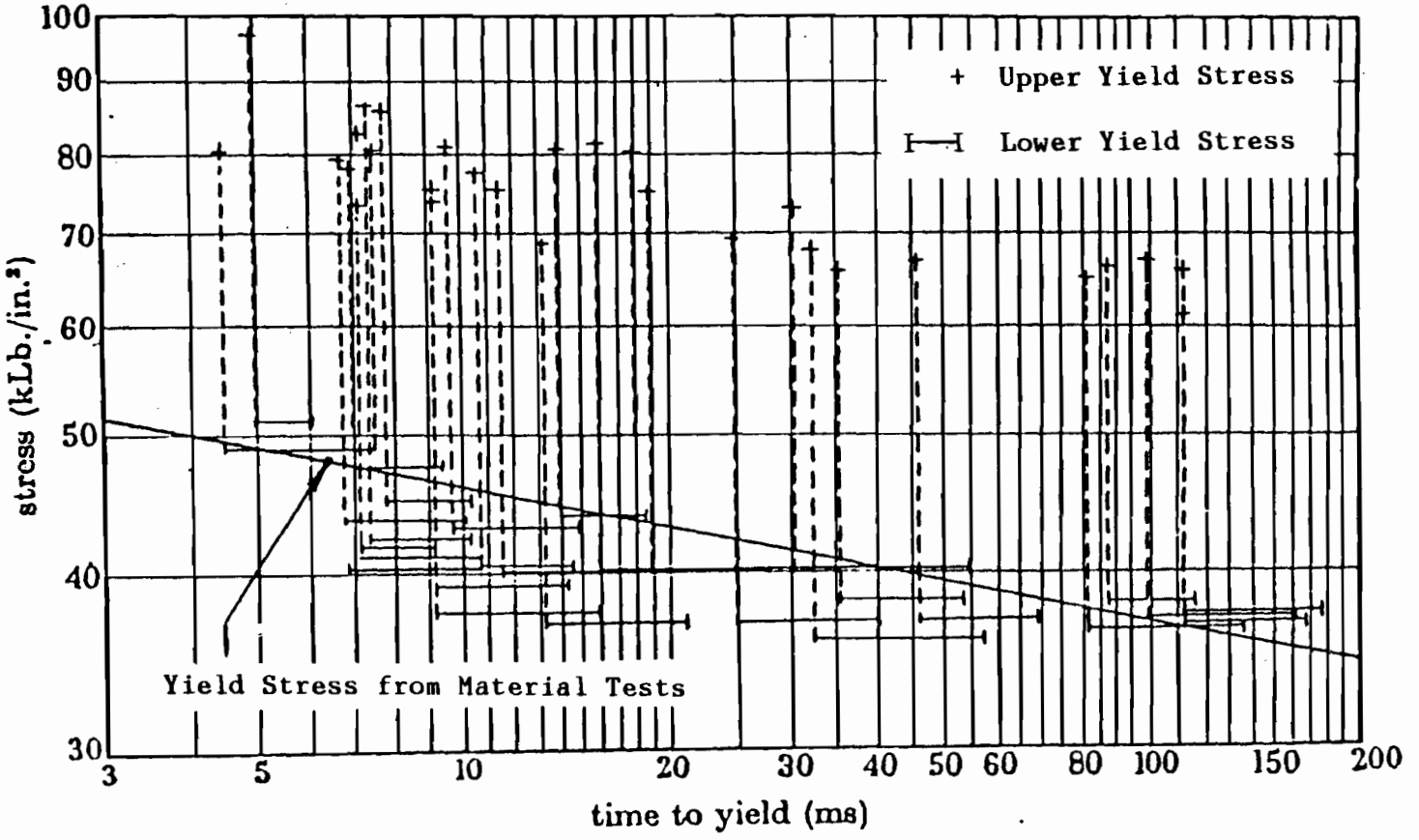

Fig. 2.55 Yield Stresses vs. Time to Yield [89]

that characteristically causes root hinges only, the strain-rate effects probably do cause almost all the errors in a simple rigid-plastic theory.. A verification of Ting 's research finding was given by Bodner[96] ,who tested cantilever specimens by detonating explosive charges which were attached to tip masses. Both cantilevers were attached to a pendulum to enable the impulse to be measured. Observation of final deformed shapes showed large root rotations, with little evidence of travelling hinges. On this basis, and using time-to-yield records from strain gages attached to the cantilever, a simple theory with an overall correction for strain-rate effects gave reasonable correlation with the test results.

Cowper and Symonds found that the following simple empirical expression with D = 40.4 in./in./sec., and p = 5, provides a reasonable estimate of dynamic yield stress recorded during many dynamic uniaxial tensile and compressive tests under constant strain rate for mild steel:[98]

$$\frac{\sigma}{\sigma_0} = 1 + \left(\frac{\dot{\varepsilon}}{D}\right)^{1/p} \qquad (2.42)$$

where σ = dynamic yield stress

σ_0 = static yield stress

$\dot{\varepsilon}$ = strain rate

D and p = material constants.

The above Cowper-Symonds constitutive relation and its derivative forms are used almost exclusively in theoretical and numerical studies on the

dynamic plastic behavior of structures made from strain-rate sensitive materials. The universal acceptance of this equation stems from the observation that analytical and numerical predictions agree remarkably well with experimental tests on beams.[98]

In 1966, Aspden and Campbell[99] were the first to conduct dynamic flexural tests in which transient records were taken of moment-rotation characteristics. They used small specimens 0.75 inches long by 0.375 inches wide by 0.125 inches thick, supported at their ends by beams, and loaded as a four point loading system by a falling weight. The bending moment transmitted to each specimen was measured by electric resistance strain gages mounted on the support beam and the strain-rate at surface of the specimen was determined by recording the velocity of the load frame using an inductive transducer. They compared their high speed flexural test results with those obtained under dynamic compression using a hydraulically operated machine, and with slow speed tests in an Instron machine. Moment-rotation curves obtained from double-beam oscilloscope traces of velocity and moment were corrected to take account of 1) the bending of the support beams, 2) zero errors, and 3) inertia effects caused by acceleration of the loading mechanism. Like Rawlings, Aspden and Campbell observed evidence of high initial peak moments of resistance. For the highest rate of strain in their beams, the dynamic 'upper yield moment' was about 80% higher than the corresponding moment in a low speed test. See Fig. 2.56 for the variation of upper and lower yield moments with strain-rate at surface of specimen. Aspden and Campbell noticed that after attaining the maximum peak moment of resistance, the value decreases below that would be predicted by integration of dynamic axial stresses

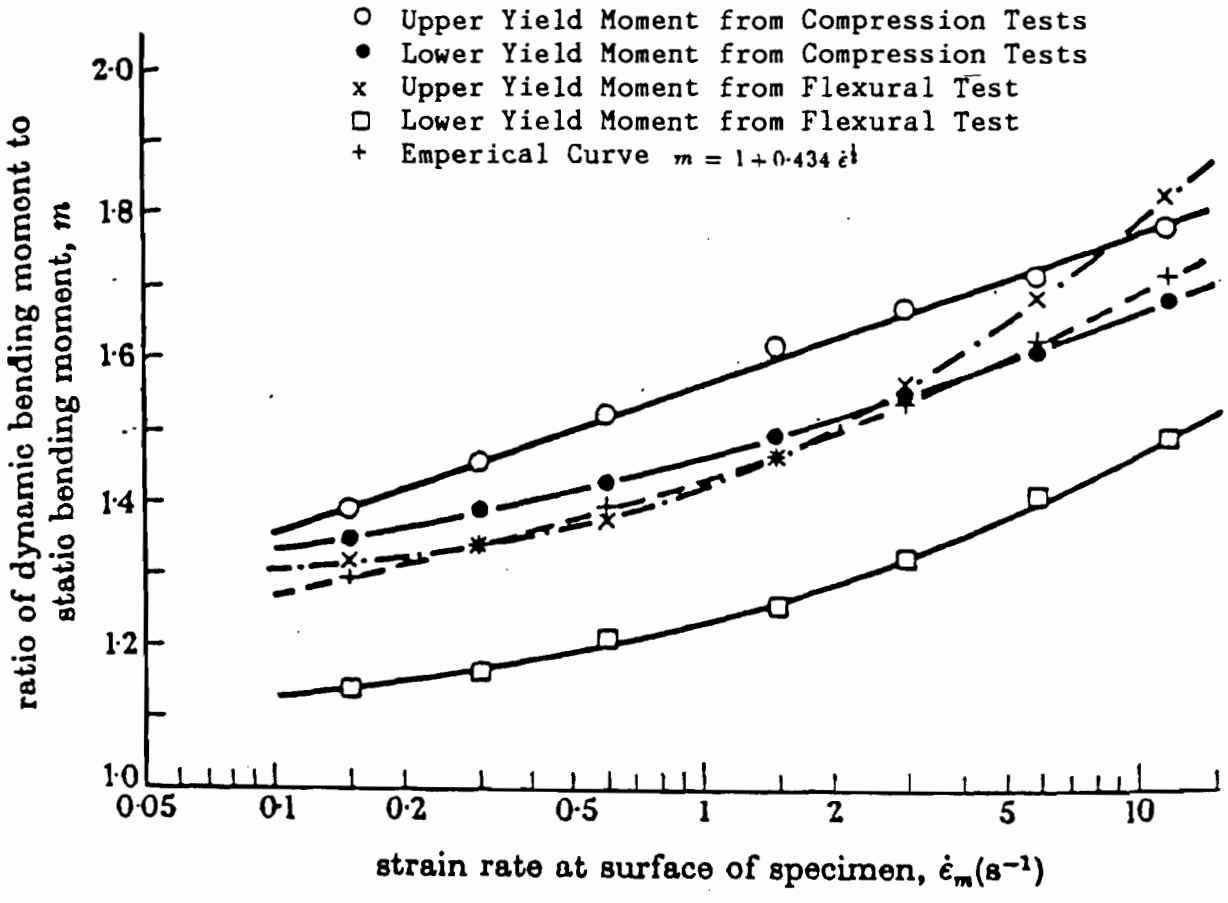

Fig. 2.56 Variation of Upper and Lower Yield Moments with Strain Rate at Surface of Specimen [99]

across the section as derived from test results by assuming plane sections remain plane. They attributed the difference of about 10% to non-uniform strain distribution throughout the experiment during the loading process. In their work, they integrated Eq. 2.42 through the thickness of a beam and found that the dynamic bending moment is related to the associated beam curvature rate according to the expression given in Eq. 2.43.

$$\frac{M}{M_0} = 1 + \frac{2p}{2p+1}\left(\frac{\dot{\kappa}H}{2D}\right)^{1/p} \qquad (2.43)$$

where M = dynamic bending moment

$M_0 = \sigma_y H^2/4$ static collapse moment

$\dot{\kappa}$ = curvature rate

H = thichness of the beam

D and p = material constants obtained from Eq. 2.42.

Recent research has been directed to analytical procedures which take into account more precise constitutive relationships including strain rate sensitivity, strain hardening, and geometric changes arising from overloads. In some of these studies, relatively sophisticated algebraic solutions have been developed, while in others, numerical procedures have been derived.

In order to develop the methods applicable for analysis of the response of beams supported at the ends by immovable frictionless pins and loaded with a uniform impulse, Jones[100] in 1967 used the rigid-plastic theory taking into account strain hardening and strain rate sensitivity. Equation 2.42 was used to acount for the material strain rate sensitivity.

Strain hardening was assumed to follow a linear relationship of the following form:

$$\frac{\sigma}{\sigma_0} = 1 + \frac{E\ \varepsilon}{r\ \sigma_0} \qquad (2.44)$$

where E/r is the equivalent modulus in the plastic range and r is the ratio of the slopes of the elastic and plastic portions of the stress-strain curve. Equations 2.42 and 2.44 were combined into the form shown in Eq. 2.45.

$$\frac{\sigma}{\sigma_0} = \left[1 + \left(\frac{\dot{\varepsilon}}{D}\right)^{1/p}\right] (1 + \nu\varepsilon) \qquad (2.45)$$

where $\nu = E / (r\ \sigma_0)$. In his treatment of the problem, Jones allowed for membrane effects by adopting interaction curves for the yield condition of a beam element subjected to axial tension and bending. Jones acknowledged the difficulty of assessing the accuracy of his theory, because of the absence of experimental results.

In 1971, Culver, Zanoni and Osgood[101] of Carnegie-Mellon University reported on thin-walled beam sections subjected to dynamic loading, as part of a large program of dynamic loading on cold-formed steel structural sections. Two methods of analysis were used in this study. One is the linear elastic and the other is the non-linear method including local buckling effects. A comparison of results showed that it was sufficient to predict bending moments from normal linear elastic analysis considering local buckling effects.

In a paper published in 1972,[102] Symonds and Jones reviewed the earlier work on plastic response to impulsive loading of beams clamped against end rotations and axial displacements, taking account of small finite transverse displacements and of strain-rate dependence of the yield stress. New solutions were derived from rigid-plastic analysis which included both effects and were compared with the experimental results. They concluded that the strain-rate dependence of the yield stress can be used in the analysis because the dynamic yield stress varies slowly with strain rate. Therefore, an estimate of dynamic yield stress at one strain rate may serve as a good approximation over several decades of strain rate. It is then assumed that the static plastic moment and axial force can be replaced by dynamic values obtained by multiplying the static magnitudes by a factor calculated from the strain rate at time t^*, after which the plastification of the cross section occurs. The strain rates at t^* are taken as representative of the initial part of the motion. If the pattern of deformation of the structure with strain-rate sensitive material is the same as that for non-rate sensitive behavior, then this substitution of new dynamic constants can give excellent results compared to those obtained by numerical integration. However, if the patterns differ considerably, then the use of dynamic correction factors may be entirely inappropriate, and can lead to large errors.

More recently, Forrestal, Wesenberg, and Sagartz[103,104] have developed a simple method for incorporating the approximate influence of material elasticity on the dynamic plastic response of beams. An exact elastic analysis is first undertaken for a dynamic beam problem which remains valid until the maximum stress reaches yield. If the beam material

is strain-rate sensitive, then this yield stress is calculated from the Cowper-Symonds constitutive law, Eq. 2.42, using the corresponding strain-rate predicted by the elastic analysis. The subsequent plastic behavior is controlled by a constant yield stress. There was an excellent agreement with the peak displacements recorded during experiments on simply supported beams using 1018 steel, type 304 stainless steel, and aluminium 6061 T6 as shown in Fig. 2.57.

b. Columns. In view of the fact that a compression member is one of the common structural components, its behavior under impact loading conditions has attracted interest for a considerable period of time.[89]

The analysis of column behavior under impact loading conditions dates back to 1933, when Koning and Taub[89] derived equations describing the axial and transverse oscillation of pin-ended columns subjected to dynamic axial load. They considered loads having a rectangular pulse form, of magnitude less than, equal to, or greater than the static Euler load. However, they did not recognize the possibility of dynamic overloads.

In the 1940s, Meier, Pian and Siddal[89] studied the response of pin-ended struts subjected to impact loads. They showed that struts could withstand loads well above Euler load without sustaining permanent damage. Pian and Siddal also conducted experiments on eccentrically loaded struts of very high slenderness ratios and demonstrated that they could withstand overloads of up to seven times the Euler value.

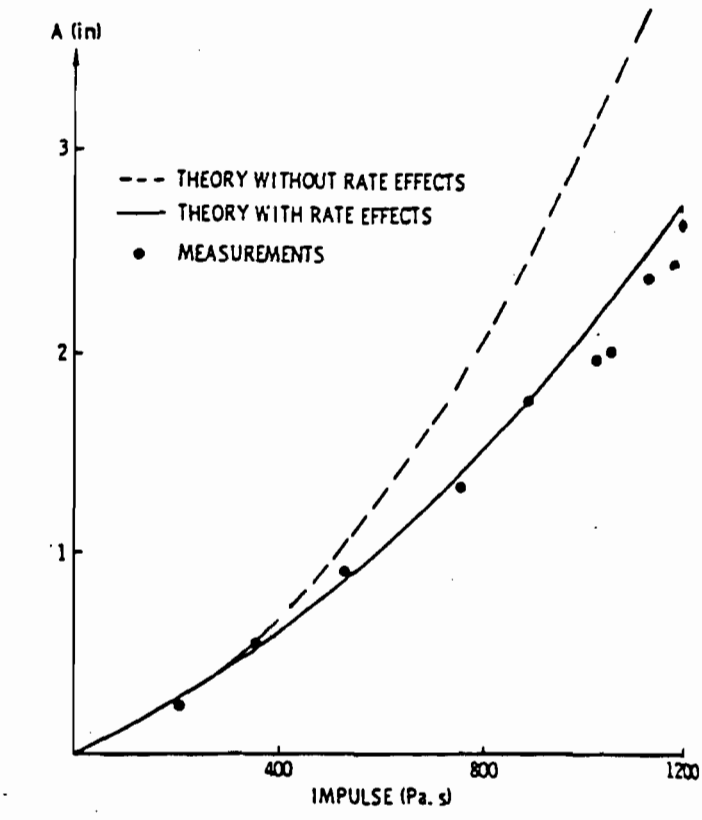

a) AISI 1018 Steel Beams[104]

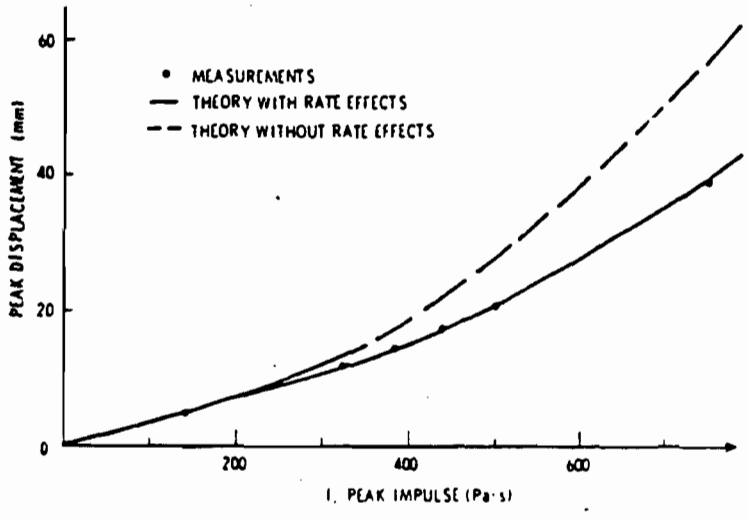

b) Type 304 Stainless Steel Beams[103]

Fig. 2.57 Peak Displacement Versus Impulse

Some of the most significant work on the analysis of strut behavior under dynamic loading is due to Hoff.[106] His analysis was directed to study the dynamics of the buckling of elastic columns in a rapid compression test. Figure 2.58 is adopted from his study which shows that under rapid loading the lateral displacements of the column are less than those calculated from static considerations. As a consequence the load supported by the column can exceed the Euler load considerably.

In 1972, Roberts[107] made an extensive theoretical and experimental investigation of pin-ended columns subjected to axial impact conditions. The experimental study involved the testing of mild steel columns of rectangular box sections. The cross sectional dimensions and the length of columns were selected to provide a range of slenderness ratios from 100 to 400. For the high speed tests, in which the impact velocity was of the order 1 to 3 m/s, the columns developed peak loads many times the Euler load, particularly for the case of columns with high slenderness ratios, for which the sustained compressive loads may be 20 or more times the Euler value.

Axial impact on thin-walled columns was examined theoretically by Culver and Vaidya[108] and experimentally by Logue[109] , both published in 1971. The theoretical work was applied to short duration impact loading which was defined by prescribing the time variations of the load at the end of the columns. Nonlinearity due to local buckling was accounted for by using nonlinear axial load-curvature relations derived with the aid of the effective width concept. The results of the analytical study were shown as response spectra curves which described the effect of initial

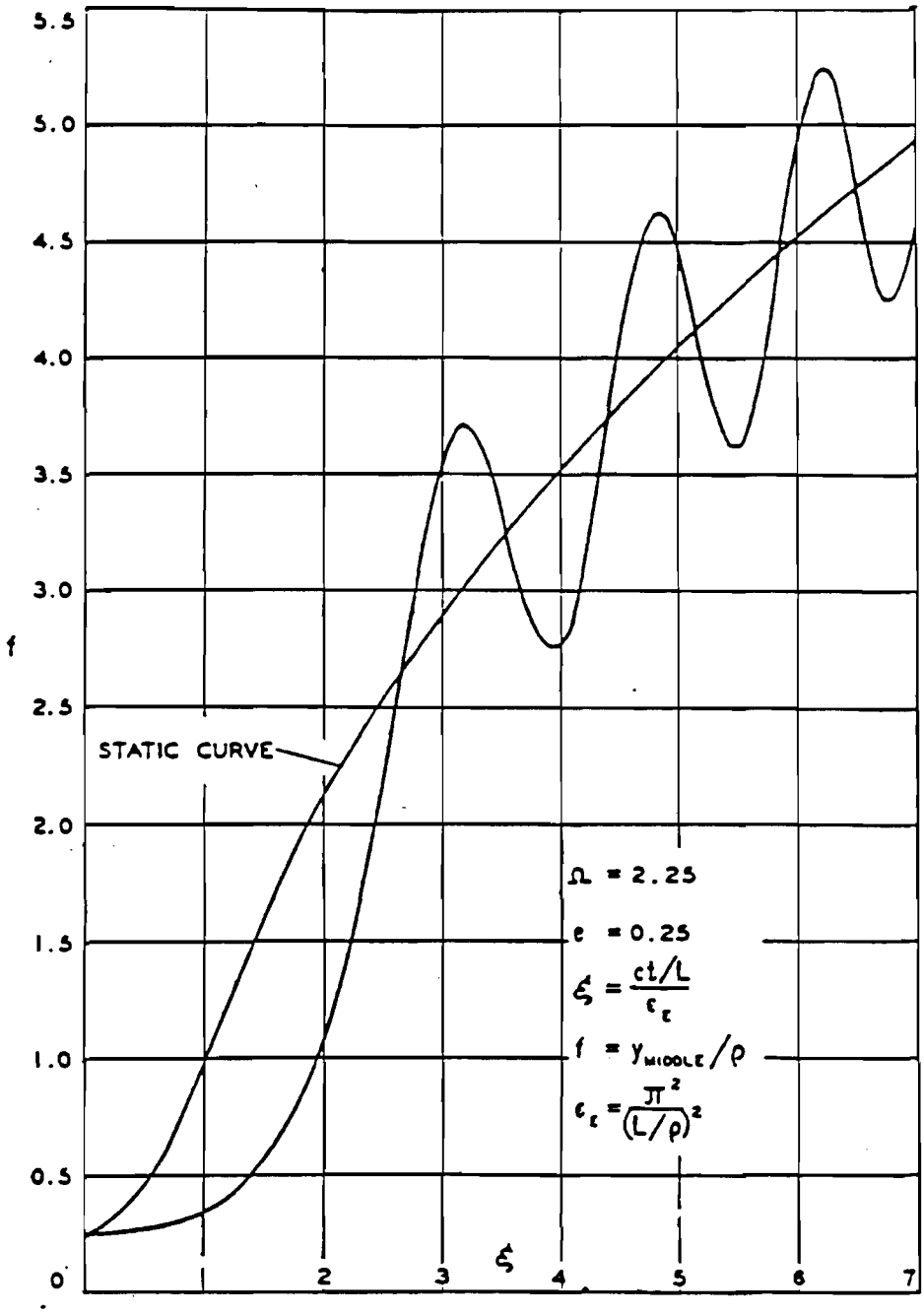

Fig. 2.58 Deflection of Mid-Point of Column[106]

deflection, pulse duration, maximum dynamic load, and the static preload on the dynamic response. It was concluded from the experimental study that maximum loads in excess of the static failure loads may be carried dynamically. However, the failure modes for thin-walled columns subjected to shock loading were not established in this study. Further study was suggested by the author to determine the maximum dynamic carrying capacity of these members.

In 1974, Soden, Al-Hassani and Johnson[110] studied the crushing behavior of circular tubes under static and dynamic axial loads. The loads and deformations of tubes with various thicknesses were recorded and three failure modes were observed and studied. The majority of tubes tested collapsed by progressive folding into diamond shaped lobes, while thick tubes failed by collapsing into circumferential rings. The initial failure loads and post-buckling loads for various modes of deformation were predicted theoretically. All stresses increased with increasing strain rate. Figure 2.59 shows the variation of first maximum stress and mean post-buckling stress for tubes with thickness to diameter ratio equal to 0.067.

Wierzbicki[111] has studied the dynamic crushing strength of strain-rate sensitive box columns. The main purpose of his study was to identify material and geometrical parameters in the problem of impact loading for sheet metal and to derive an expression for the strain rate correction factor. As a particular structural component, a straight rectangular box column was considered to be representive of front or rear longitudinal members of an automobile body. He stated that during a

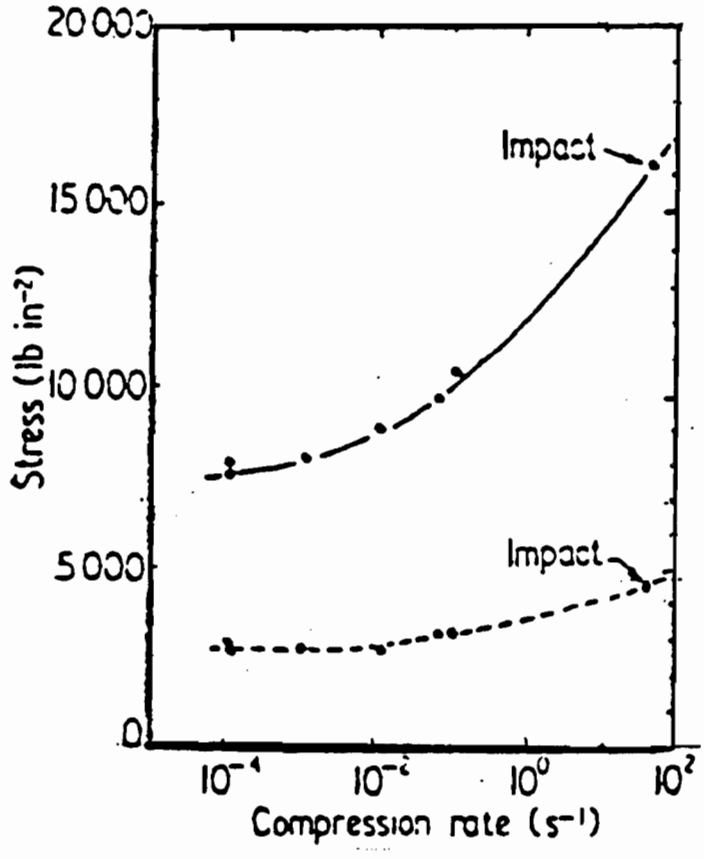

Fig. 2.59 Variation of First Maximum Stress (Solid Curve) and Mean Post-Buckling Stress (Broken Curve) with Compression Rate,[110] for Column with t/D= 0.067

vehicle collision the strain rates in the zones of localized deformation can be of the order of 10 to 100 in/in/sec. Consequently, dynamic forces in compressed mild steel members are much greater than static ones. An approximate analysis was presented to determine dynamic strength and energy absorption of axially loaded thin-walled box columns. In this analysis, the dynamic compressive force is a product of a static crushing strength of the column and a strain-rate correction factor. The strain-rate correction factor was found to be dependent on the initial impact velocity and parameters describing the sensitivity of the material to strain rate. He compared his analytical solution with the results of experimental work conducted by Ohkubo, Akamatsu, and Shirasawa[112] on closed-hat section members and the experimental work of Wimmer[113] on box sections. Wierzbicki concluded that in order to validate his theory, a much wider range of sectional dimensions and impact velocities is needed.

Wierzbicki and Abramowicz[114] used a simple method to calculate the dynamic correction factor for thin-walled strain-rate sensitive structures. For the experiments run at two crushing speeds v_1 and v_2 with associated strain rates $\dot{\varepsilon}_1$ and $\dot{\varepsilon}_2$, the correponding ratio of mean crushing forces $P_m^{\,1}$ and $P_m^{\,2}$ is equal to the dynamic correction factor given as follows:

$$R = \frac{P_m^{\,1}}{P_m^{\,2}} = \left(\frac{\dot{\varepsilon}_1}{\dot{\varepsilon}_2}\right)^{\frac{1}{\bar{n}}} = \left(\frac{v_1}{v_2}\right)^{\frac{1}{\bar{n}}} \qquad (2.46)$$

where $\bar{n}$ is the material strain-rate sensitivity calculated from the following equation:

$$\frac{\sigma}{\sigma_0} = \left(\frac{\dot{\varepsilon}}{\dot{\varepsilon}_0}\right)^{\frac{1}{\bar{n}}} . \qquad (2.47)$$

It is observed from Eq. 2.46 that the dynamic correction factor does not involve any geometrical and material parameters except the constant $\bar{n}$.

In another work published in 1984, Abramowicz and Jones[115] conducted 84 dynamic crushing tests on thin-walled square steel tubes with various lengths and two different cross sections. The columns were crushed axially on a drop hammer rig. Approximate theoretical predictions were developed for the axial progressive crushing of square box columns using a kinematic method of analysis. The effective crushing distance is considered in the analysis along with the influence of material strain-rate sensitivity. The theoretical study predicts four deformation modes which govern the behavior for different ranges of the parameter c/h (c being the width of a square box-section and h being the wall thickness). New asymmetric deformation modes were predicted theoretically and confirmed by the experimental tests. These asymmetric modes cause an inclination of a column which could lead to collapse in the sense of overall buckling even for relatively short columns. The following equation was presented for the ratio of dynamic to static mean crush force:

$$\bar{P}_m^d / \bar{P}_m = 1 + \alpha\, v^{\beta} \qquad (2.48)$$

where α and β = constants given in Table 2.13 for different modes

v = impact velocity (m/sec.).

Equation 2.48 gave reasonable agreement with the corresponding experimental results of Abamowicz and Jones.[115]

Also listed in Table 2.13 are the values of constants α and β used in Eq. 2.48 obtained from various references for calculation of the dynamic correction factor for thin-walled steel columns having different cross sections and different lengths.

Table 2.13

α and β Values of Equation 2.48 for the Calculation of Dynamic Correction Factor for Thin-Walled Steel Columns with Various Cross-Sections

Author and Reference Number	Cross Section	α	β
Wierzbicki (Ref. 111)	Box Sections	0.1000	0.714
Ohkubo, Akamatsu, and Shirasawa (Ref. 112)	Closed Hat Sections (70x60x1.2 mm)	0.0668	1.000
Wimmer (Ref. 113)	Box Sections (50x50x1.2 mm)	0.0700	0.820
Abramowicz and Jones (Ref. 115)	Box, Symmetric Mode (37x37x1.152 mm)	0.183	0.256
Abramowicz and Jones (Ref. 115)	Box, Symmetric Mode (49x49x1.63 mm)	0.170	0.256
Abramowicz and Jones (Ref. 115)	Box, Asymmetric Mode (37x37x1.152 mm)	0.193	0.256
Abramowicz and Jones (Ref. 115)	Box, Asymmetric Mode (49x49x1.63 mm)	0.180	0.256

III. EXPERIMENTAL PROGRAM

A. GENERAL

This chapter includes the experimental investigation of 1) material properties as presented in Section III.B, and 2) structural strengths of cold-formed steel members as presented in Section III.C.

B. MATERIAL PROPERTIES

1. Materials. Currently, numerous grades of high strength sheet steels are commercially available for automotive structural components[1]. Three types of sheet steels (35XF, 50XF, and 100XF) were selected for the purpose of studying the effect of strain rate on tensile and compressive mechanical properties of sheet steels. The chemical compositions for these sheet steels are listed in Table 3.1.

2. Uniaxial Tests. All three virgin materials listed in Table 3.1 were uniaxially tested in tension and compression in the longitudinal (parallel to the direction of rolling) and transverse (perpendicular to the direction of rolling) directions under three different strain rates of 10^{-4}, 10^{-2}, and 1.0 in./in./sec. Two of the three materials (50XF and 35XF) were also tested in tension in both directions to determine the combined effects of cold-stretching and strain rate. The uniform cold-stretchings used for the tests were 0.02 in./in.(20 mils) and 0.08 in./in.(80 mils). In order to determine the combined effects of strain rate and aging, half of the coupons (non-aged coupons) were tested in an average of two days after the cold stretching operation. The remaining half of the cold-stretched coupons (aged coupons) were tested to failure

Table 3.1

Chemical Compositions of the Sheet Steels Used

AISI Designa.	Thick. in.	C	Mn	P	S	Si	V	Cu	Al	Cb	Zr
035XF	0.085	.070	.40	.007	.017	--	.08	--	--	--	--
050XF	0.077	.081	.96	.017	.003	.27	--	--	.04	--	--
100XF	0.062	.070	.43	.006	.023	--	--	.11	.056	.064	.08

Table 3.2

Classification of the MTS Extensometer

Range	Maximum Strain In./In.	Maximum Error In./In.	ASTM Classification
100%	0.50	0.00065	Between Classes B-2 and C
50 %	0.25	0.00030	Between Classes B-2 and C
20 %	0.10	0.00011	Between Classes B-1 and B- 2
10 %	0.05	0.00002	Between Classes A and B- 1

under different strain rates at least 30 days after the cold stretching operation.

a. Tension Tests.

i) ASTM Specifications. All tension tests followed the procedures outlined in the ASTM Specifications listed below:

E8-69 Tension Testing of Metalic Materials

E83-67 Standard Method of Verification and Classification of Extensometers

E111-82 Standard Test Method for Young's Modulus, Tangent Modulus and Chord Modulus

ii) Specimens. The tensile specimens tested in the longitudinal and transverse directions were prepared by the Machine Shop of the Department of Civil Engineering at the University of Missouri-Rolla. The test specimens were cut from the quarter points of the steel sheets as shown in Figure 3.1. The sketch in Figure 3.2 shows the tensile specimen dimensions for the three materials (35XF, 50XF, and 100XF). A total of 124 coupons were tested in this phase of study. They are summarized in Table 3.3.

iii) Equipment. All the specimens were tested in a 110 kips MTS 880 Test System located in the UMR Engineering Research Laboratory. Figure 3.3 shows the Test System along with the remaining equipment used for the tension tests under controlled strain rates. Other equipment used for the tests includes the MTS controller, the data acquisition system, Data General graphic monitor, Data General MV-10000 mini computer to store and manipulate the data, MTS Model No. 732.25b-20 extensometer (Fig.

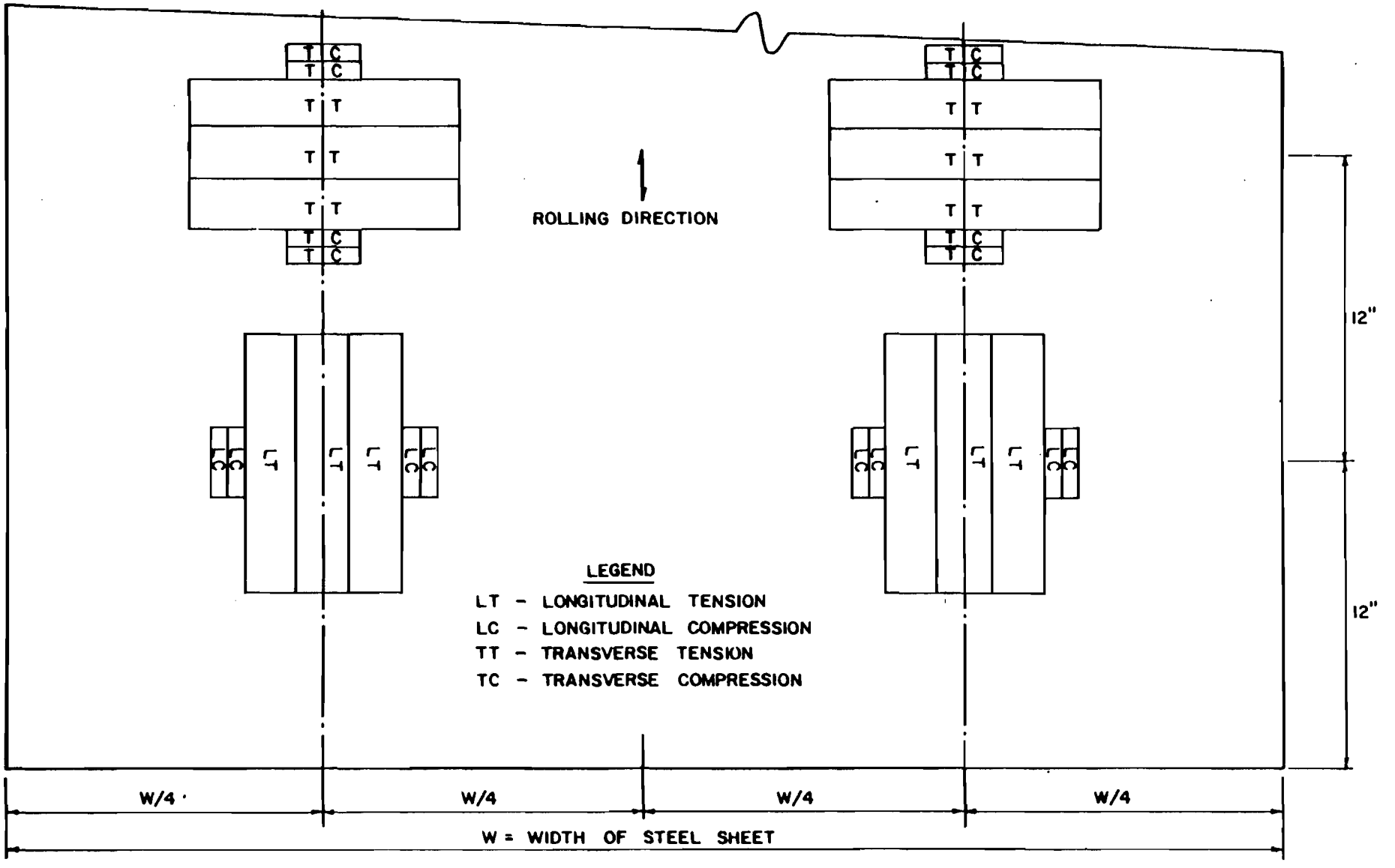

Fig. 3.1 Location of Tension and Compression Coupons[12]

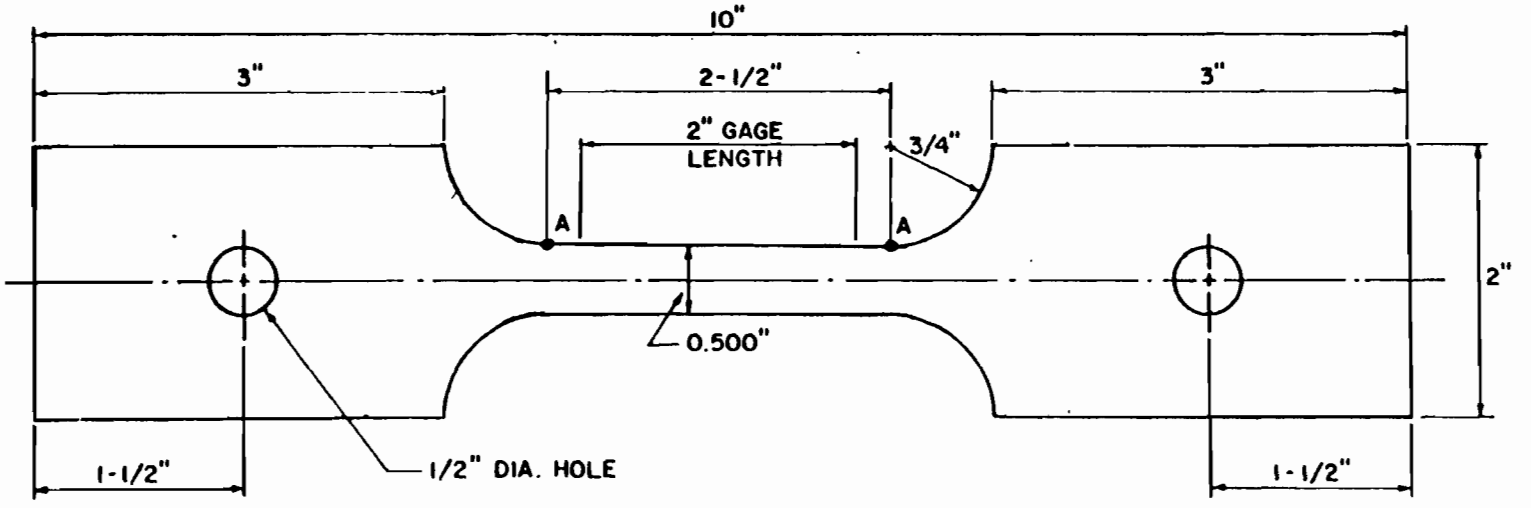

Fig. 3.2 Nominal Dimensions of Tension Coupons Used for 100XF, 50XF, and 35XF [12]

Table 3.3

Number of Performed Tensile Coupon Tests

Cold-Stretched Condition	Type of Material	Number of Coupons Used
Virgin Materials		
Longitudinal Tension (LT)	100XF-LT	7
	50XF-LT	9
	35XF-LT	9
Transverse Tension (TT)	100XF-TT	6
	50XF-TT	9
	35XF-TT	6
2% Cold-Stretched Non-Aged Materials		
Longitudinal Tension (LT)	50XF-LT	6
	35XF-LT	6
Transverse Tension (TT)	50XF-TT	2
	35XF-TT	4
8% Cold-Stretched Non-Aged Materials		
Longitudinal Tension (LT)	50XF-LT	6
	35XF-LT	6
Transverse Tension (TT)	50XF-TT	4
	35XF-TT	4
2% Cold-Stretched Aged Materials		
Longitudinal Tension (LT)	50XF-LT	6
	35XF-LT	6
Transverse Tension (TT)	50XF-TT	4
	35XF-TT	4
8% Cold-Stretched Aged Materials		
Longitudinal Tension (LT)	50XF-LT	6
	35XF-LT	6
Transverse Tension (TT)	50XF-TT	4
	35XF-TT	4

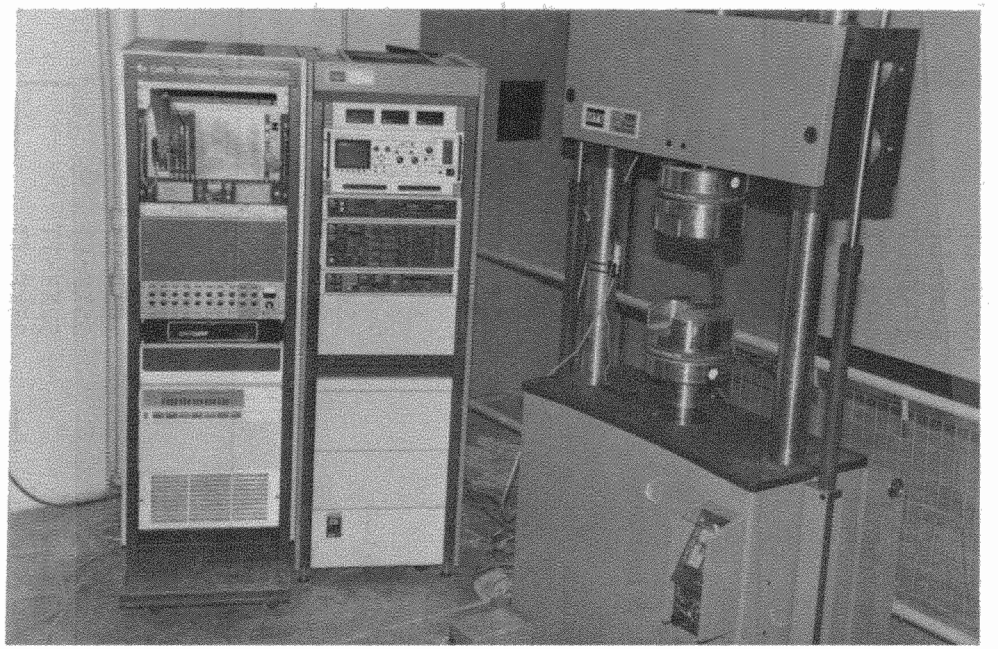

Fig. 3.3 Material Test System (MTS) 880 Used for Tension Tests

3.4), and IBM PS/2 Model 30 personal computer with IBM color plotter and NEC Pinwriter P5XL printer.

An MTS extensometer with a 2-in. gage length was used to measure the strains from zero load to failure. The classification of this extensometer according to ASTM Designation E-83 was found to be dependent on the extensometer range used in the tests. Table 3.2 contains the classifications of the four extensometer ranges according to the MTS transducer calibration data.

The load was measured by an MTS System Model 380041-06 load cell and associated conditioning, which was calibrated prior to testing according to the procedure of the National Bureau of Standards.

Figure 3.5 shows the MTS 880 automated test system which consists of four components: the load frame, the control console, the CAMAC (Computer Automated Measurement and Control) data acquisition system, and Data General MV-10000 computer. The testing machine is of a servohydraulic closed-loop type. Figure 3.6 shows the simplified block diagram of the servo control loop. The moving piston is driven by a double-action hydraulic cylinder; so that it can operate under tension and compression. The fluid pressure in the chamber is controlled by a servovalve. This servovalve responds to the difference between the measured signal and the desired signal. The signal is amplified to drive the valve so as to remove the error. There are three main modes of operating the machine, commonly referred to as stroke, strain, and load. Under the stroke mode, the movement of the piston is the controlling variable. Under the load mode, it is the load acting on the specimen. Under the strain mode, it is the strain, as read from the extensometer. For each of these three

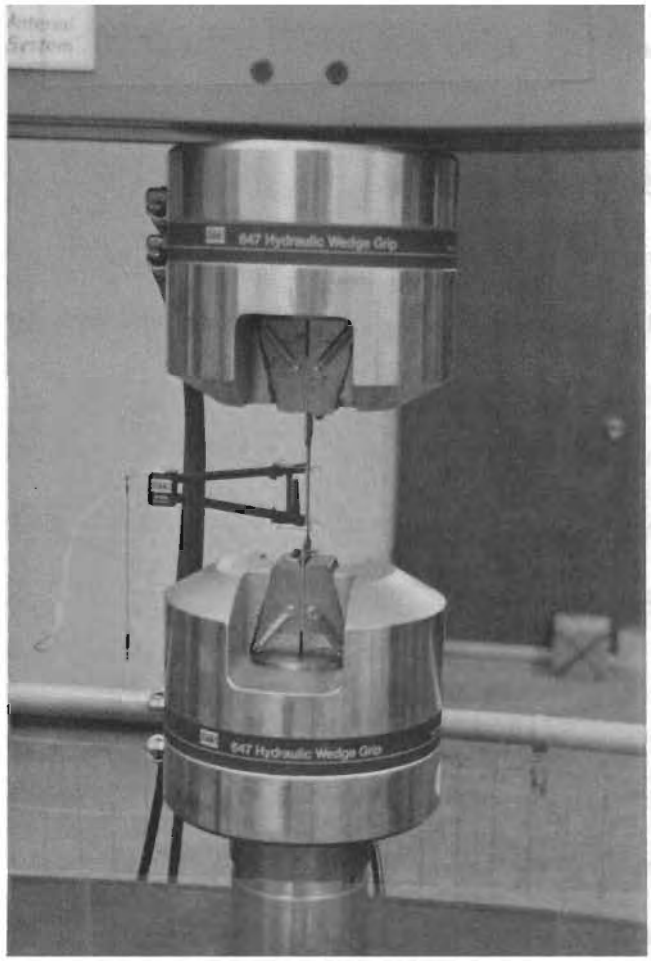

Fig. 3.4 Test Setup Showing the Attachment of Extensometer

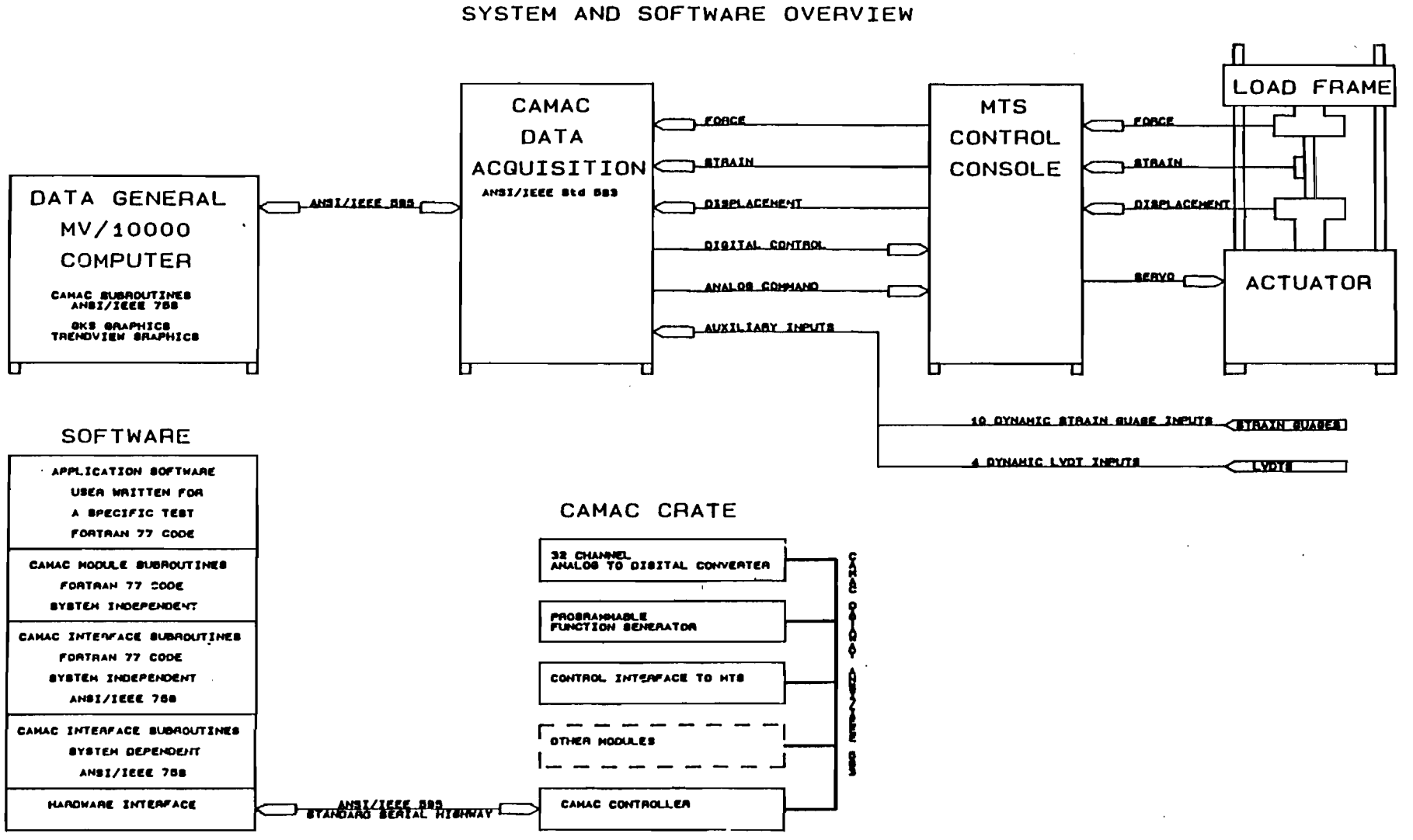

Fig. 3.5 MTS 880 Automated Test System and Software Overview

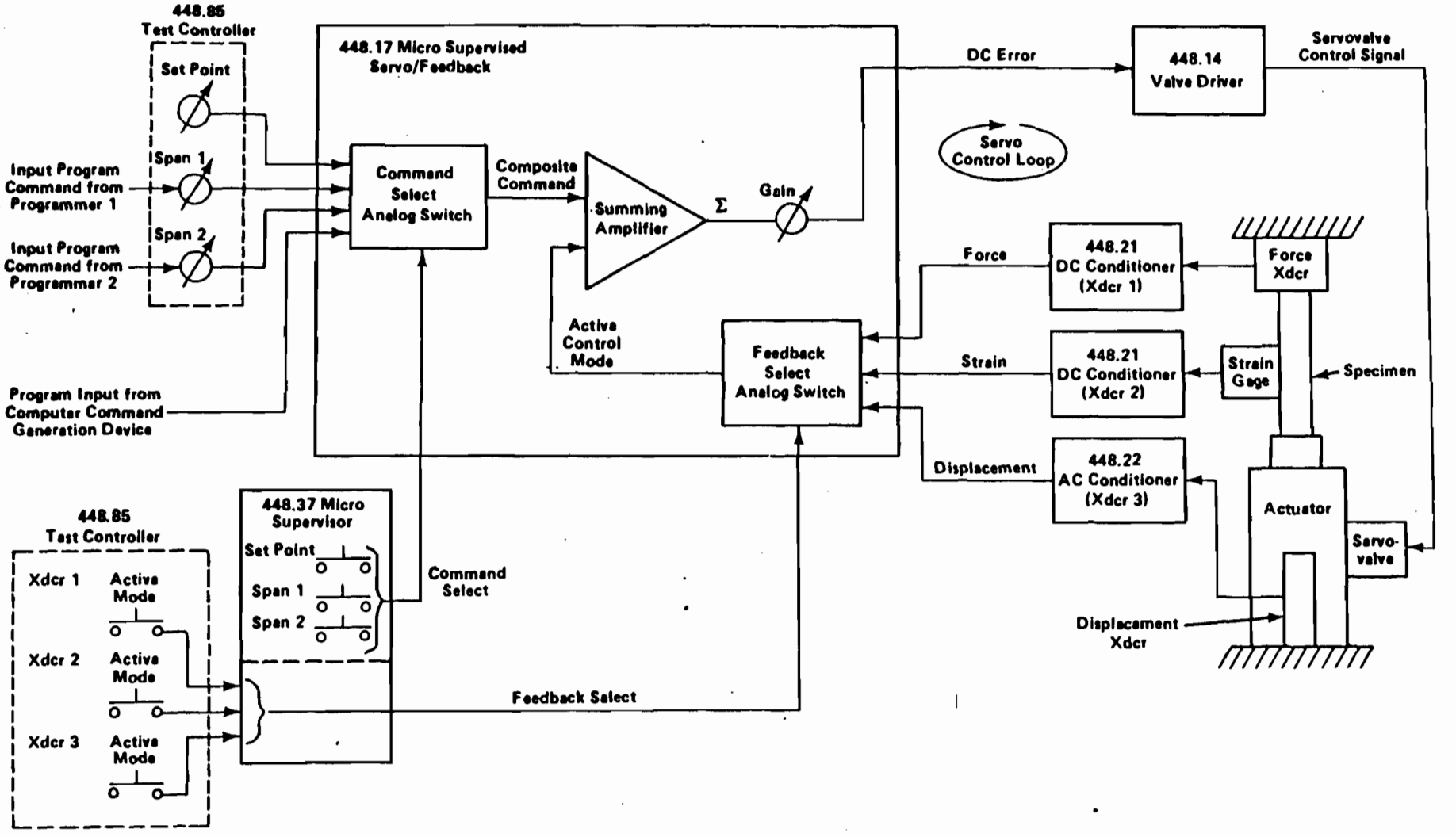

Fig. 3.6 MTS 880 Test Controller Servo Control Loop

modes, different time functions can be established by the function generator to match the application needed. Tensile tests under a constant strain rate can be made by setting a ramp function under the strain mode. The slope of this ramp is the desired strain rate. Each of these modes has four different ranges of operation i.e., 100%, 50%, 20%, and 10%. Table 3.4 summarizes the transducer ranges and the corresponding load, strain, or displacement values. The test results can be processed by the Data General mini-computer and displayed graphically as desired. The data acquisition used in this system conforms to the CAMAC standards. The main data acquisition module used in this system is a Kinetic Systems Model 4022 Transient Recorder. The unit has 32 simultaneous sampling input channels at a resolution of 12 bits. The unit is capable of acquiring sets of data at the maximum rate of 25,000 sets of readings per second. The recorder has a storage capacity of 1,000,000 samples. The simultaneous sampling feature of the system eliminates the timing skew between data points. After the data has been acquired, it is downloaded into the computer for analysis. The transient recorder includes a direct readout for "present value" monitoring, which allows the data to be displayed in real-time as the test runs.

iv) Procedure. Prior to testing, the dimensions of the tensile specimens were measured to the nearest 0.001 in., cleaned with acetone,and the gage length (2 in.) was marked in ink. The grips of the machine were alligned by operating the machine under stroke mode. The specimen was then placed in the grips such that the longitudinal axis of the specimen coincided with the center line of the grips. The load mode was selected to place the specimen in the grips before running the test. Next, the

Table 3.4

MTS Transducer Ranges and the Corresponding Load, Strain, or Displacement Values

Transducer	Range	Value	
Load	100 %	100.0	Kips
	50 %	50.0	Kips
	20 %	20.0	Kips
	10 %	10.0	Kips
Strain	100 %	0.50	In./In.
	50 %	0.25	In./In.
	20 %	0.10	In./In.
	10 %	0.05	In./In.
Stroke	100 %	10.0	In.
	50 %	5.00	In.
	20 %	2.00	In.
	10 %	1.00	In.

Table 3.5

Function Generator Ramp Time and the Corresponding Strain Rate (Tensile Tests)

Ramp Time 1 sec.	Strain Rate in./in./sec.
5000	0.0001
500	0.001
50	0.01
5	0.1
0.5	1.0

extensometer was attached to the specimen such that the extensometer knife edges lined up with the gage marks as illustrated in Figure 3.4. The function generator was then programmed to produce the desired ramp. The slope of this ramp equals to the strain rate selected for the test (see Fig. 3.7). Table 3.5 shows the ramp time and the corresponding strain-rate value. Transfer from load mode to strain mode was made before the test was started. For almost all the tests, load range 4, strain range 1, and stroke range 1 were selected. As the test proceeded, the stress-strain graph was plotted simultaneously on the graphic display terminal. The stress and strain data were stored by the Data General computer for later plotting and determination of mechanical properties.

A constant strain-rate is very difficult to maintain with the conventional testing machine, especially at high strain rate. The strain rate was controlled electronically by the new MTS 880 Test System, which allowed the exact strain rates to be performed without any difficulty. Figures 3.8 to 3.10 show the strain versus time curves for different strain rates.

The cold-stretching coupons were loaded to the desired 2% strain or 8% strain by using strain as a control mode with a strain rate of 0.1 in./in./sec. The span in the MTS system controller was used to stop the test when the desired strain was reached.

b. Compression Tests.

i) ASTM Specifications. The compression tests followed the procedures outlined in the ASTM Specifications listed below:

E9-70 Standard Methods of Compression Testing of Metallic Materials at Room Temperature

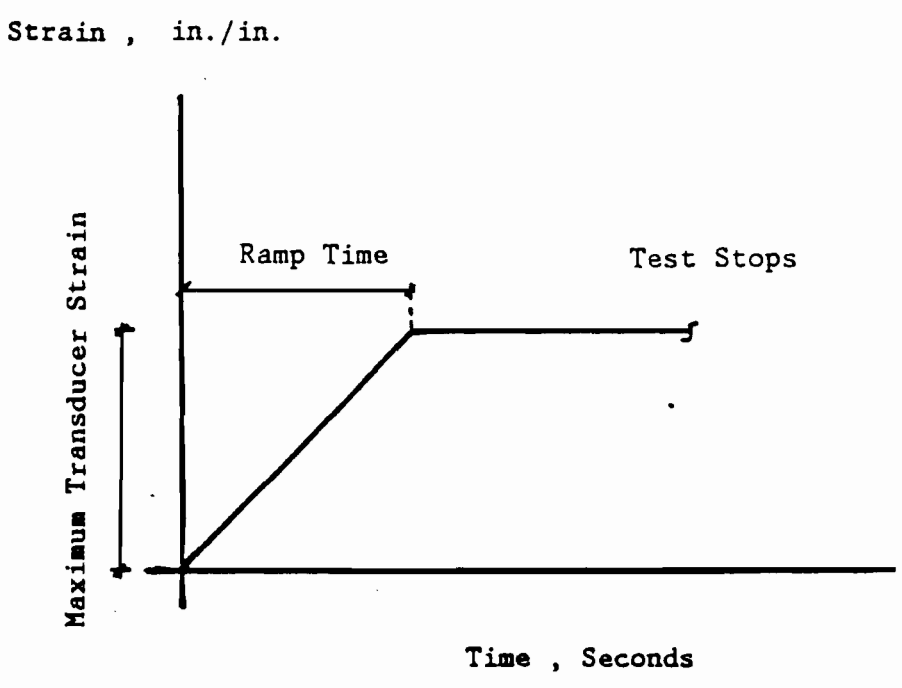

Fig. 3.7 Typical Function Generator Ramp Waveform

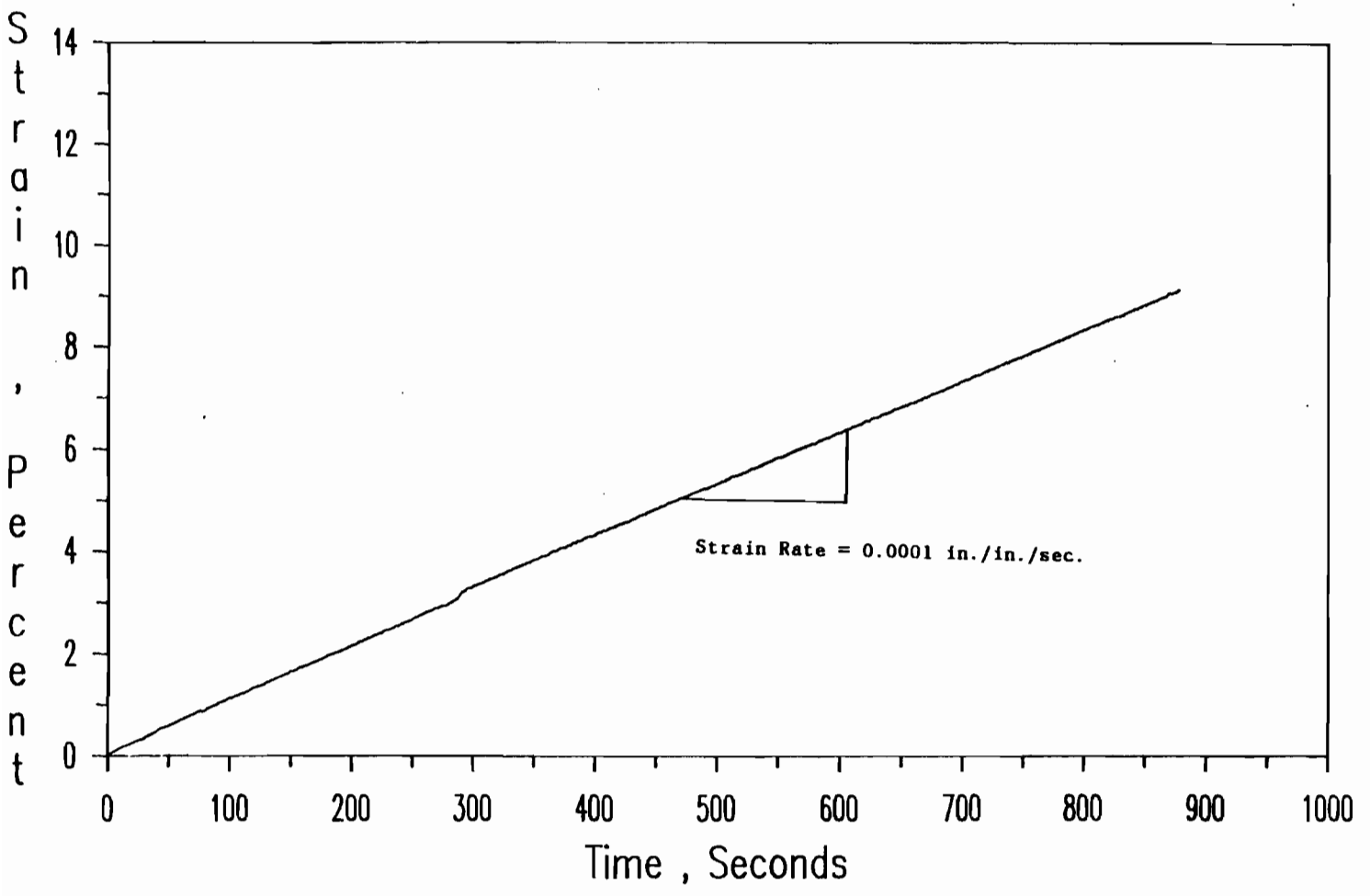

Fig. 3.8 Strain-Time Curve for 100$\dot{X}$F-LT-1, (Virgin Material)

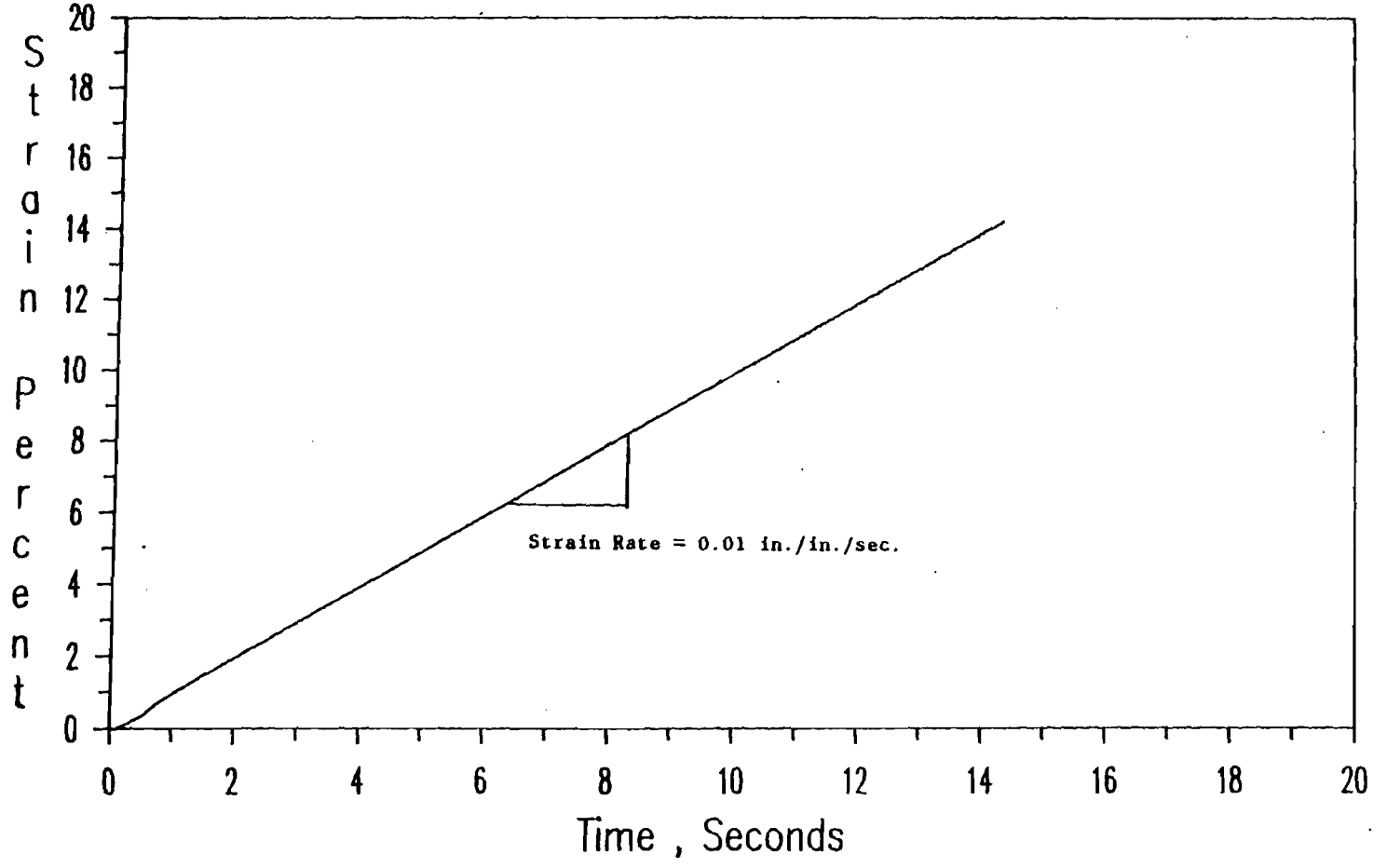

Fig. 3.9 Strain-Time Curve for 100XF-LT-3, (Virgin Material)

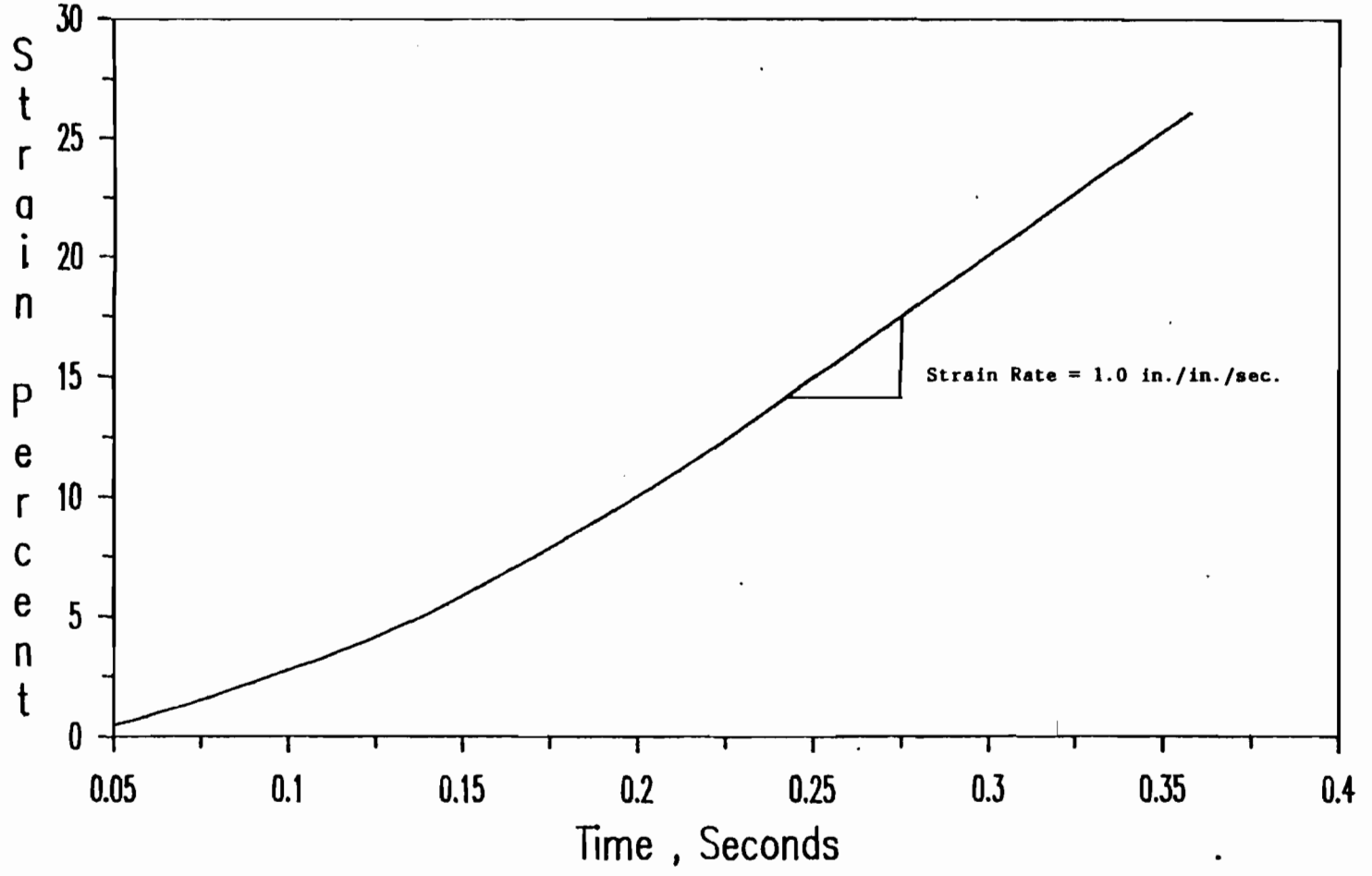

Fig. 3.10 Strain-Time Curve for 50XF-LT-7, (Virgin Material)

E83-67 Standard Method of Verification and Classification of Extensometers

E111-82 Standard Test Method for Young's Modulus, Tangent Modulus and Chord Modulus

ii) Specimens. The compression specimens tested in the longitudinal and transverse directions were prepared by the Machine Shop of the Department of Civil Engineering at the University of Missouri-Rolla. The test specimens were cut from the quarter points of the steel sheets. The sketch in Figure 3.11 shows the compression specimen dimensions for the three materials (35XF, 50XF, and 100XF). The specimen dimensions were selected to fit a Montgomery-Templin compression test fixture. The notches along one edge were for the installation of the knife edges of the compressometer. Special care was taken to ensure that the ends of the specimens were parallel and thus the same length was used for both longitudinal sides of the specimen. A total of 54 coupons were tested in this phase of study. They are summarized in Table 3.6.

iii) Equipment. All compression tests were performed in the same 110 kips 880 Material Test System (Figure 3.12) as described in Section III.B.2.a for tension tests. New MTS Compression Platens were installed for conducting the compression tests. The load was applied to the compression specimen by means of a specially made subpress (Figure 3.13(A)). The subpress base and ram are constructed of a hardened steel in order to minimize their deformation when applying the load. The compression specimen was held in a Montgomery-Templin compression test fixture (Figure 3.13(B)) which contains a series of rollers that may be tightened against the specimen to prevent buckling.

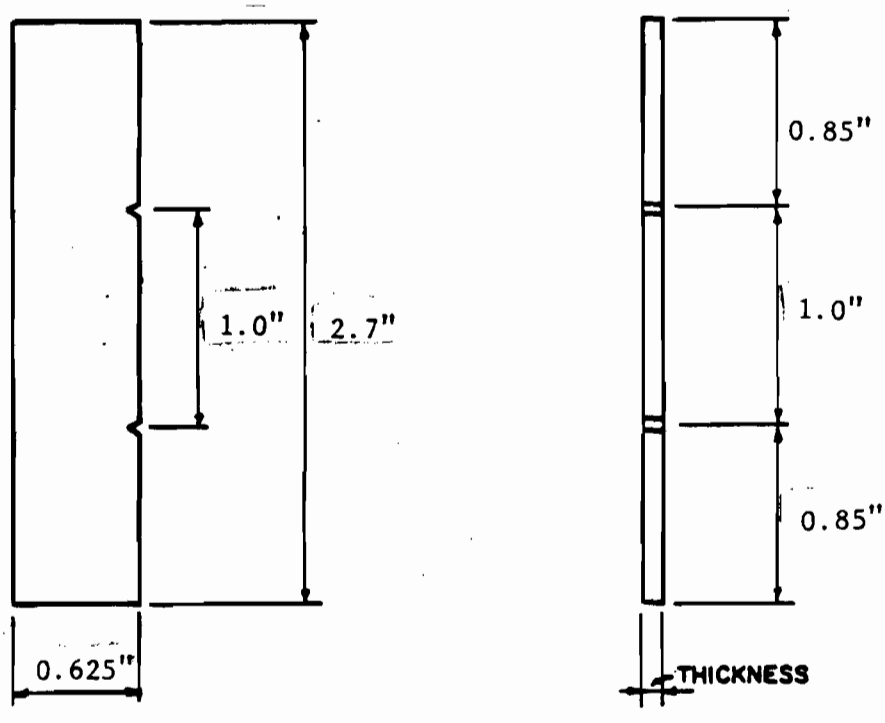

Fig. 3.11 Nominal Dimensions of Compression Coupons Used for All Sheet Steels

Table 3.6

Number of Performed Compressive Coupon Tests

Direction of Testing	Type of Material	Number of Coupons Used
Longitudinal Compression (LC)	100XF-LC	9
	50XF-LC	9
	35XF-LC	9
Transverse Compression (TC)	100XF-TC	9
	50XF-TC	9
	35XF-TC	9

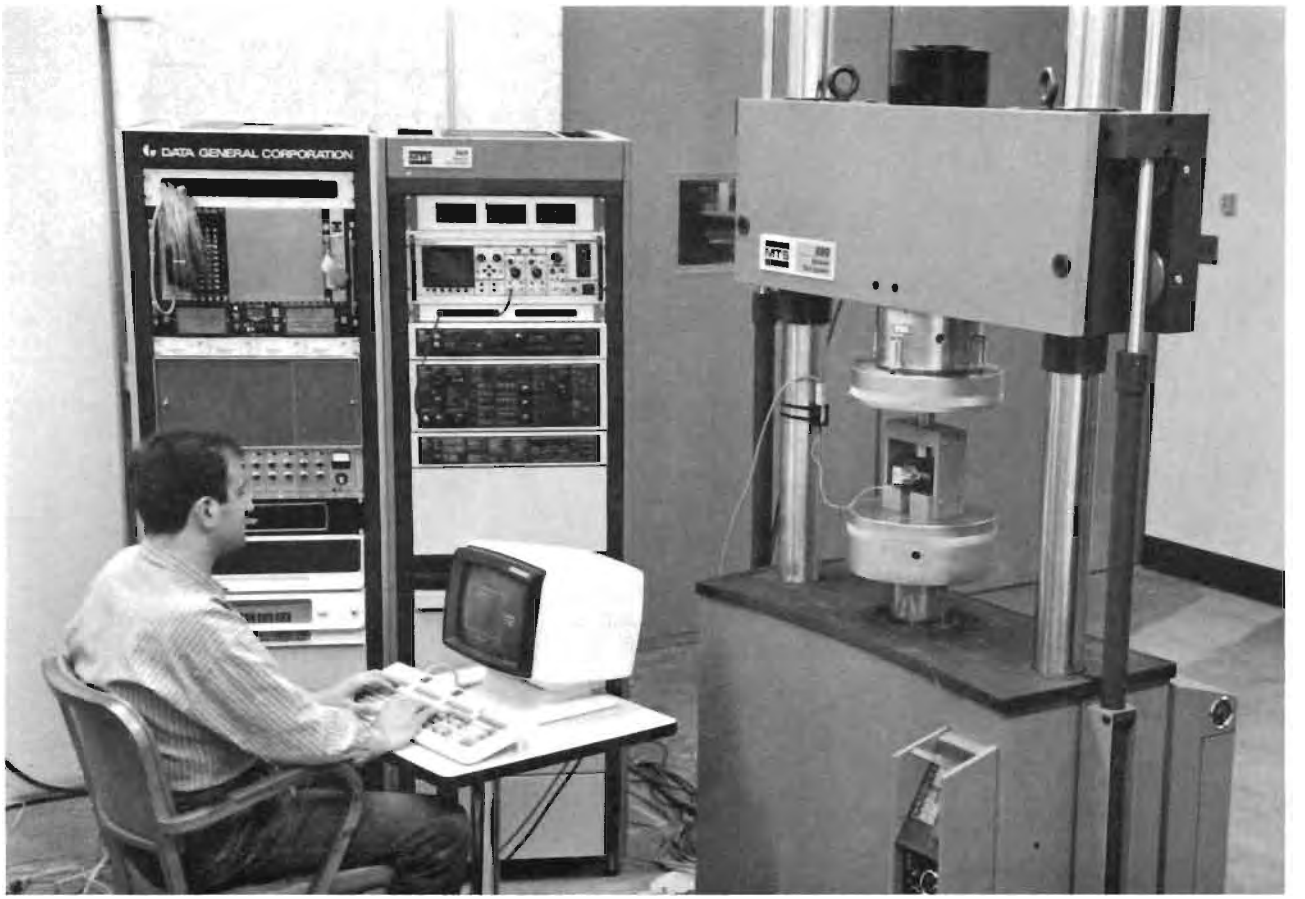

Fig. 3.12 MTS Load Frame, MTS Controller, CAMAC Data Acquisition System, and Data General Graphic Display Terminal Used for Compression Tests

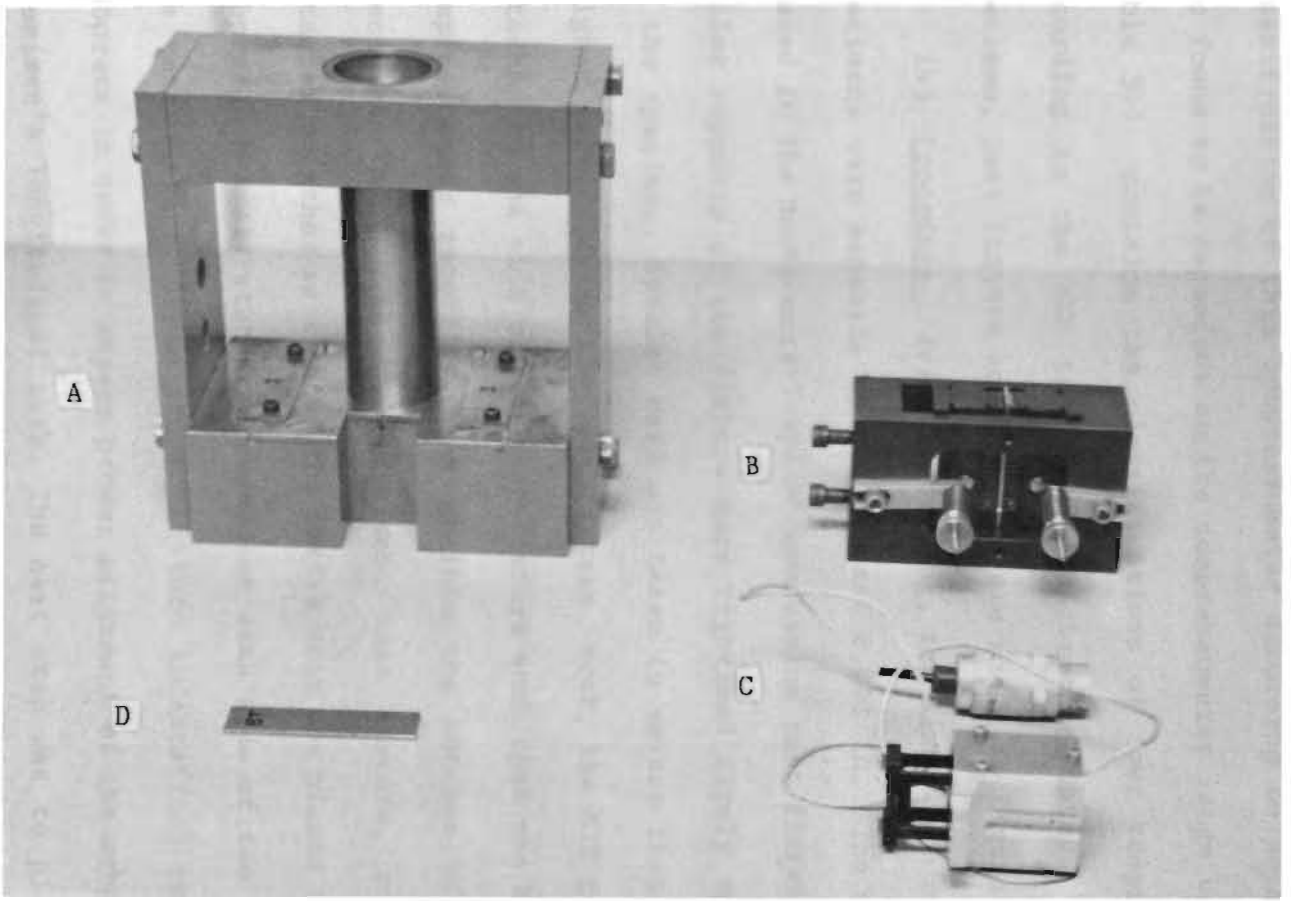

Fig. 3.13 Compression Subpress, Jig, Compressometer, and Test Specimen Used for Compression Tests

A- Compression Subpress
B- Compression Jig
C- MTS Compressometer
D- Test Specimen

An MTS compressometer (Figure 3.13(C)) with a 1-in. gage length was used to measure strains from zero to 2 percent in./in. A special fixture was designed to fit the MTS compressometer in the compression jig. The classification of this compressometer according to ASTM Designation E83 was found to be dependent on the compressometer range used in the tests. Table 3.7 contains the classifications of four compressometer ranges according to the MTS transducer calibration data. The assembly of specimen, test fixture and subpress are shown in Figure 3.14.

iv) Procedure. Prior to testing, the dimensions of the compressive specimens were measured to the nearest 0.001 in. The specimen was then placed in the Montgomery-Templin compression test fixture and the lateral roller supports of the fixture were tightened firmly against both sides of the specimen. Special care was taken to ensure that the specimen was aligned vertically in the test fixture. Next, the MTS compressometer was attached to one side of the test fixture such that the knife edges of the compressometer smoothly inserted into the notches of the compression specimen. Then, with the specimen, test fixture, and compressometer attached together as a unit, the entire unit was placed in the compression subpress. A small stub is provided on each side of the bottom surface of the test fixture. These stubs fit into indentations on the base of the subpress in order to ensure proper alignment of the subpress ram with the specimen's longitudinal axis. The next step was to place the subpress, with the test fixture, compressometer, and specimen attached, between the compression platens of the MTS loading frame such that the longitudinal axis of the subpress lined up with the centers of the platens. The function generator was then programmed to produce the desired ramp. Table

Table 3.7

Classification of the MTS Compressometer

Range	Maximum Strain in./in.	Maximum Error in./in.	ASTM Classification
100%	0.20	0.000100	Class B-1
50 %	0.10	0.000050	Between Classes A and B-1
20 %	0.04	0.000012	Between Classes A and B-1
10 %	0.02	0.000008	Class A

Table 3.8

Function Generator Ramp Time and the Corresponding Strain Rate (Compressive Tests)

Ramp Time sec.	Strain Rate in./in./sec.
200	0.0001
20	0.001
2	0.01
0.2	0.1
0.02	1.0

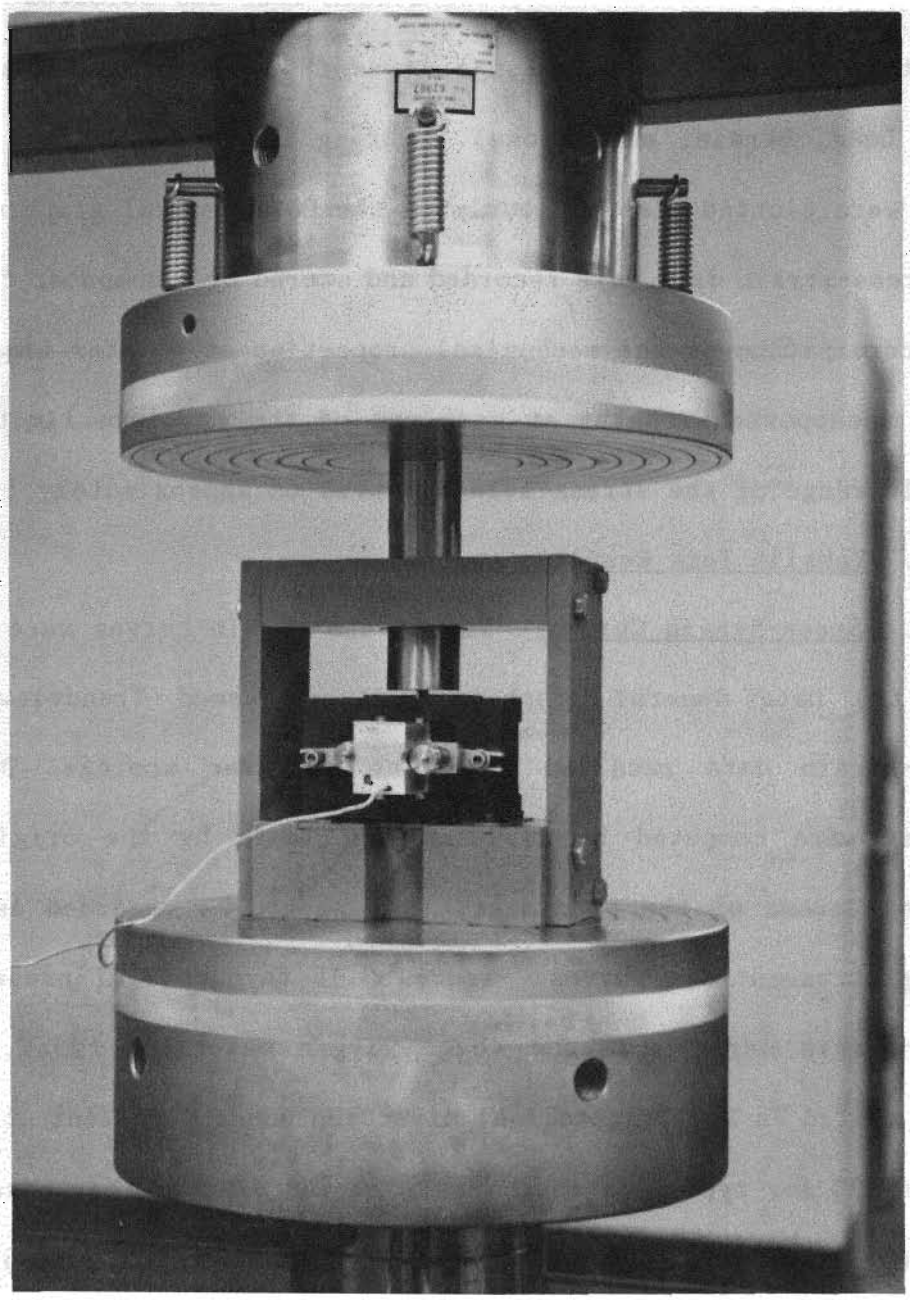

Fig. 3.14 Assembly of Compression Subpress, Jig, and Compressometer (Back View)

3.8 shows the function generator ramp time and the corresponding strain-rate value. For all the tests, the strain mode was selected to maintain a constant strain rate and Range 4 was chosen for the three MTS modes (i.e., Load, Strain, and Stroke). During the tests, the stress-strain curves were plotted simultaneously on the Data General graphic terminal. The stress-strain data were recorded and stored by a computer for plotting and determination of the mechanical properties at a later time. Buckling of the unsupported lengths at each end of the specimen limited the obtainable range of the stress-strain curves to approximately 1.8 percent.

3. Tensile Test Results.

a. Stess-Strain Curves. The stress-strain curves were plotted by using the Data General graphics software named Trendview with the stress-strain data recalled from the computer storage. Because the stresses were computed by dividing the loads by the original cross-sectional areas of the specimens, they should be regarded as the engineering stress-strain curves. Figures 3.15 through 3.17 present typical stress-strain curves for the three virgin materials (35XF, 50XF, and 100XF) tested in the longitudinal direction under different strain rates. See Ref. 23 for typical stress-strain curves of the other cases investigated in this study. For the purpose of comparison, each figure includes three stress-strain curves representing the test data obtained from the same material for different strain rates. In order to study the effect of aging on the mechanical properties of 50XF-LT steel, Figures 3.18 to 3.20 compare three stress-strain curves for 50XF-LT steel with different amount of cold stretching tested under a constant strain rate.

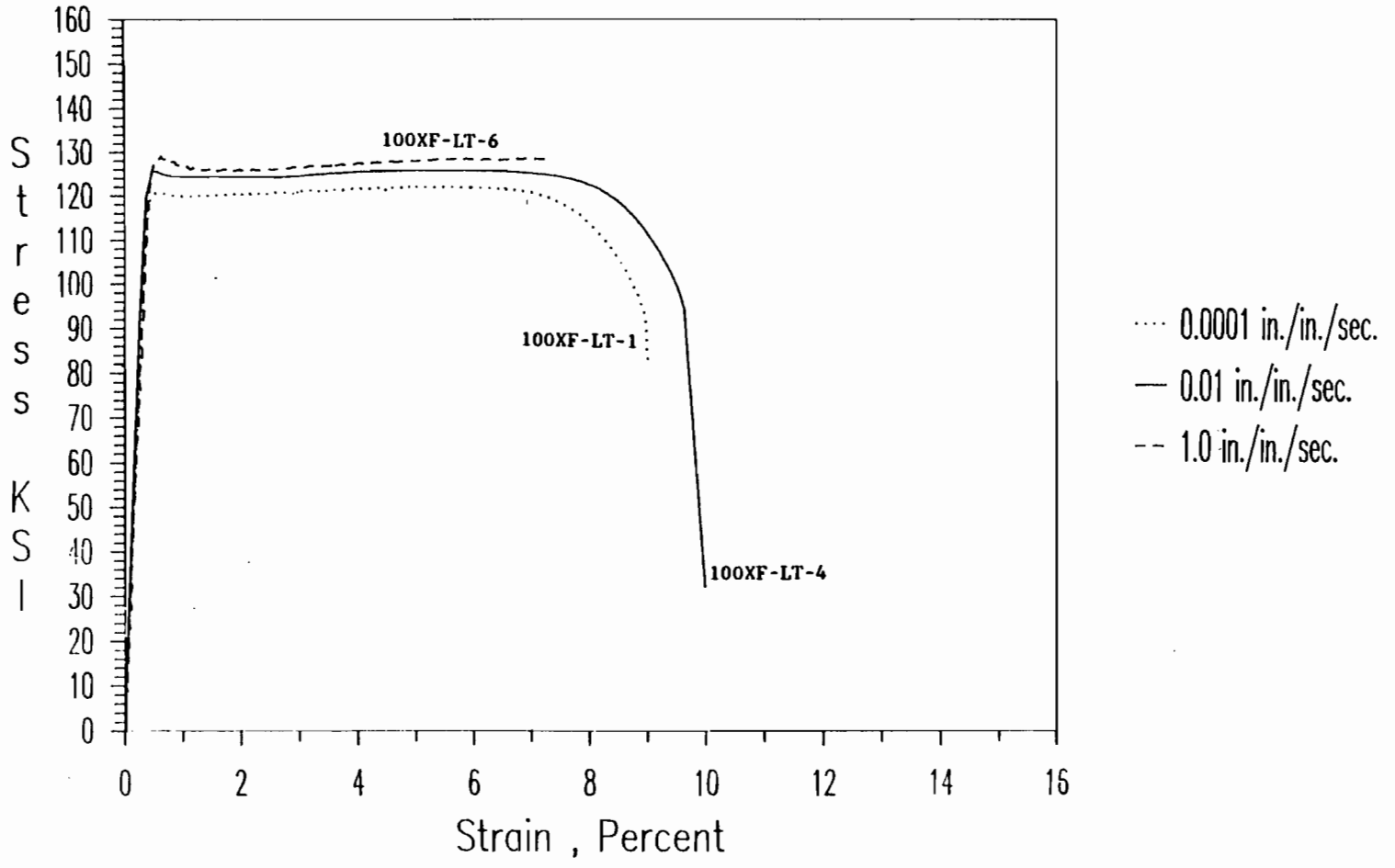

Fig. 3.15 Stress-Strain Curves for 100XF-LT-1, 100XF-LT-4, and 100XF-LT-6, (Virgin Material)

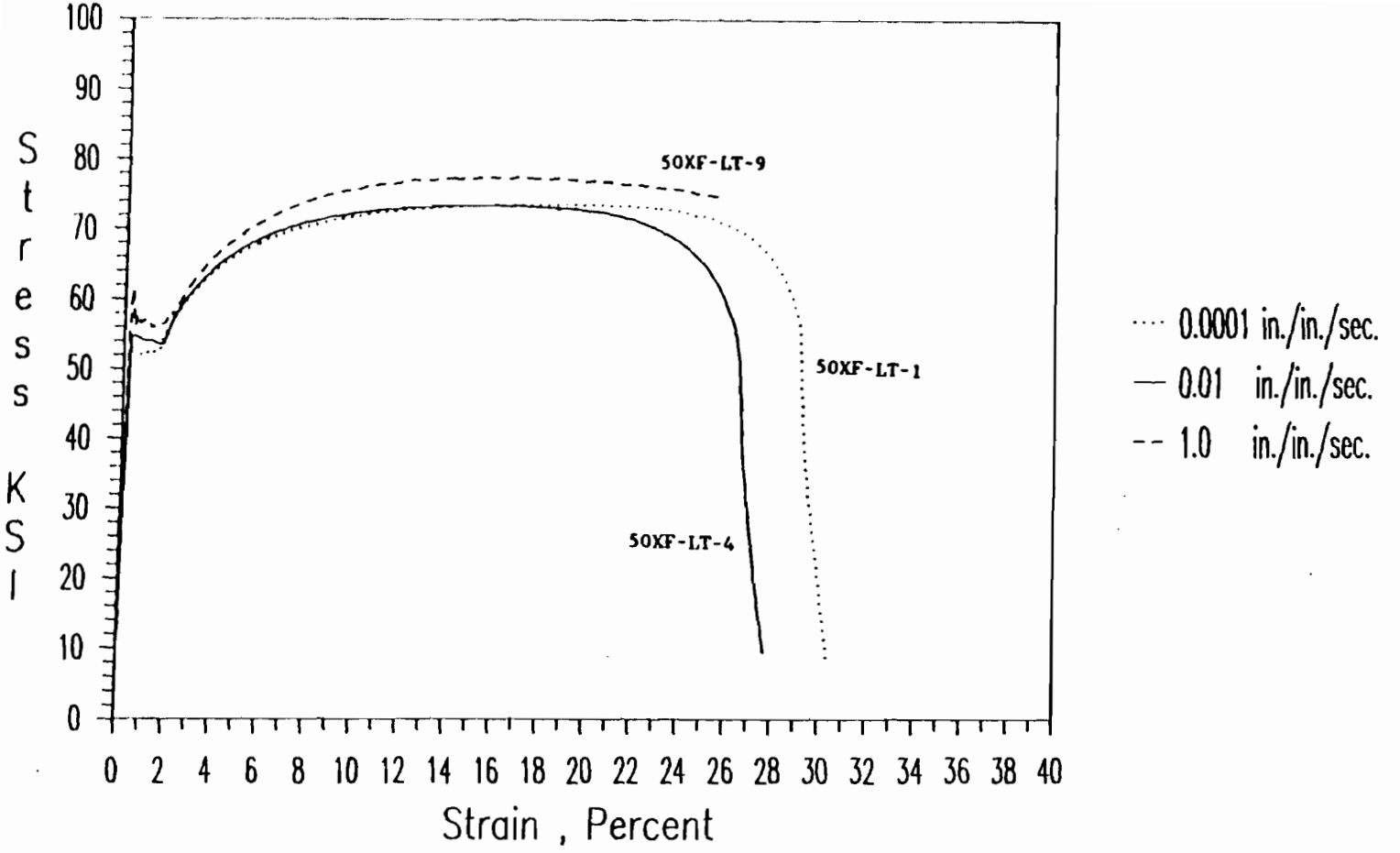

Fig. 3.16 Stress-Strain Curves for 50XF-LT-1, 50XF-LT-4, and 50XF-LT-9, (Virgin Material)

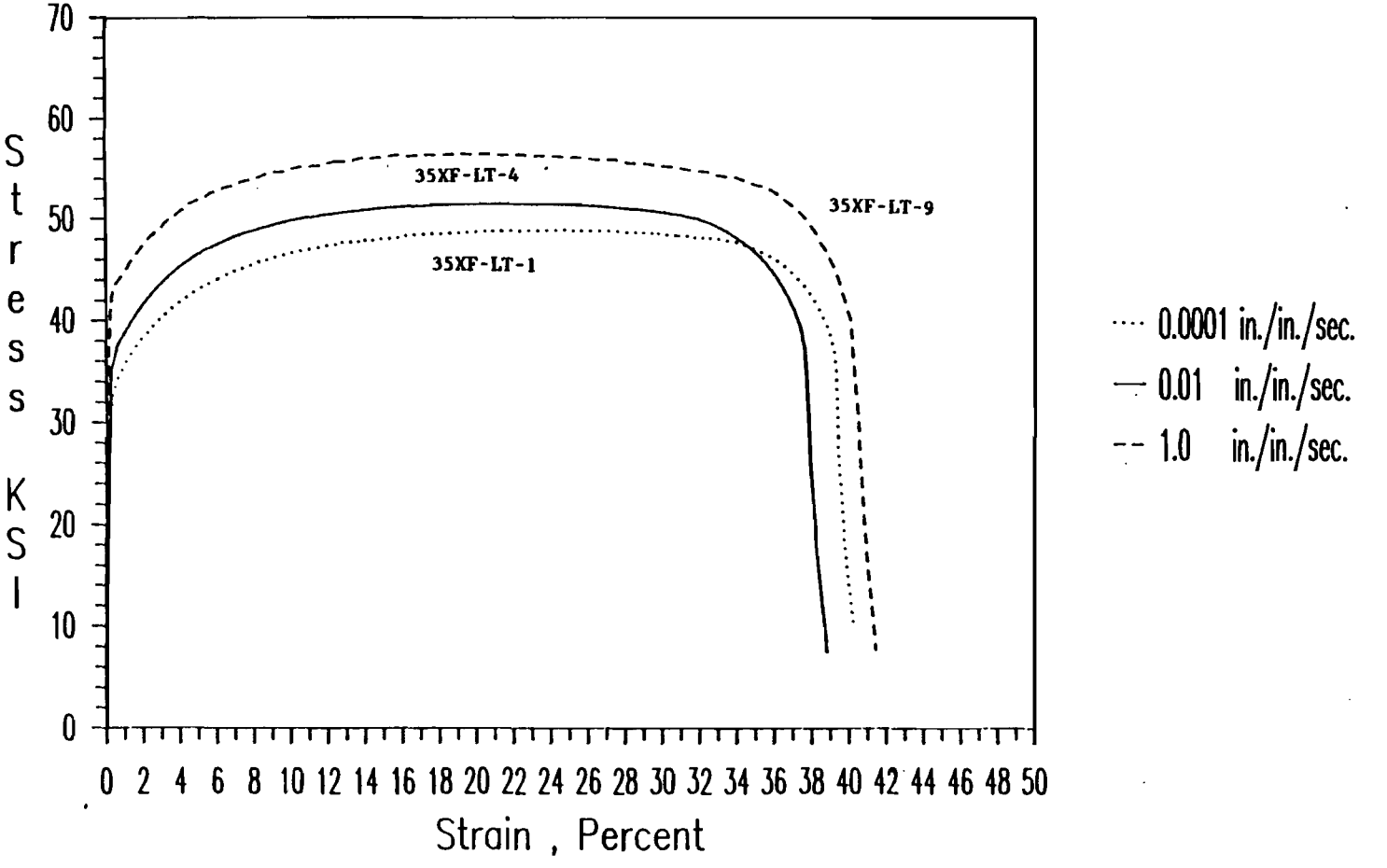

Fig. 3.17 Stress-Strain Curves for 35XF-LT-1, 35XF-LT-4, and 35XF-LT-9, (Virgin Material)

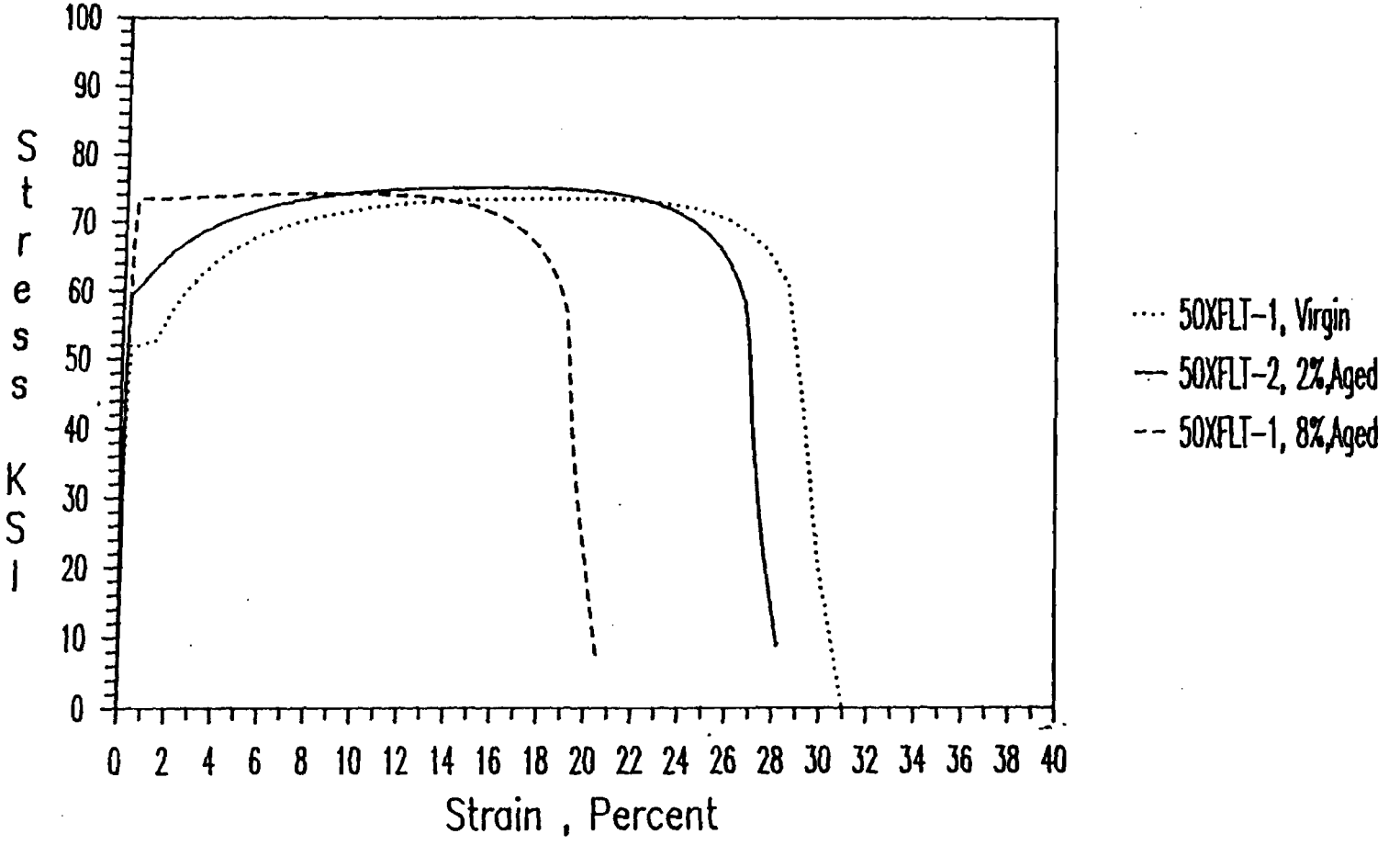

Fig. 3.18 Stress-Strain Curves for 50XF-LT Steel at Strain Rate of 0.0001 in./in./sec.

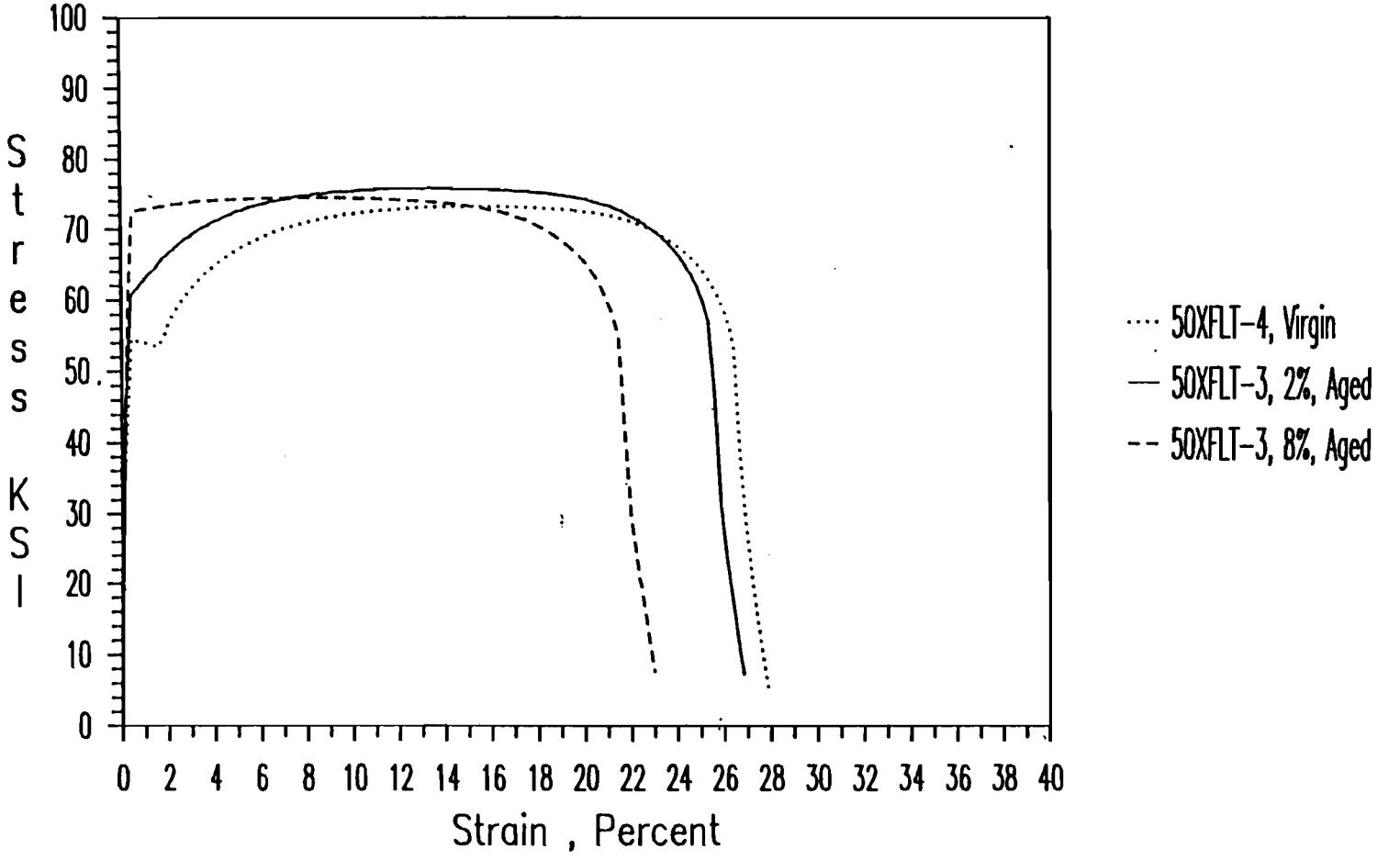

Fig. 3.19 Stress-Strain Curves for 50XF-LT Steel at Strain Rate of 0.01 in./in./sec.

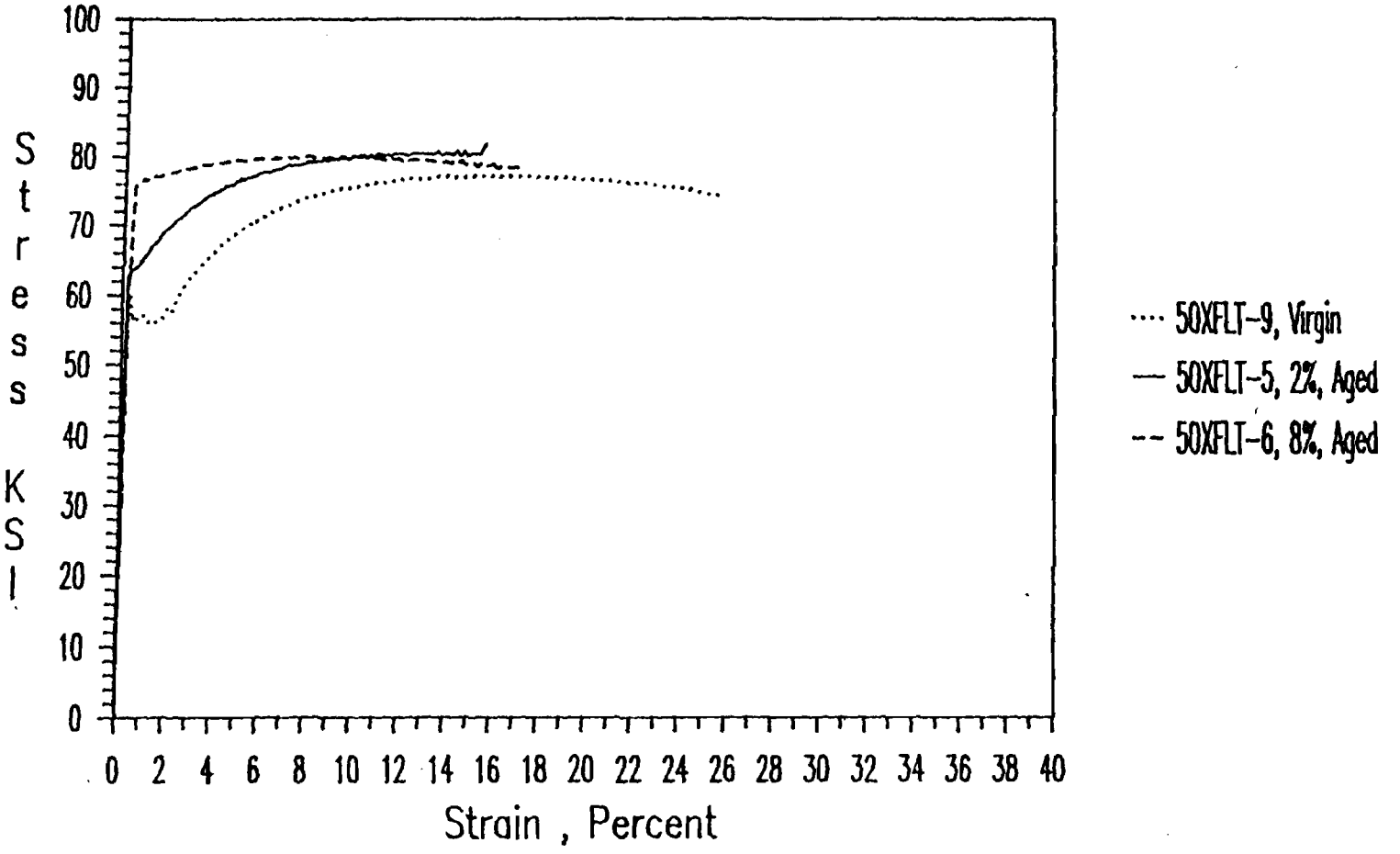

Fig. 3.20 Stress-Strain Curves for 50XF-LT Steel at Strain Rate of 1.0 in./in./sec.

b. Mechanical Properties. The procedures used for determining the mechanical properties of sheet steels are discussed in the subsequent sections (Sections III.B.3.b.i through III.B.3.b.iii). The mechanical properties so determined are the yield point F_y, the tensile strength F_u, and elongation in 2-in. gage length. These tested mechanical properties are presented in Tables 3.9 through 3.19 for each individual test. Tables 3.20 through 3.25 present the average values of the mechanical properties for each material tested in either longitudinal tension (LT) or transverse tension (TT), but with different amount of cold stretching (i.e., virgin material, 2%, or 8%) under different strain rates (0.0001, 0.01, or 1.0 in./in./sec.).

i) Yield Strength or Yield Point, F_y. The method commonly used to determine the yield point of sheet steels depends on whether the stress-strain curve is of the gradual or sharp-yielding type. For the types of sheet steels tested in this phase of study, the stress-strain curves of the 100XF and 50XF sheet steels are the sharp-yielding type, while the stress-strain curves of the 35XF steel are the gradual-yielding type. Because the 50XF sheet steel exhibited a considerable amount of strain hardening, the stress-strain curves became the gradual-yielding type after the material was cold-stretched to a selected strain of either 2% or 8%.

The yield point of the sharp-yielding steel was determined as the stress where the stress-strain curve becomes horizontal. Typical sharp yielding stress-strain curves are shown in Figure 3.15 for the 100XF steel in the longitudinal direction. For this case, the lower yield point is

Table 3.9

Tested Mechanical Properties of 100XF Sheet Steel

Virgin Material

Test No.	Strain Rate in./in./sec.	F_y (ksi)	F_u (ksi)	Elongation in 2-in. Gage Length (percent)
LT-1	0.0001	122.44	122.44	9.4
LT-2	0.0001	126.07	126.07	9.7
LT-3	0.01	123.98	123.98	10.3
LT-4	0.01	125.91	125.91	10.3
LT-5	0.01	127.52	127.52	9.8
LT-6	1.0	129.06	129.06	---
LT-7	1.0	128.75	128.75	---
TT-1	0.0001	138.20	138.20	4.9
TT-2	0.0001	137.34	137.34	4.9
TT-3	0.01	140.11	140.11	6.1
TT-4	0.01	139.05	139.05	4.4
TT-5	1.0	144.11	144.11	8.0
TT-6	1.0	143.03	143.03	5.1

Table 3.10

Tested Mechanical Properties of 50XF Sheet Steel

Virgin Material

Test No.	Strain Rate in./in./sec.	F_y (ksi)	F_u (ksi)	Elongation in 2-in. Gage Length (percent)
LT-1	0.0001	49.80	73.87	29.9
LT-2	0.0001	49.39	72.54	32.0
LT-3	0.0001	49.32	72.51	31.0
LT-4	0.01	51.89	75.44	27.2
LT-5	0.01	50.83	74.07	27.4
LT-6	0.01	52.09	75.11	26.4
LT-7	1.0	54.71	79.18	26.2
LT-8	1.0	54.99	79.64	25.4
LT-9	1.0	54.29	77.36	25.7
TT-1	0.0001	50.38	73.73	26.8
TT-2	0.0001	51.13	73.39	28.3
TT-3	0.0001	50.25	73.21	24.8
TT-4	0.01	54.22	75.26	25.9
TT-5	0.01	52.77	74.80	26.7
TT-6	0.01	52.64	74.16	27.0
TT-7	1.0	56.21	79.86	28.3
TT-8	1.0	54.31	79.85	27.9
TT-9	1.0	56.13	80.03	27.1

Table 3.11

Tested Mechanical Properties of 50XF Sheet Steel

2% Cold Stretched, Non-Aged Material

Test No.	Strain Rate in./in./sec.	F_y (ksi)	F_u (ksi)	Elongation in 2-in. Gage Length (percent)
LT-1	0.0001	56.37	72.62	26.5
LT-2	0.0001	56.44	73.41	27.5
LT-3	0.01	58.46	74.81	25.4
LT-4	0.01	58.88	74.20	25.7
LT-5	1.0	63.19	80.58	26.1
LT-6	1.0	62.16	80.06	27.9
TT-1	0.0001	59.29	74.90	23.1
TT-2	1.0	68.48	81.29	24.6

Table 3.12

Tested Mechanical Properties of 50XF Sheet Steel

8% Cold Stretched, Non-Aged Material

Test No.	Strain Rate in./in./sec.	F_y (ksi)	F_u (ksi)	Elongation in 2-in. Gage Length (percent)
LT-1	0.0001	71.22	73.73	24.6
LT-2	0.0001	71.86	73.99	23.8
LT-3	0.01	73.87	76.21	21.6
LT-4	0.01	75.06	76.81	20.3
LT-5	1.0	77.00	80.77	21.6
LT-6	1.0	78.18	81.55	19.8
TT-1	0.0001	72.59	74.90	20.0
TT-2	0.0001	74.71	76.86	23.6
TT-3	1.0	77.90	82.07	19.4
TT-4	1.0	77.78	81.94	17.5

Table 3.13

Tested Mechanical Properties of 50XF Sheet Steel

2% Cold Stretched, Aged Material

Test No.	Strain Rate in./in./sec.	F_y (ksi)	F_u (ksi)	Elongation in 2-in. Gage Length (percent)
LT-1	0.0001	58.78	74.84	30.3
LT-2	0.0001	59.68	75.31	27.7
LT-3	0.01	60.49	76.05	26.4
LT-4	0.01	60.55	76.27	26.7
LT-5	1.0	63.45	81.39	----
LT-6	1.0	62.97	81.16	28.8
TT-1	0.0001	60.33	74.96	26.5
TT-2	0.0001	60.20	75.13	28.9
TT-3	1.0	65.43	83.62	22.1
TT-4	1.0	64.15	82.57	22.1

Table 3.14

Tested Mechanical Properties of 50XF Sheet Steel

8% Cold Stretched, Aged Material

Test No.	Strain Rate in./in./sec.	F_y (ksi)	F_u (ksi)	Elongation in 2-in. Gage Length (percent)
LT-1	0.0001	73.33	74.41	20.1
LT-2	0.0001	72.94	73.21	20.0
LT-3	0.01	72.51	74.49	22.4
LT-4	0.01	73.80	75.92	20.5
LT-5	1.0	75.60	77.19	----
LT-6	1.0	75.93	80.69	----
TT-1	0.0001	75.06	75.41	17.1
TT-2	0.0001	73.54	74.49	21.5
TT-3	1.0	78.11	81.82	19.1
TT-4	1.0	77.26	81.47	16.4

Table 3.15

Tested Mechanical Properties of 35XF Sheet Steel

Virgin Material

Test No.	Strain Rate in./in./sec.	F_y (ksi)	F_u (ksi)	Elongation in 2-in. Gage Length (percent)
LT-1	0.0001	32.42	49.22	39.7
LT-2	0.0001	32.57	49.19	40.2
LT-3	0.0001	33.63	49.64	36.7
LT-4	0.01	36.42	51.68	38.1
LT-5	0.01	36.65	52.02	36.0
LT-6	0.01	36.12	51.59	36.5
LT-7	1.0	42.53	56.82	41.6
LT-8	1.0	41.87	56.48	40.2
LT-9	1.0	42.70	56.60	40.9
TT-1	0.0001	33.53	49.41	34.9
TT-2	0.0001	33.49	49.19	37.5
TT-3	0.01	36.21	50.98	39.0
TT-4	0.01	36.57	51.10	35.3
TT-5	1.0	43.00	55.70	36.9
TT-6	1.0	43.47	56.15	34.1

Table 3.16

Tested Mechanical Properties of 35XF Sheet Steel

2% Cold Stretched, Non-Aged Material

Test No.	Strain Rate in./in./sec.	F_y (ksi)	F_u (ksi)	Elongation in 2-in. Gage Length (percent)
LT-1	0.0001	39.20	49.08	36.2
LT-2	0.0001	39.89	49.86	39.3
LT-3	0.01	42.62	52.11	31.4
LT-4	0.01	42.29	52.44	33.5
LT-5	1.0	47.44	57.05	39.8
LT-6	1.0	47.20	57.05	38.7
TT-1	0.0001	38.06	47.73	32.7
TT-2	0.0001	38.14	48.18	34.5
TT-3	1.0	46.36	55.81	32.1
TT-4	1.0	46.45	56.04	37.5

Table 3.17

Tested Mechanical Properties of 35XF Sheet Steel

8% Cold Stretched, Non-Aged Material

Test No.	Strain Rate in./in./sec.	F_y (ksi)	F_u (ksi)	Elongation in 2-in. Gage Length (percent)
LT-1	0.0001	46.05	49.41	29.9
LT-2	0.0001	46.57	49.08	29.7
LT-3	0.01	48.54	52.00	30.0
LT-4	0.01	49.75	52.67	29.5
LT-5	1.0	53.23	57.72	31.5
LT-6	1.0	52.57	56.71	38.5
TT-1	0.0001	44.77	47.84	29.0
TT-2	0.0001	46.14	47.73	22.1
TT-3	1.0	52.35	56.26	28.5
TT-4	1.0	52.59	56.49	26.9

Table 3.18

Tested Mechanical Properties of 35XF Sheet Steel

2% Cold Stretched, Aged Material

Test No.	Strain Rate in./in./sec.	F_y (ksi)	F_u (ksi)	Elongation in 2-in. Gage Length (percent)
LT-1	0.0001	40.02	49.32	31.8
LT-2	0.0001	39.89	50.10	35.7
LT-3	0.01	41.80	51.77	37.3
LT-4	0.01	41.25	51.16	36.1
LT-5	1.0	47.52	56.91	35.9
LT-6	1.0	47.28	56.80	40.9
TT-1	0.0001	38.89	48.73	29.8
TT-2	0.0001	39.27	48.90	31.8
TT-3	1.0	45.02	55.78	34.3
TT-4	1.0	45.23	55.34	32.6

Table 3.19

Tested Mechanical Properties of 35XF Sheet Steel

8% Cold Stretched, Aged Material

Test No.	Strain Rate in./in./sec.	F_y (ksi)	F_u (ksi)	Elongation in 2-in. Gage Length (percent)
LT-1	0.0001	45.69	48.19	34.8
LT-2	0.0001	46.61	49.11	30.7
LT-3	0.01	48.85	51.74	30.6
LT-4	0.01	49.70	52.34	30.7
LT-5	1.0	53.82	57.52	32.0
LT-6	1.0	53.53	57.55	31.1
TT-1	0.0001	45.25	47.60	25.3
TT-2	0.0001	45.64	47.65	28.7
TT-3	1.0	50.83	55.48	28.5
TT-4	1.0	51.25	56.01	28.1

Table 3.20

Average Tested Mechanical Properties of 100XF Sheet Steel

Longitudinal Tension, Virgin Material

Strain Rate in./in./sec.	F_y (ksi)	F_u (ksi)	Elongation (percent)
0.0001	124.25	124.25	9.5
0.01	125.80	125.80	10.2
1.0	128.91	128.91	----

Table 3.21

Average Tested Mechanical Properties of 100XF Sheet Steel

Transverse Tension, Virgin Material

Strain Rate in./in./sec.	F_y (ksi)	F_u (ksi)	Elongation (percent)
0.0001	137.77	137.77	4.9
0.01	139.58	139.58	5.3
1.0	143.57	143.57	6.6

Table 3.22

Average Tested Mechanical Properties of 50XF Sheet Steel

Longitudinal Tension

Amount of Cold Stretching	Strain Rate in./in./sec.	F_y (ksi)	F_u (ksi)	Elongation (percent)
Virgin	0.0001	49.50	72.97	31.0
Virgin	0.01	51.60	74.87	27.0
Virgin	1.0	54.66	78.73	25.8
2%, Non-Aged	0.0001	56.40	73.01	27.0
2%, Non-Aged	0.01	58.67	74.50	25.5
2%, Non-Aged	1.0	62.67	80.32	27.0
8%, Non-Aged	0.0001	71.54	73.86	24.2
8%, Non-Aged	0.01	74.47	76.51	20.9
8%, Non-Aged	1.0	77.59	81.16	20.7
2%, Aged	0.0001	59.23	75.07	29.0
2%, Aged	0.01	60.52	76.16	26.5
2%, Aged	1.0	63.21	81.27	28.8
8%, Aged	0.0001	73.13	73.81	20.0
8%, Aged	0.01	73.15	75.20	21.5
8%, Aged	1.0	75.77	78.94	-----

Table 3.23

Average Tested Mechanical Properties of 50XF Sheet Steel

Transverse Tension

Amount of Cold Stretching	Strain Rate in./in./sec.	F_y (ksi)	F_u (ksi)	Elongation (percent)
Virgin	0.0001	50.59	73.44	26.7
Virgin	0.01	53.21	74.74	26.5
Virgin	1.0	55.55	79.91	27.8
2%, Non-Aged	0.0001	59.29	74.90	23.1
2%, Non-Aged	1.0	68.48	81.29	24.6
8%, Non-Aged	0.0001	73.65	75.88	21.8
8%, Non-Aged	1.0	77.84	82.00	18.5
2%, Aged	0.0001	60.27	75.05	27.7
2%, Aged	1.0	64.79	83.09	22.1
8%, Aged	0.0001	74.30	74.95	19.3
8%, Aged	1.0	77.69	81.65	17.7

Table 3.24

Average Tested Mechanical Properties of 35XF Sheet Steel

Longitudinal Tension

Amount of Cold Stretching	Strain Rate in./in./sec.	F_y (ksi)	F_u (ksi)	Elongation (percent)
Virgin	0.0001	32.87	49.35	38.9
Virgin	0.01	36.40	51.76	36.8
Virgin	1.0	42.37	56.63	40.9
2%, Non-Aged	0.0001	39.55	49.47	37.7
2%, Non-Aged	0.01	42.45	52.27	32.5
2%, Non-Aged	1.0	47.32	57.05	39.3
8%, Non-Aged	0.0001	46.31	49.25	29.7
8%, Non-Aged	0.01	49.15	52.33	29.8
8%, Non-Aged	1.0	52.90	57.21	35.0
2%, Aged	0.0001	39.95	49.71	33.8
2%, Aged	0.01	41.53	51.47	36.7
2%, Aged	1.0	47.40	56.85	38.4
8%, Aged	0.0001	46.15	48.65	32.7
8%, Aged	0.01	49.27	52.04	30.7
8%, Aged	1.0	53.67	57.53	31.5

Table 3.25

Average Tested Mechanical Properties of 35XF Sheet Steel

Transverse Tension

Amount of Cold Stretching	Strain Rate in./in./sec.	F_y (ksi)	F_u (ksi)	Elongation (percent)
Virgin	0.0001	33.51	49.30	36.2
Virgin	0.01	36.39	51.04	37.1
Virgin	1.0	43.23	55.93	35.5
2%, Non-Aged	0.0001	38.10	47.95	33.6
2%, Non-Aged	1.0	46.41	55.93	34.8
8%, Non-Aged	0.0001	45.45	47.79	25.6
8%, Non-Aged	1.0	52.47	56.37	27.7
2%, Aged	0.0001	39.08	48.81	30.8
2%, Aged	1.0	45.13	55.56	33.5
8%, Aged	0.0001	45.45	47.63	27.0
8%, Aged	1.0	51.04	55.75	28.3

given in Table 3.9. The same method was used to determine the yield points included in Table 3.10 for the 50XF sheet steel.

For the gradual-yielding type stress-strain curves as shown in Figure 3.17, the yield point of 35XF steel was determined by the intersection of the stress-strain curve and the straight line drawn parallel to the elastic portion of the stress-strain curve at an offset of 0.002 in./in. A Fortran 77 code was written to determine the yield points presented in Tables 3.11 through 3.19 for the gradual-yielding type curves using the Least Square Method.

ii) Ultimate Tensile Strength, F_u. The ultimate tensile strength was determined from each of the tension tests as the maximum stress that the given tensile coupon could withstand before fracture. This value was calculated by the computer for each test and is presented in Tables 3.9 through 3.19.

iii) Ductility. Ductility is a very important property of high strength sheet steels not only for the structural behavior of the member, but also for the fabrication of the desired structural shape. In this study, ductility was determined by the total elongation in a 2-in. gage length. For this method, the maximum strain recorded by the computer before fracture was taken as the ductility. The maximum elongation was also verified by placing the fractured ends of the specimen together and measuring the distance between the gage marks.

4. Compressive Test Results.

a. Stess-Strain Curves. Figures 3.21 through 3.23 present typical compressive stress-strain curves for the three virgin materials (35XF, 50XF, and 100XF) tested in the longitudinal direction under different

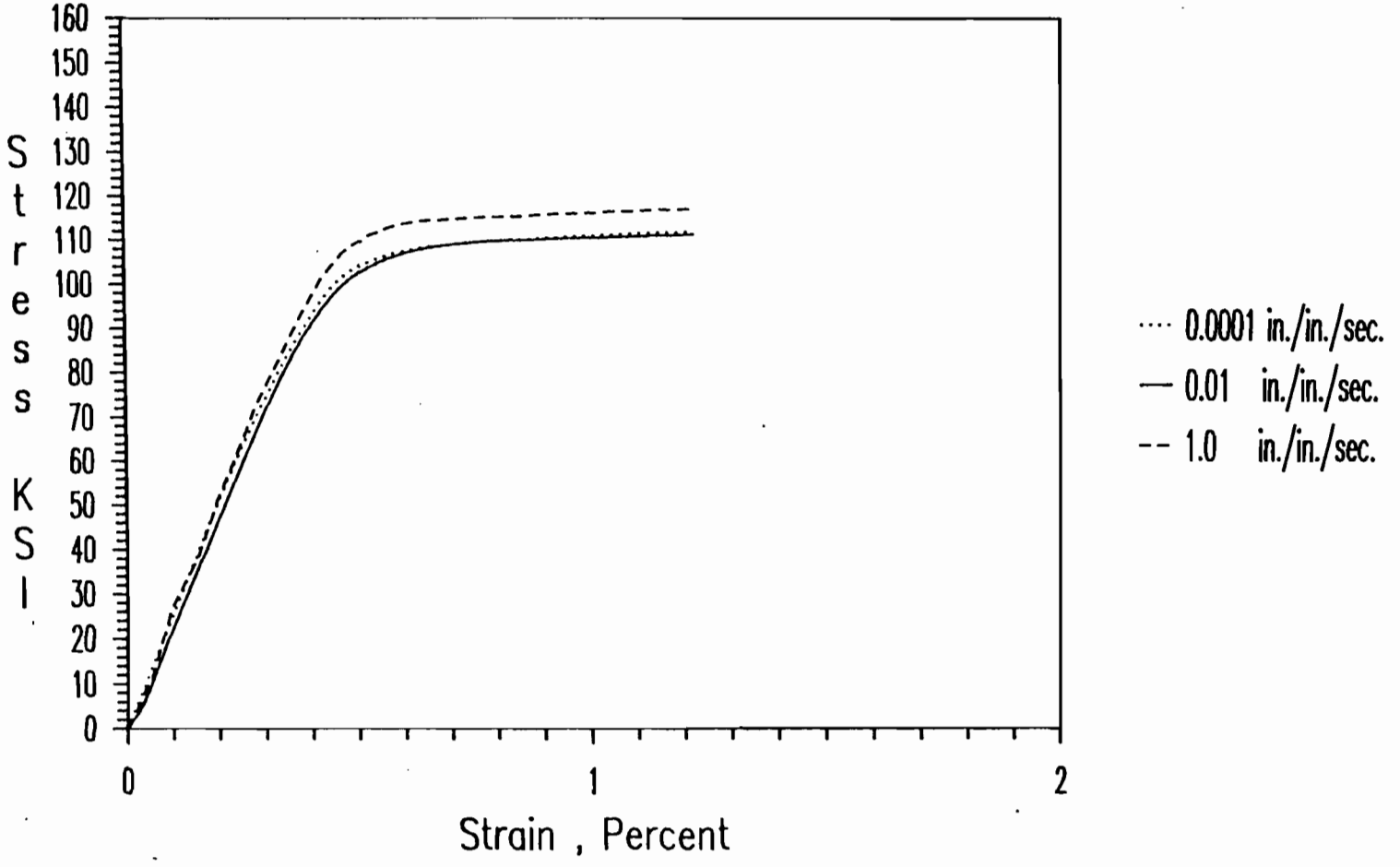

Fig. 3.21 Stress-Strain Curves for 100XF-LC Steel Under Different Strain Rate

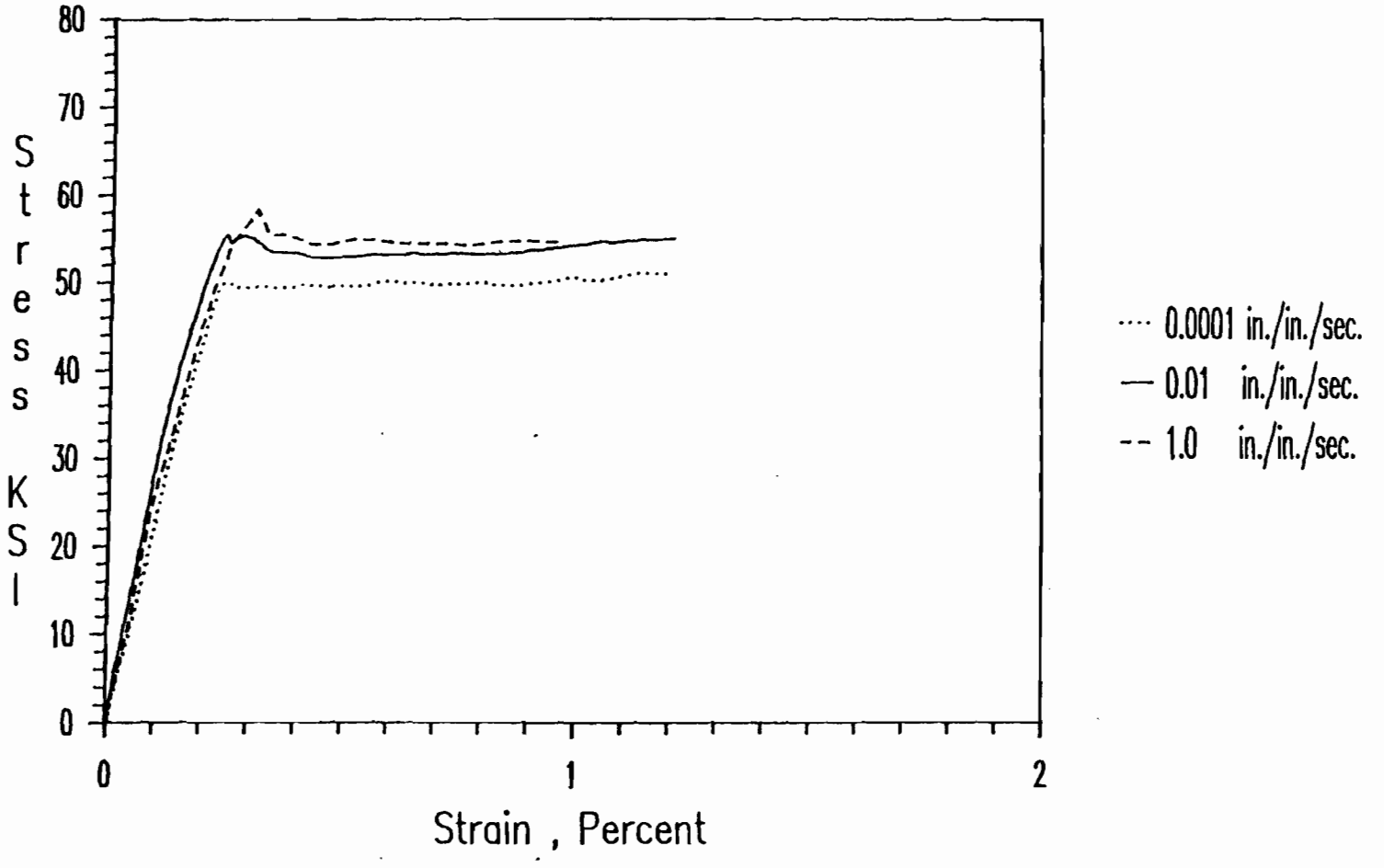

Fig. 3.22 Stress-Strain Curves for 50XF-LC Steel Under Different Strain Rates

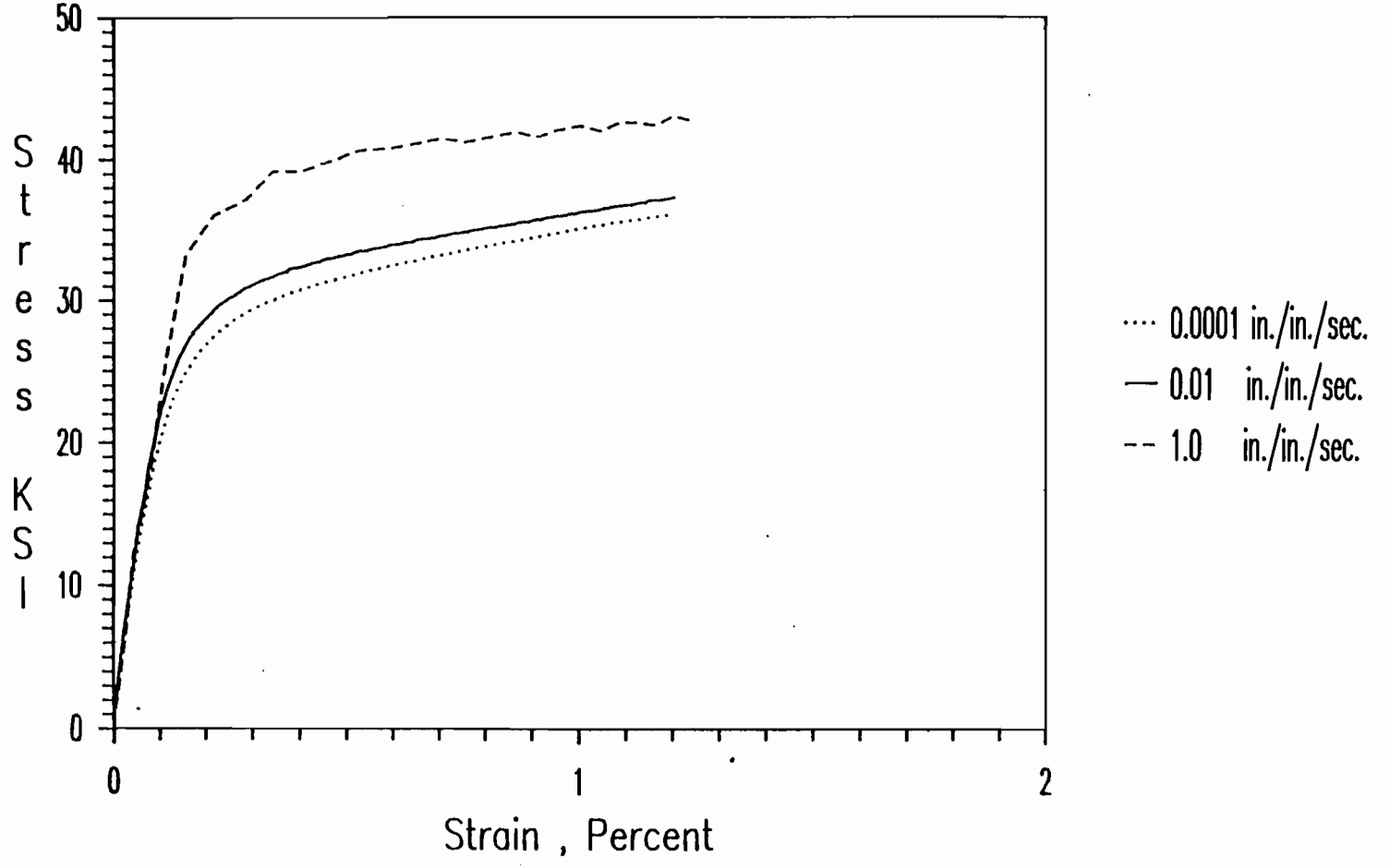

Fig. 3.23 Stress-Strain Curves for 35XF-LC Steel Under Different Strain Rates

strain rates. See Ref. 24 for typical compressive stress-strain curves for the same materials tested in the transverse direction. For the purpose of comparison, each figure includes three stress-strain curves representing the test data obtained from the same material for three different strain rates.

b. Mechanical Properties. The procedures used for determining the mechanical properties of sheet steels are discussed in the subsequent sections (Sections III.B.4.b.i and III.B.4.b.ii). The mechanical properties so determined are the proportional limit F_{pr}, and the yield point F_y. These tested mechanical properties are presented in Tables 3.26 through 3.31 for each individual test. Tables 3.32 through 3.37 present the average values of the mechanical properties for each material tested in either longitudinal compression (LC) or transverse compression (TC) under different strain rates (0.0001, 0.01, or 1.0 in./in./sec.).

i) Proportional Limit, F_{pr}. The proportional limit is usually defined as the point above which the stress-strain curve becomes nonlinear. Since it is often difficult to pinpoint the exact location of the true proportional limit, standard methods are normally used so that comparable values of proportional limit may be determined by different researchers. One such method that is commonly used for aircraft structures and also for cold-formed stainless steel members is the 0.01 percent offset method. For this method a straight line with a slope equal to the modulus of elasticity is drawn parallel to the stress-strain curve and offset such that it intersects the strain axis at 0.01 percent strain. The intersection of this line with the stress-strain curve is defined as the proportional limit.

Table 3.26

Tested Mechanical Properties of 100XF Sheet Steel

Longitudinal Compression

Test No.	Strain Rate in./in./sec.	F_{pr} (ksi)	F_y (ksi)	F_{pr}/F_y
LC-1	0.0001	72.87	107.28	0.68
LC-2	0.0001	71.17	108.23	0.66
LC-3	0.0001	69.71	106.37	0.65
LC-4	0.01	87.90	110.51	0.79
LC-5	0.01	88.98	112.18	0.79
LC-6	0.01	*****	111.08	****
LC-7	1.0	*****	115.16	****
LC-8	1.0	*****	116.61	****
LC-9	1.0	*****	112.97	****

Table 3.27

Tested Mechanical Properties of 100XF Sheet Steel

Transverse Compression

Test No.	Strain Rate in./in./sec.	F_{pr} (ksi)	F_y (ksi)	F_{pr}/F_y
TC-1	0.0001	103.82	123.66	0.84
TC-2	0.0001	102.53	120.41	0.85
TC-3	0.0001	104.63	126.91	0.82
TC-4	0.01	113.27	126.42	0.90
TC-5	0.01	113.18	125.14	0.90
TC-6	0.01	113.91	126.91	0.90
TC-7	1.0	*******	129.98	*****
TC-8	1.0	*******	132.62	*****
TC-9	1.0	*******	132.59	*****

Table 3.28

Tested Mechanical Properties of 50XF Sheet Steel

Longitudinal Compression

Test No.	Strain Rate in./in./sec.	F_{pr} (ksi)	F_y (ksi)	F_{pr}/F_y
LC-1	0.0001	37.63	49.95	0.75
LC-2	0.0001	39.05	49.70	0.79
LC-3	0.0001	39.24	49.40	0.79
LC-4	0.01	42.92	52.82	0.81
LC-5	0.01	41.25	52.82	0.78
LC-6	0.01	35.99	51.90	0.69
LC-7	1.0	*****	54.88	****
LC-8	1.0	*****	54.50	****
LC-9	1.0	*****	54.99	****

Table 3.29

Tested Mechanical Properties of 50XF Sheet Steel

Transverse Compression

Test No.	Strain Rate in./in./sec.	F_{pr} (ksi)	F_y (ksi)	F_{pr}/F_y
TC-1	0.0001	38.69	51.07	0.76
TC-2	0.0001	42.65	51.04	0.84
TC-3	0.0001	43.19	51.13	0.84
TC-4	0.01	50.00	53.46	0.93
TC-5	0.01	50.47	53.38	0.94
TC-6	0.01	51.47	53.36	0.96
TC-7	1.0	*****	55.52	*****
TC-8	1.0	*****	55.88	*****
TC-9	1.0	*****	55.22	*****

Table 3.30

Tested Mechanical Properties of 35XF Sheet Steel

Longitudinal Compression

Test No.	Strain Rate in./in./sec.	F_{pr} (ksi)	F_y (ksi)	F_{pr}/F_y
LC-1	0.0001	17.76	29.95	0.59
LC-2	0.0001	17.98	29.79	0.60
LC-3	0.0001	17.63	29.74	0.59
LC-4	0.01	23.15	32.50	0.71
LC-5	0.01	17.94	31.52	0.57
LC-6	0.01	19.00	31.73	0.60
LC-7	1.0	*****	36.69	*****
LC-8	1.0	*****	36.27	*****
LC-9	1.0	*****	37.76	*****

Table 3.31

Tested Mechanical Properties of 35XF Sheet Steel

Transverse Compression

Test No.	Strain Rate in./in./sec.	F_{pr} (ksi)	F_y (ksi)	F_{pr}/F_y
TC-1	0.0001	23.48	32.76	0.72
TC-2	0.0001	22.45	32.44	0.69
TC-3	0.0001	23.42	32.67	0.72
TC-4	0.01	28.60	37.95	0.75
TC-5	0.01	30.34	36.71	0.83
TC-6	0.01	27.26	35.40	0.77
TC-7	1.0	*****	43.17	****
TC-8	1.0	*****	41.00	****
TC-9	1.0	*****	46.17	****

Table 3.32

Average Tested Mechanical Properties of 100XF Sheet Steel

Longitudinal Compression

Strain Rate in./in./sec.	F_{pr} (ksi)	F_y (ksi)	F_{pr}/F_y
0.0001	71.25	107.29	0.66
0.01	88.44	111.26	0.79
1.0	*****	114.91	****

Table 3.33

Average Tested Mechanical Properties of 100XF Sheet Steel

Transverse Compression

Strain Rate in./in./sec.	F_{pr} (ksi)	F_y (ksi)	F_{pr}/F_y
0.0001	103.66	123.66	0.84
0.01	113.45	126.16	0.90
1.0	******	131.73	****

Table 3.34

Average Tested Mechanical Properties of 50XF Sheet Steel

Longitudinal Compression

Strain Rate in./in./sec.	F_{pr} (ksi)	F_y (ksi)	F_{pr}/F_y
0.0001	38.64	49.68	0.78
0.01	40.05	52.51	0.76
1.0	*****	54.79	****

Table 3.35

Average Tested Mechanical Properties of 50XF Sheet Steel

Transverse Compression

Strain Rate in./in./sec.	F_{pr} (ksi)	F_y (ksi)	F_{pr}/F_y
0.0001	41.51	51.08	0.81
0.01	50.65	53.40	0.95
1.0	*****	55.54	****

Table 3.36

Average Tested Mechanical Properties of 35XF Sheet Steel

Longitudinal Compression

Strain Rate in./in./sec.	F_{pr} (ksi)	F_y (ksi)	F_{pr}/F_y
0.0001	17.79	29.83	0.60
0.01	20.03	31.92	0.63
1.0	*****	36.91	****

Table 3.37

Average Tested Mechanical Properties of 35XF Sheet Steel

Transverse Compression

Strain Rate in./in./sec.	F_{pr} (ksi)	F_y (ksi)	F_{pr}/F_y
0.0001	23.12	32.62	0.71
0.01	28.73	36.69	0.78
1.0	*****	43.45	*****

In this study, the 0.01 percent offset method was chosen to obtain the values of the proportional limit for the steels tested in compression under the strain rates of 0.0001 and 0.01 in./in./sec. as demonstrated graphically in Figure 3.24 for the 35XF-TC-4 curve and listed in tables 3.24 through 3.29. Because of the waving effect of the impact load on the stress-strain curves of the tests conducted at the high strain rate of 1.0 in./in./sec., reliable values for the proportional limit were difficult to obtain.

ii) Yield Strength or Yield Point, F_y. For the types of sheet steels tested in this study in compression, the stress-strain curves of the 50XF sheet steel are the sharp-yielding type, while the stress-strain curves of the 35XF and 100XF steels are the gradual-yielding type.

The yield point of the sharp-yielding steel was determined as the stress where the stress-strain curve becomes horizontal. Typical sharp-yielding stress-strain curves are shown in Figure 3.22 for the 50XF steel in the longitudinal direction. For this case, the lower yield point is given in Tables 3.28 and 3.29 for longitudinal and transverse directions, respectively.

For the gradual-yielding type stress-strain curves as shown in Figure 3.24 for 35XF-TC-4, the yield point of 35XF steel was determined by the intersection of the stress-strain curve and the straight line drawn parallel to the elastic portion of the stress-strain curve at an offset of 0.002 in./in. A Fortran 77 code was written to determine the yield points presented in Tables 3.26, 3.27, 3.30 and 3.31 for the gradual-yielding type curves using the Least Square Method.

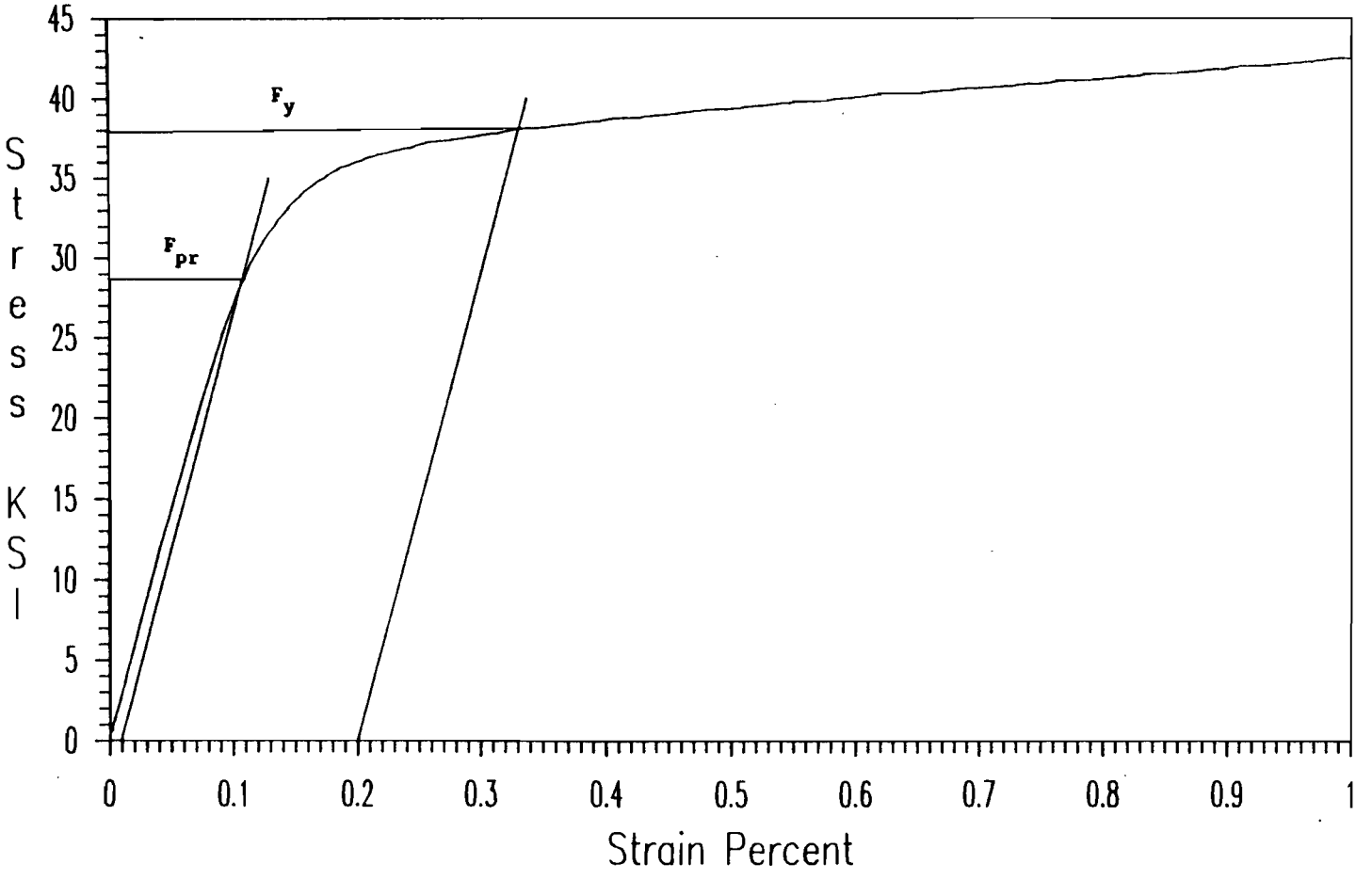

Fig. 3.24 Stress-Strain Curve for Determination of Mechanical Properties of 35XF-TC-4

C. STRUCTURAL MEMBERS

In cold-formed steel design, the effective width approach has been adopted in several specifications to predict the load-carrying capacities of structural members in building and other cold-formed steel structures. Because the effective width formulas included in the current AISI Specification and the Automotive Steel Design Manual [22] are primarily based on the results of static tests of cold-formed steel members corresponding to a strain rate of approximately 1.7×10^{-6} in./in./sec. [3], the objective of this experimental investigation was to study whether the available effective design formulas using dynamic material properties can be adequately used for the design of structural members subjected to dynamic loads. It should be noted that according to ASTM Specification E8, the stress rate should be 100 ksi/min. for obtaining the material static stress-strain curve. This stress rate could be converted to strain rate of $5.65\ 10^{-5}$ in./in./sec. by using Hooke's Law and modulus of elasticity of 29,500 ksi.

In this phase of experimental investigation, 15 hat-section beams and 18 box-shaped stub columns were tested for the study of stiffened elements, while 15 channel-beams and 19 I-shaped stub columns were tested for unstiffened elements. The configurations of test specimens are shown in Figs. 3.25 and 3.26. All specimens used for this phase of study were fabricated from 35XF sheet steels. The stub column specimens were cold-formed by Butler Manufacturing Company in Grandview, Missouri, while the beam specimens were cold-formed by Holloway Machine Company in Springfield, Missouri. The designation of test spcimens used in this study of structural members is presented in Table 3.38. The number of

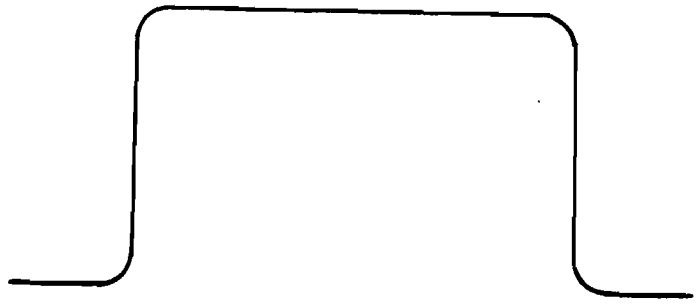

a. Beams

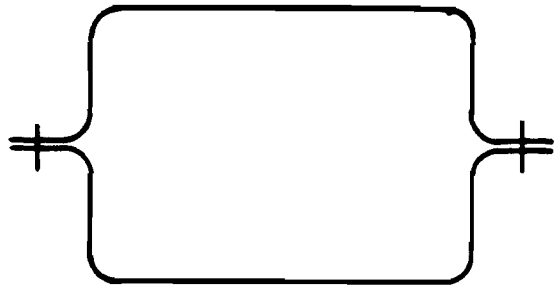

b. Stub Columns

Figure 3.25 Configurations of Test Specimens for Members Having Stiffened Compression Flanges

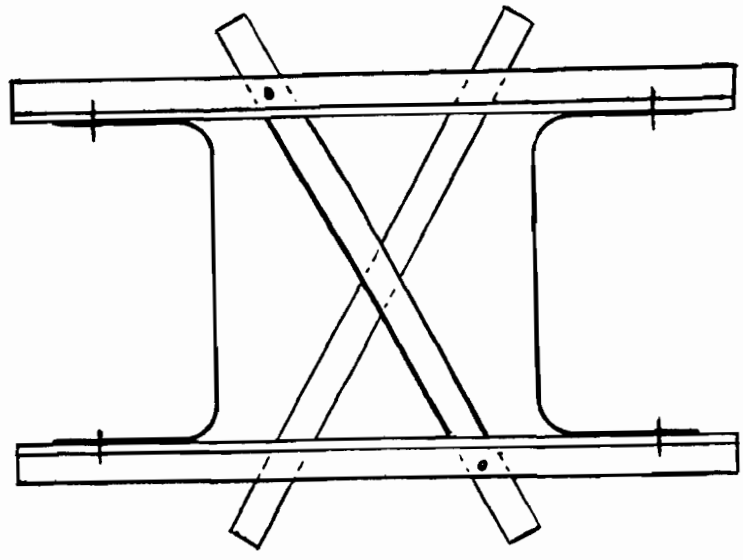

a. Beams

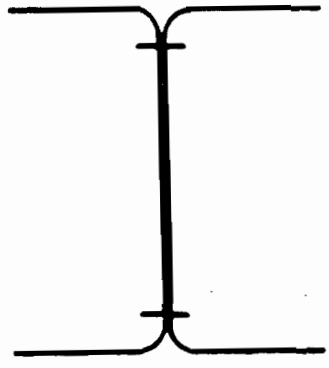

b. Stub Columns

Figure 3.26 Configurations of Test Specimens for Members Having Unstiffened Compression Flanges

Table 3.38

Designation of Test Specimens Used in This Study

1st Digit - Section Type	1st Letter - w/t Ratio	2nd Digit - Strain-Rate (in./in./sec.)	2nd Letter - Test No.
1- Box-Shaped Section Stub-Column Test (Fig. 3.1b)	A- Small Ratio	0- 0.00001	A- 1st Test
	B- Medium Ratio	1- 0.0001	B- 2nd Test
	C- Large Ratio	2- 0.01	
2- I-Shaped Section Stub-Column Test (Fig. 3.2b)		3- 0.1	
3- Hat Section for Beam Test (Fig. 3.1a)			
4- Channel Section for Beam Test (Fig. 3.2a)			

tests are given in Tables 3.39 through 3.42. As shown in these tables, a total of 67 specimens have been tested under different strain rates.

The strain rates used in the tests varied from 10^{-5} to 0.1 in./in./sec. as given in Tables 3.39 through 3.42. Also included in these tables is the actuator speed used for the tests. The ranges of w/t ratios used in this study were from 26.67 to 76.08 for stiffened elements, and from 8.93 to 20.69 for unstiffened elements.

1. Material Properties. The 35XF sheet steel used to fabricate the structural members is the same as that used to cut the tensile and compressive coupons. The mechanical properties of this sheet steel in tension and compression have been established under different strain rates and included in Section III.B. Table 3.43 gives the average values of mechanical properties including yield stress (F_y), proportional limit (F_{pr}), tensile strength (F_u), and elongation in 2-in. gage length tested under different strain rates. The thickness of this sheet steel is 0.085 in. Typical stress-strain curves for longitudinal tension and longitudinal compression of this material under different strain rates were shown previously in Figs. 3.17 and 3.23, respectively.

2. Beam Tests for Stiffened Elements.

a. Specimens. Fifteen (15) beam specimens were tested to study the local buckling and post-buckling strengths of stiffened elements of the 35XF steel material using different strain rates. The strain rates used for the tests ranged from 10^{-5} to 0.01 in./in./sec. Three different beam sections were used. Figure 3.27 shows the hat sections designed for the

Table 3.39

Number of Performed Stub Column Tests

Box Sections Having Stiffened Compression Elements

Spec. No.	Test Speed in./min.	Strain Rate (in./in./sec.)	w/t	L/r	No. of Tests Performed
1A1A	0.072	0.0001	27.15	12.26	1
1A1B	0.072	0.0001	27.39	12.26	1
1A2A	7.2	0.01	26.92	12.26	1
1A2B	7.2	0.01	27.06	12.26	1
1A3A	72.0	0.1	27.31	12.26	1
1A3B	72.0	0.1	27.40	12.26	1
1B1A	0.084	0.0001	38.93	10.98	1
1B1B	0.084	0.0001	38.17	10.98	1
1B2A	8.4	0.01	38.86	10.98	1
1B2B	8.4	0.01	39.10	10.98	1
1B3A	84.0	0.1	38.86	10.98	1
1B3B	84.0	0.1	38.96	10.98	1
1C1A	0.09	0.0001	52.69	11.27	1
1C1B	0.09	0.0001	52.96	11.27	1
1C2A	9.0	0.01	52.20	11.27	1
1C2B	9.0	0.01	53.06	11.27	1
1C3A	90.0	0.1	53.15	11.27	1
1C3B	90.0	0.1	53.39	11.27	1
Total					18

Table 3.40

Number of Performed Stub Column Tests

I-Sections Having Unstiffened Compression Elements

Spec. No.	Test Speed in./min.	Strain Rate (in./in./sec.)	w/t	L/r	No. of Tests Performed
2A1A	0.054	0.0001	8.93	18.73	1
2A1B	0.054	0.0001	9.04	18.73	1
2A2A	5.4	0.01	8.93	18.73	1
2A2B	5.4	0.01	9.10	18.73	1
2A3A	54.0	0.1	8.93	18.73	1
2A3B	54.0	0.1	8.96	18.73	1
2B1A	0.06	0.0001	13.34	17.65	1
2B1B	0.06	0.0001	13.41	17.65	1
2B2A	6.0	0.01	13.40	17.65	1
2B2B	6.0	0.01	13.37	17.65	1
2B3A	60.0	0.1	13.34	17.65	1
2B3B	60.0	0.1	13.42	17.65	1
2C0A	0.0084	0.00001	20.69	15.64	1
2C1A	0.084	0.0001	20.85	15.64	1
2C1B	0.084	0.0001	20.76	15.64	1
2C2A	8.4	0.01	20.97	15.64	1
2C2B	8.4	0.01	20.81	15.64	1
2C3A	84.0	0.1	20.93	15.64	1
2C3B	84.0	0.1	20.87	15.64	1
Total					19

Table 3.41

Number of Performed Beam Tests

Hat Sections Having Stiffened Compression Flanges

Spec. No.	Test Speed in./min.	Strain Rate (in./in./sec.)	w/t	L (in.)	No. of Tests Performed
3A0A	0.023	0.00001	29.15	47	1
3A1A	0.23	0.0001	30.00	47	1
3A1B	0.23	0.0001	29.85	47	1
3A2A	23.0	0.01	29.05	47	1
3A2B	23.0	0.01	30.17	47	1
3B0A	0.038	0.00001	55.91	77	1
3B1A	0.38	0.0001	55.11	77	1
3B1B	0.38	0.0001	55.91	77	1
3B2A	38.0	0.01	55.82	77	1
3B2B	38.0	0.01	55.97	77	1
3C0A	0.15	0.00001	76.17	95	1
3C1A	1.50	0.0001	76.64	95	1
3C1B	1.50	0.0001	76.57	95	1
3C2A	150.0	0.01	76.62	95	1
3C2B	150.0	0.01	76.03	95	1
Total					15

Table 3.42

Number of Performed Beam Tests

Channel Sections Having Unstiffened Compression Flanges

Spec. No.	Test Speed in./min.	Strain Rate (in./in./sec.)	w/t	L (in.)	No. of Tests Performed
4A0A	0.043	0.00001	9.28	41	1
4A1A	0.43	0.0001	9.16	41	1
4A1B	0.43	0.0001	9.16	41	1
4A2A	43.0	0.01	9.22	41	1
4A2B	43.0	0.01	9.03	41	1
4B0A	0.045	0.00001	15.13	47	1
4B1A	0.45	0.0001	15.16	47	1
4B1B	0.45	0.0001	14.93	47	1
4B2A	45.0	0.01	15.04	47	1
4B2B	45.0	0.01	15.16	47	1
4C0A	0.082	0.00001	20.93	69	1
4C1A	0.82	0.0001	20.99	69	1
4C1B	0.82	0.0001	20.93	69	1
4C2A	82.0	0.01	20.99	69	1
4C2B	82.0	0.01	20.93	69	1
Total					15

Table 3.43

Average Mechanical Properties of 35XF Sheet Steel used in the Experimental Study Under Different Strain Rates

Strain Rate in./in./sec.	$(F_y)_c$ (ksi)	$(F_{pr})_c$ (ksi)	$(F_y)_t$ (ksi)	$(F_u)_t$ (ksi)	Elongation (%)
0.0001	29.83	17.79	32.87	49.35	38.90
0.01	31.92	20.03	36.40	51.76	36.80
1.0	36.91	*****	42.37	56.63	40.90

Notes:

1) $(F_y)_c$ and $(F_{pr})_c$ are based on longitudinal compression coupon tests.

2) $(F_y)_t$ and $(F_u)_t$ and Elongation are determined from longitudinal tension coupon tests.

3) Elongation was measured by using a 2-in. gage length.

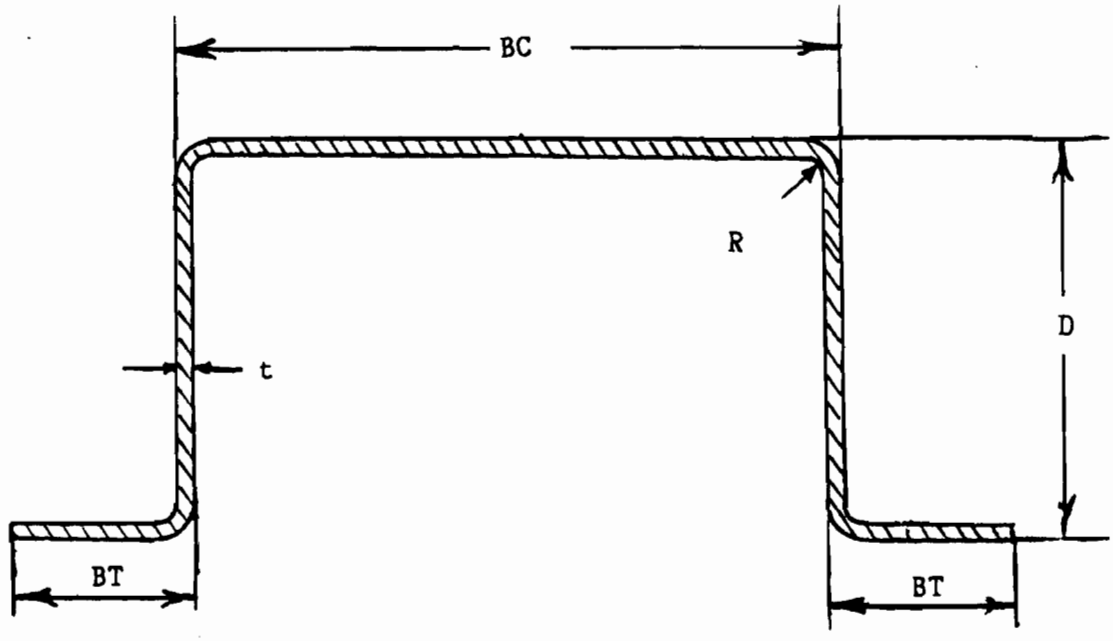

Figure 3.27 Hat Sections Used for Beam Tests

study of post-buckling strength of stiffened elements. Table 3.44 gives the average cross-sectional dimensions of hat sections, thicknesses of sheet steels, w/t ratios, span lengths of specimens, and failure loads. The width-to-thickness ratios, w/t, ranged from 29.62 to 76.08.

All steel sheets were sheared to the designed sizes before the specimens were formed. All specimens were formed with an inside bend radius of 5/32 in.

b. Strain Measurements. Twelve foil strain gages were placed on the compression flange, tension flanges, and webs of each beam specimen for measuring compressive and tensile strains. Figure 3.28 shows the locations of strain gages, numbered from 1 to 12, placed on beam specimens. Eight strain gages (No. 3 through 8, 11, and 12) were placed at the midspan of beam specimens. In addition, two paired strain gages ((1,2) and (9,10)) were placed along the longitudinal centerline of the compression flange at a distance equal to the overall width of the compression flange on each side of the midspan of the specimens. All three paired strain gages along the centerline of the compression flange were used to detect local buckling of the compression flange. As shown in Fig. 3.29, the critical buckling load is determined from the load-versus-strain diagram by using the modified strain reversal method, which is discussed in Ref. 119. Strain gages (No. 5 and 6) placed along both edges of the compression flange were used to measure edge strains. The edge stress of stiffened elements can be determined from these strain readings using the stress-strain curve. On each side of the tension flanges, a strain gage (No. 11 or 12) was placed along the edge of each tension

Table 3.44

Dimensions of Beam Specimens with Stiffened Flanges

Fabricated from 35XF Sheet Steel

Specimen	BC (in.)	D (in.)	BT (in.)	t	w/t (in.)	L (in.)	P_u (kips)
3A0A	2.960	1.510	1.010	0.085	29.15	43.00	5.69
3A1A	3.033	1.462	1.012	0.085	30.00	43.00	5.43
3A1B	3.020	1.477	1.017	0.085	29.85	43.00	5.72
3A2A	2.952	1.515	1.020	0.085	29.05	43.00	6.31
3A2B	3.047	1.470	1.012	0.085	30.17	43.00	6.39
3B0A	5.235	2.445	1.235	0.085	55.91	73.00	6.38
3B1A	5.167	2.460	1.255	0.085	55.11	73.00	6.54
3B1B	5.235	2.435	1.230	0.085	55.91	73.00	6.49
3B2A	5.227	2.435	1.220	0.085	55.82	73.00	6.97
3B2B	5.240	2.440	1.232	0.085	55.97	73.00	7.63
3C0A	6.957	2.926	1.490	0.085	76.17	91.00	6.53
3C1A	6.997	2.947	1.483	0.085	76.64	91.00	6.99
3C1B	6.991	2.954	1.481	0.085	76.57	91.00	6.96
3C2A	6.995	2.934	1.483	0.085	76.62	91.00	7.45
3C2B	6.945	2.945	1.485	0.085	76.03	91.00	7.42

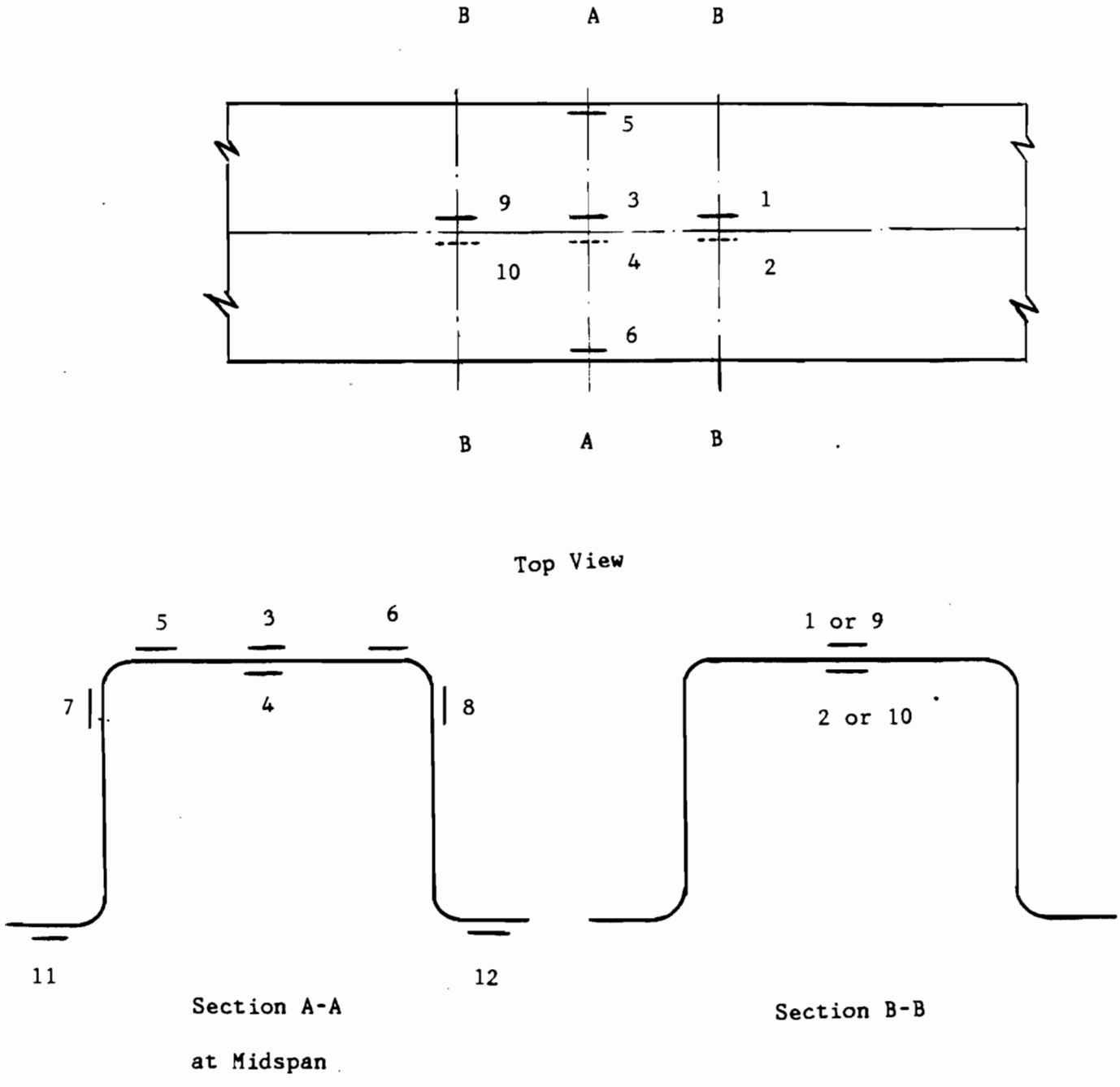

Figure 3.28 Locations of Strain Gages on Hat Sections

Table 3.44

Dimensions of Beam Specimens with Stiffened Flanges

Fabricated from 35XF Sheet Steel

Specimen	BC (in.)	D (in.)	BT (in.)	t	w/t (in.)	L (in.)	P_u (kips)
3A0A	2.960	1.510	1.010	0.085	29.15	43.00	5.69
3A1A	3.033	1.462	1.012	0.085	30.00	43.00	5.43
3A1B	3.020	1.477	1.017	0.085	29.85	43.00	5.72
3A2A	2.952	1.515	1.020	0.085	29.05	43.00	6.31
3A2B	3.047	1.470	1.012	0.085	30.17	43.00	6.39
3B0A	5.235	2.445	1.235	0.085	55.91	73.00	6.38
3B1A	5.167	2.460	1.255	0.085	55.11	73.00	6.54
3B1B	5.235	2.435	1.230	0.085	55.91	73.00	6.49
3B2A	5.227	2.435	1.220	0.085	55.82	73.00	6.97
3B2B	5.240	2.440	1.232	0.085	55.97	73.00	7.63
3C0A	6.957	2.926	1.490	0.085	76.17	91.00	6.53
3C1A	6.997	2.947	1.483	0.085	76.64	91.00	6.99
3C1B	6.991	2.954	1.481	0.085	76.57	91.00	6.96
3C2A	6.995	2.934	1.483	0.085	76.62	91.00	7.45
3C2B	6.945	2.945	1.485	0.085	76.03	91.00	7.42

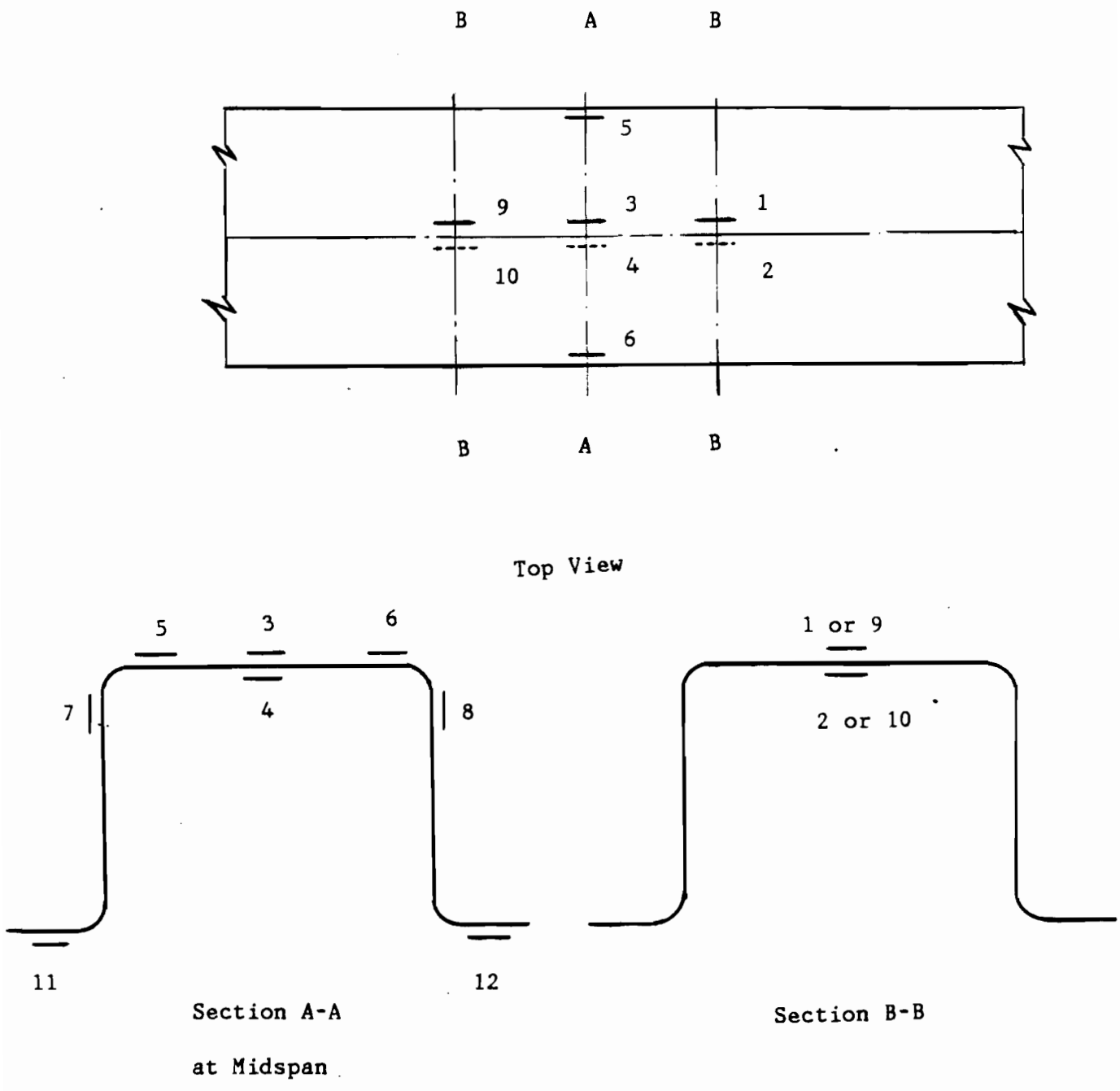

Figure 3.28 Locations of Strain Gages on Hat Sections

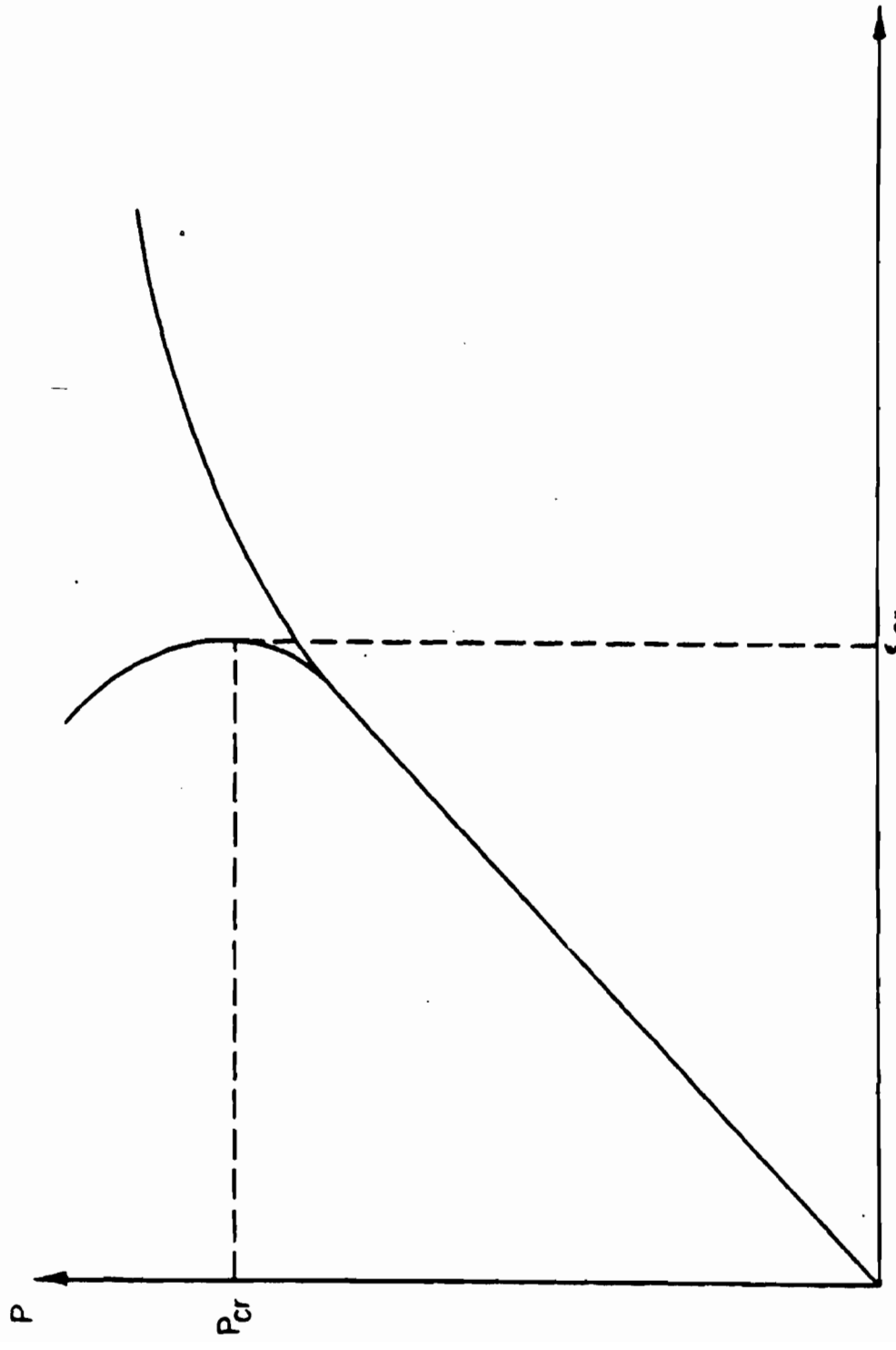

Figure 3.29 Modified Strain Reversal Method Used to Determine the Critical Buckling Load

flange as shown in Fig. 3.28 to study the shift of the neutral axis during the test. Strain gages (No. 7 and 8) placed on the top of the webs were used to study the distribution of compressive stress in the web.

c. Instrumentation and Test Procedure. All beam specimens were tested using the 880 Material Test System described in Section III.B.2.a.iii. The data acquisition system used in this study is the same as that used for the study of material tests. It has 64 simultaneously sampling input channels. Two channels were connected to the MTS machine to record loads and actuator displacements as the test runs. Thirty channels were connected to a 2120 Measurements Group Strain Gage Conditioner and Amplifier System to measure the strain gage outputs. Four channels were connected to Daytronic Linear Variable Differential Transformer (LVDT) Conditioners to measure the LVDT outputs. After the data have been acquired, it was downloaded into the computer for analysis. A Data General mini-computer was used to coordinate the electronic equipment and to store and analyze the test data.

Following fabrication of the test specimen and placement of strain gages, the beam specimen was placed in the 880 MTS test system on the top of an 8-feet long W-Shape steel beam which was supported by the lower compression platen of the MTS machine. The test setup for beam specimens is shown in Figs. 3.30 and 3.31. As shown in Fig. 3.30, the beam was simply supported and the load was applied from the lower compression platen to the specimen. T-sections were used at L/8 points to support the beam for preventing web crippling failure. Six 1/4-in. dia., high strength bolts were used to connect each T-section to the web of the specimen. To prevent premature web crippling failure, one 4-in. wide

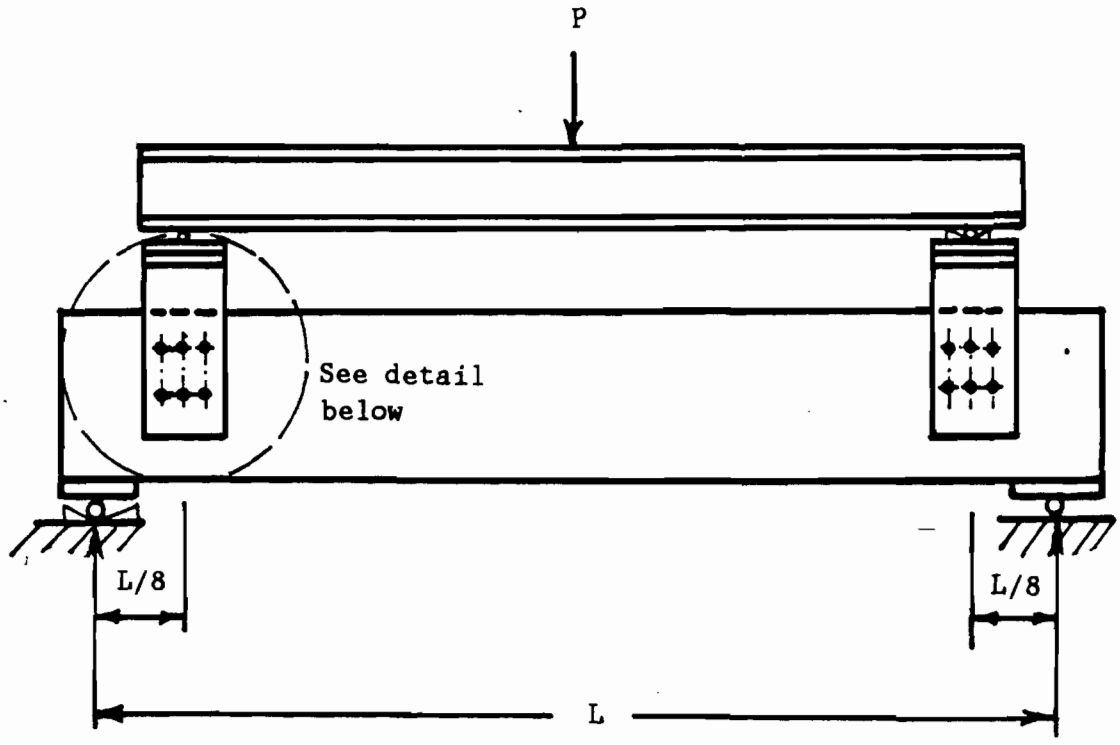

(a) Test Setup

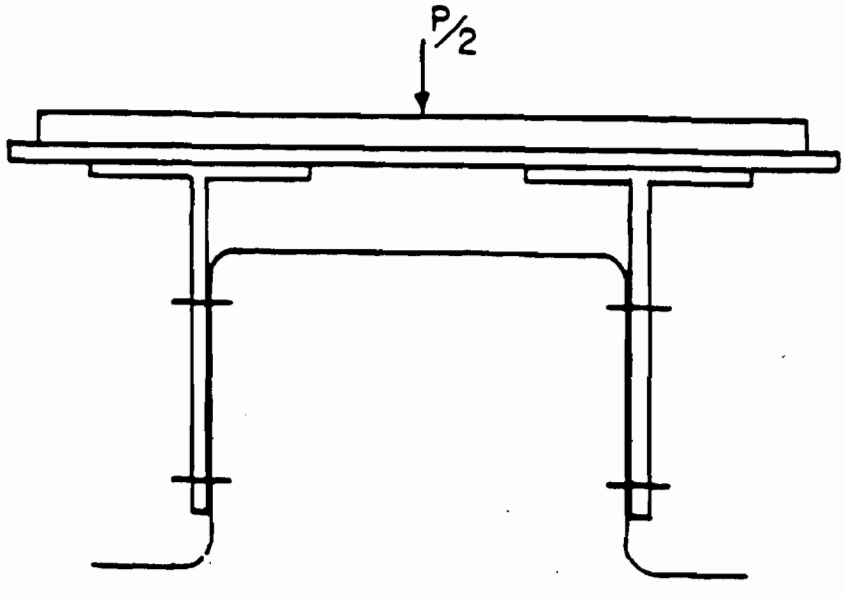

(b) Detail at Loading Points

Figure 3.30 Test Setup for Beams with a Stiffened Flange

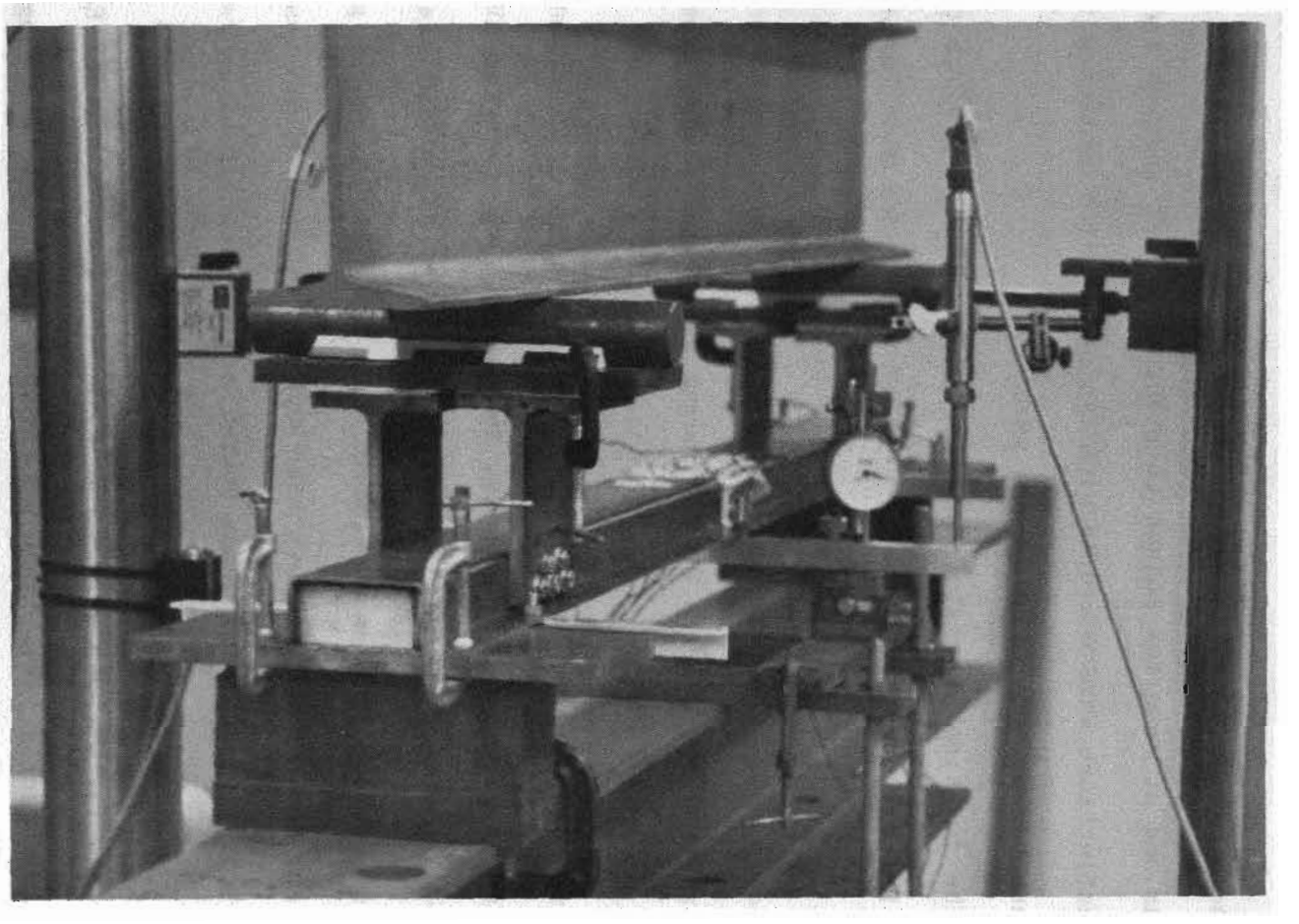

Figure 3.31 End View for the Hat Beam Test Setup

bearing plate and a wooden block placed between specimen webs were used at each end of the specimen. The tension flanges at both ends of the beam specimens are clamped to bearing plates. During the fabrication of specimens, three aluminum bars were connected to the tension flanges at midspan and at quarter points to prevent the hat section from opening. Beam deflections were measured with two LVDTs which contacted the midspan aluminum bar at both sides of the specimen.

The function generator was then programmed to produce the desired ramp. For all the tests, the range 2 of the stroke mode (maximum stroke = 2.5 in.) was selected as the control mode to maintain a constant actuator speed. The strain rates used in the tests ranged from 10^{-5} to 0.01 in./in./sec. and the corresponding test times ranged from 3000 to 3 sec.

During the tests, the applied load, actuator displacement, strains from twelve strain gage outputs, and deflections from two LVDT outputs were recorded and stored in the CAMAC memory. The CAMAC sampling rate depends on the test time and varied from 5 to 25000 readings per second. This rate depends on the test time and was set before the test started. Table 3.45 gives the frequency number and the corresponding readings per second. Following the completion of the test, the data were downloaded and stored in the Data General Computer for later analysis. Each of the 64 CAMAC channels takes 16384 data points during the test (regardless of the test time). The test data file occupied 2 megabytes of the DG memory. All specimens were loaded to failure.

d. Test Results. For the study of post-buckling strengths of stiffened elements, beam specimens were designed to have various w/t ra-

Table 3.45

The CAMAC Frequencies and the

Corresponding Sampling Rates

Frequency Number	Reading Per Seconds
0	5
1	10
2	25
3	50
4	100
5	250
6	500
7	1000
8	2500
9	5000
10	10000
11	25000

tios for the compression flange. Local buckling of the compression flange can be detected from the readings of the paired strain gages located on the centerline of the flange. Waving of the compression flange was observed as the load continued to increase beyond the buckling load. Because of the redistribution of compressive stress across the compression flange, the specimen failed when the maximum strength of the compression flange was reached. Typical failure of the beam specimen is shown in Fig. 3.32. Failure of test specimens always occurred in the middle portion of the beam close to the L/8 points.

The location of the neutral axis was determined from strain gage readings. Figure 3.33 shows the positions of the neutral axis. The neutral axis shifted away from the top flange as the load increased. As mentioned above, beam deflection was carefully measured at both sides of the midspan of the specimen. In the early stage of the slow test, beam deflection increased linearly corresponding to the applied load. The nonlinear load-deflection relationship was noted when local buckling occurred in the compression flange of the specimen. A typical strain-time curve for the slow strain-rate test is presented in Fig. 3.34. Typical load-strain curves for the paired strain gages at the middle of the stiffened flange are shown in Fig. 3.35. This plot is used for determination of critical buckling load.

3. Stub Column Tests for Stiffened Elements

a. Specimens. In this phase of experimental investigation, eighteen (18) stub column specimens were tested to study the effect of strain rate

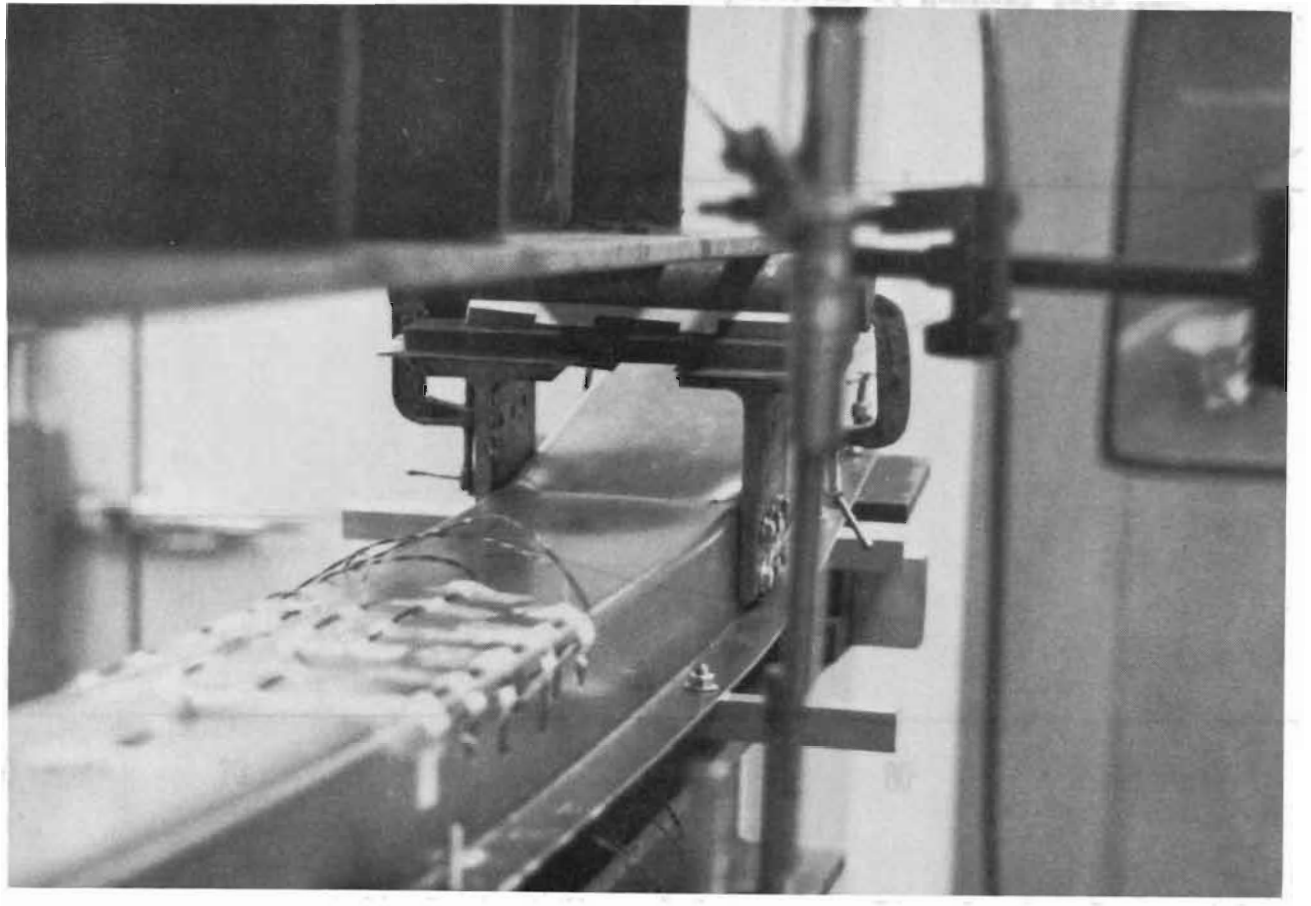

Figure 3.32 Typical Failure of Hat Beams with a Stiffened Flange

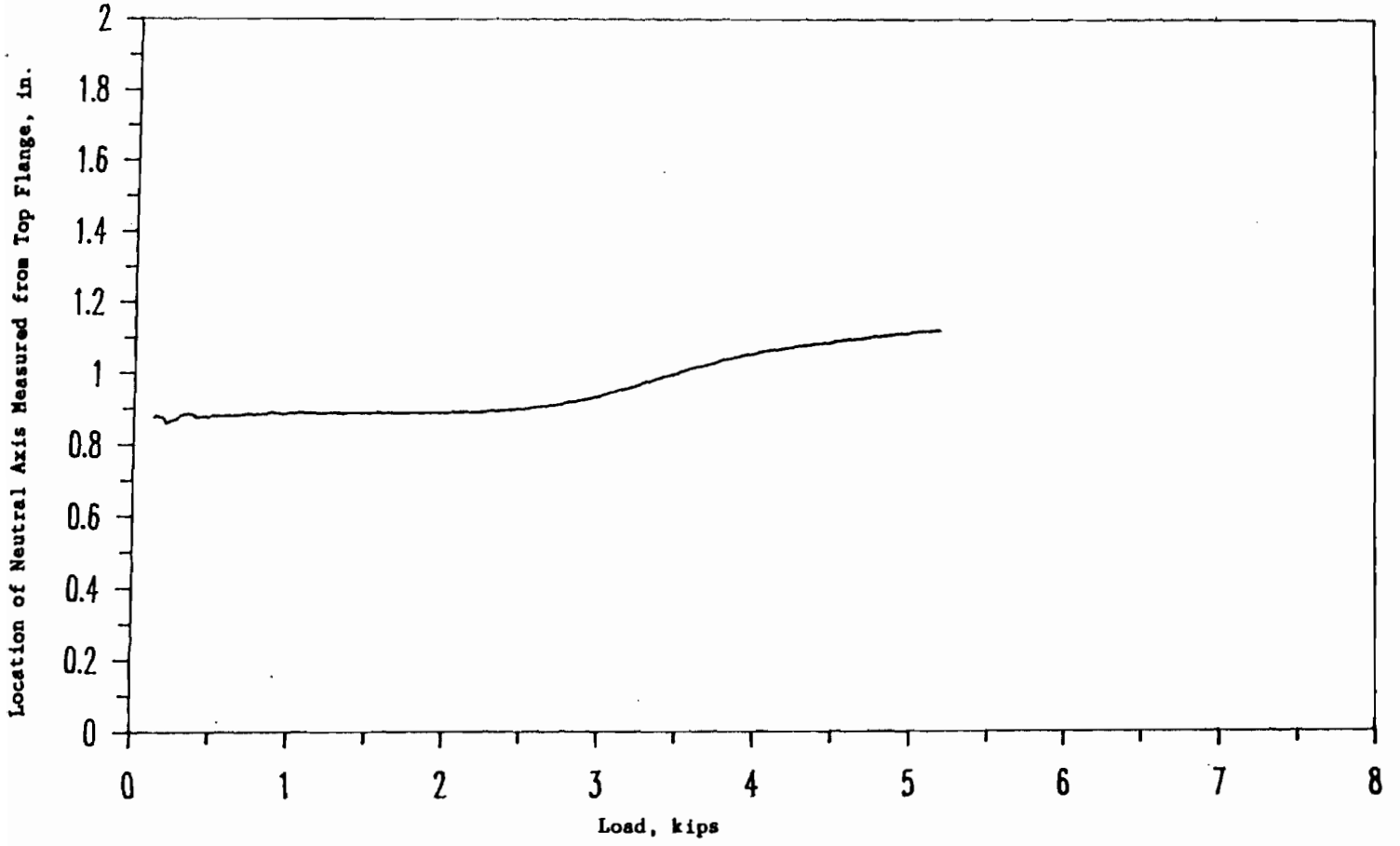

Figure 3.33 Typical Plot of Load vs. Location of Neutral Axis for Beams with a Stiffened Flange (Specimen 3A0A)

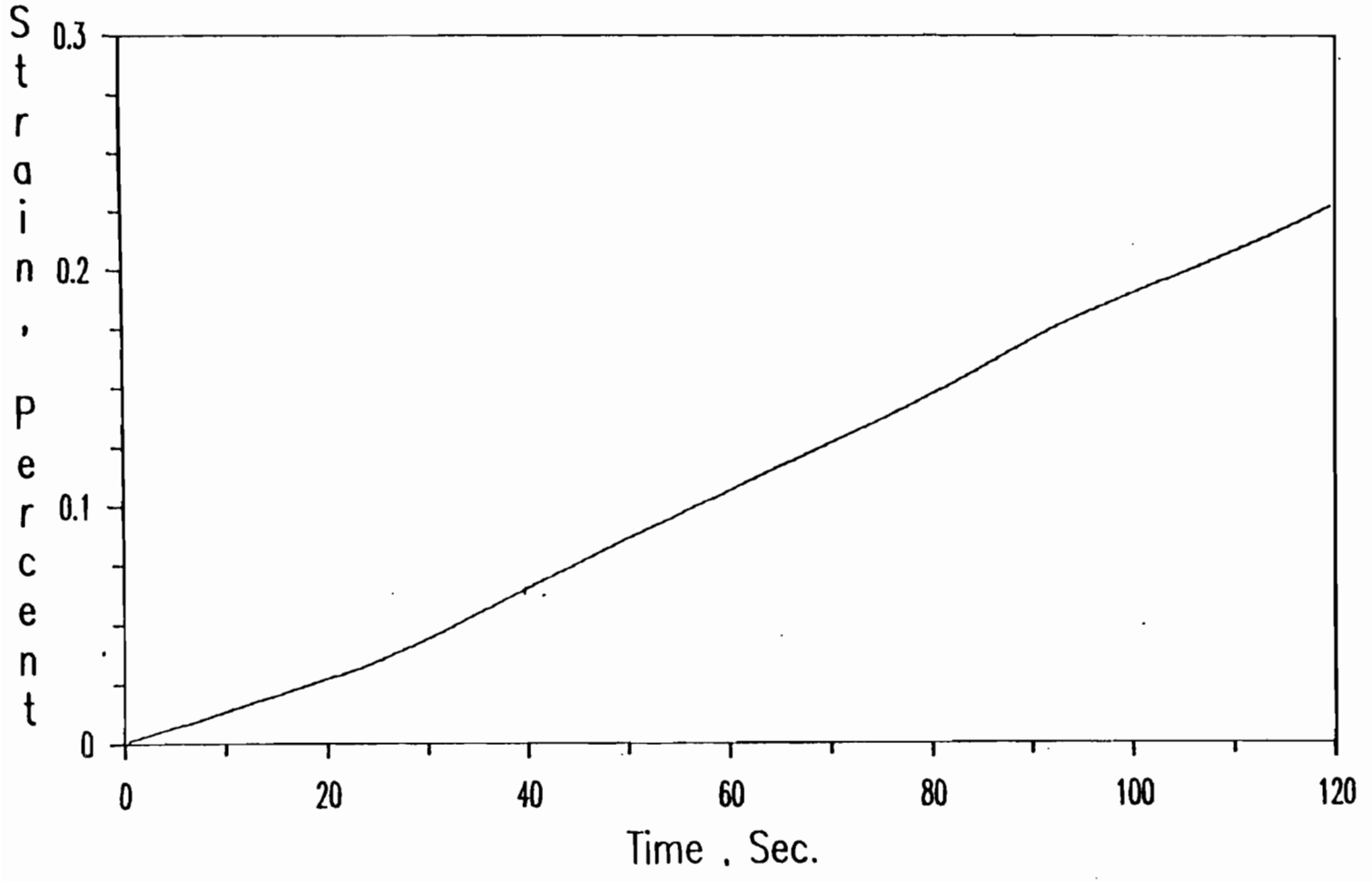

Figure 3.34 Typical Plot of Strain vs. Time for Hat Beams with a Stiffened Flange (Strain Gage # 5 for Specimen 3A1A)

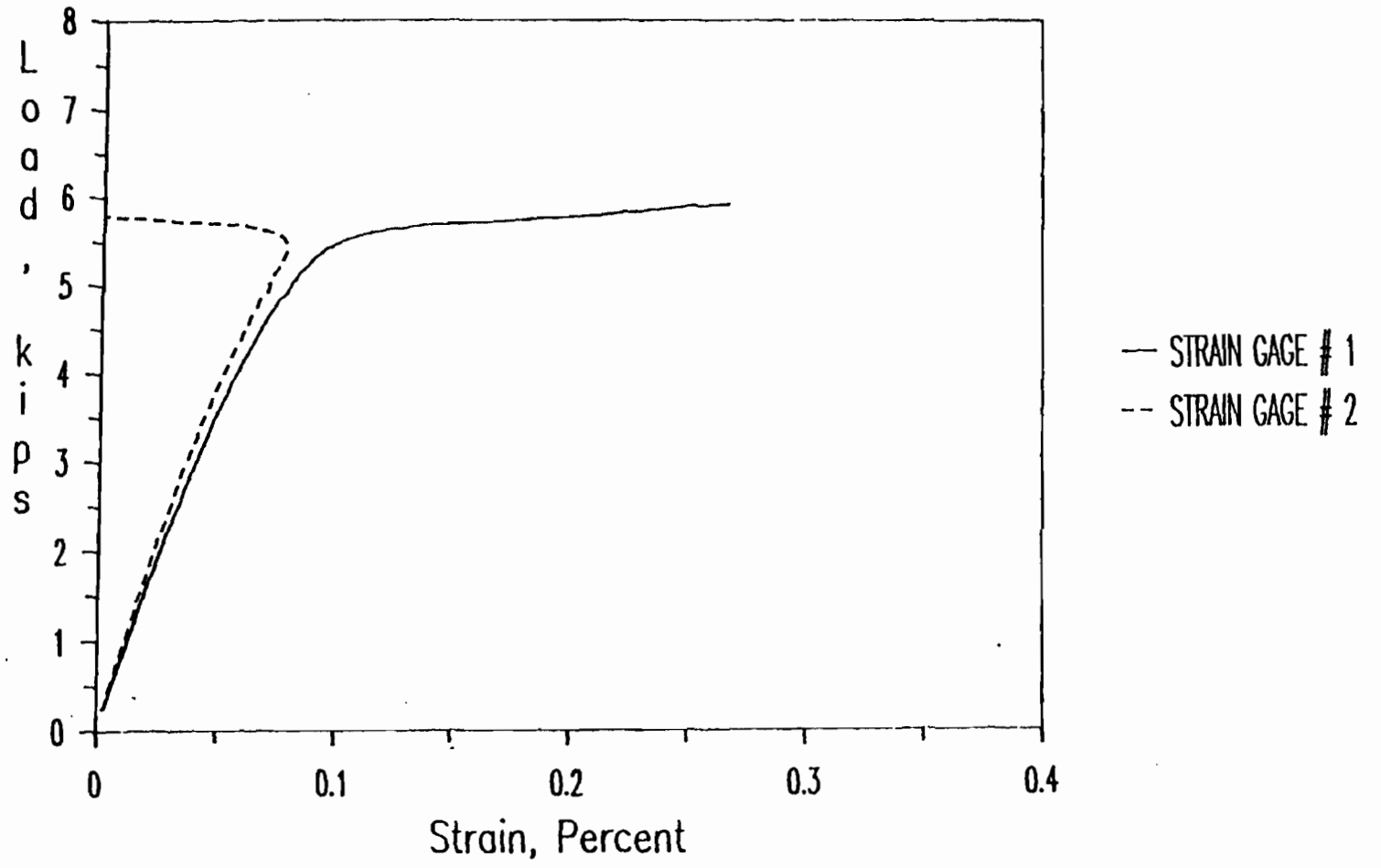

Figure 3.35 Load-Strain Curves of Strain Gages # 1 and 2 Installed at the Center of the Stiffened Flange (Specimen 3C0A)

on the local and post-buckling strengths of stiffened elements for 35XF steel material.

As shown in Fig. 3.36, box-shaped stub columns were used for this phase of study. All stub columns were fabricated by connecting two identical hat sections through the unstiffened flanges. High strength bolts (1/4-in. dia.) with washers were used for the fabrication of stub columns. The spacing of bolts was determined on the basis of the requirements of the AISI Specification. The steel sheets were sheared to the designed sizes of each hat section. Great care was taken when the stub-column specimens were fabricated. Both ends of the stub-column specimens were milled to ensure that they were flat and parallel.

Table 3.46 gives the average cross sectional dimensions of stub-column specimens, the measured thicknesses of sheet steels, and the failure loads. In this phase of experimental study, the w/t ratios of stiffened elements ranged from 26.67 to 53.15. The strain rates ranged from 0.0001 to 0.1 in./in./sec. The webs of all hat sections were designed to be fully effective. The unstiffened flanges were connected to satisfy the requirements of the AISI Specification.

The lengths of stub-column specimens are also given in Table 3.46. In order to avoid overall column buckling, the length of each stub-column specimen is longer than three times the largest dimension of the cross section of the specimen and less than 20 times the least radius of gyration as recommended in Ref. 116. This criterion was also adopted in Part VII (Test Procedure) of the 1986 AISI Cold Formed Steel Design Manual.

b. Strain Measurements. Eight foil strain gages were used to measure strains at midheight of the stub column specimen. The location

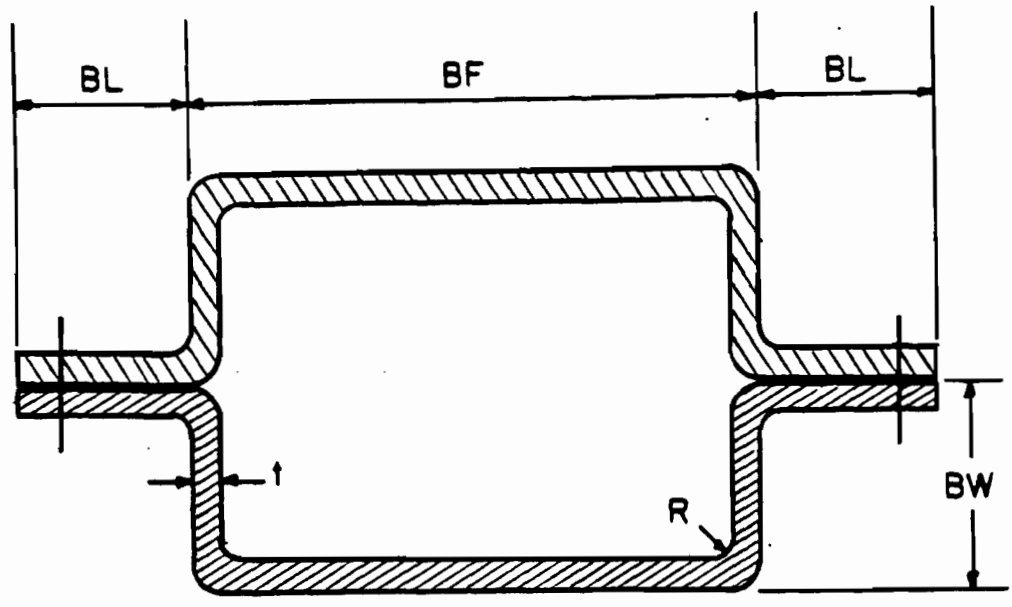

Figure 3.36 Cross Sections of Box-Shaped Stub Columns Used for the Study of Stiffened Elements

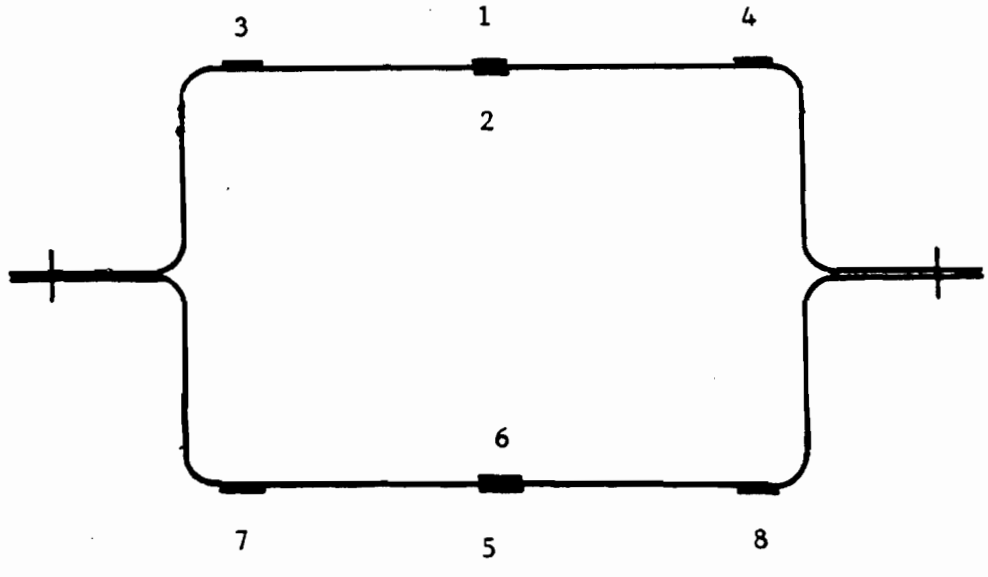

Figure 3.37 Locations of Strain Gages at Midheight of Box-Shaped Stub Columns

Table 3.46

Dimensions of Stub Columns with Stiffened Flanges

Fabricated from 35XF Sheet Steel

Specimen	BF (in.)	BW (in.)	BL (in.)	w/t	Gross Area ($in.^2$)	L (in.)	P_u (kips)
1A1A	2.790	1.492	0.916	27.15	1.2060	12.03	46.12
1A1B	2.811	1.482	0.915	27.39	1.2060	12.02	44.89
1A2A	2.771	1.484	0.918	26.92	1.2010	12.03	50.02
1A2B	2.783	1.482	0.916	27.06	1.2060	12.03	49.29
1A3A	2.804	1.470	0.916	27.31	1.2009	12.03	53.54
1A3B	2.812	1.467	0.915	27.40	1.2009	12.03	54.37
1B1A	3.792	1.990	0.922	38.93	1.5477	14.99	49.19
1B1B	3.812	1.985	0.918	39.17	1.5480	13.97	53.54
1B2A	3.786	1.978	0.918	38.86	1.5412	13.84	56.28
1B2B	3.806	1.982	0.919	39.10	1.5463	13.94	57.01
1B3A	3.786	1.992	0.919	38.86	1.5463	13.84	64.78
1B3B	3.794	1.982	0.918	38.96	1.5440	13.94	60.87
1C1A	4.961	2.523	0.919	52.69	1.9266	15.06	56.76
1C1B	4.984	2.513	0.922	52.96	1.9282	15.06	56.52
1C2A	4.920	2.524	0.920	52.20	1.9203	14.81	61.02
1C2B	4.993	2.519	0.922	53.06	1.9317	15.12	64.58
1C3A	5.000	2.526	0.919	53.15	1.9343	15.09	73.96
1C3B	5.021	2.510	0.922	53.39	1.9334	15.00	69.27

of strain gages, numbered from 1 to 8, is shown in Fig. 3.37. An additional eights strain gages were added only to the hat sections with large w/t ratio (w/t= 53.15). They were placed at a distance equal to half of the overall width of the compression flange as shown in Fig. 3.38. The critical buckling load of the specimen was determined from the load-versus-strain diagram using the modified strain reversal method as discussed in Ref. 119. The strains used in the load-versus-strain diagrams were obtained from the output of paired gages (No. 1,2,5,6 and 9 through 16) located at the centerline of each flange. Additional strain gages attached to the edges of compression flanges were used to measure the maximum edge strains for stiffened elements. Prior to testing, all strain gages were used to align the stub-column specimen.

c. Instrumentation and Test Procedure. The 880 MTS material test system and the CAMAC data acquisition system used for the beam tests were also used for stub column tests.

Following fabrication of the specimen and placement of strain gages, the stub column was placed in the MTS testing machine. At the beginning of the test, a small preload was applied to the specimen and the resulting strains were recorded for all strain gages to see whether the strain distribution was uniform over the cross section of the specimen. If necessary, thin layers of aluminum foil were added to the ends of stub columns in the regions of low strain. This procedure was repeated until the strain distribution was essentially uniform over the cross section. Figure 3.39 shows the box-shaped stub column test setup.

The function generator was then programmed to produce the desired ramp. For all tests, the stroke mode was selected as the control mode to

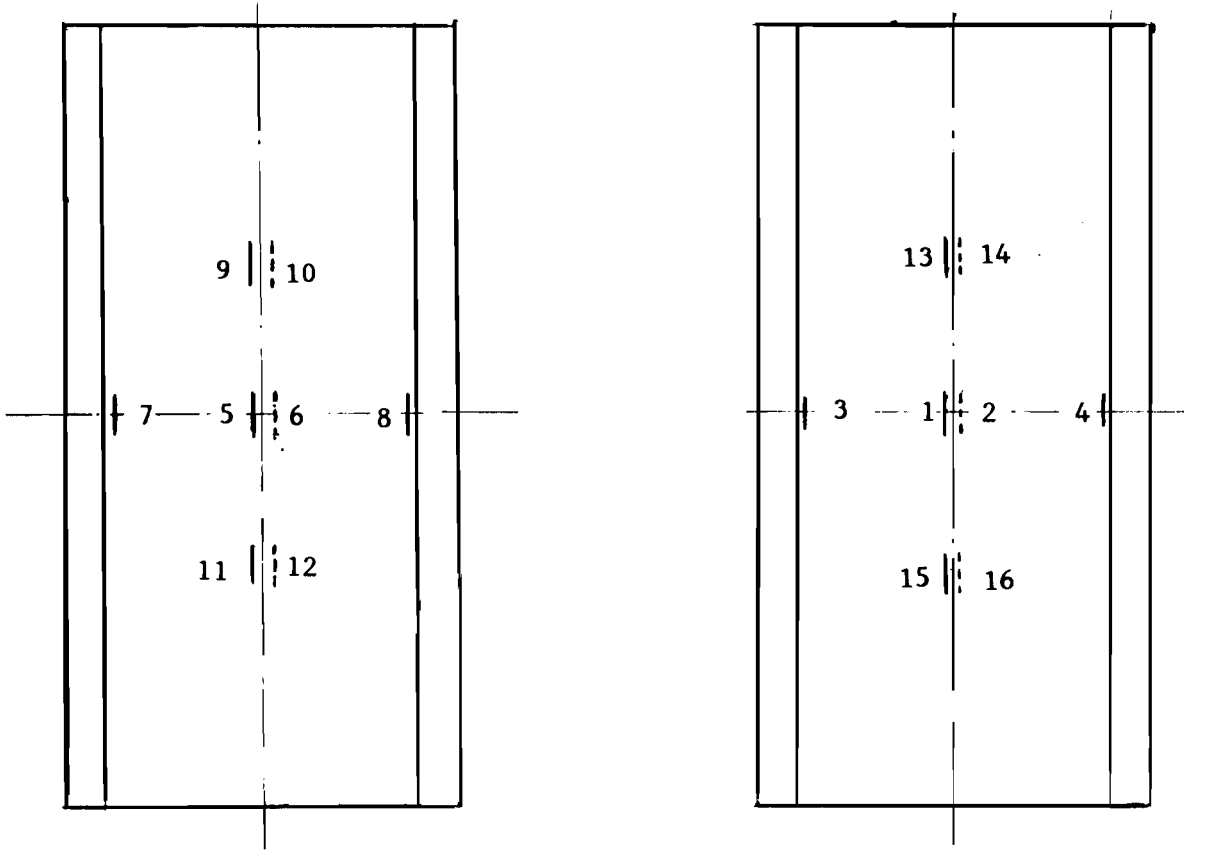

Figure 3.38 Locations of Strain Gages along the Specimen Length for Box-Shaped Stub Column Having Large w/t Ratio

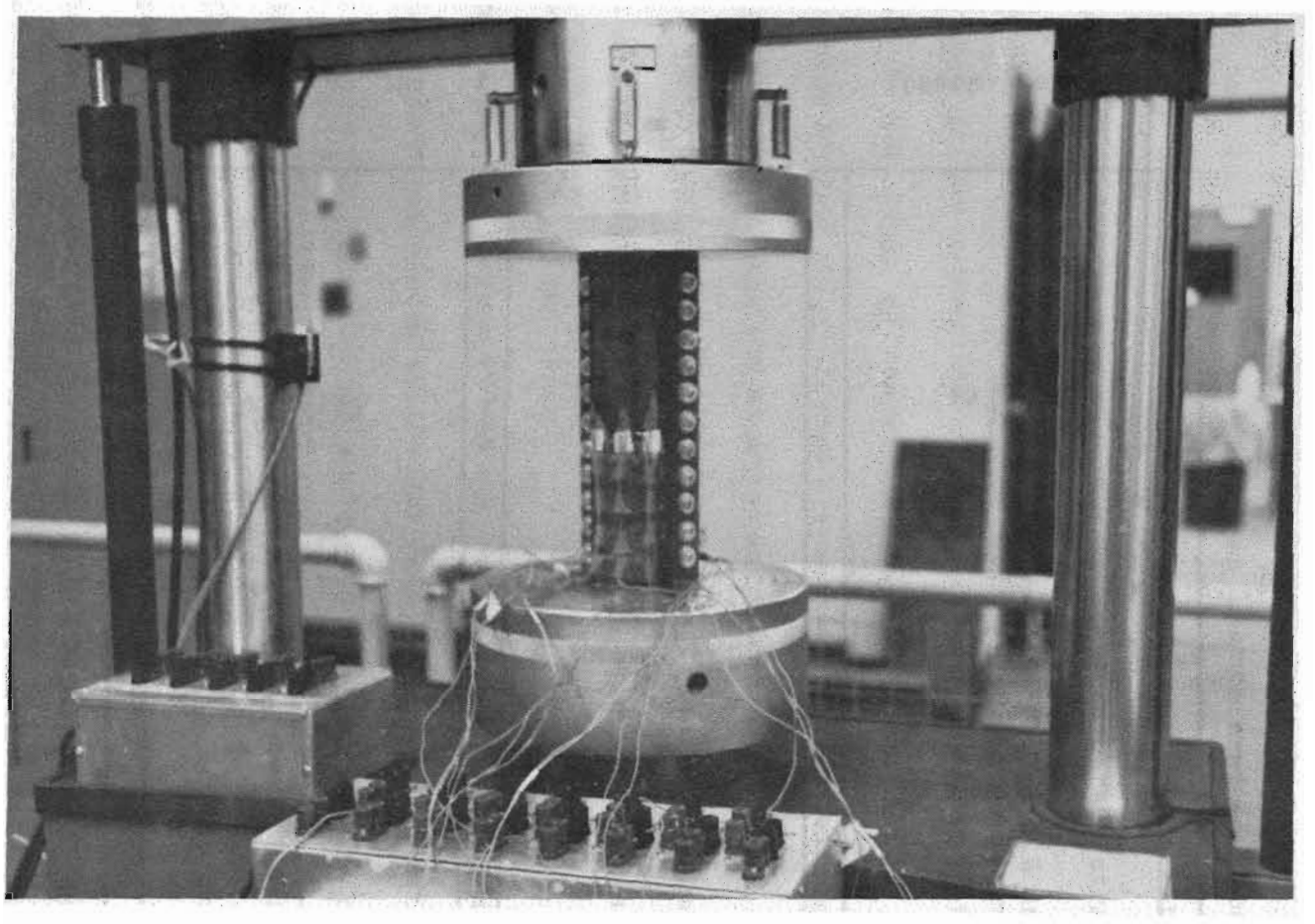

Figure 3.39 Test Setup of Stub Columns with Stiffened Flanges

(Specimen 1B3B)

maintain a constant actuator speed which was obtained from multiplying the selected strain rate by the overall length of the specimen. For all tests, load range 1 (maximum load of 100 kips) and stroke range 4 (maximum displacement of 0.5 inch) were selected. Because the maximum actuator speed is 2.5 in./sec., a strain rate higher than 0.1 in./in./sec could not be obtained. The strain rates used in the tests ranged from 10^{-4} to 0.1 in./in./sec. and the corresponding test times ranged from 416 to 0.2 sec.

d. Test Results. The failure mode of the specimens varied with the width-to-thickness ratio of the compression flange. For stiffened elements with large w/t ratios, local buckling always occurred in the elastic range. Due to the stress redistribution across the cross section of the compression flange, the edge stress of the stiffened element continued to increase until the maximum edge stress was reached and the specimen failed. For stiffened elements with moderate w/t ratios, the compression flange normally buckled in or near the inelastic range. Yield failure occurred in stiffened elements with small w/t ratios, so that very little, if any, waving of the stiffened compression element occurred before failure. It was noted that the specimens with small w/t ratio failed always at either top or bottom ends. The specimen with moderate w/t ratio failed either at the end or at the middle or both, while the specimen with large w/t ratio failed most of the time at or near the middle height of the specimen regardless of the strain rate used in the test. Figure 3.40 shows a typical failure mode of box-shaped stub column specimens with moderate w/t ratios.

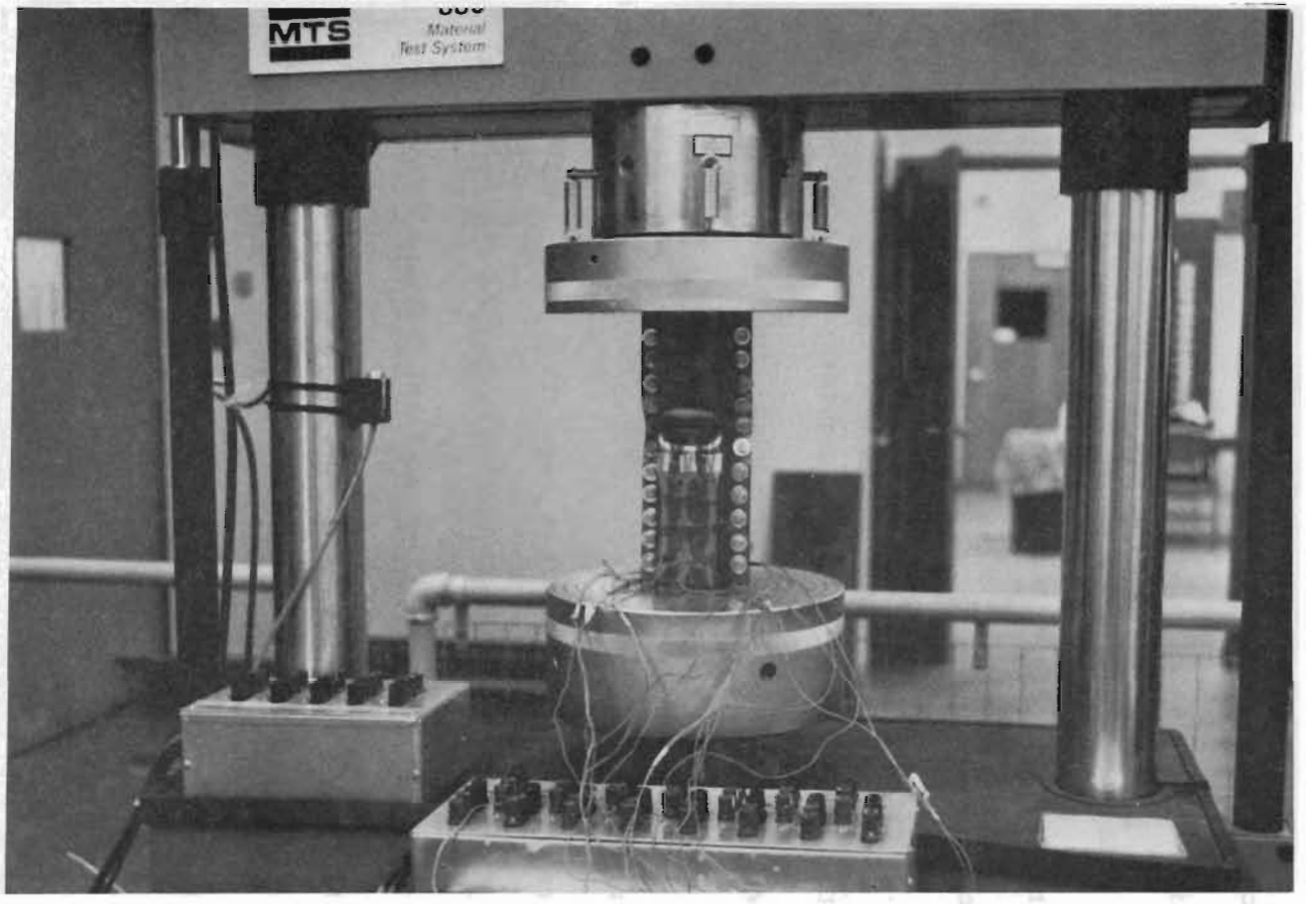

Figure 3.40 Failure of Stub Columns with Stiffened Flanges (Front View)

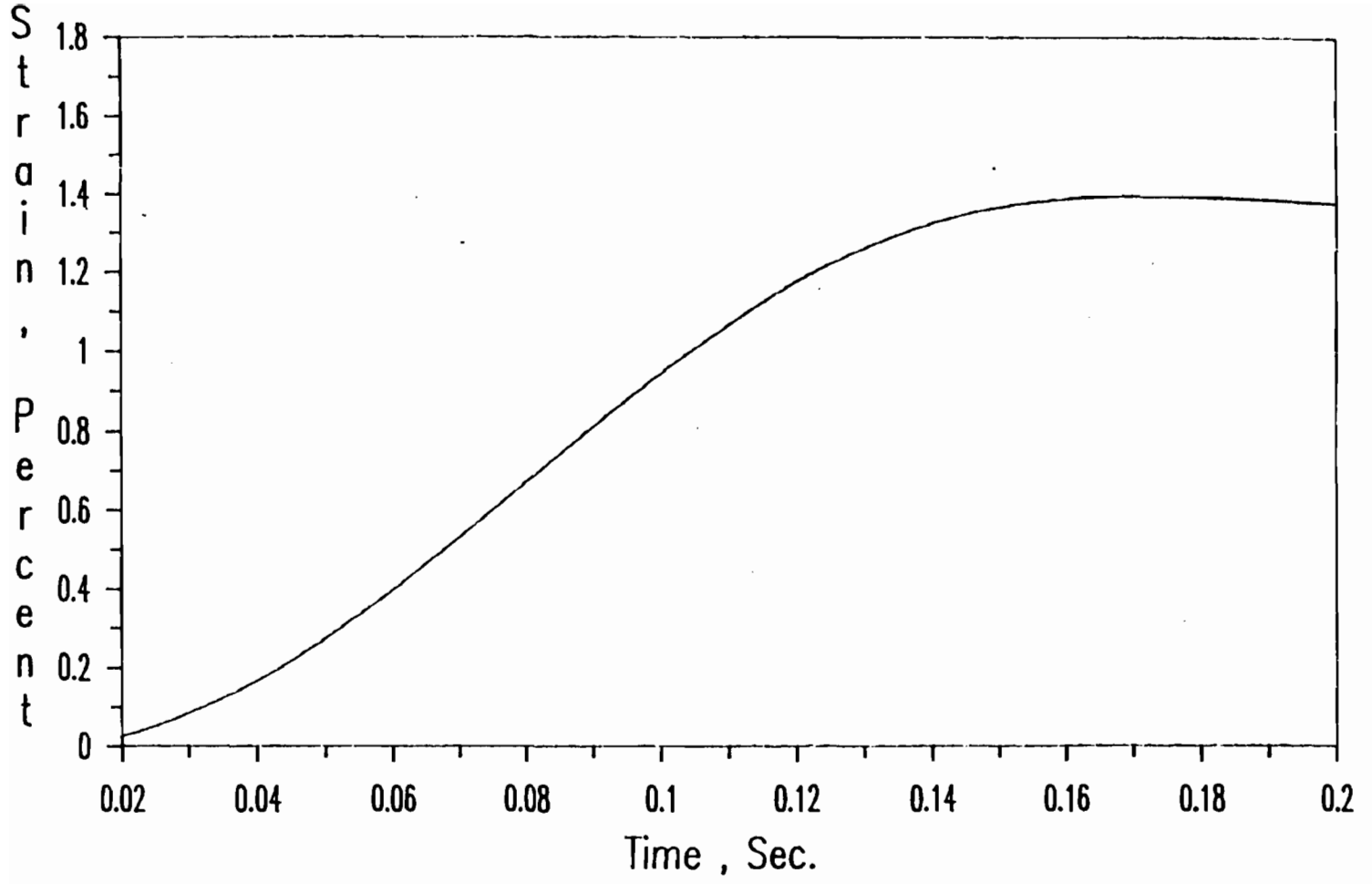

Figure 3.41 Typical Plot of Strain vs. Time for Stub Columns with Stiffened Flanges (Strain Gage # 3 for Specimen 1A3B)

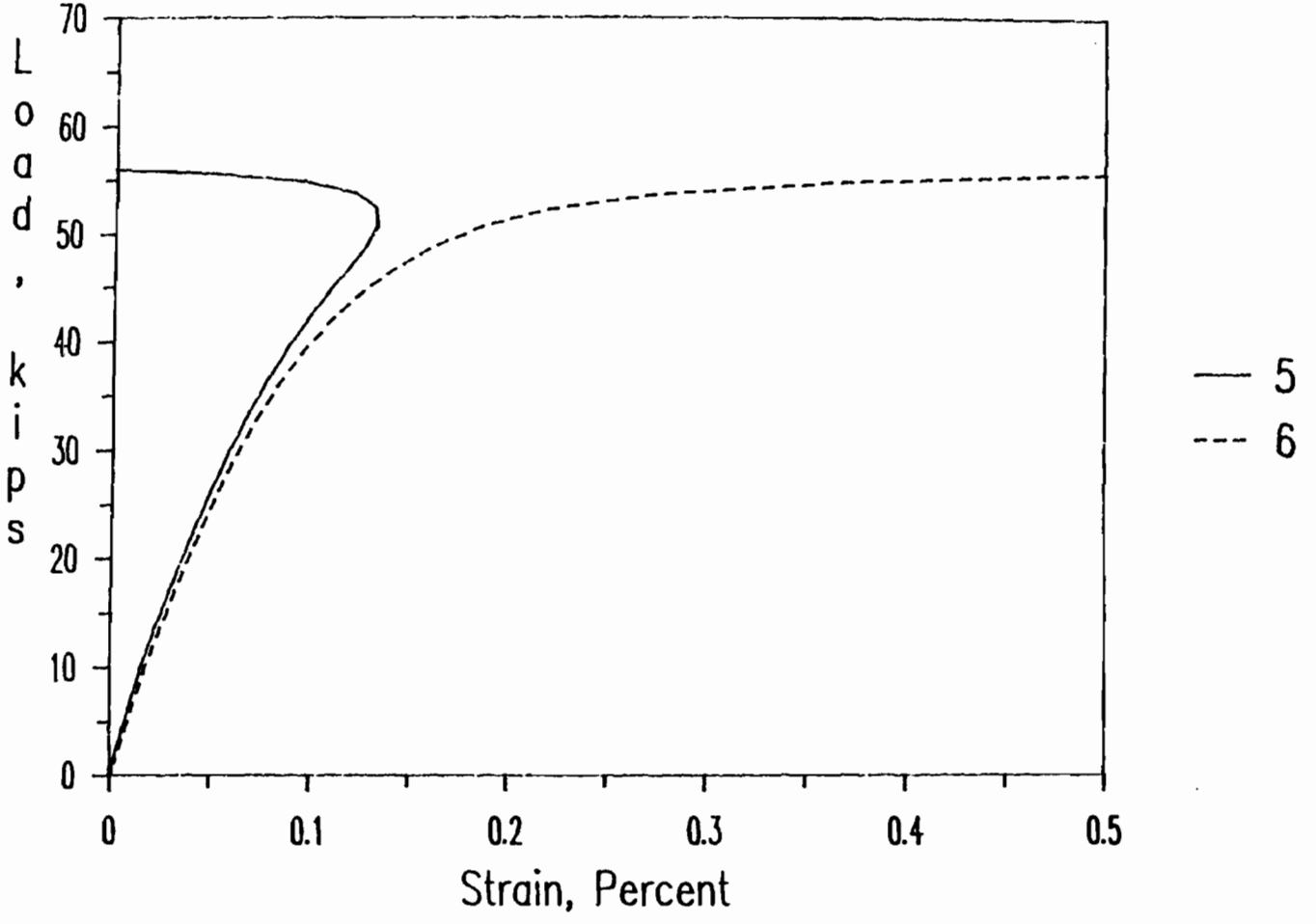

Figure 3.42 Load-Strain Curves of Strain Gages # 5 and 6, Installed at the Center of a Stiffened Flange (Specimen 1C1B)

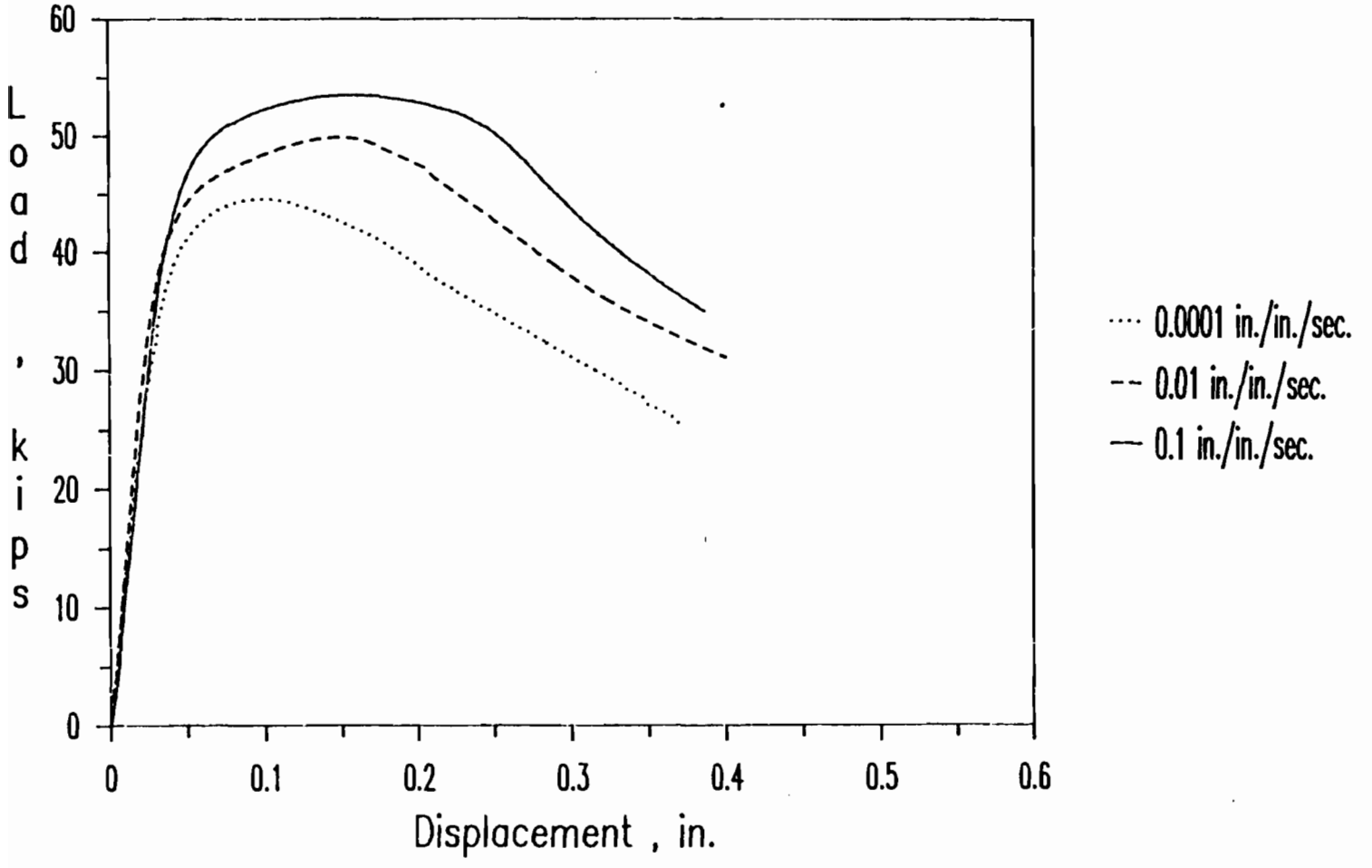

Figure 3.43 Load-Displacement Curves for Stub-Column Specimens 1A1A, 1A2A, and 1A3A

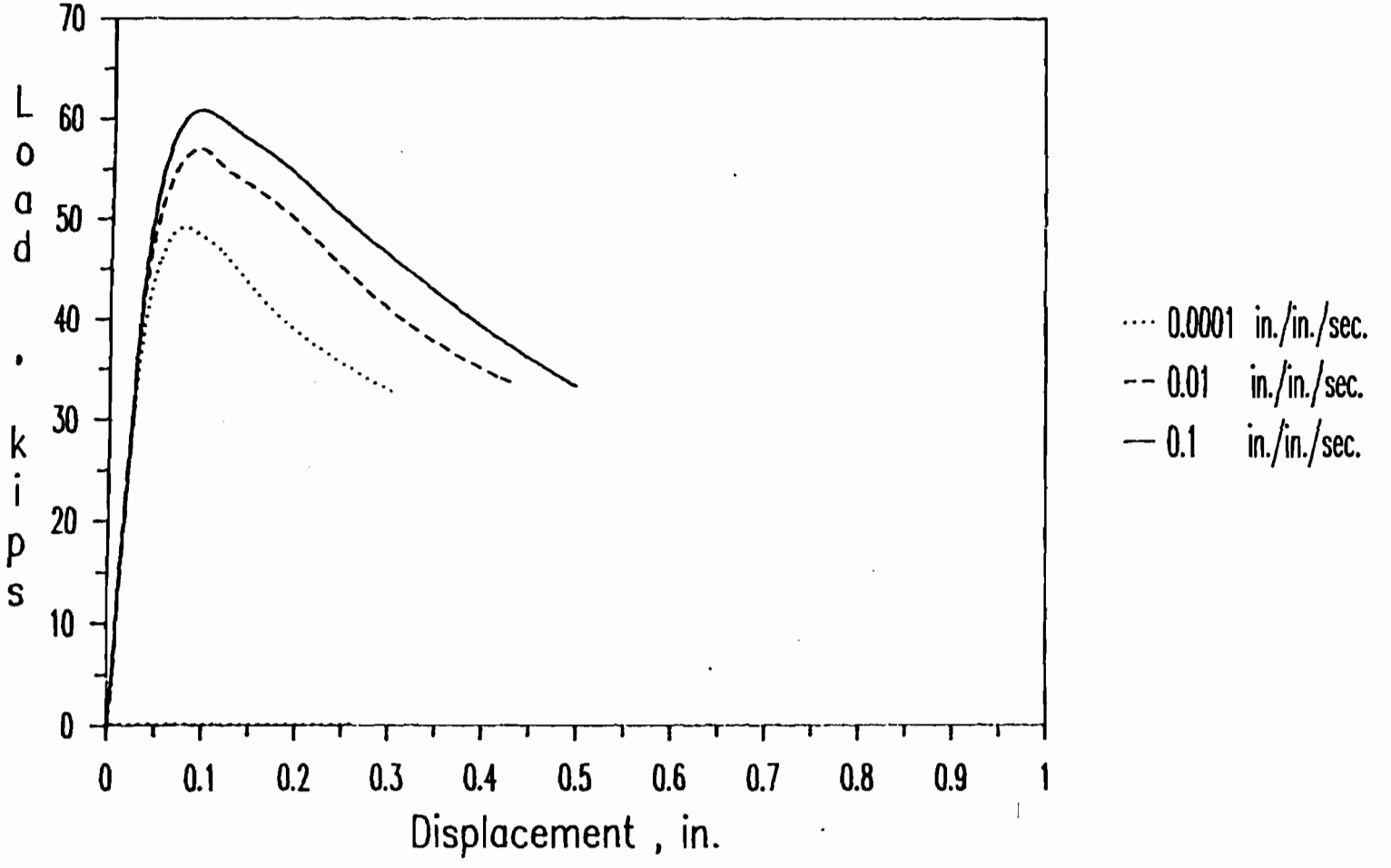

Figure 3.44 Load-Displacement Curves for Stub-Column Specimens 1B1A, 1B2A, and 1B3A

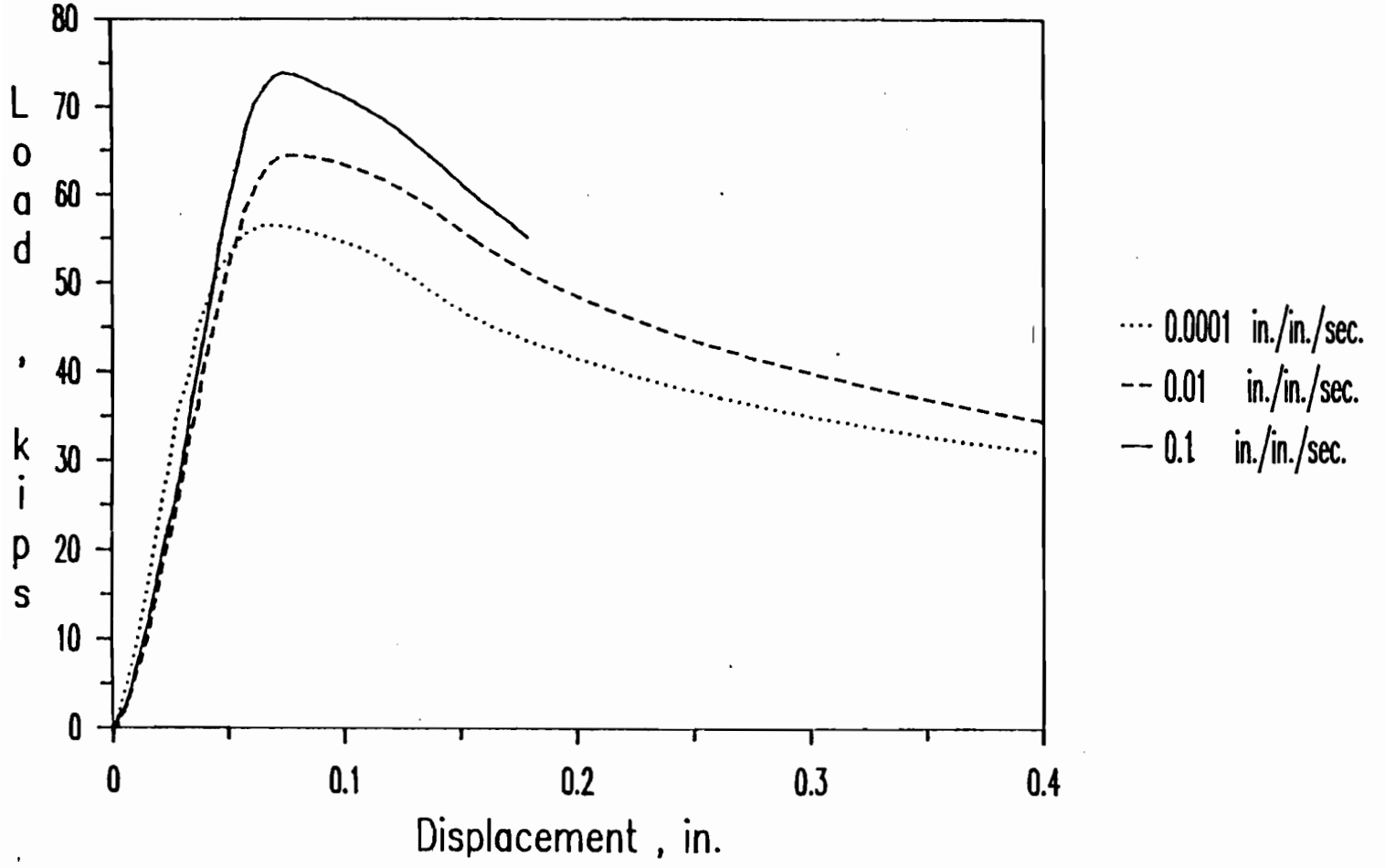

Figure 3.45 Load-Displacement Curves for Stub-Column Specimens 1C1A, 1C2A, and 1C3A

A typical strain-time curve for a high strain-rate test is presented in Fig. 3.41. Typical load-strain curves for the paired strain gages at the middle of the stiffened flange are shown in Fig. 3.42. For the purpose of comparison, Figures 3.43 through 3.45 present three typical load-displacement curves for the specimens having the same w/t ratio but tested under different strain rates.

4. Beam Tests for Unstiffened Elements.

a. Specimens. Fifteen (15) channel-beam specimens were tested to study the effect of strain rate on local and post-buckling strengths of unstiffened elements using 35XF steel material. Three different beam sections were studied. Aluminum bars were used to connect two channel specimens together to fabricate the beam specimen as demonstrated in Figure 3.46. The purpose of using the aluminum bars was to prevent the specimen from lateral buckling during the test. High strength, 1/4 in. dia. bolts were used in the fabrication of the test specimens. The cross section of the channel-beam specimens is also shown in Fig. 3.46. Table 3.47 gives the average cross-sectional dimensions of channel-beam specimens and the failure loads. The span lengths of beam specimens are also given in Table 3.47. The w/t ratios of unstiffened elements ranged from 8.93 to 20.69.

All steel sheets were sheared to the designed sizes before the channel sections were formed. All specimens were formed with an inside bend radius of 5/32 in.

b. Strain Measurements. Eight foil strain gages were placed at the midspan of the test specimen on the compression and tension flanges for

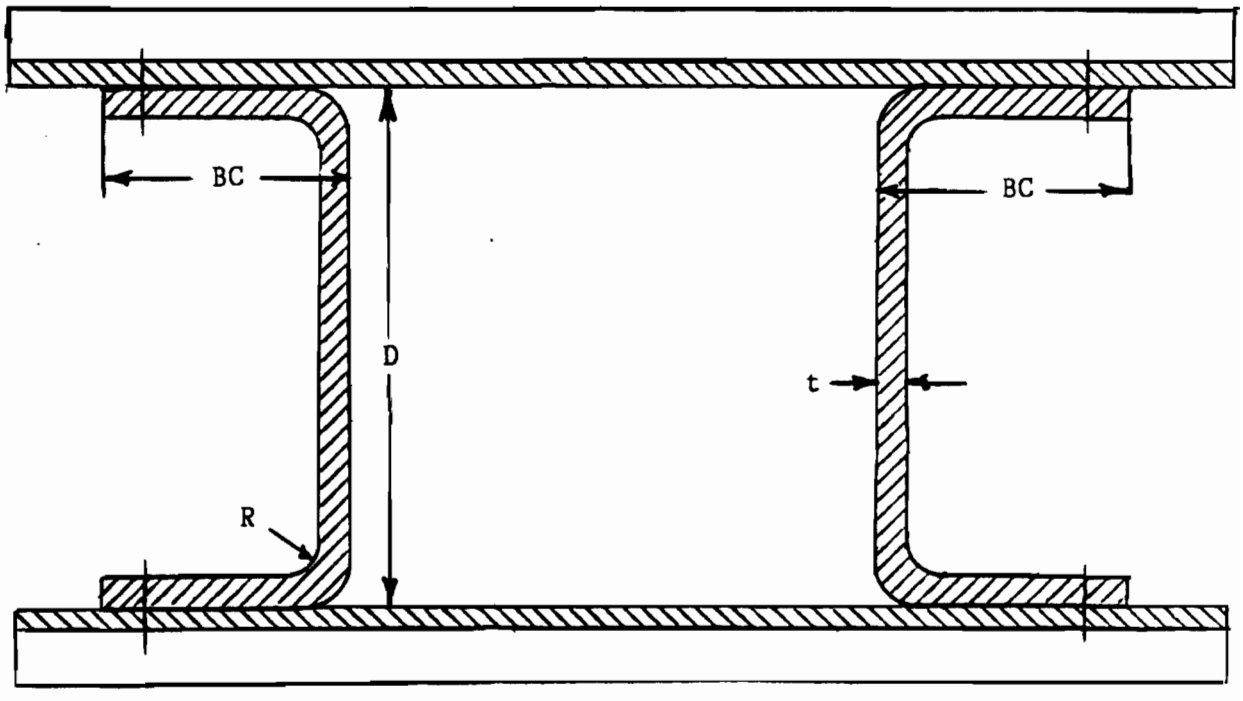

Figure 3.46 Cross Sections of Channel Beams Used for the Study of Unstiffened Elements

Table 3.47

Dimensions of Beam Specimens with Unstiffened Flanges

Fabricated from 35XF Sheet Steel

Specimen	BC (in.)	D (in.)	t (in.)	w/t	L (in.)	P_u (kips)
4A0A	1.030	2.020	0.085	9.28	37.00	6.41
4A1A	1.020	2.007	0.085	9.16	37.00	7.15
4A1B	1.020	2.025	0.085	9.16	37.00	7.18
4A2A	1.025	2.012	0.085	9.22	37.00	7.53
4A2B	1.009	2.020	0.085	9.03	37.00	7.63
4B0A	1.527	2.517	0.085	15.13	43.00	9.77
4B1A	1.530	2.510	0.085	15.16	43.00	10.12
4B1B	1.510	2.530	0.085	14.93	43.00	9.87
4B2A	1.520	2.520	0.085	15.04	43.00	10.97
4B2B	1.530	2.510	0.085	15.16	43.00	10.98
4C0A	2.020	3.020	0.085	20.93	65.00	8.49
4C1B	2.025	3.010	0.085	20.99	65.00	8.83
4C1C	2.020	3.010	0.085	20.93	65.00	9.15
4C2A	2.025	3.030	0.085	20.99	65.00	10.23
4C2B	2.020	3.020	0.085	20.93	65.00	10.22

measuring compressive and tensile strains. The locations of strain gages (numbered from 1 to 8) placed on beam specimens are shown in Fig. 3.47. These paired strain gages ((1,2) and (5,6)) were used to detect local buckling of the compression flanges. The modified strain reversal method was used to determine the critical buckling load from the load-versus-strain diagram, as recommended in Ref. 119.

Strain gages placed along the unsupported edges of the unstiffened compression flanges were used to measure edge strains. The edge stress of unstiffened elements can be determined from these strain readings using the stress-strain curve. Strain gages on the tension flange were used to study the shift of the neutral axis.

c. Instrumentation and Test Procedure. The equipment and testing procedure were identical to those used in the beam tests for the study of stiffened elements as discussed in Section III.C.2.c. The test setup for channel-beams is shown in Figs. 3.48 and 3.49.

The load was applied to the beam specimen by the 880 MTS machine. Four-inch wide bearing plates were used under the loading points and at the ends of specimens. The stroke range 3 with maximum displacement equal to 1 in. was selected to be the control mode. The strain rates used in the tests ranged from 10^{-5} to 0.01 in./in./sec. and the corresponding test times ranged from 1400 to 1.4 sec.

During the tests, the applied load, actuator displacement, strains from eight strain gage outputs, and midspan deflections from two LVDT outputs were recorded at a preset frequency rate. As mentioned previously, the frequency rate depends on the test time.

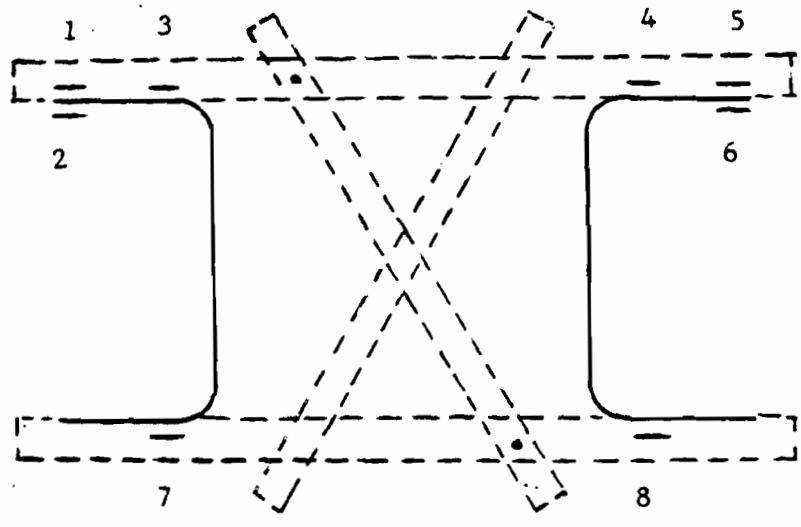

Figure 3.47 Locations of Strain Gages at Midspan Section of Channel Beams

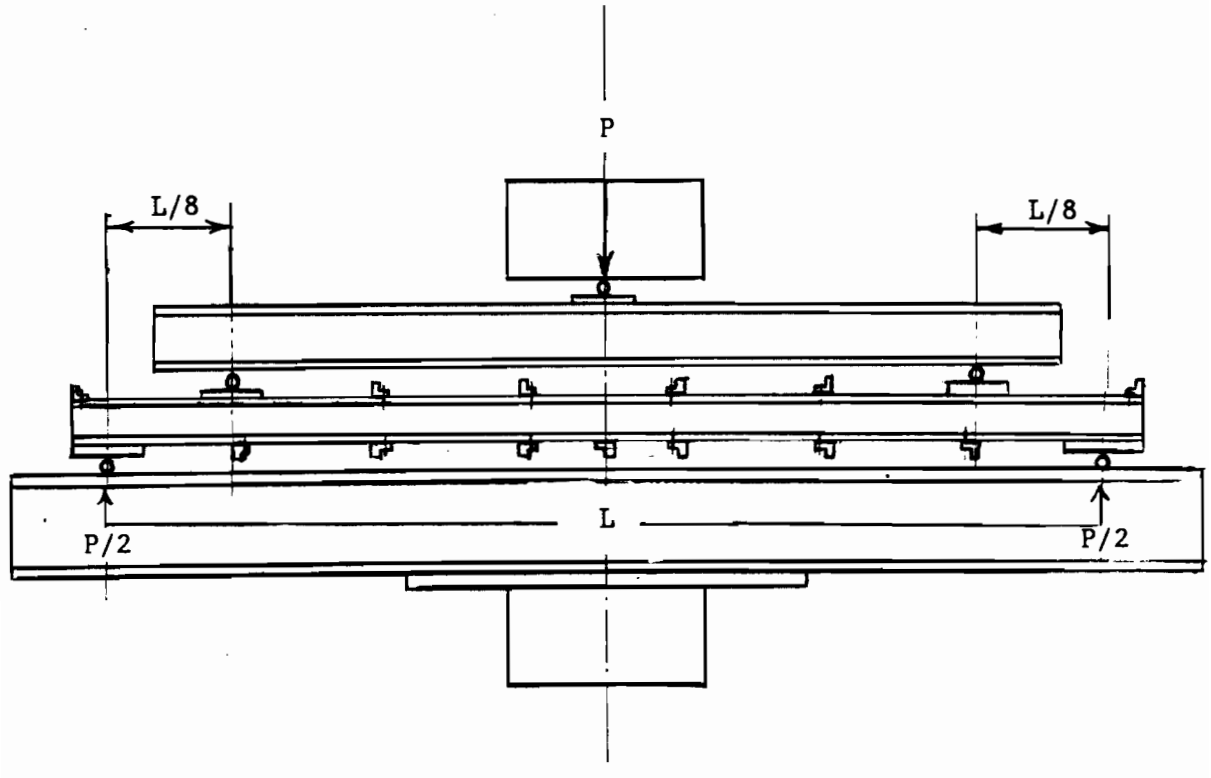

Figure 3.48 Test Setup for Channel Beams with Unstiffened Flanges

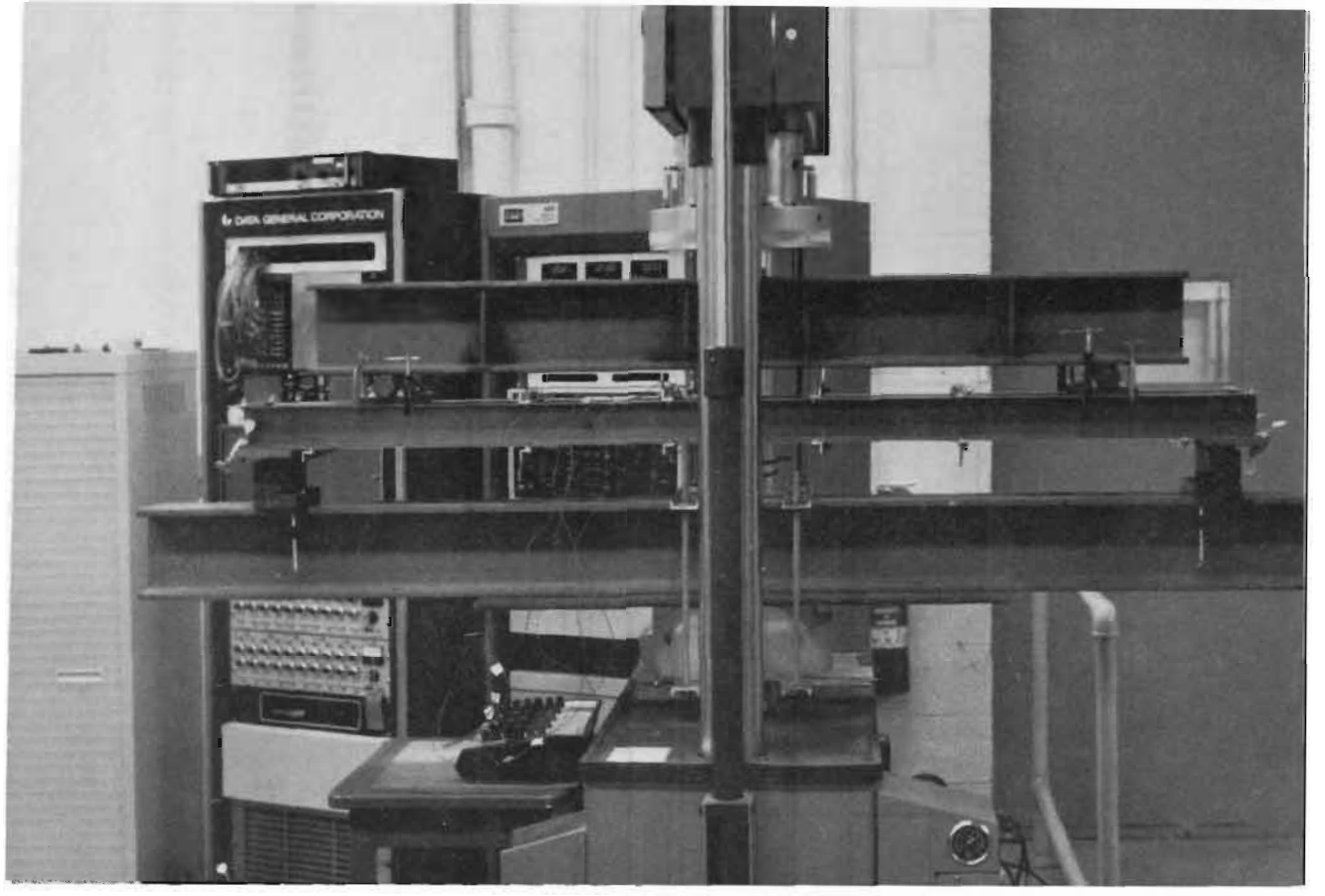

Figure 3.49 Photograph of Test Setup for Channel Beams with Unstiffened Flanges

d. Test Results. During the testing, waving of the compression flange was observed as the load continued to increase beyond the buckling load. Curling of the compression flanges near loading plates was observed in most specimens with small or moderate w/t ratios. For the specimens with large w/t ratio the curling always occured in the middle portion of the beam. As expected, the specimen failed between the loading points. The beam specimen failed when the maximum strength of the compression flange was reached. Possible failure by lateral buckling was prevented by providing lateral supports. Figure 3.50 shows typical flexural failure of channel-beams with unstiffened elements having large w/t ratios.

A typical strain-time curve for a medium strain-rate test is presented in Fig. 3.51. Typical load-strain curves for the paired strain gages at the middle of the stiffened flange are shown in Fig. 3.52. For the purpose of comparison, Figures 3.53 through 3.55 present three typical load-displacement curves for the specimens having the same w/t ratio but tested under different strain rates.

5. Stub Column Tests for Unstiffened Elements

a. Specimens. In this study, eighteen (18) I-shaped stub-column specimens have been tested for the study of local buckling and post-buckling strength of unstiffened elements of the 35XF steel material using different strain rates. The strain rates used for the tests ranged from 10^{-5} to 0.1 in./in./sec. Figure 3.56 shows the cross section of an I-shaped stub column. Table 3.48 gives the average cross-sectional dimensions of stub-column specimens and the failure loads. For the unstiffened

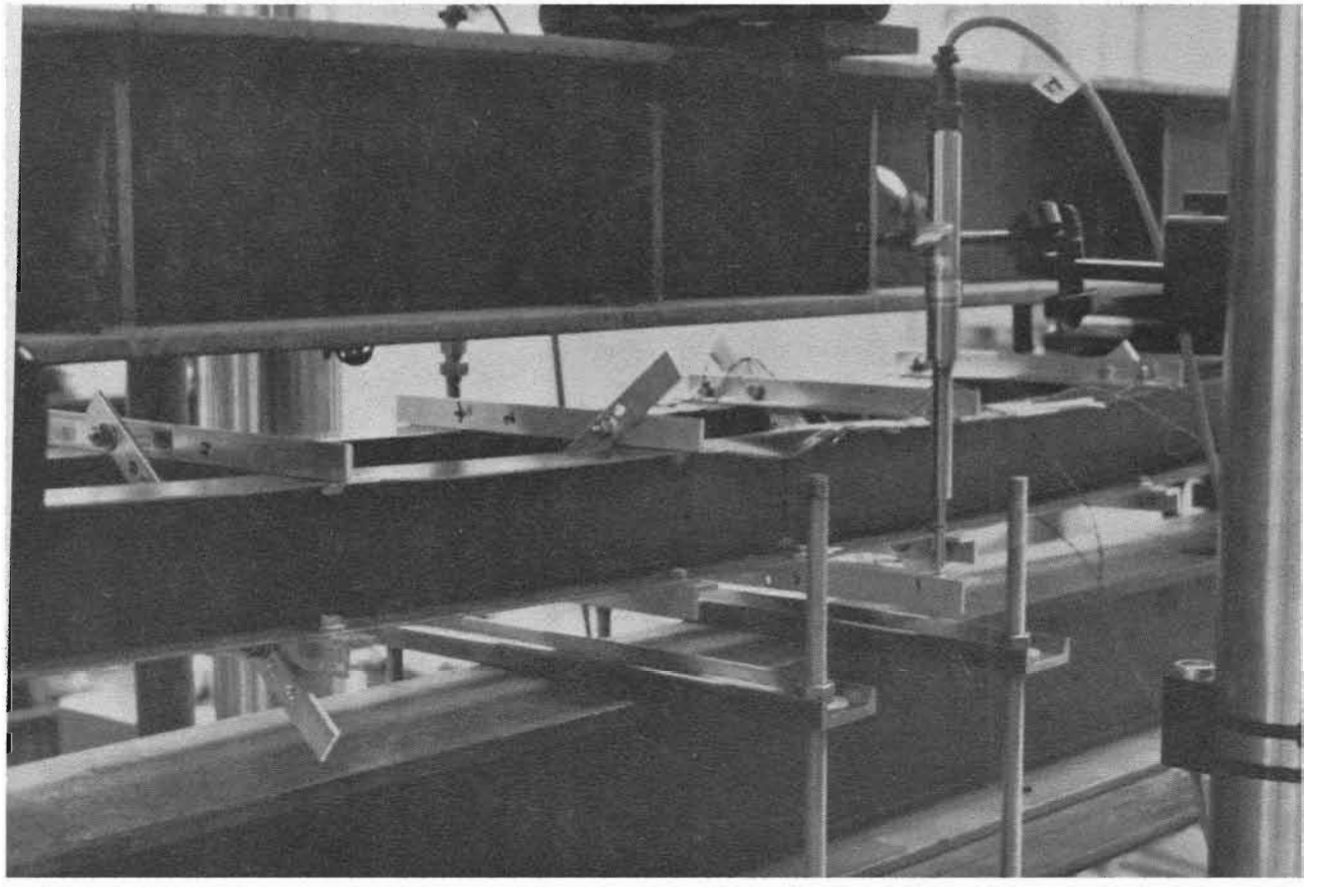

Figure 3.50 Typical Failure of Channel Beams with Unstiffened Flanges

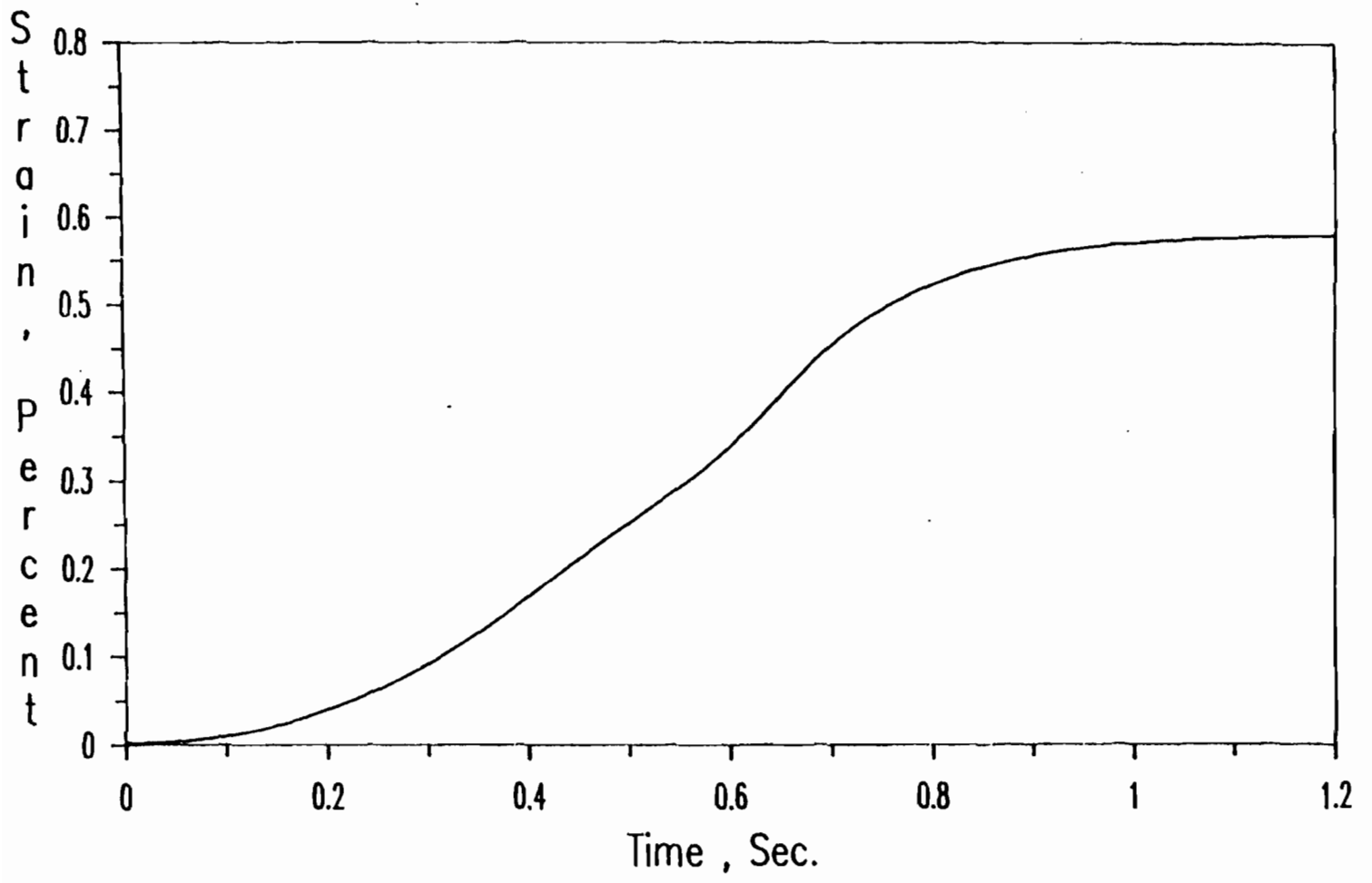

Figure 3.51 Typical Plot of Strain vs. Time for Channel Beams with Unstiffened Flanges (Strain Gage # 3 for Specimen 4C2B)

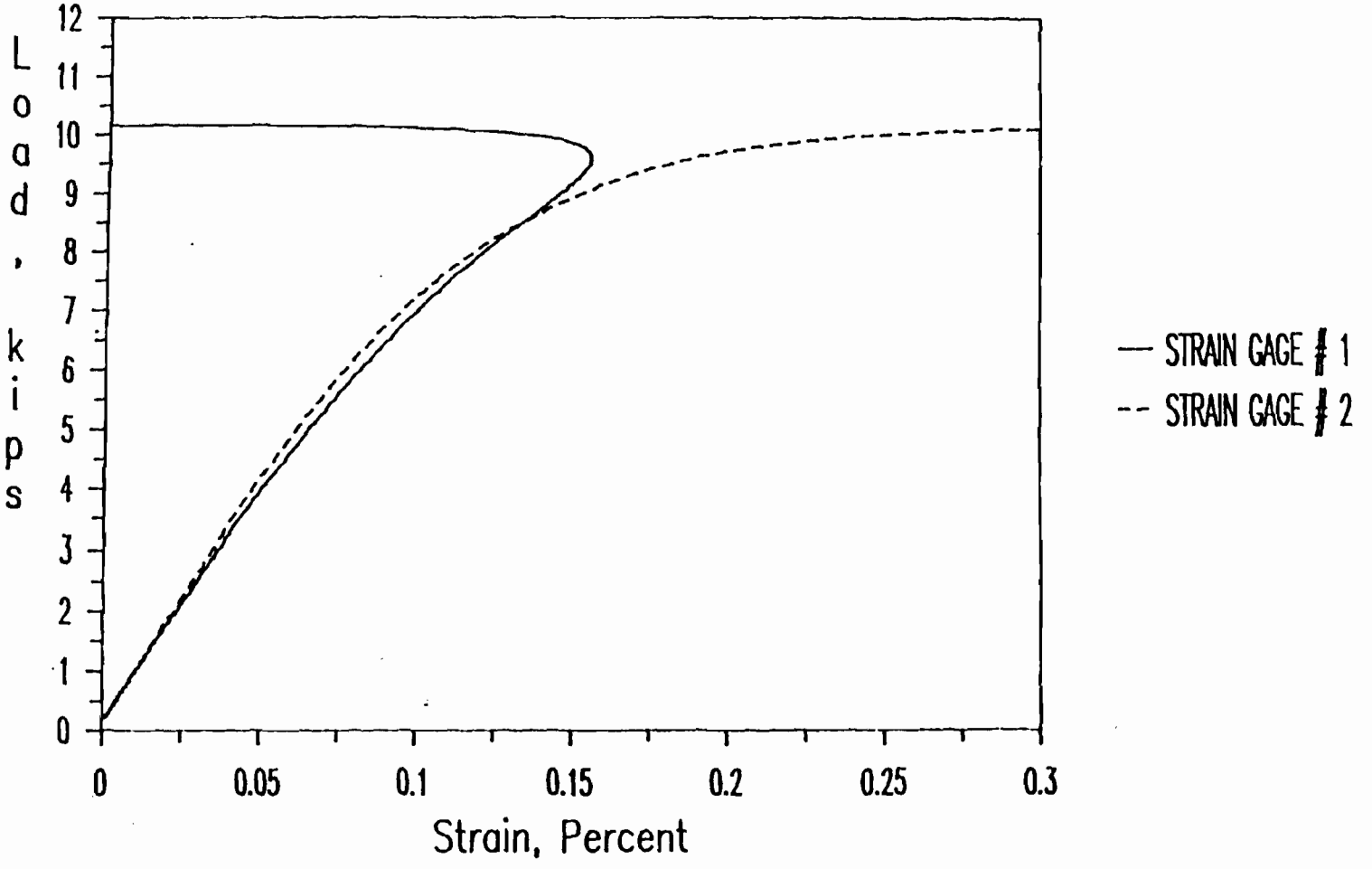

Figure 3.52 Load-Strain Curves of Strain Gages # 1 and 2 Installed at the Tip of an Unstiffened Flange (Spec. 4C2A)

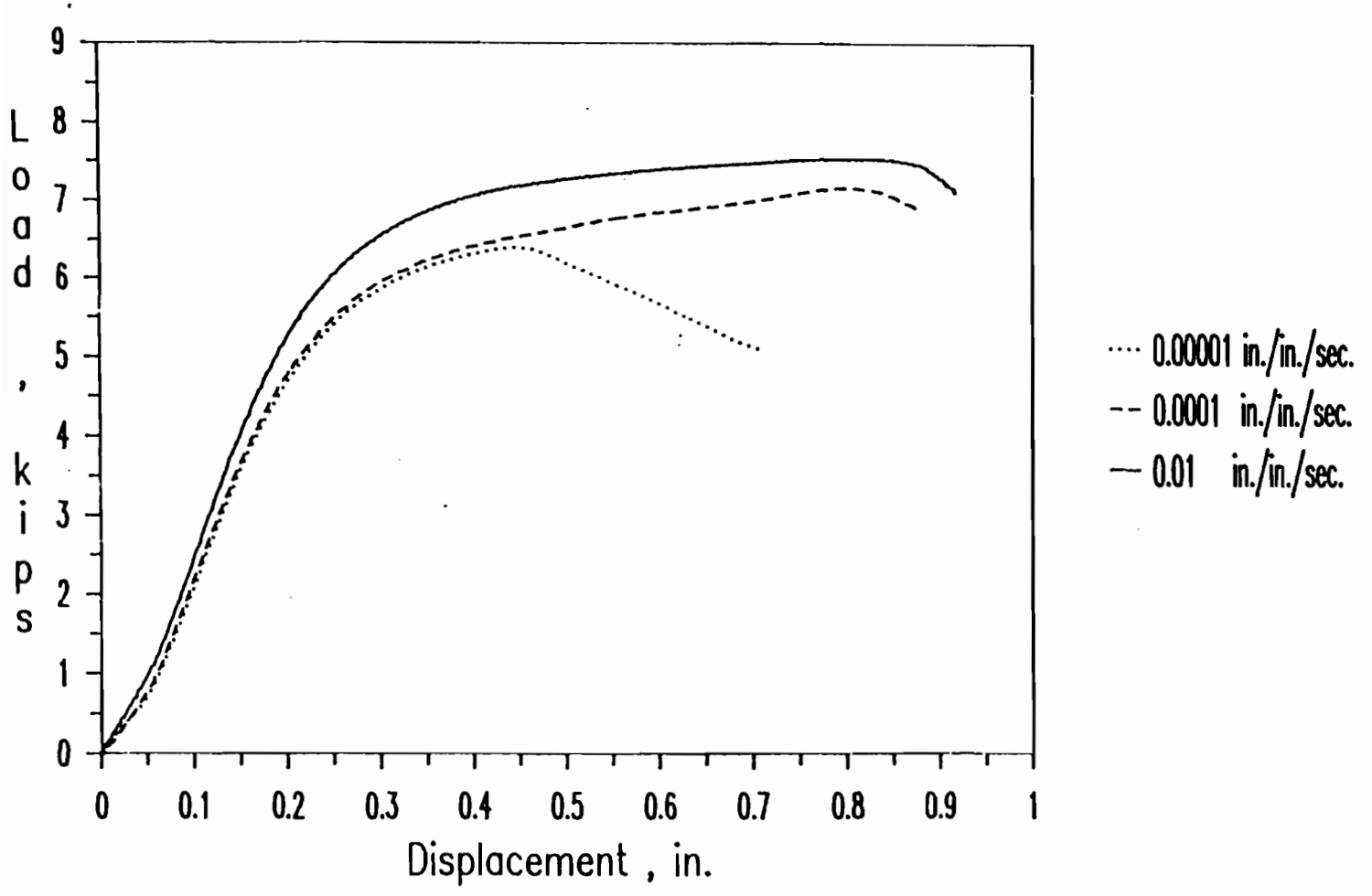

Figure 3.53 Load-Displacement Curves for Channel Beam Specimens 4A0A, 4A1A, and 4A2A

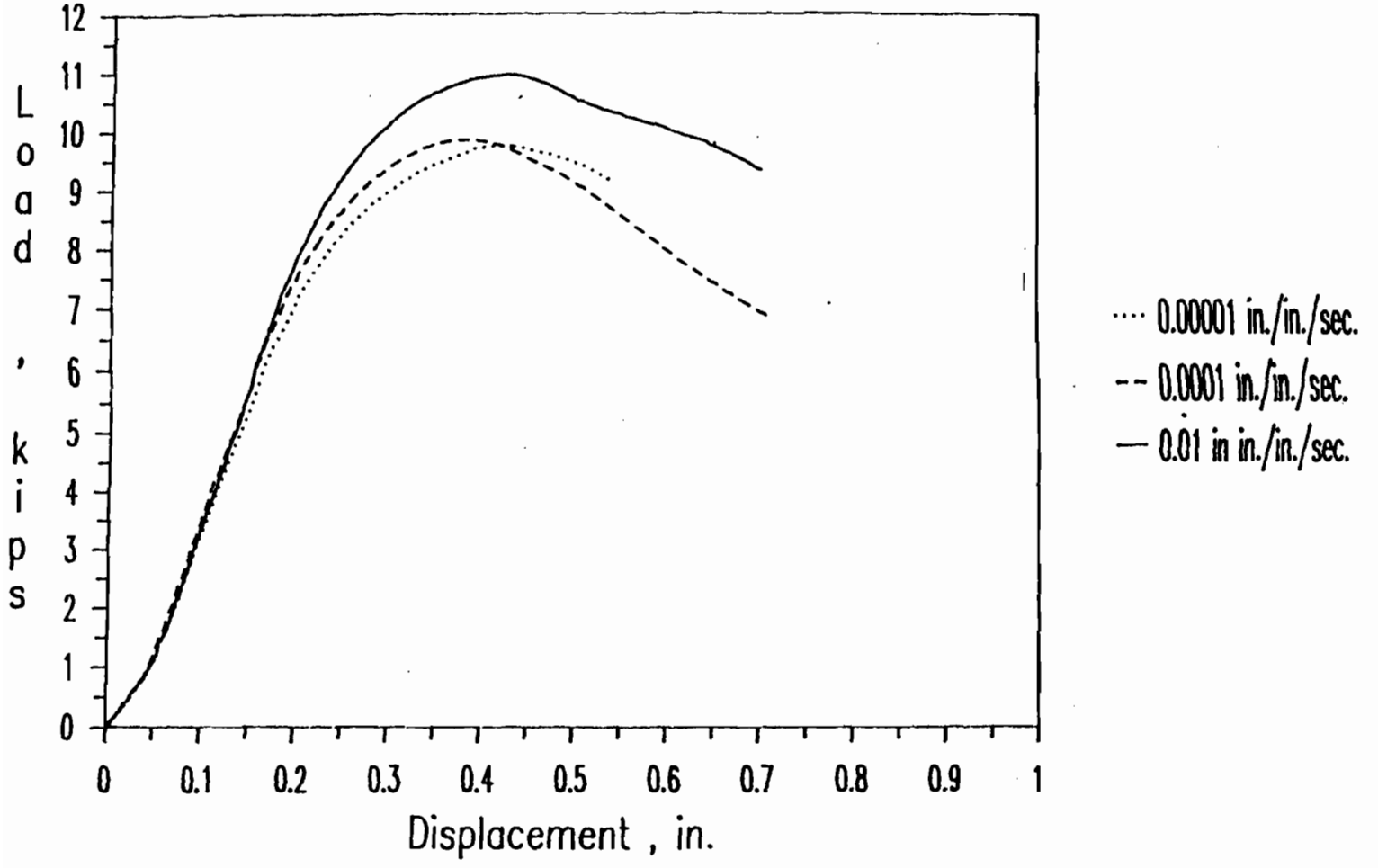

Figure 3.54 Load-Displacement Curves for Channel Beam Specimens 4B0A, 4B1A, and 4B2A

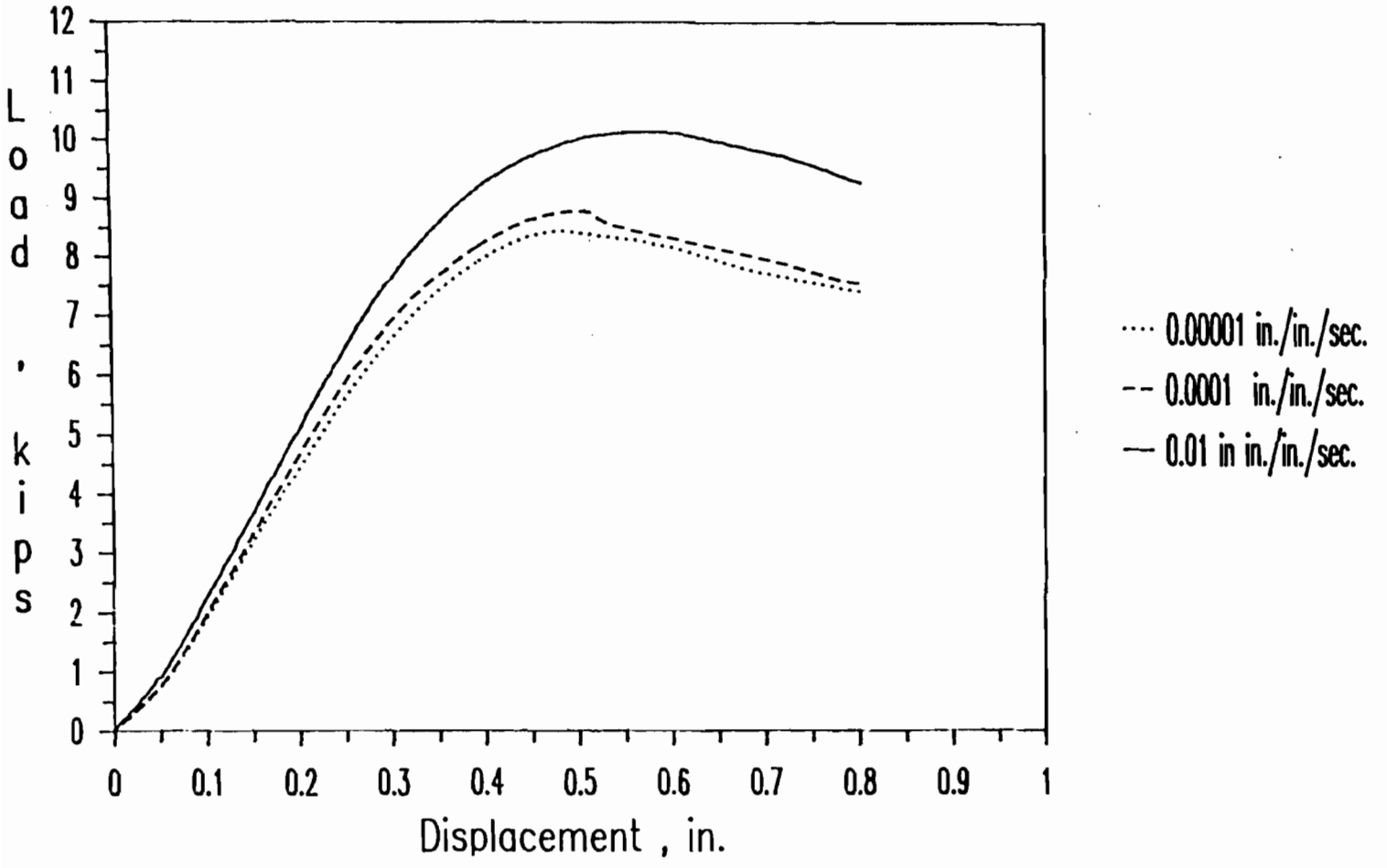

Figure 3.55 Load-Displacement Curves for Channel Beam Specimens 4C0A, 4C1A, and 4C2A

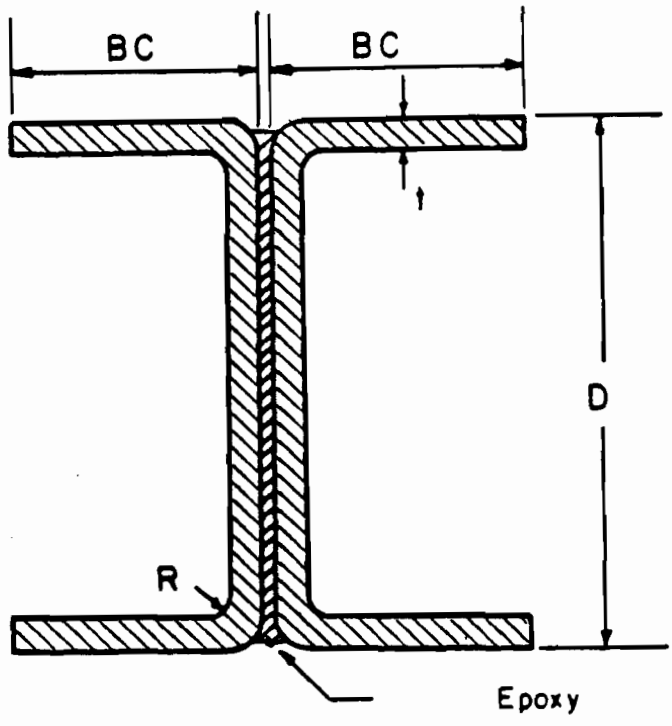

Figure 3.56 Cross Sections of I-Shaped Stub Columns

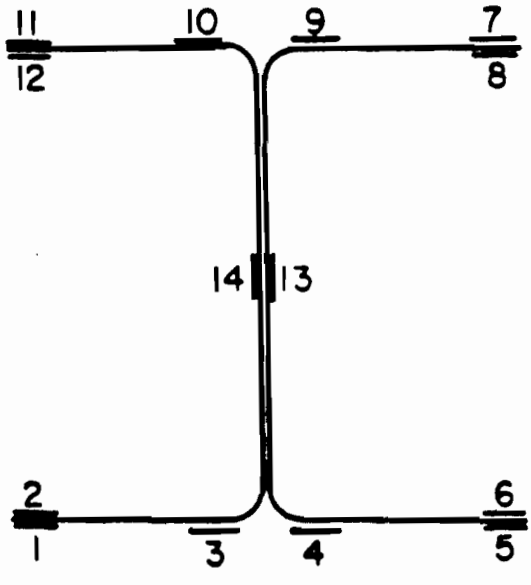

Figure 3.57 Locations of Strain Gages at Midheight of I-Shaped Stub Columns

Table 3.48

Dimensions of Stub Columns with Unstiffened Flanges

Fabricated from 35XF Sheet Steel

Specimen	BC (in.)	D (in.)	w/t	Gross Area ($in.^2$)	L (in.)	P_u (kips)
2A1A	1.000	2.000	8.93	0.6220	7.90	25.26
2A1B	1.010	2.018	9.04	0.6285	7.97	25.35
2A2A	1.000	2.040	8.93	0.6288	7.95	26.04
2A2B	1.015	2.002	9.10	0.6275	7.94	27.70
2A3A	1.000	2.040	8.93	0.6288	7.98	31.41
2A3B	1.003	2.014	8.96	0.6254	7.94	29.41
2B1A	1.375	3.025	13.34	0.9238	9.95	34.20
2B1B	1.381	2.981	13.41	0.9184	9.97	34.20
2B2A	1.380	2.987	13.40	0.9190	9.96	36.30
2B2B	1.378	3.007	13.37	0.9217	9.94	37.52
2B3A	1.375	3.020	13.34	0.9229	10.01	41.67
2B3B	1.382	3.006	13.42	0.9229	9.99	42.70
2C0A	2.000	3.000	20.69	1.1320	14.00	36.30
2C1A	2.014	2.976	20.85	1.1327	14.00	37.23
2C1B	2.006	3.018	20.76	1.1371	13.94	37.66
2C2A	2.024	2.967	20.97	1.1346	14.09	41.28
2C2B	2.010	3.015	20.81	1.1380	13.95	41.52
2C3A	2.020	2.970	20.93	1.1337	14.06	47.92
2C3B	2.015	2.977	20.87	1.1332	13.91	46.16

flanges studied in this program, the range of w/t ratios was from 8.9 to 20.7.

The stub-column specimens were fabricated by bonding two identical channels back to back. Surfaces to be joined were paper sanded and cleaned with methyl alcohol and bonded by a thin layer of PC-7 epoxy. The webs of the channels were held together by C-clamps after glue was placed on the web. Thin wires with 0.002 in. dia. were placed between the specimen webs to maintain uniform epoxy thickness. C-clamps were released after 24 hours. Great care was taken when the stub-columns were fabricated. Prior to testing, the ends of stub-column specimens were milled flat and parallel.

The lengths of stub-column specimens are also given in Table 3.48. In order to prevent overall column buckling, the length of each stub column is longer than three times the largest dimension of the cross section of the specimen and less than 20 times the least radius of gyration as recommended in Ref. 116. This criterion was also adopted in Part VII (Test Procedure) of the 1986 AISI Design Manual. The dimensions of the webs of all stub column specimens were chosen to be fully effective.

b. Strain Measurements. Fourteen foil strain gages were used to measure strains at the midheight of the stub-column specimens. The locations of strain gages are shown in Fig. 3.57. The paired strain gages placed along the tips of compression flanges were used to determine the critical buckling load of stub columns. The buckling load of the specimen was determined from the modified strain reversal method. Strain gages (No. 3, 4, 9, and 10) were placed at the supported edges of the compression flanges to measure maximum edge strains at each load level for

calculating the maximum edge stress in the unstiffened flanges. Paired strain gages (No. 13 and 14) were placed along the centerline of the web to monitor any premature failure of the web. All strain gages were used to align the stub-column specimen.

c. Instrumentation and Test Procedure. Equipment and test procedures used in this phase were the same as those used in the stub column tests for stiffened elements described in Section III.C.3.c. The test setup for stub-column specimens with unstiffened elements is shown in Fig. 3.58. The strain rates used in the tests ranged from 10^{-5} to 0.1 in./in./sec. and the corresponding test times ranged from 3600 to 0.2 sec.

d. Test Results.

During the test, no bonding failure was observed prior to the attainment of the maximum load. The failure mode of stub-column specimens with unstiffened elements varied with the width-to-thickness ratio of the unstiffened compression flanges. The unstiffened flanges with large w/t ratios showed large waving deformations, whereas the unstiffened compression flanges with small w/t ratios showed no noticeable waving until failure. A typical failure mode of stub-column specimens with unstiffened compression flanges is shown in Fig. 3.59. A typical strain-time curve for a high strain-rate test is presented in Fig. 3.60. It was observed during the I-shaped stub column tests that the webs of the test specimens showed no sign of buckling before the load reached the ultimate value. Typical stress-strain curves for the paired strain gages at the tip of the unstiffened flange are shown in Fig. 3.61. For the purpose of comparison, Figures 3.62 through 3.64 present three typical load-

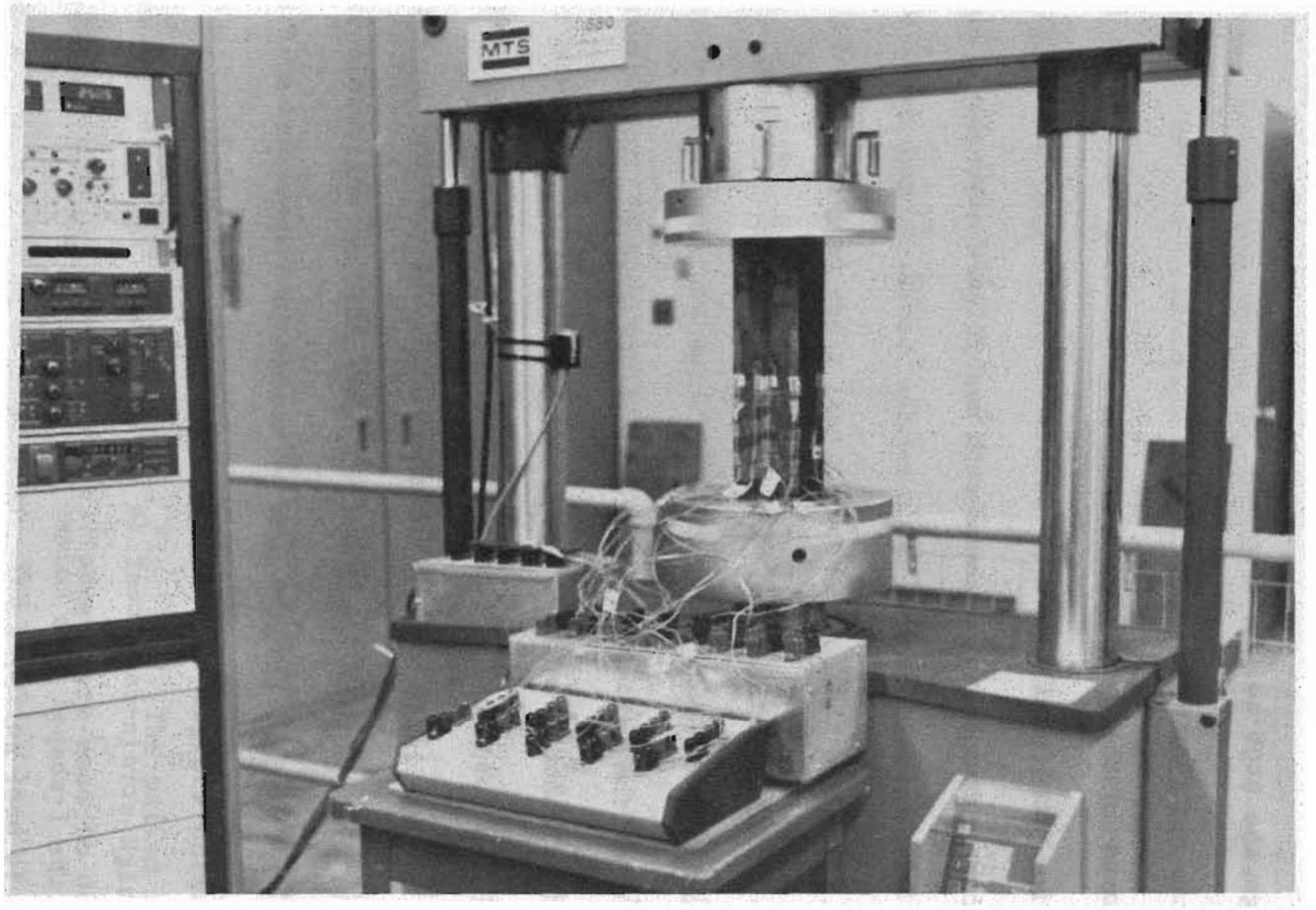

Figure 3.58 Test Setup of Stub Columns with Unstiffened Flanges

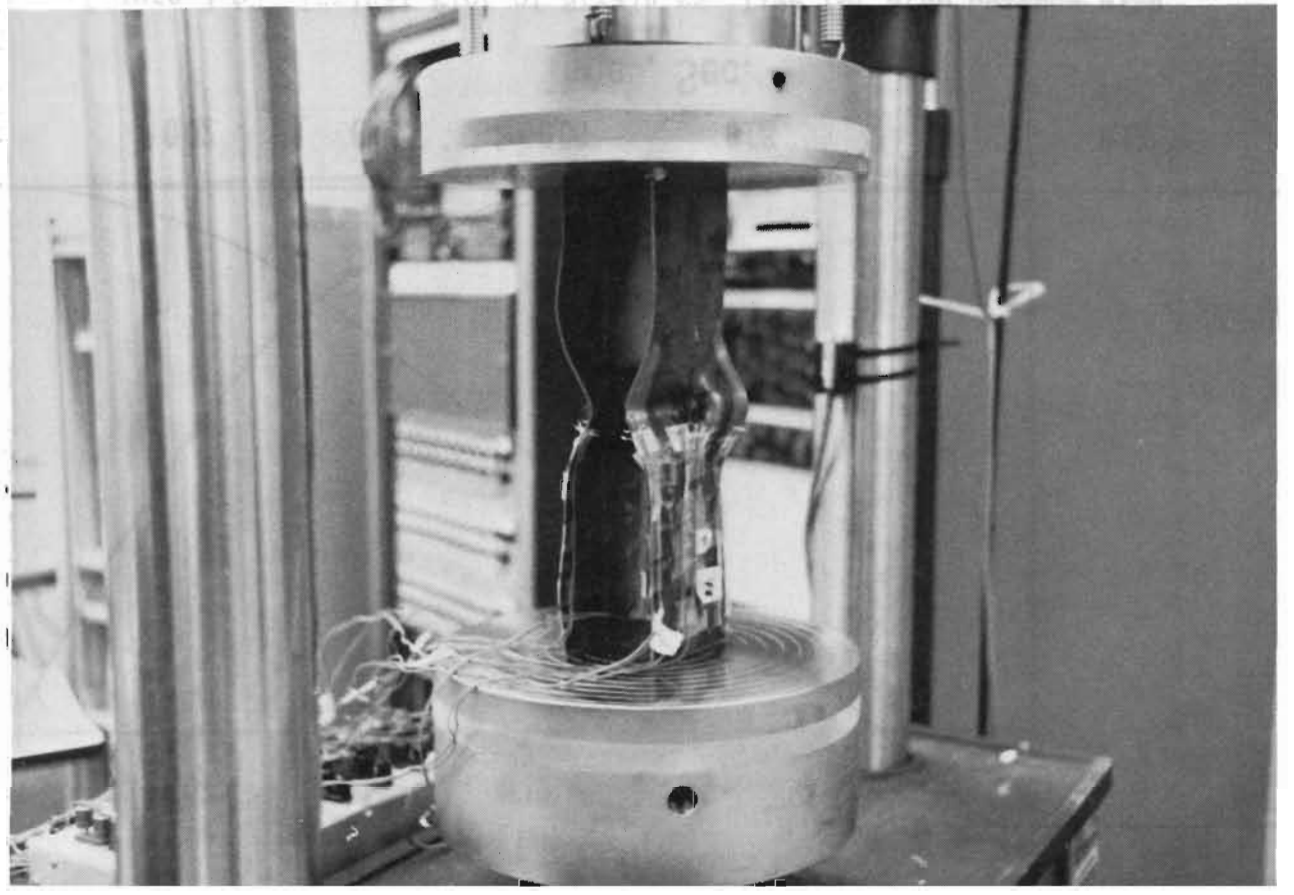

Figure 3.59 Typical Failure of Stub Columns with Unstiffened Flanges

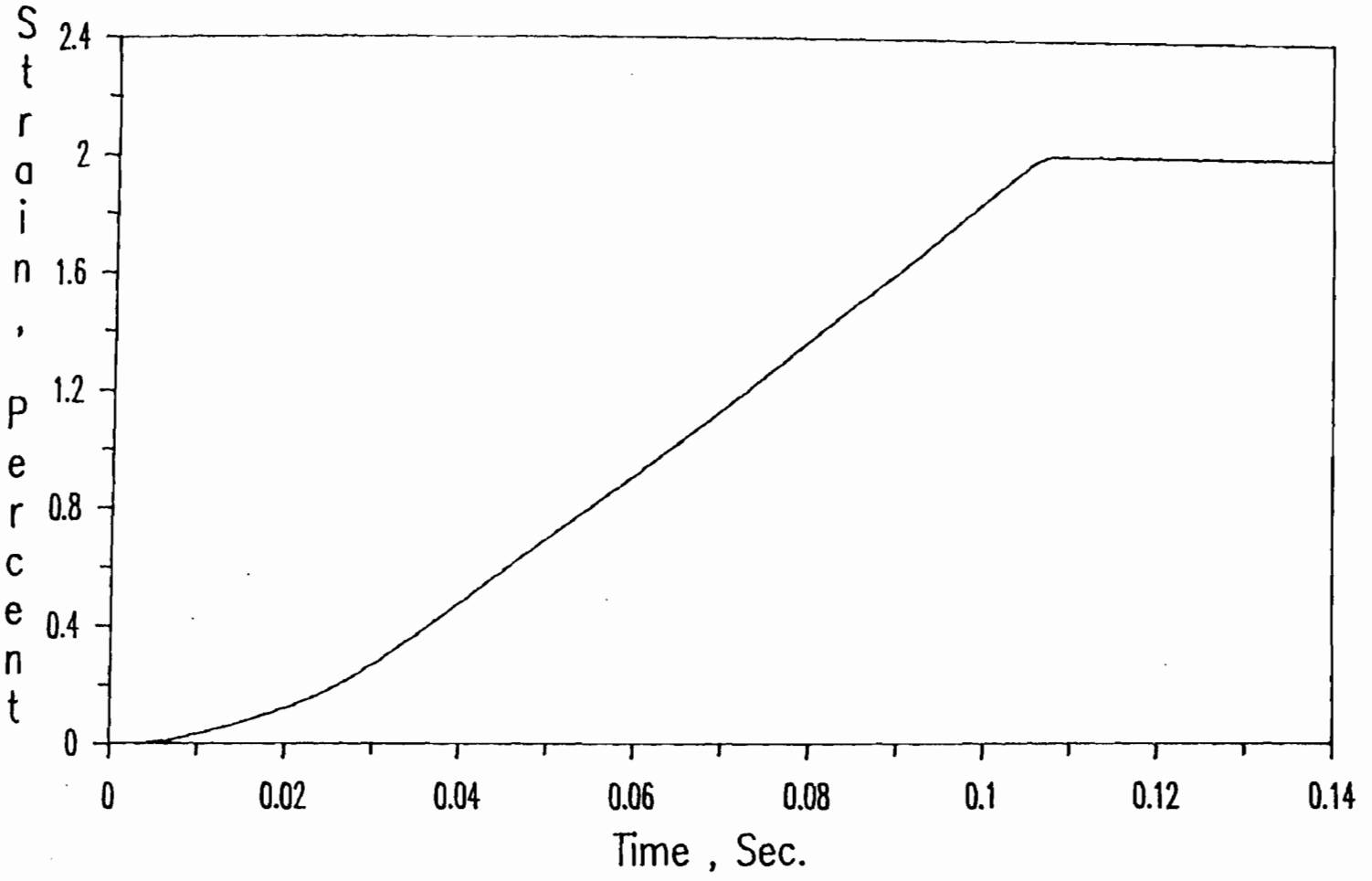

Figure 3.60 Typical Plot of Strain vs. Time for Stub Columns with Unstiffened Flanges (Strain Gage # 3 for Specimen 2B3A)

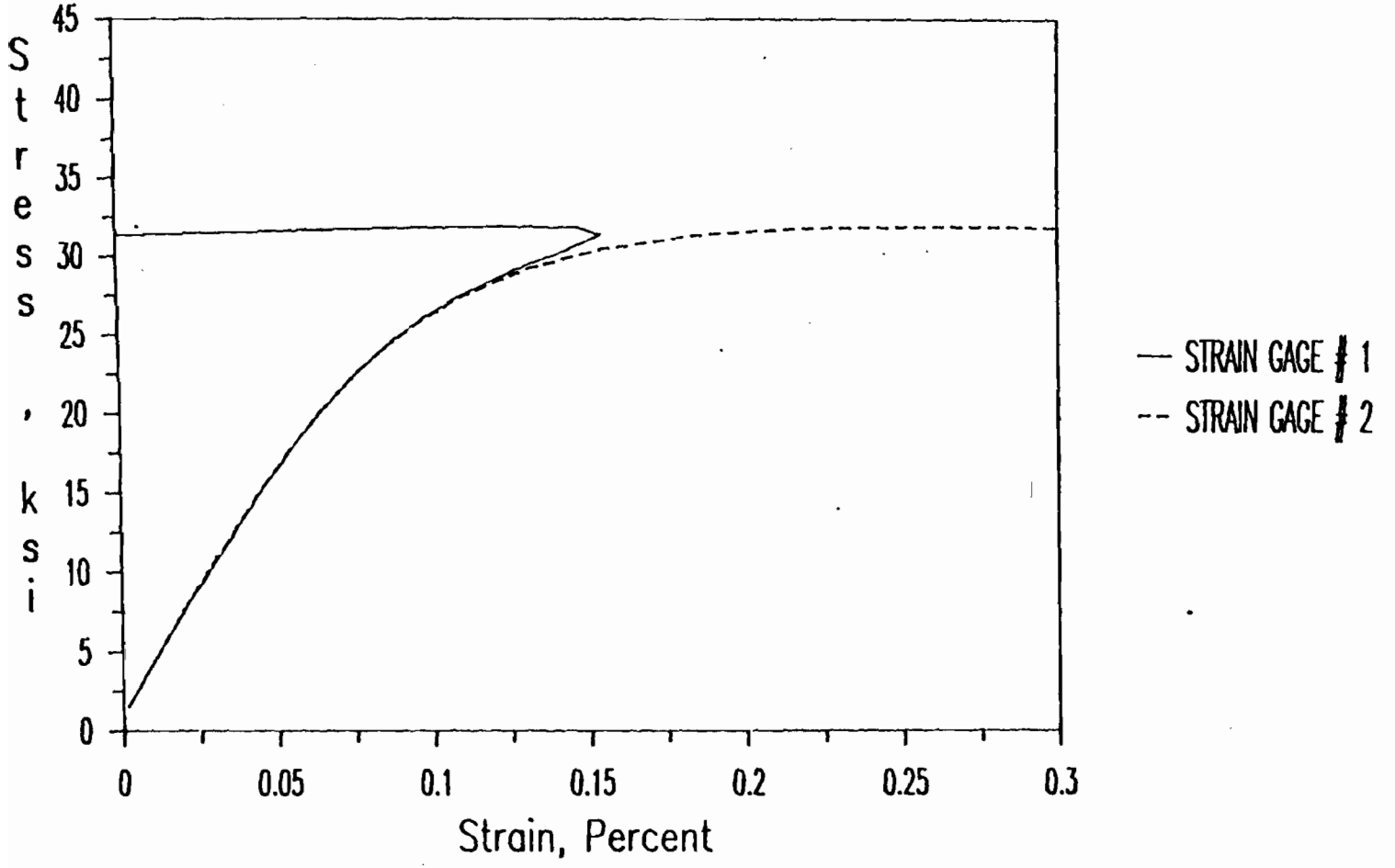

Figure 3.61 Load-Strain Curves of Strain Gages # 1 and 2 Installed at the Tip of an Unstiffened Flange (Spec. 2C0A)

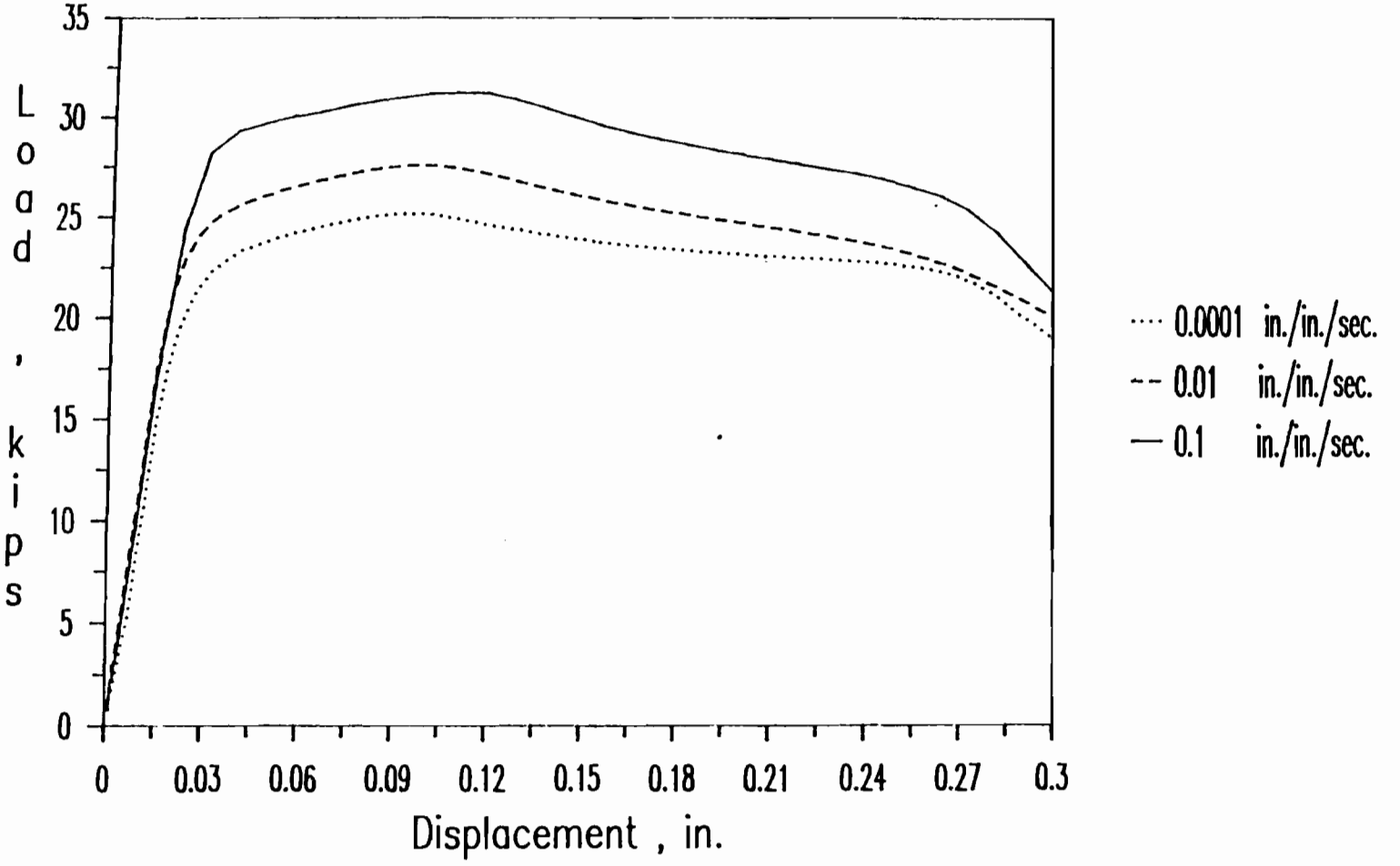

Figure 3.62 Load-Displacement Curves for I-Shaped Stub Columns 2A1A, 2A2A, and 2A3A

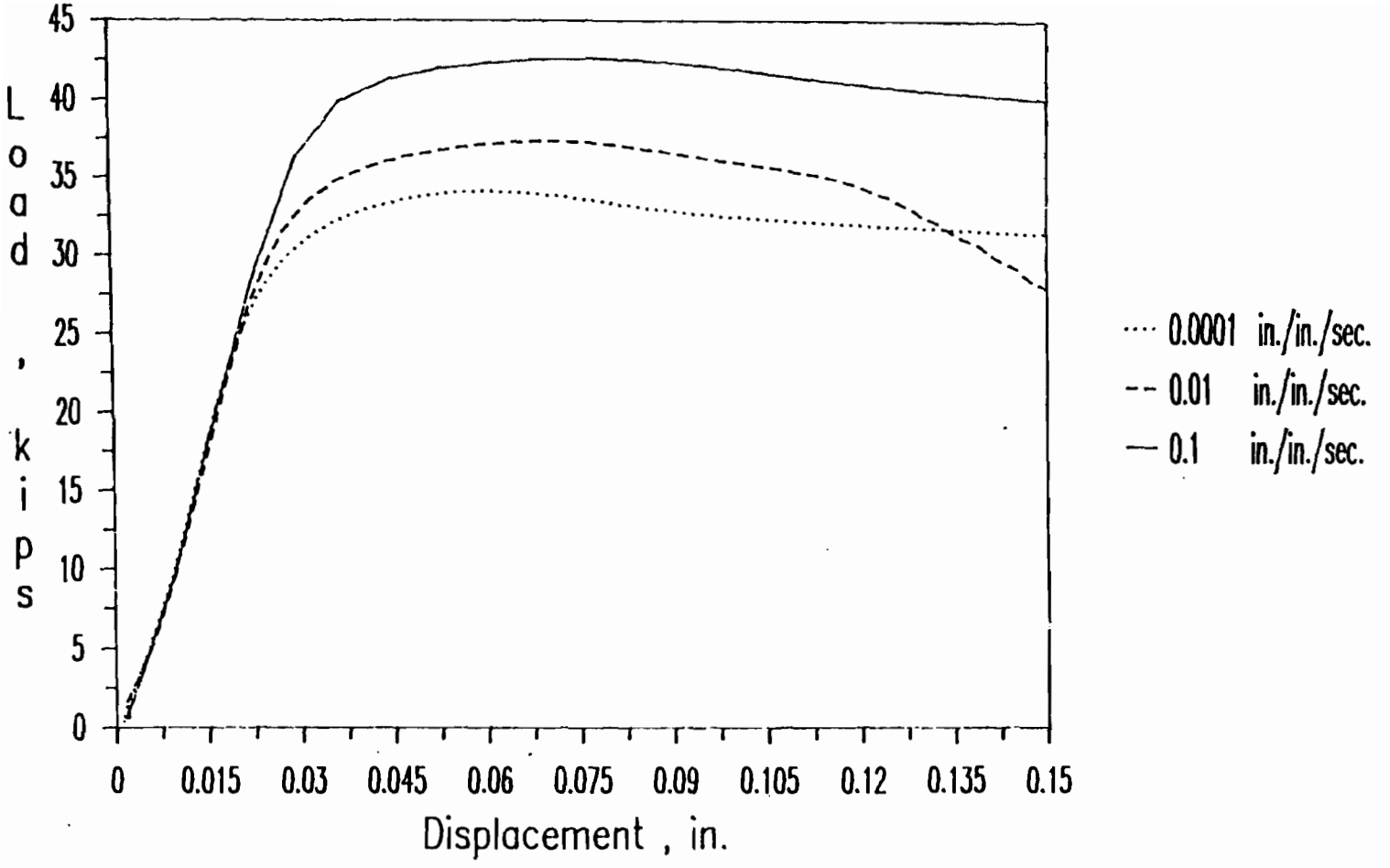

Figure 3.63 Load-Displacement Curves for I-Shaped Stub Columns 2B1A, 2B2A, and 2B3A

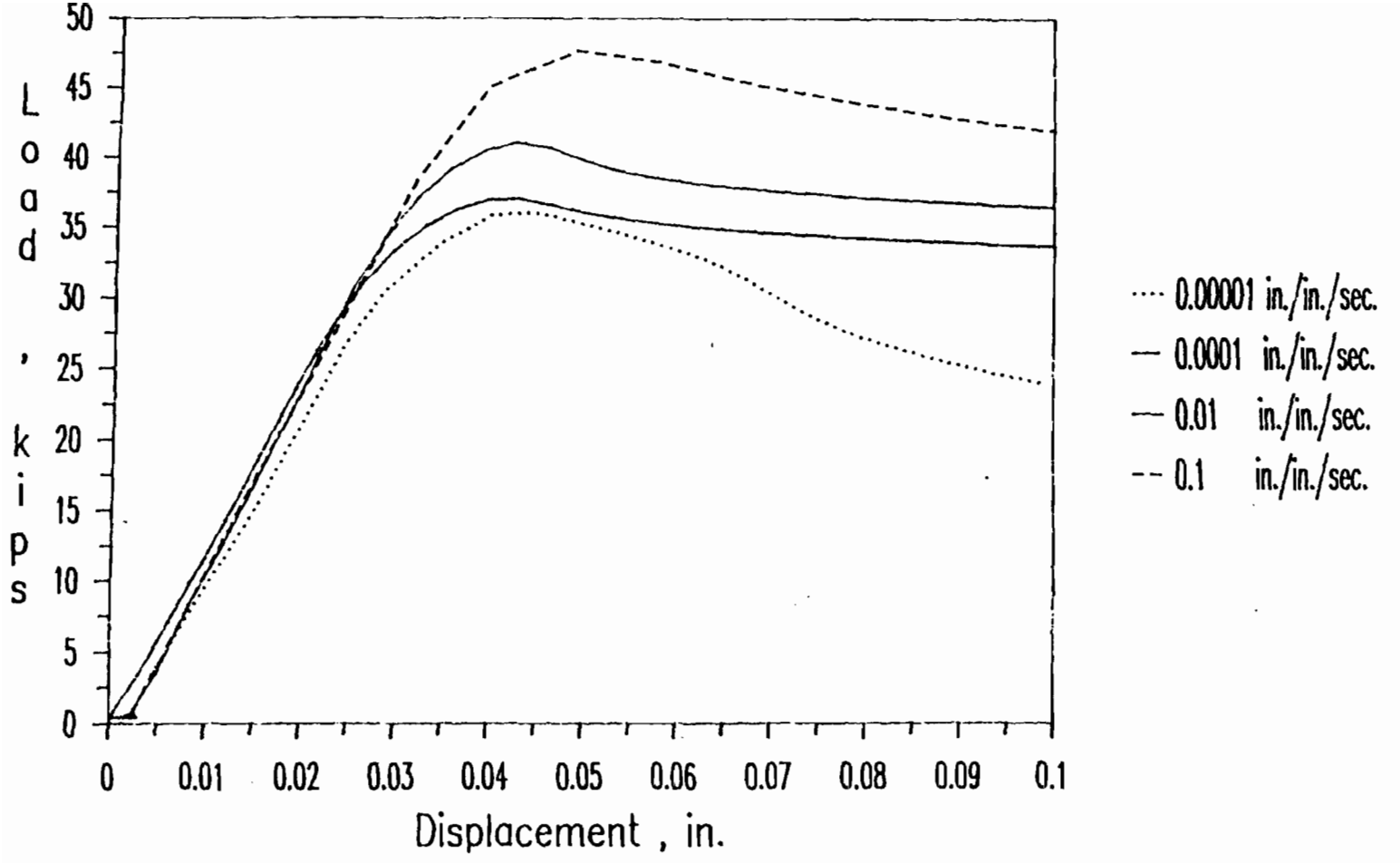

Figure 3.64 Load-Displacement Curves for I-Shaped Stub Columns 2C0A,2C1A, 2C2A, and 2C3A

displacement curves for the specimens having the same w/t ratio but tested under different strain rates.

IV. EVALUATION OF EXPERIMENTAL DATA

A. GENERAL

The material test results presented earlier in Section III.B are discussed in Section IV.B of this chapter with an emphasis on the effects of strain rate on the mechanical properties of sheet steels. The materials used in the coupon experimental program included virgin steels for tensile and compressive tests and steels with different amounts of cold stretching for tensile tests only. They were tested in both longitudinal and transverse directions under different strain rates. The strain rates varied from 0.0001 to 1.0 in./in./sec. The mechanical properties of 35XF sheet steel developed from material tests are used later in the evaluation of structural member test data.

Sections IV.C.1 through IV.C.4 of this chapter evaluate the experimental results of beams and stub columns fabricated from 35XF sheet steels and tested under different strain rates. The strain rates varied from 0.00001 to 0.1 in./in./sec. These sections compare the test results and the failure loads predicted by the current AISI Automotive Steel Design Manual[22] for structural members tested in this study. Also discussed in these sections is the effect of strain rate on the structural strengths of test specimens. Comparison between tested and predicted midspan deflections for beam tests is presented in Section IV.C.5.

B. EVALUATION OF MATERIAL TEST DATA

1. Mechanical Properties. The test results indicate that all mechanical properties are affected by the strain rate and the amount of cold stretching. Tables 4.1 and 4.2 compare the dynamic mechanical properties determined at the strain rate of 1.0 in./in./sec. and the static properties determined at the strain rate of 0.0001 in./in./sec. The effects of strain rate on proportional limit, yield stress, and tensile strength are discussed in the following sections.

a. Proportional Limit F_{pr}. The proportional limits are obtained for compression tests only. The proportional limits for tensile tests could not be obtained accurately because of limited number of data points recorded by the MTS extensometer in the linear range of the tensile stress-strain curves. The proportional limits of sheet steels tested in compression increased with the strain rate. The percentage increases in proportional limits for the three materials studied in compression are: 9% to 24% for 100XF steel, 4% to 22% for 50XF steel, and 14% to 24% for 35XF steel when the strain rate increased from 0.0001 to 0.01 in./in./sec. to 1.0 in./in./sec.

b. Yield Strength or Yield Point, F_y. In Tables 4.1 and 4.2, the dynamic yield strength, $(F_y)_d$, and the static yield strength, $(F_y)_s$, are compared by using a ratio of $(F_y)_d/(F_y)_s$. In the above expressions, $(F_y)_d$ is the yield strength determined for the strain rate of 1.0 in./in./sec. while $(F_y)_s$ is the yield strength determined for the strain rate of 0.0001 in./in./sec. It can be seen that for all cases, the yield strength of sheet steel increases with the strain rate. The increases in

Table 4.1

Ratios of Dynamic to Static Mechanical Properties for Three Sheet Steels Based on Tables 3.20 to 3.25

Type of Sheet Steel	$(F_y)_d/(F_y)_s$	$(F_u)_d/(F_u)_s$	$(\text{Elong.})_d/(\text{Elong.})_s$
100XF-LT-Virgin	1.04	1.04	---
100XF-TT-Virgin	1.04	1.04	1.3
50XF-LT-Virgin	1.10	1.08	0.8
50XF-LT-2%, Non-Aged	1.11	1.10	1.0
50XF-LT-8%, Non-Aged	1.08	1.10	0.85
50XF-LT-2%, Aged	1.07	1.08	0.99
50XF-LT-8%, Aged	1.04	1.07	----
50XF-TT-Virgin	1.10	1.09	1.04
50XF-TT-2%, Non-Aged	1.15	1.09	1.06
50XF-TT-8%, Non-Aged	1.06	1.08	0.85
50XF-TT-2%, Aged	1.07	1.11	0.80
50XF-TT-8%, Aged	1.05	1.09	0.92
35XF-LT-Virgin	1.29	1.15	1.05
35XF-LT-2%, Non-Aged	1.20	1.15	1.04
35XF-LT-8%, Non-Aged	1.14	1.16	1.18
35XF-LT-2%, Aged	1.19	1.14	1.14
35XF-LT-8%, Aged	1.16	1.18	0.96
35XF-TT-Virgin	1.29	1.13	0.98
35XF-TT-2%, Non-Aged	1.22	1.17	1.04
35XF-TT-8%, Non-Aged	1.15	1.18	1.08
35XF-TT-2%, Aged	1.15	1.14	1.09
35XF-TT-8%, Aged	1.12	1.17	1.05

Notes :

$(F_y)_d$ = dynamic yield stress for the strain rate of 1.0 in./in./sec.

$(F_y)_s$ = static yield stress for the strain rate of 0.0001 in./in./sec.

$(F_u)_d$ = dynamic ultimate stress for the strain rate of 1.0 in./in./sec.

$(F_u)_s$ = static ultimate stress for the strain rate of 0.0001 in./in./sec.

Table 4.2

Ratios of Dynamic to Static Compressive Yield Stresses for Three Sheet Steels Based on Tables 3.32 to 3.36

Type of Sheet Steel	$(F_y)_d/(F_y)_s$
100XF-LC	1.07
100XF-TC	1.07
50XF-LC	1.10
50XF-TC	1.09
35XF-LC	1.24
35XF-TC	1.33

Notes :

$(F_y)_d$ = dynamic yield stress for the strain rate of 1.0 in./in./sec.

$(F_y)_s$ = static yield stress for the strain rate of 0.0001 in./in./sec.

yield strength for the three steels studied in tension are: 4% for 100XF steel, 4% to 15% for 50XF steel, and 12% to 29% for 35XF steel, while the percentage increases in yield strength for the three steels studied in compression are: 7% for 100XF steel, 9% to 10% for 50XF steel, and 24% to 33% for 35XF steel when the strain rate increased from 0.0001 to 1.0 in./in./sec. It is observed from these tables that the increases in yield strength for the virgin materials are independent of the test direction (Longitudinal or Transverse). However, for 35XF steel tested in compresstion the increase in yield stress in the transverse direction is larger than that in the longitudinal direction. It is also noted that the percentage increase in proportional limit obtained from compression testes are larger than the percentage increase in yield stress when the strain rate increased from 0.0001 in./in./sec. to 1.0 in./in./sec. The effect of the strain rate on yield strength decreases as the static yield stress and/or the amount of cold stretching increases. Previous study[120] indicated that the increase in yield strength due to cold work is caused mainly by strain hardening and strain aging. However, in the present investigation no significant increase in yield strength was observed due to the strain aging effect. It was also observed that strain aging has little or no effect on the type of stress-strain curve.

c. Ultimate Tensile Strength, F_u. Similar to the effect of strain rate on yield strength, the ultimate tensile strengths of sheet steels increased with the strain rate. The increases in ultimate tensile strengths for the three materials studied in tension are: 4% for 100XF steel, 7% to 11% for 50XF steel, and 13% to 18% for 35XF steel when the strain rate increased from 0.0001 to 1.0 in./in./sec. As mentioned in

Chapter III, the ultimate compressive strengths could not be obtained because the buckling of the unsupported lengths at each end of the compressive specimen limited the obtainble range of the stress-strain curves to approximately 1.8 percent. It is noted from Table 4.1 that the amounts of increase in ultimate tensile strength due to the increase in strain rate are approximately the same for both longitudinal tension and transverse tension.

2. Strain Rate Sensitivity. In the literature review, Equation 2.13 gives the relation between the stress and the strain rate at a given strain as follows:

$$\sigma = C\,\dot{\epsilon}^{m} \tag{4.1}$$

By applying Equation 4.1 to two different strain rates and eliminating C we have:

$$m = \ln(\sigma_2 / \sigma_1) / \ln(\dot{\epsilon}_2 / \dot{\epsilon}_1) \tag{4.2}$$

for two given values of the flow stress of a material at two different strain rates. The strain-rate sensitivity exponent m may be calculated by using Equation 4.2.

Tables 4.3 and 4.4 list the values of the strain-rate sensitivities, which were calculated on the basis of Equation 4.2. The value of m_1 was calculated for the yield strengths corresponding to the strain rates of 0.0001 in./in./sec. and 0.01 in./in./sec., while the value of m_2 was calculated for the yield strengths corresponding to the strain rates of 0.01 in./in./sec. and 1.0 in./in./sec. In Table 4.3 whenever only two strain rates were used in the tests, the value of m_3 was calculated for the yield strengths corresponding to the strain rates of 0.0001

Table 4.3

Values of Strain Rate Sensitivities m for Three Sheet Steels Based on the Changes of the Yield Stresses at Different Strain Rates, (Tensile Coupon Tests)

Type of Sheet Steel	m_1	m_2	m_3
100XF-LT-Virgin	0.003	0.005	0.004
100XF-TT-Virgin	0.003	0.006	0.004
50XF-LT-Virgin	0.009	0.013	0.011
50XF-LT-2%, Non-Aged	0.009	0.014	0.011
50XF-LT-8%, Non-Aged	0.009	0.009	0.009
50XF-LT-2%, Aged	0.005	0.009	0.007
50XF-LT-8%, Aged	0.000	0.008	0.004
50XF-TT-Virgin	0.011	0.009	0.010
50XF-TT-2%, Non-Aged	-----	-----	0.016
50XF-TT-8%, Non-Aged	-----	-----	0.006
50XF-TT-2%, Aged	-----	-----	0.008
50XF-TT-8%, Aged	-----	-----	0.005
35XF-LT-Virgin	0.022	0.033	0.027
35XF-LT-2%, Non-Aged	0.015	0.023	0.019
35XF-LT-8%, Non-Aged	0.013	0.016	0.014
35XF-LT-2%, Aged	0.008	0.029	0.019
35XF-LT-8%, Aged	0.014	0.018	0.016
35XF-TT-Virgin	0.018	0.037	0.028
35XF-TT-2%, Non-Aged	-----	-----	0.021
35XF-TT-8%, Non-Aged	-----	-----	0.015
35XF-TT-2%, Aged	-----	-----	0.016
35XF-TT-8%, Aged	-----	-----	0.013

Notes:

m_1 = strain rate sensitivity based on the changes of yield stress between strain rates of 0.0001 and 0.01 in./in./sec.

m_2 = strain rate sensitivity based on the changes of yield stress between strain rates of 0.01 and 1.0 in./in./sec.

m_3 = strain rate sensitivity based on the changes of yield stress between strain rates of 0.0001 and 1.0 in./in./sec.

Table 4.4

Values of Strain Rate Sensitivities m for Three Sheet Steels Based on the Changes of the Yield Stresses at Different Strain Rates, (Compressive Coupon Tests)

Type of Sheet Steel	m_1	m_2
100XF-LC	0.008	0.007
100XF-TC	0.004	0.009
50XF-LC	0.012	0.009
50XF-TC	0.010	0.008
35XF-LC	0.015	0.031
35XF-TC	0.025	0.037

Notes:

m_1= strain rate sensitivity based on the changes of yield stress between strain rates of 0.0001 in./in./sec. and 0.01 in./in./sec.

m_2= strain rate sensitivity based on the changes of yield stress between strain rates of 0.01 in./in./sec. and 1.0 in./in./sec.

in./in./sec. and 1.0 in./in./sec. From Tables 4.3 and 4.4, it can be seen that, in general, the value of m in tension and compression increases as the strain rate increases. The strain rate sensitivity decreases progressively as the static yield strength level increases. For tension tests with different amounts of cold-stretching, the strain-rate sensitivity decreases as the amount of cold stretching increases.

3. Prediction of Yield Strength for High Strain Rates. Figures 4.1 through 4.6 copmare the average values of tensile and compressive yield strengths for the three materials (35XF, 50XF, and 100XF) in the virgin condition and tested in the longitudinal direction under different strain rates. The data plotted in these figures are in terms of yield stress vs. logarithmic strain rate. For each case, the following second degree polynomial was developed using the Least Square Method in the strain-rate range of 0.0001 to 1.0 in./in./sec.

$$Y = A + B\,X + C\,X^2 \qquad (4.3)$$

where

Y = yield stress

$X = \log(\dot{\epsilon})$

A, B, and C = polynomial constants.

The polynomial parameters A, B, and C are given at the top of the curve for each case in Figures 4.1 through 4.6. The values of the tensile and compressive yield strengths of the steels used in this investigation at higher strain rate (larger than 1.0 and up to 1000 in./in./sec.) could

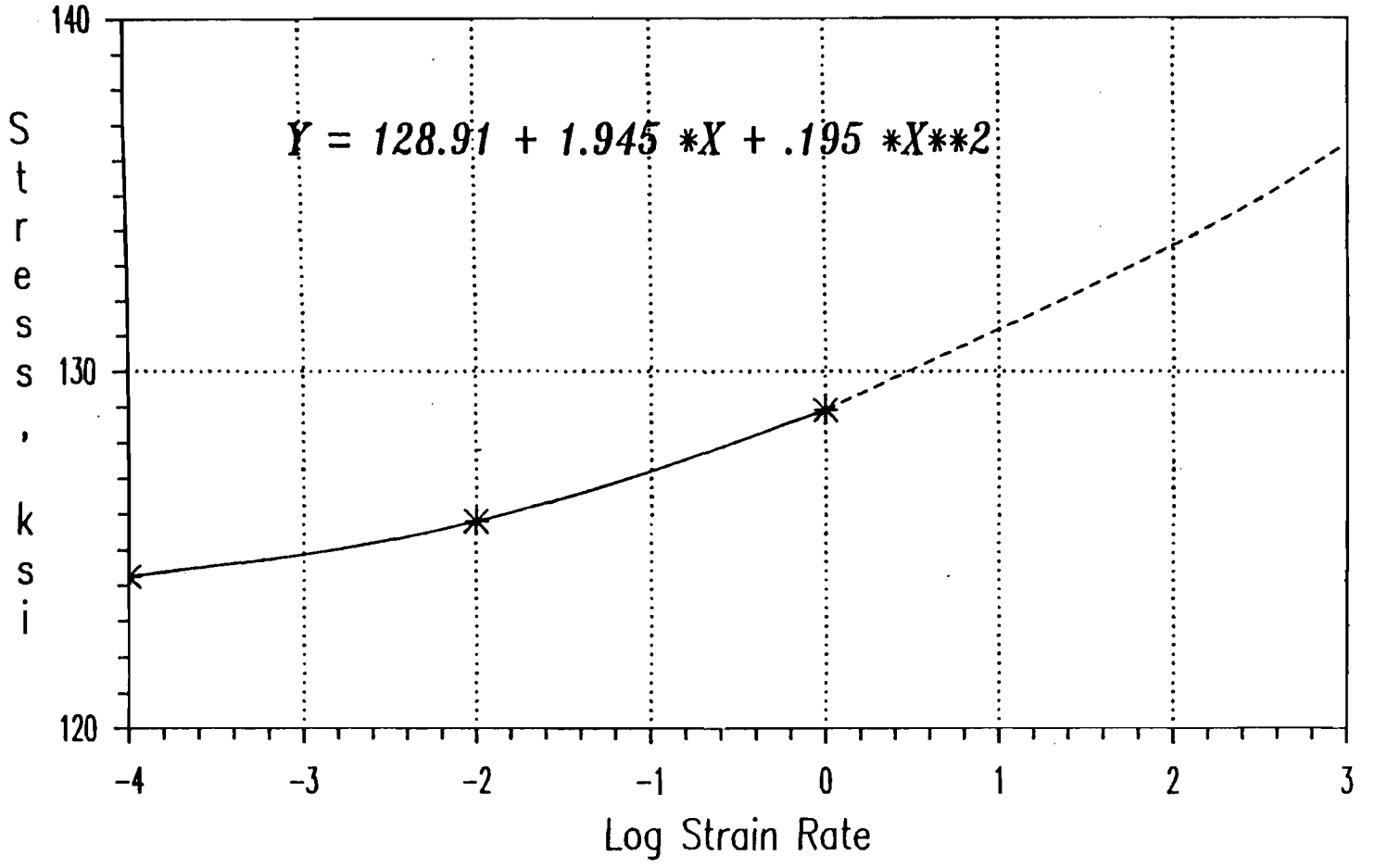

Fig. 4.1 Tensile Yield Stress vs. Logarithmic Strain-Rate Curve for 100XF-LT, (Virgin Material)

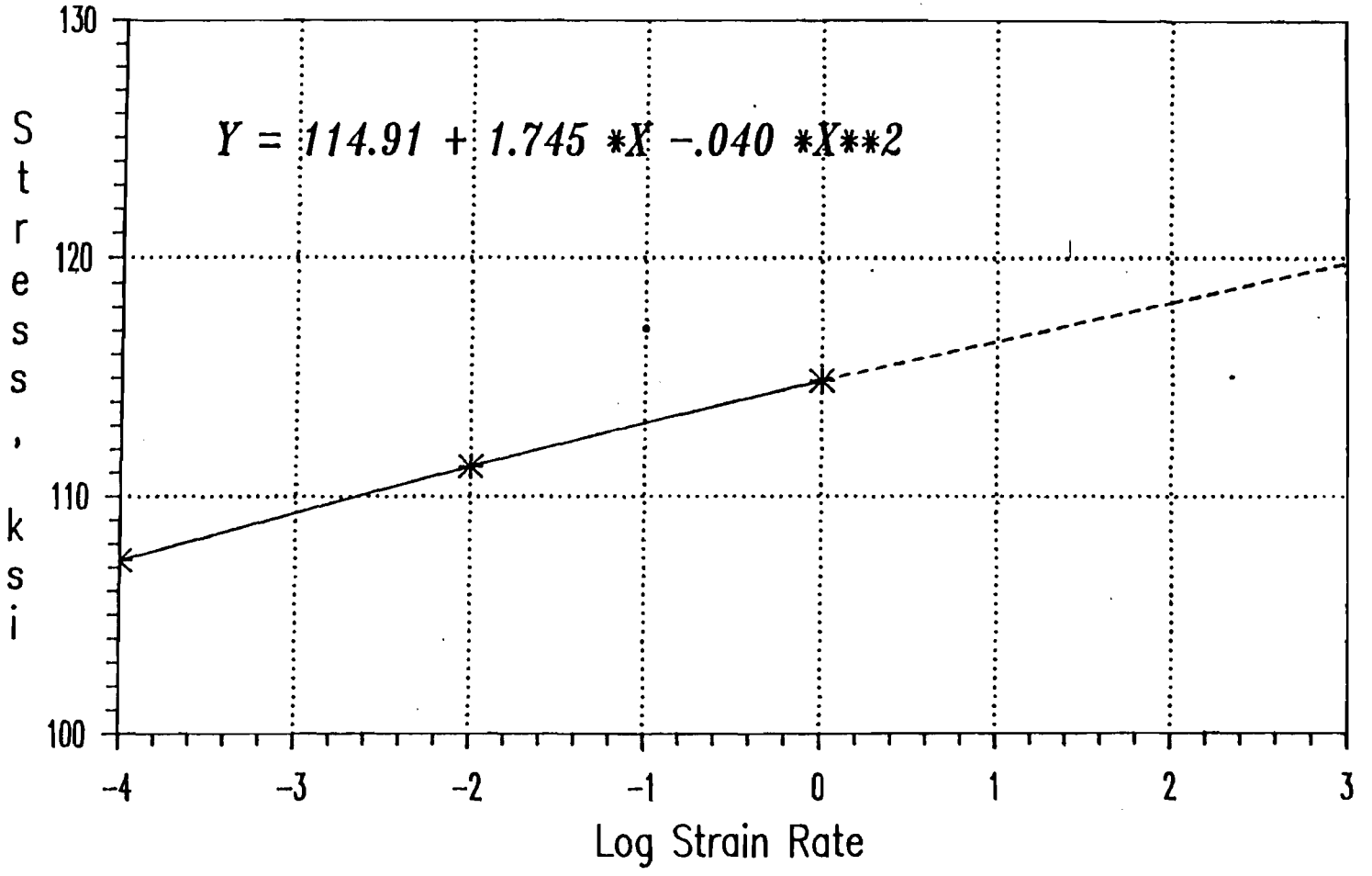

Fig. 4.2 Compressive Yield Stress vs. Logarithmic Strain-Rate Curve for 100XF-LC, (Virgin Material)

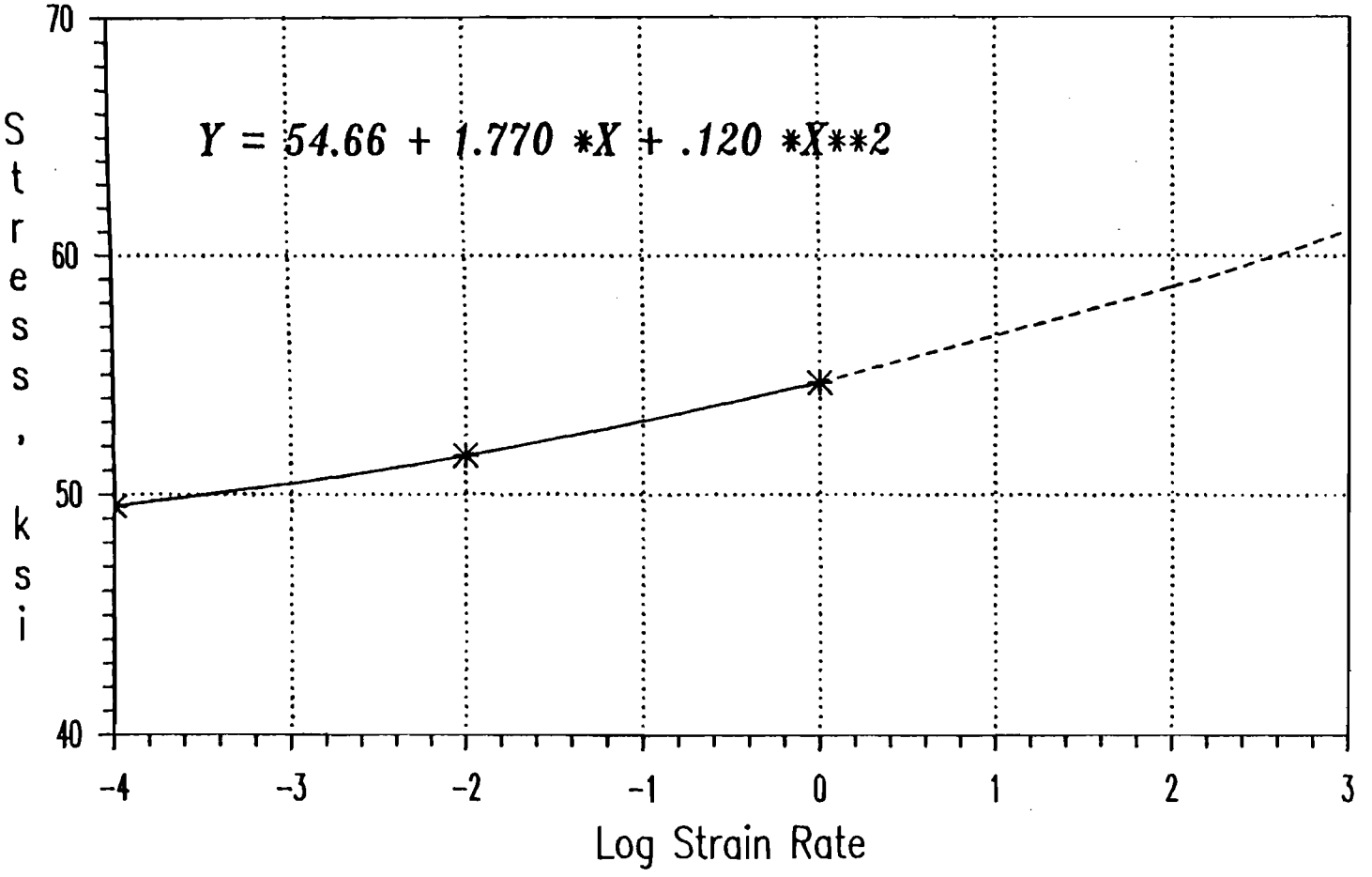

Fig. 4.3 Tensile Yield Stress vs. Logarithmic Strain-Rate Curve for 50XF-LT, (Virgin Material)

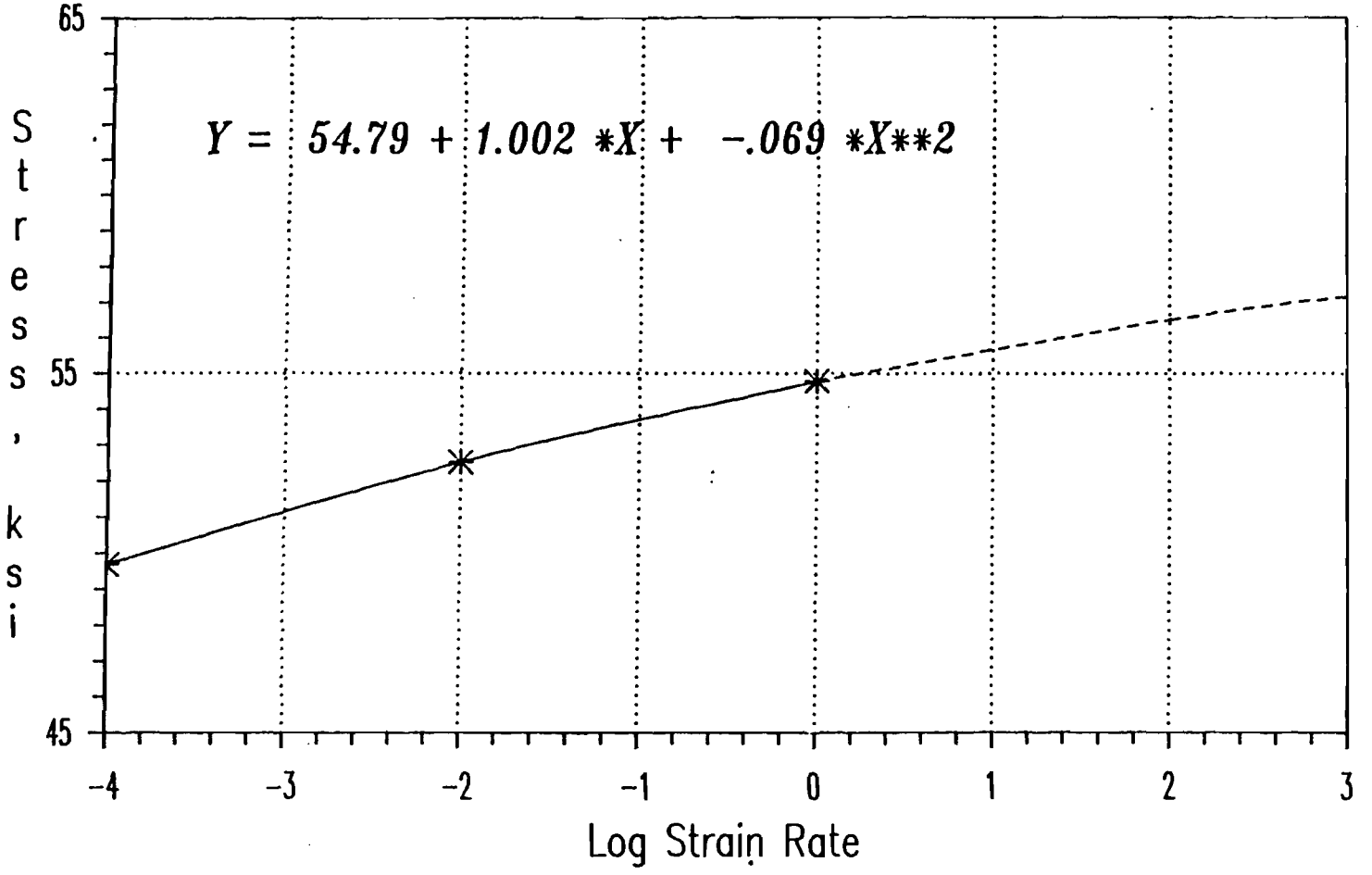

Fig. 4.4 Compressive Yield Stress vs. Logarithmic Strain-Rate Curve for 50XF-LC, (Virgin Material)

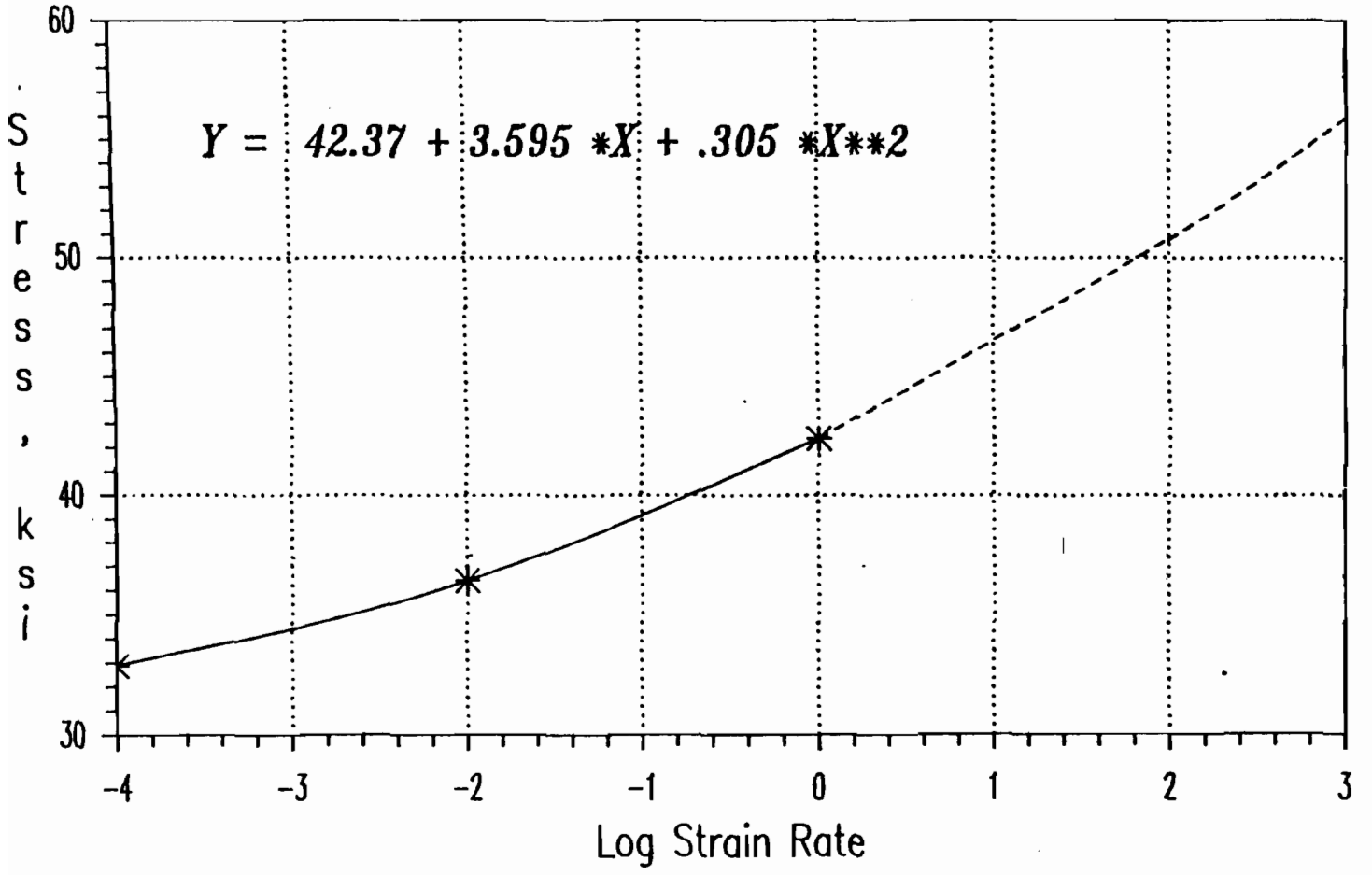

Fig. 4.5 Tensile Yield Stress vs. Logarithmic Strain-Rate Curve for 35XF-LT, (Virgin Material)

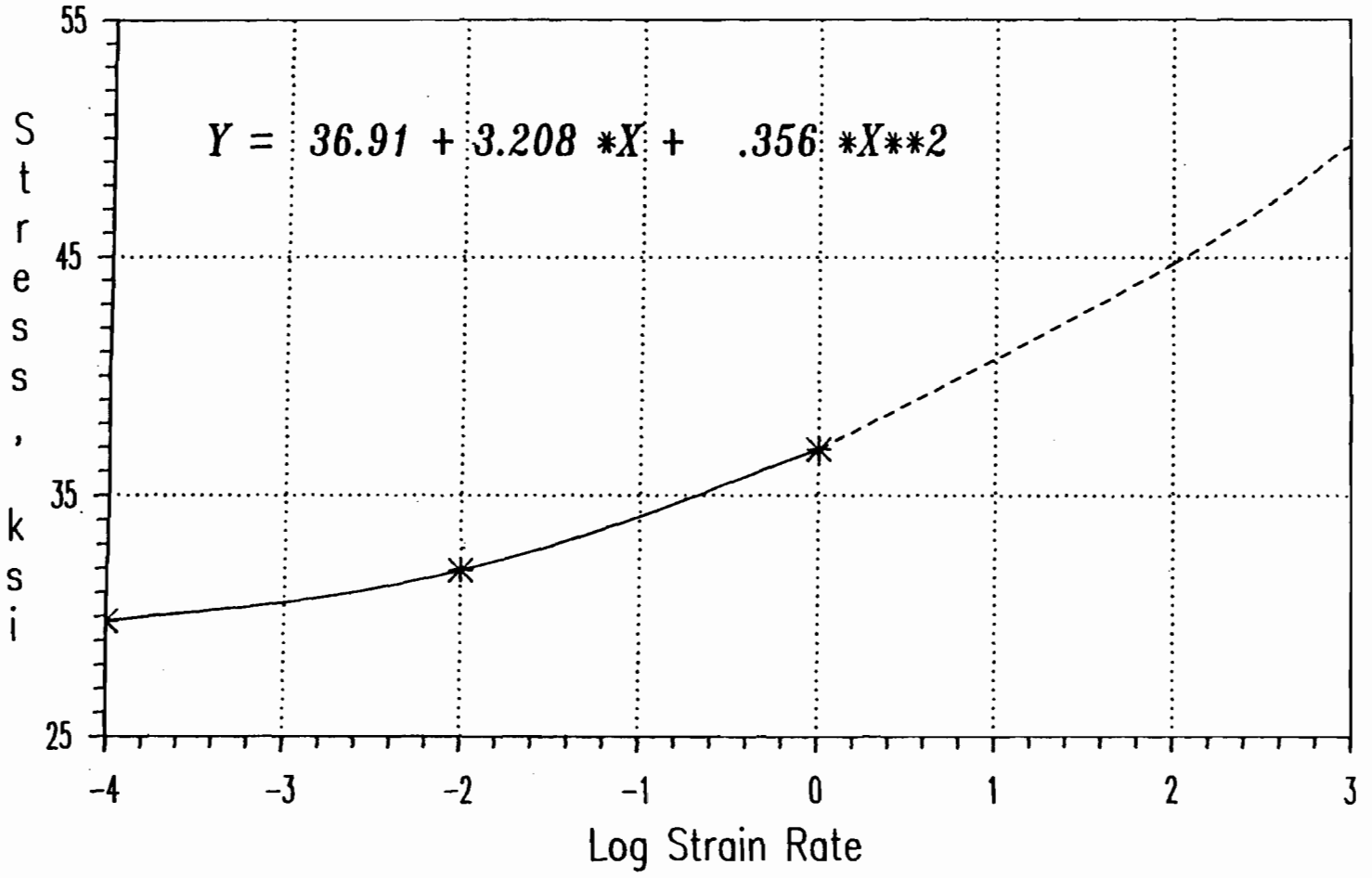

Fig. 4.6 Compressive Yield Stress vs. Logarithmic Strain-Rate Curve for 35XF-LC, (Virgin Material)

be extrapolated by using the equation or the curve for each individual case.

In Ref. 24 the polynomial constants A, B, and C are given for other cases such as: ultimate tensile strengths, yield and tensile ultimate strengths of the three materials tested in the transverse direction, and yield and ultimate strengths of the three materials tested with different amounts of cold stretching.

C. EVALUATION OF STRUCTURAL MEMBER EXPERIMENTAL DATA

1. Beam Tests for the Study of Stiffened Elements. Hat sections have been designed and fabricated for beam tests to study the post-buckling strengths of stiffened compression elements using 35XF sheet steels. All beam specimens were subjected to two point loads located at L/8 from end supports as shown in Figs. 3.30 and 3.31. Lateral torsional buckling of beam specimens was not critical according to the design of specimens. The webs of hat-section beams were designed to be fully effective. The weight of the test specimen and the weight of the cross beam placed on the top of the specimen (approx. 70 lbs.) are small as compared to the ultimate loads and were neglected in the evaluation of test results. The tested tensile yield stress was used for computing yield moment (M_y) and ultimate moment (M_u) for all beam specimens studied in this investigation.

a. Critical Local Buckling Strength. The compression flange of beam specimens may buckle locally in either the elastic or the inelastic range,

depending on the w/t ratio of the flange. The elastic critical local buckling stress of the stiffened flange subjected to uniform compression can be computed by using Eq. (2.25).

$$(f_{cr})_E = \frac{k\pi^2 E}{12(1-\mu^2)(w/t)^2} \qquad (2.25)$$

where

k = buckling coefficient

E = modulus of elasticity

w = width of plate

t = thickness of plate

μ = Poisson's ratio.

If the local critical buckling stress exceeds the proportional limit, the stiffened flange buckles in the inelastic range. The inelastic buckling stress, $(f_{cr})_I$, can be computed by using the following equation, which is based on the tangent modulus concept[121].

$$(f_{cr})_I = F_y - \frac{F_{pr}(F_y - F_{pr})}{(f_{cr})_E} \qquad (4.4)$$

where

F_y = yield stress of steel

F_{pr} = proportional limit of steel

$(f_{cr})_E$ = elastic local critical buckling stress defined in Eq. (2.25)

Therefore, the computed critical local buckling moment, $(M_{cr})_{comp}$, of a beam corresponding to the initiation of local buckling of its compression flange can be calculated as follows:

$$(M_{cr})_{comp} = S_{xc} \; f_{cr} \qquad (4.5)$$

where

f_{cr} = critical local buckling stress of the compression flange

S_{xc} = elastic section modulus of the full cross section relative to the compression flange.

The predicted and tested critical local buckling moments of beam specimens are listed in columns (5) and (6) of Table 4.5, respectively. The predicted critical buckling moments were computed by using Eq. (4.5). The tested critical local buckling moments were determined from the product of bending arm (L/8) and one half of the tested critical local buckling load ($P_{cr}/2$) as follows:

$$(M_{cr})_{test} = \frac{P_{cr} \; L}{16} \qquad (4.6)$$

In the above equation, the tested critical local buckling loads (P_{cr}) were determined from load-strain diagrams by using a modified strain reversal method as discussed in Ref. 119. L is the span length of the beam specimen. The values of S_{xc}, f_{cr}, P_{cr}, and L are also given in Table 4.5.

Table 4.5

Comparison of Computed and Tested Critical Buckling Moments
Beam Specimens with a Stiffened Flange (Based on k=4.0)
(35XF Sheet Steel)

Specimen	S_{xc} ($in.^3$) (1)	f_{cr} (ksi) (2)	$(P_{cr})_{test}$ (kips) (3)	L (in.) (4)	$(M_{cr})_{comp}$ (in.-kips) (5)	$(M_{cr})_{test}$ (in.-kips) (6)	(6)/(5) (7)
3A0A	0.342	28.12	N/A	43.00	9.62	N/A	N/A
3A1A	0.335	28.02	N/A	43.00	9.39	N/A	N/A
3A1B	0.338	28.04	N/A	43.00	9.48	N/A	N/A
3A2A	0.343	30.22	N/A	43.00	10.36	N/A	N/A
3A2B	0.338	30.09	N/A	43.00	10.17	N/A	N/A
3B0A	1.011	23.55	5.833	73.00	23.81	26.61	1.117
3B1A	1.010	23.73	6.214	73.00	23.97	28.35	1.183
3B1B	1.005	23.55	5.774	73.00	23.67	26.34	1.113
3B2A	1.003	25.66	6.106	73.00	25.74	27.86	1.082
3B2B	1.009	25.63	N/A	73.00	25.86	N/A	N/A
3C0A	1.615	18.38	5.042	91.00	29.68	28.68	0.966
3C1A	1.635	18.16	5.291	91.00	29.69	30.10	1.014
3C1B	1.638	18.19	5.217	91.00	29.79	29.67	0.996
3C2A	1.626	18.17	5.823	91.00	29.54	33.12	1.121
3C2B	1.624	18.45	5.760	91.00	29.96	32.76	1.093
Mean							1.076
Standard Deviation							0.066

The load versus strain diagrams of the hat sections with small w/t ratios (3A Sections) showed no sign of critical local buckling. As presented in Table 4.5, most of the tested critical local buckling moments were greater than the predicted values. This is because a minimum value of 4.0 was used as the buckling coefficient for stiffened compression flanges ignoring any effect of rotational edge restraint provided by the adjoining webs. The mean value of nine $(M_{cr})_{test}/(M_{cr})_{comp}$ ratios is equal to 1.076 with a standard deviation of 0.066. The tested critical local buckling loads of the hat sections with relatively large w/t ratios (3C Sections) increased with increasing strain rate.

It was observed from 3C beam specimens that the number of half sine waves in the stiffened compression flange is the same for all tests regardless of the strain rate used for the test.

b. Ultimate Flexural Strength. The ultimate section strength can be calculated either on the basis of initiation of yielding in the effective section or on the basis of the inelastic reserve capacity.

i) Yield Flexural Strength. Based on the initiation of yielding in the effective section, the computed yield moment, $(M_y)_{comp}$, of a beam can be calculated by using the following equation:

$$(M_y)_{comp} = F_y S_e \qquad (4.7)$$

where

F_y = static or dynamic yield stress of steel

S_e = elastic section modulus of the effective section

calculated with the extreme compression or tension stress at F_y.

Tables 4.6(a) and 4.6(b) compare the computed and tested yield moments. Table 4.6(a) uses static yield stress for all tests, while Table 4.6(b) uses static or dynamic yield stress taking into account the effect of strain rate on yield stress value as discussed in Refs. 23. and 24. In these tables, the computed yield moment $(M_{y)comp}$ is listed in column (5) for each specimen. These yield moments were calculated by using Eq. (4.4) with effective section moduli (S_e) computed from the AISI effective width formula. The yield stress value is listed in column (2). Note that this value is a constant in Table 4.6(a), but it increases with strain rate in Table 4.6(b). The tested yield moments listed in column (6) were determined from the product of bending arm (L/8) and one half of the yield loads (P_y) determined from load-strain diagrams as follows:

$$(M_y)_{test} = \frac{P_y L}{16} \qquad (4.8)$$

The tested yield load and the effective section modulus computed for the extreme compression or tension stress at F_y are also given in Tables 4.6(a) and 4.6(b). As presented in these tables, all tested yield moments were greater than the predicted values. As expected, the ratios of tested to computed yield moments listed in Table 4.6(a) are larger than those listed in Table 4.6(b), because the latter table takes into account the effect of strain rate on yield stress. In both tables the ratio of tested to computed yield moments increases with strain rate for most of the

Table 4.6(a)

Comparison of Computed and Tested Yield Moments
Beam Specimens with a Stiffened Flange
(35XF Sheet Steel)
(Based on Static Yield Stress)

Specimen	S_e	F_y	$(P_y)_{test}$	L	$(M_y)_{comp}$	$(M_y)_{test}$	(6)/(5)
	($in.^3$)	(ksi)	(kips)	(in.)	(in.-kips)	(in.-kips)	
	(1)	(2)	(3)	(4)	(5)	(6)	(7)
3A0A	.268	32.02	3.773	43.00	8.58	10.14	1.182
3A1A	.258	32.02	3.936	43.00	8.25	10.58	1.282
3A1B	.262	32.02	4.137	43.00	8.39	11.12	1.325
3A2A	.271	32.02	4.799	43.00	8.68	12.90	1.486
3A2B	.260	32.02	4.844	43.00	8.32	13.02	1.565
3B0A	.635	32.02	5.824	73.00	20.32	26.57	1.307
3B1A	.646	32.02	4.894	73.00	20.69	22.33	1.079
3B1B	.629	32.02	5.668	73.00	20.15	25.86	1.283
3B2A	.626	32.02	6.511	73.00	20.04	29.71	1.482
3B2B	.632	32.02	7.130	73.00	20.23	32.53	1.608
3C0A	.924	32.02	6.038	91.00	29.58	34.34	1.161
3C1A	.930	32.02	6.825	91.00	29.79	38.82	1.303
3C1B	.932	32.02	6.112	91.00	29.86	34.76	1.164
3C2A	.925	32.02	6.873	91.00	29.61	39.09	1.320
3C2B	.930	32.02	6.684	91.00	29.78	38.01	1.276
Mean							1.321
Standard Deviation							0.148

Table 4.6(b)

Comparison of Computed and Tested Yield Moments
Beam Specimens with a Stiffened Flange
(35XF Sheet Steel)
(Based on Dynamic Yield Stress)

Specimen	S_e	F_y	$(P_y)_{test}$	L	$(M_y)_{comp}$	$(M_y)_{test}$	(6)/(5)
	($in.^3$)	(ksi)	(kips)	(in.)	(in.-kips)	(in.-kips)	
	(1)	(2)	(3)	(4)	(5)	(6)	(7)
3A0A	.268	32.02	3.773	43.00	8.58	10.14	1.182
3A1A	.258	32.87	3.936	43.00	8.46	10.58	1.251
3A1B	.262	32.87	4.137	43.00	8.62	11.12	1.290
3A2A	.271	36.40	4.799	43.00	9.87	12.90	1.307
3A2B	.260	36.40	4.844	43.00	9.45	13.02	1.378
3B0A	.635	32.02	5.824	73.00	20.32	26.57	1.307
3B1A	.645	32.87	4.894	73.00	21.21	22.33	1.053
3B1B	.629	32.87	5.668	73.00	20.66	25.86	1.252
3B2A	.623	36.40	6.511	73.00	22.66	29.71	1.311
3B2B	.628	36.40	7.130	73.00	22.87	32.53	1.422
3C0A	.924	32.02	6.038	91.00	29.58	34.34	1.161
3C1A	.929	32.87	6.825	91.00	30.53	38.82	1.271
3C1B	.931	32.87	6.112	91.00	30.61	34.76	1.135
3C2A	.917	36.40	6.873	91.00	34.33	39.09	1.139
3C2B	.922	36.40	6.684	91.00	34.52	38.01	1.101
Mean							1.237
Standard Deviation							0.102

cases. As shown in Table 4.6(a), the average value of $(M_y)_{test}/(M_y)_{comp}$ ratios is equal to 1.321 with a standard deviation of 0.148, while in Table 4.6(b) the mean value of $(M_y)_{test}/(M_y)_{comp}$ ratios is equal to 1.237 with a standard deviation of 0.102.

ii) Inelastic Reserve Capacity. The inelastic reserve capacity of flexural members, which allows partial yielding of a cross section, is recognized in the 1986 AISI Automotive Design Manual. It can be used to predict the ultimate load capacities of flexural members provided that such members satisfy the specific requirements.

The ultimate strengths of hat sections or track sections with yielded tension flanges may be calculated on the basis of inelastic reserve capacity. Figure 4.7 shows the stress distribution in sections with yielded tension flanges at ultimate moment. The following equations can be used to compute the values of y_c, y_t, y_p, and y_{tp} shown in Fig. 4.1 and the ultimate moment, M_u. For the purpose of simplicity, midline dimensions were used in the calculations.[26]

$$y_c = \frac{b_t - b_c + 2d}{4} \qquad (4.9)$$

$$y_t = d - y_c \qquad (4.10)$$

$$y_p = \frac{y_c}{C_y} \qquad (4.11)$$

$$y_{cp} = y_c - y_p \qquad (4.12)$$

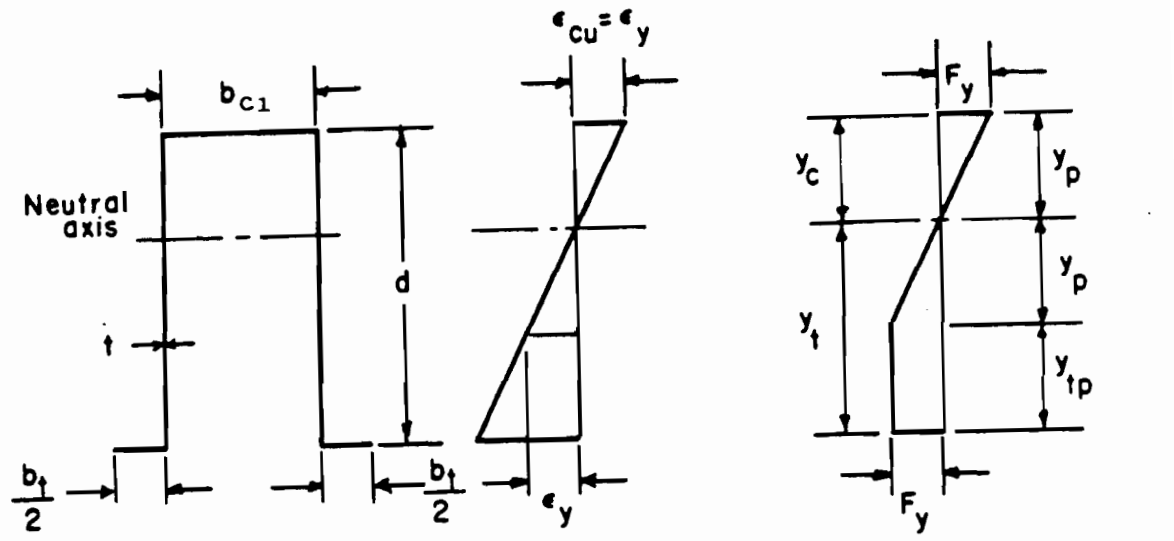

(a)

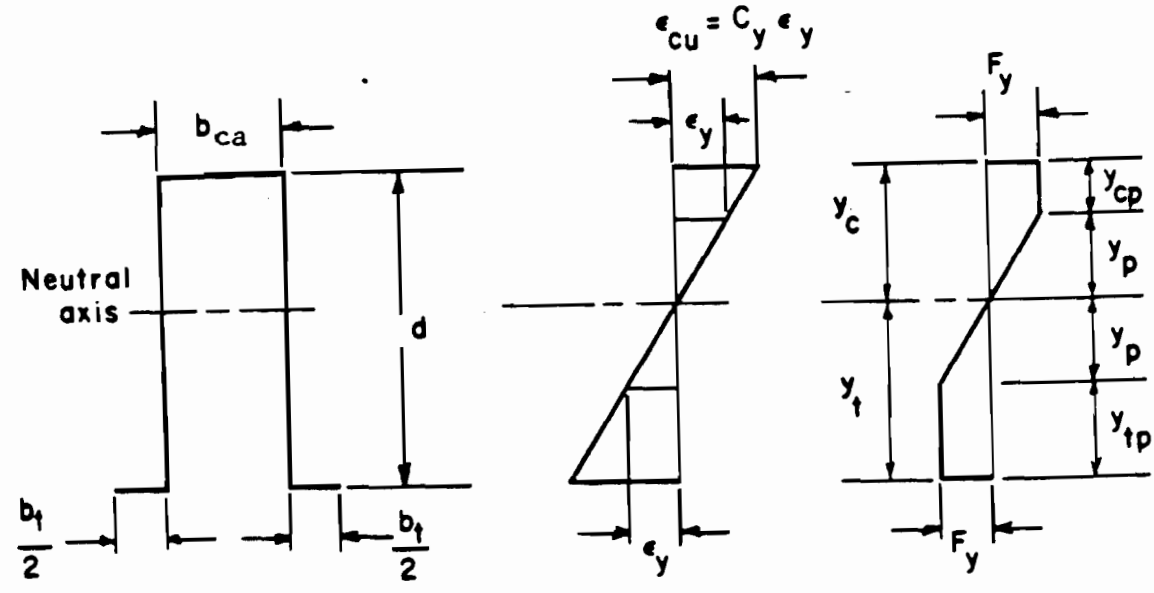

(b)

Fig. 4.7 Stress Distribution in Sections with Yielded Tension Flanges at Ultimate Moments[26]

$$y_{tp} = y_t - y_p \qquad (4.13)$$

$$M_u = F_y t\left[b_c y_c + 2y_{cp}(y_p + \frac{y_{cp}}{2}) + \frac{4}{3}(y_p)^2 + 2y_{tp}(y_p + \frac{y_{tp}}{2}) + b_t y_t \right] \qquad (4.14)$$

where

b_c = effective width of the compression flange

b_t = total width of the tension flange

d = depth of the section

t = thickness of the section

C_y = compression strain factor for stiffened compression elements without intermediate stiffeners, which can be determined as follows:

$$C_y = 3 \qquad \text{for} \quad w/t \leq \lambda_1 \qquad (4.15(a))$$

$$C_y = 3 - 2(\frac{w/t - \lambda_1}{\lambda_2 - \lambda_1}) \qquad \text{for} \quad \lambda_1 < w/t < \lambda_2 \qquad (4.15(b))$$

$$C_y = 1 \qquad \text{for} \quad w/t \geq \lambda_2 \qquad (4.15(c))$$

where $\lambda_1 = \dfrac{1.11}{\sqrt{F_y/E}}$ (4.16)

$$\lambda_2 = \frac{1.28}{\sqrt{F_y/E}} \quad . \tag{4.17}$$

According to the AISI Automotive Design Manual, the ultimate moments computed by using the inelastic reserve capacity procedure should not exceed the limit of:

$$(M_u)_{comp} = 1.25\ S_e\ F_y \tag{4.18}$$

Tables 4.7(a) and 4.7(b) present the predicted and tested ultimate moments. Similar to Tables 4.6(a) and 4.6(b), Table 4.7(a) uses static yield stress while Table 4.7(b) uses static or dynamic yield stress corresponding to the strain-rate value used in the test. It was found that the computed ultimate moments using Eq. (4.14) for all hat-beam tests exceed the values computed by Eq. (4.18) and listed in column (5) of Tables 4.7(a) and 4.7(b). The tested ultimate moments were determined by the product of bending arm (L/8) and one half of the ultimate load $(P_u)/2$ as follows:

$$(M_u)_{test} = \frac{P_u\ L}{16} \tag{4.19}$$

Table 4.7(a)

Comparison of Computed and Tested Failure Moments Based on the Effective Width Formulas in the 1986 AISI Automotive Steel Design Manual for Beam Specimens with a Stiffened Flange
(35XF Sheet Steel)
(Based on Static Yield Stress)

Specimen	Strain Rate (in./in./sec.) (1)	F_y (ksi) (2)	$(P_u)_{test}$ (kips) (3)	L (in.) (4)	$(M_u)_{comp}$ (in.-kips) (5)	$(M_u)_{test}$ (in.-kips) (6)	(6)/(5) (7)
3A0A	0.00001	32.02	5.69	43.00	10.73	15.29	1.425
3A1A	0.0001	32.02	5.43	43.00	10.33	14.59	1.412
3A1B	0.0001	32.02	5.72	43.00	10.49	15.37	1.465
3A2A	0.01	32.02	6.31	43.00	10.85	16.96	1.563
3A2B	0.01	32.02	6.39	43.00	10.41	17.17	1.649
3B0A	0.00001	32.02	6.38	73.00	25.41	29.11	1.146
3B1A	0.0001	32.02	6.54	73.00	25.86	29.84	1.154
3B1B	0.0001	32.02	6.49	73.00	25.17	29.61	1.037
3B2A	0.01	32.02	6.97	73.00	25.05	31.80	1.176
3B2B	0.01	32.02	7.63	73.00	25.29	34.81	1.376
3C0A	0.00001	32.02	6.53	91.00	36.98	37.14	1.004
3C1A	0.0001	32.02	6.99	91.00	37.22	39.75	1.068
3C1B	0.0001	32.02	6.96	91.00	37.30	39.58	1.061
3C2A	0.01	32.02	7.45	91.00	37.02	42.37	1.144
3C2B	0.01	32.02	7.42	91.00	37.22	42.20	1.134
Mean							1.254
Standard Deviation							0.200

Table 4.7(b)

Comparison of Computed and Tested Failure Moments Based on the Effective Width Formulas in the 1986 AISI Automotive Steel Design Manual for Beam Specimens with a Stiffened Flange (35XF Sheet Steel) (Based on Dynamic Yield Stress)

Specimen	Strain Rate (in./in./sec.) (1)	F_y (ksi) (2)	$(P_u)_{test}$ (kips) (3)	L (in.) (4)	$(M_u)_{comp}$ (in.-kips) (5)	$(M_u)_{test}$ (in.-kips) (6)	(6)/(5) (7)
3A0A	0.00001	32.02	5.69	43.00	10.73	15.29	1.425
3A1A	0.0001	32.87	5.43	43.00	10.57	14.59	1.380
3A1B	0.0001	32.87	5.72	43.00	10.77	15.37	1.427
3A2A	0.01	36.40	6.31	43.00	12.34	16.96	1.374
3A2B	0.01	36.40	6.39	43.00	11.81	17.17	1.454
3B0A	0.00001	32.02	6.38	73.00	25.40	29.11	1.146
3B1A	0.0001	32.87	6.54	73.00	26.51	29.84	1.126
3B1B	0.0001	32.87	6.49	73.00	25.82	29.61	1.147
3B2A	0.01	36.40	6.97	73.00	28.32	31.80	1.123
3B2B	0.01	36.40	7.63	73.00	28.59	34.81	1.217
3C0A	0.00001	32.02	6.53	91.00	36.97	37.14	1.004
3C1A	0.0001	32.87	6.99	91.00	38.16	39.75	1.042
3C1B	0.0001	32.87	6.96	91.00	38.26	39.58	1.034
3C2A	0.01	36.40	7.45	91.00	42.91	42.37	0.987
3C2B	0.01	36.40	7.42	91.00	43.15	42.20	0.978
Mean							1.191
Standard Deviation							0.169

Ultimate loads were determined from the maximum loads reached during the tests and are listed in column (3). In both Tables 4.7(a) and 4.7(b), the tested ultimate moments of specimens were compared with the calculated ultimate moments. It is noted from column (7) of these tables that the ratio of the tested ultimate moment to the computed value decreases with increasing w/t ratio. As shown in Table 4.7(a), the average value of $(M_u)_{test}/(M_u)_{comp}$ ratios is equal to 1.254 with a standard deviation of 0.200, while in Table 4.6(b) the mean value of $(M_u)_{test}/(M_u)_{comp}$ ratios is equal to 1.191 with a standard deviation of 0.169.

Figures 4.8 through 4.10 show graphically typical moment-displacement curves for 3B sections under different strain rates. The computed critical local buckling, yield, and ultimate moments are marked in these figures for comparison with the tested values and are obtained from Tables (4.5, 4.6(b), and 4.8(b)), respectively. It is observed from these figures that the critical local buckling moments are greater than the yield moments because the stress in the compression flange at the initiation of yielding (Fig. 4.11(b)) is less than the critical local buckling stress. The critical local buckling moments in these figures were calculated according to the stress distribution shown in Fig. 4.11(c).

Tables 4.8 and 4.9 were prepared to study the effect of strain rate on ultimate momemts of hat-beam specimens. Table 4.8 lists average ultimate moments. Each ultimate moment value listed in this table is the average of two similar tests except that for the test conducted at the strain rate of 0.00001 in./in./sec. for which only one test was performed

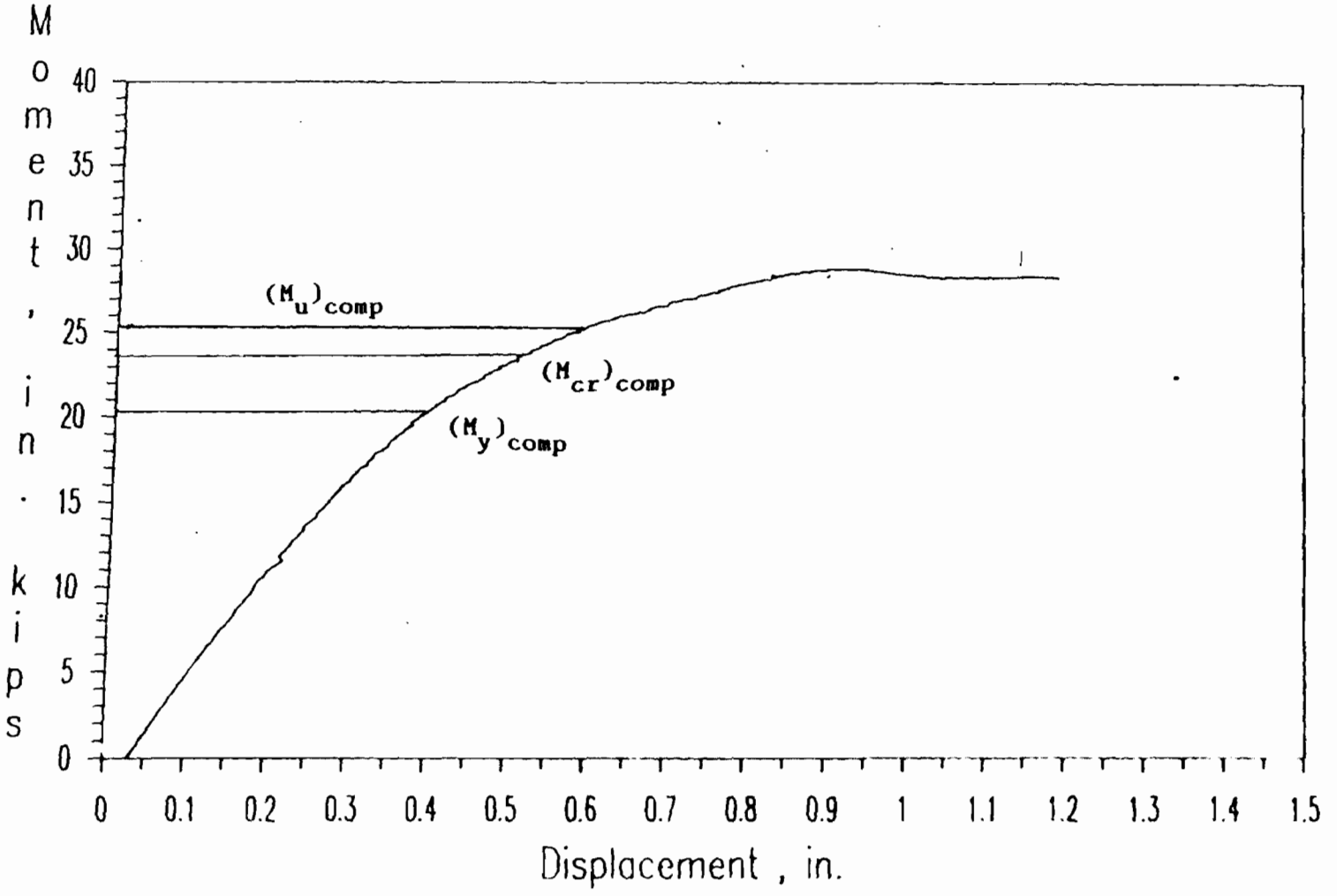

Fig. 4.8 Moment-Displacement Curve for Hat-Beam Specimen 3B0A

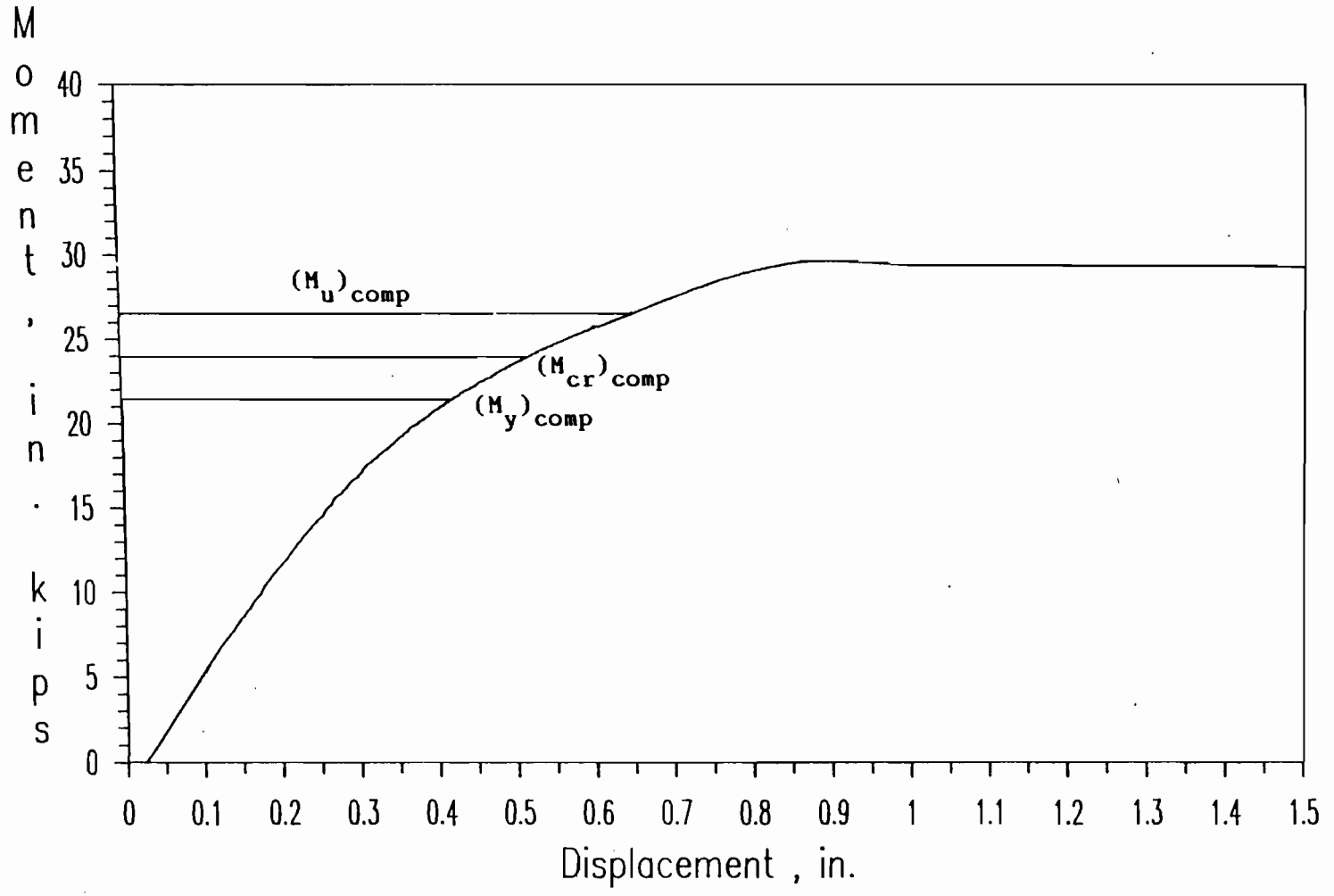

Fig. 4.9 Moment-Displacement Curve for Hat-Beam Specimen 3B1A

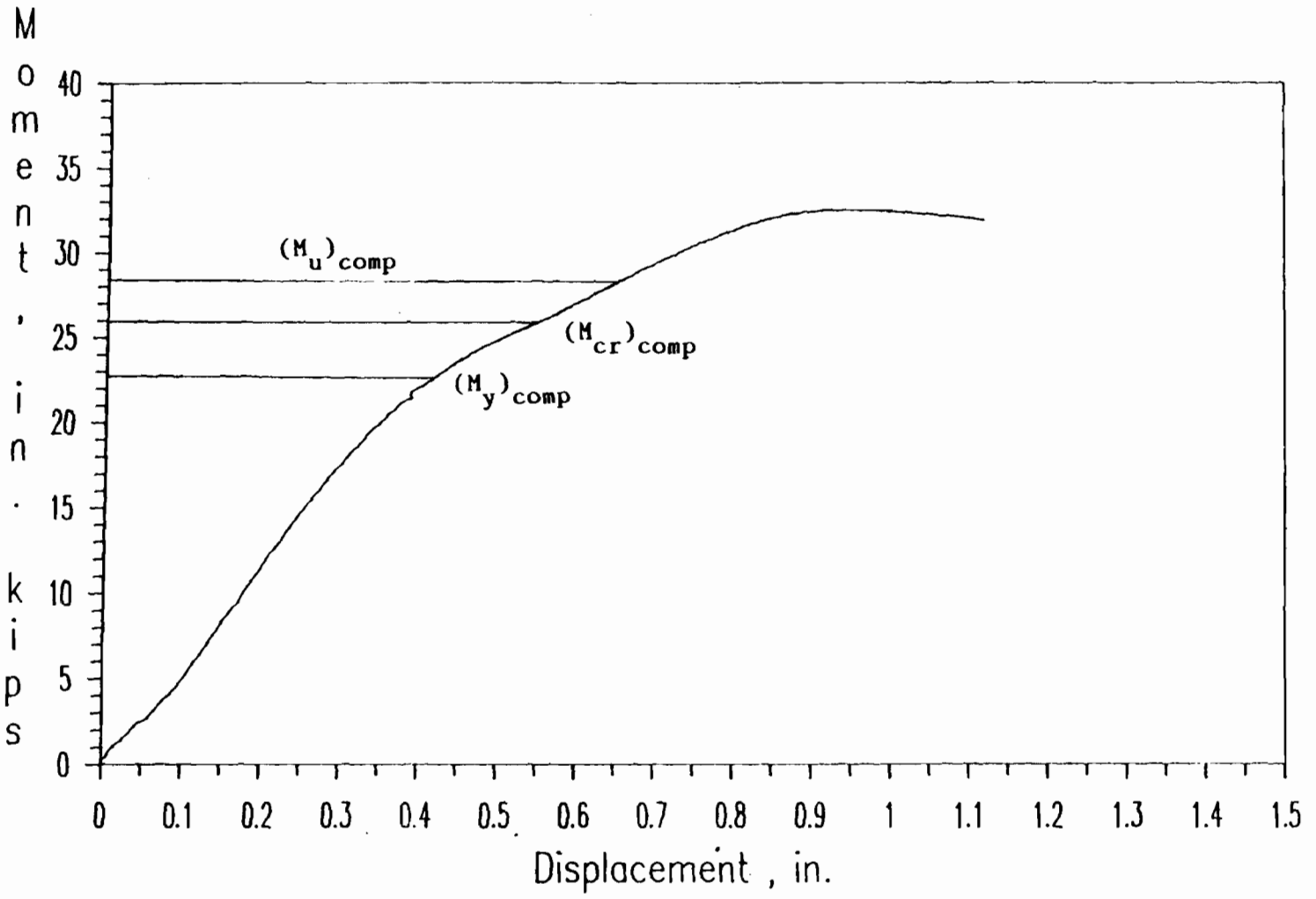

Fig. 4.10 Moment-Displacement Curve for Hat-Beam Specimen 3B2B

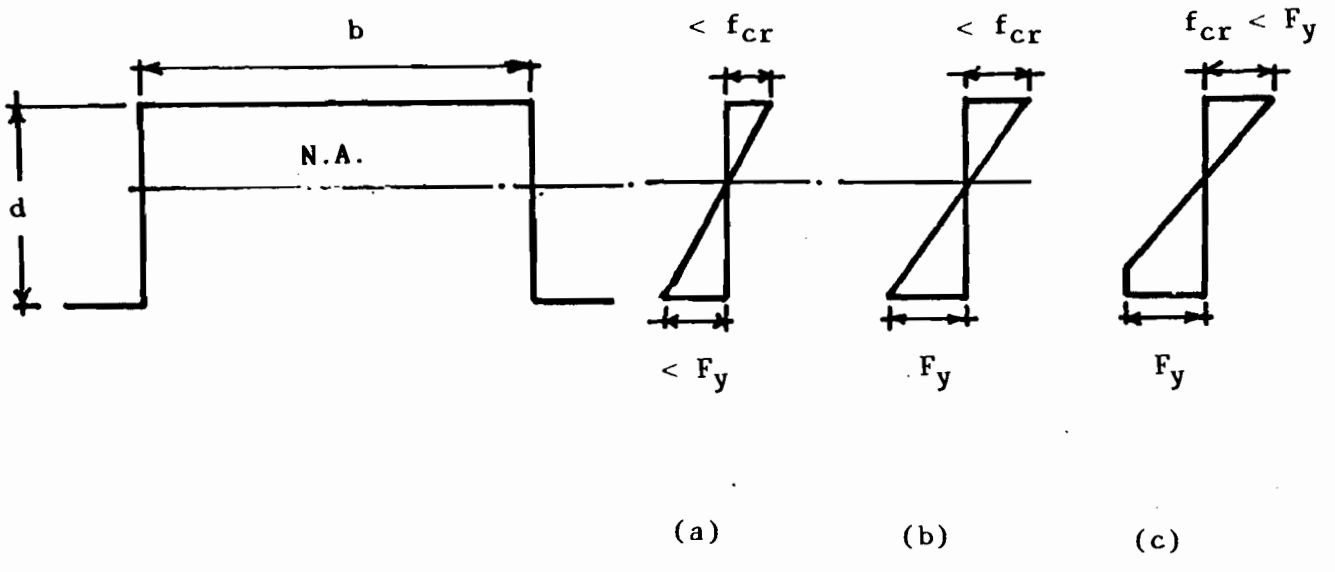

Fig. 4.11 Stress Distribution in Tested Hat Sections

Table 4.8

Average Tested Ultimate Moments for Hat-Beam Specimens with a Stiffened Flange (35XF Sheet Steel)

Strain Rate	Ultimate Moment, $(M_u)_{test}$, in.-kips		
in./in./sec.	w/t		
	29.62	56.09	76.08
0.00001	15.29	29.11	37.14
0.0001	14.98	29.72	39.66
0.01	17.06	33.30	42.28

Table 4.9

Average Ultimate Moment Ratios for Hat-Beam Specimens Having Stiffened Flanges (35XF Sheet Steel)

w/t	$(M_u)_0/(M_u)_1$	$(M_u)_2/(M_u)_1$
29.69	1.02	1.14
56.09	0.98	1.12
76.08	0.94	1.07

Notes :

$(M_u)_0$= Average ultimate moment for the hat-beam specimens tested at the strain rate of 0.00001 in./in./sec.

$(M_u)_1$= Average ultimate moment for the hat-beam specimens tested at the strain rate of 0.0001 in./in./sec.

$(M_u)_2$= Average ultimate moment for the hat-beam specimens tested at the strain rate of 0.01 in./in./sec.

for each w/t ratio. For the purpose of comparison, Table 4.9 lists the ratios of average ultimate moments obtained from Table 4.8. Each value listed in this table represents the ratio of two ultimate moments for tests having the same w/t ratio but conducted at two different strain rates. It is noted from Tables 4.8 and 4.9 that the ultimate moment increases with strain rate for all w/t ratios. The percentage increase of the ultimate moments for specimens having the same w/t ratio is larger at higher strain rate as compared to this increase at lower strain rate for most of the cases.

Figure 4.12 shows graphically the effect of strain rate on the ultimate moments of the hat-beam specimens. The horizontal axis represents logarithmic strain rate while the vertical axis represents the ratio of dynamic to static ultimate moments. The tests performed at strain rate of 0.0001 in./in./sec. are considered to be the static loading condition.

2. Stub Column Tests for the Study of Stiffened Elements. Box-shaped sections (Fig. 3.36) were designed and fabricated for stub column tests to study the post-buckling strengths of stiffened elements by using 35XF sheet steels. All stub columns were subjected to uniform compression. Overall column buckling is prevented by the design of stub columns. All webs of the stub columns were designed to be fully effective based on the 1986 AISI Automotive Design Manual. According to the same manual, all unstiffened elements are fully effective. The tested compressive yield stress was used for the evaluation of all stub column specimens studied in this investigation.

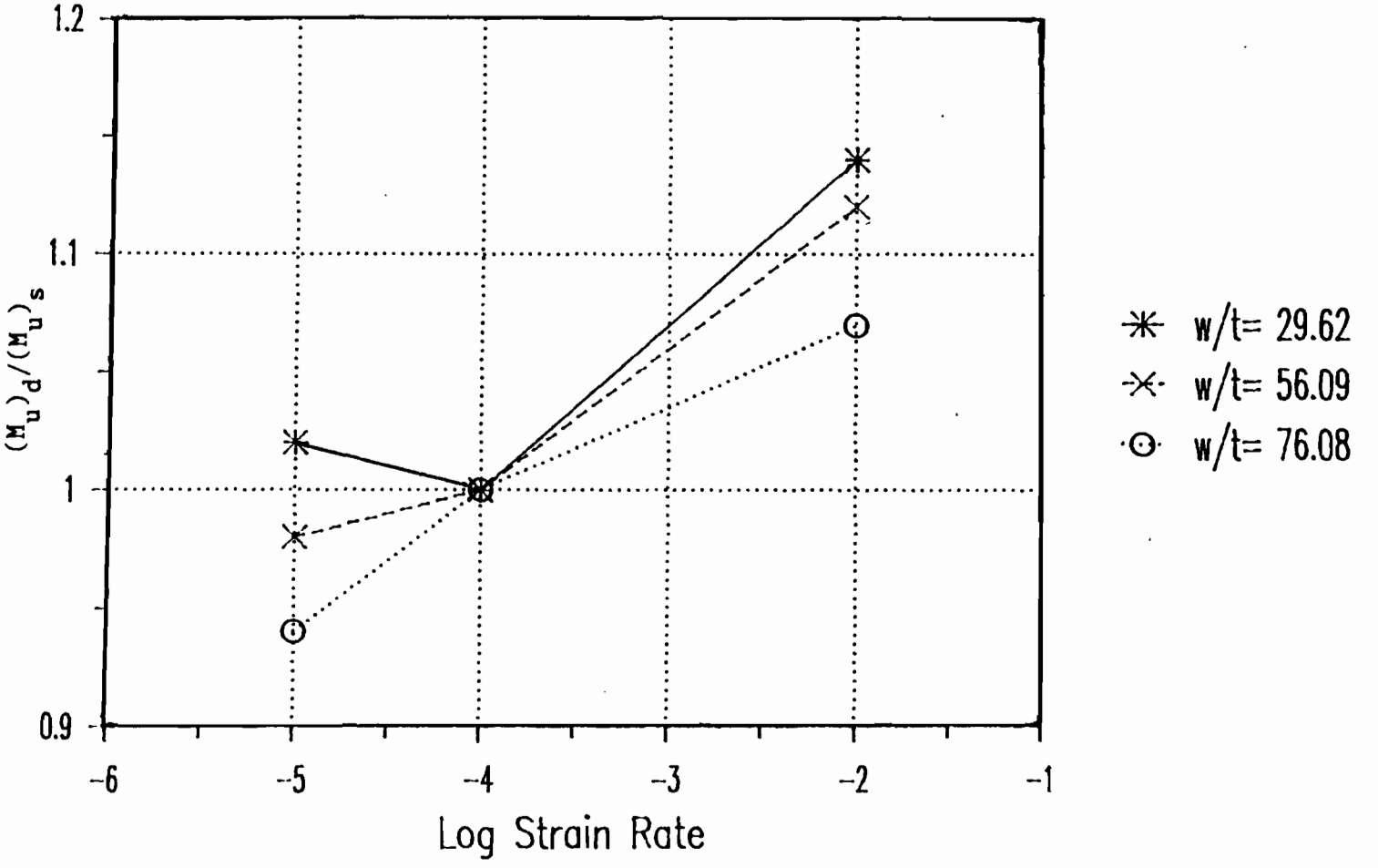

Fig. 4.12 Ratios of Dynamic to Static Average Ultimate Moments vs. Logarithmic Strain Rate for Hat-Beam Specimens

a. Critical Local Buckling Load. As discussed in Section IV.C.1.a, the critical local buckling stress, f_{cr}, of a stiffened element can be computed by using Eq. (2.25) or Eq. (4.4), depending on the w/t ratio of the stiffened element. Therefore, the critical local buckling loads of stub columns can be computed by using the following equation:

$$P_{cr} = A_g f_{cr} \tag{4.20}$$

where

f_{cr} = critical local buckling stress of stiffened element

A_g = gross cross-sectional area of stub column.

The total cross-sectional areas of stub columns with stiffened elements are given in Table 3.46. The critical local buckling stress for each specimen, listed in column (1) of Table 4.10, is the average value of two critical local buckling stresses of stiffened compression flanges of stub columns. No signs of critical local buckling were observed from the load-strain diagrams of box-shaped stub columns with small and medium w/t ratios (1A and 1B sections).

Table 4.10 compares the computed and tested critical local buckling loads for stub column specimens fabricated from 35XF sheet steels. The tested critical local buckling loads listed in column (3) of Table 4.10 were determined from load-strain diagrams by using a modified strain reversal method. The buckling coefficient used to calculate the buckling stress of stiffened elements in Eq. (4.4) was equal to 4.0. The mean value of $(P_{cr})_{test}/(P_{cr})_{comp}$ ratios is equal to 1.168 with a standard deviation

Table 4.10

Comparison of Computed and Tested Critical Buckling Loads
Stub Columns with Stiffened Flanges (Based on k=4.0)
(35XF Sheet Steel)

Specimen	f_{cr} (ksi) (1)	$(P_{cr})_{comp}$ (kips) (2)	$(P_{cr})_{test}$ (kips) (3)	(3)/(2) (4)
1A1A	28.35	34.19	N/A	N/A
1A1B	28.32	34.15	N/A	N/A
1A2A	30.30	36.39	N/A	N/A
1A2B	30.28	36.52	N/A	N/A
1A3A	32.16	38.62	N/A	N/A
1A3B	32.15	38.61	N/A	N/A
1B1A	26.79	41.46	N/A	N/A
1B1B	26.75	41.41	N/A	N/A
1B2A	28.55	44.00	N/A	N/A
1B2B	28.51	44.08	N/A	N/A
1B3A	30.22	46.73	N/A	N/A
1B3B	30.20	46.63	N/A	N/A
1C1A	24.25	46.72	50.56	1.082
1C1B	24.20	46.66	50.90	1.091
1C2A	25.83	49.60	58.09	1.171
1C2B	25.63	49.51	55.94	1.130
1C3A	26.88	51.99	66.15	1.272
1C3B	26.81	51.83	65.51	1.264
Mean				1.168
Standard Deviation				0.076

of 0.076. It is noted from column (4) of Table 4.10 that the ratio of tested to computed critical local buckling load $(P_{cr})_{test}/(P_{cr})_{comp}$ increases with increasing strain rate for stub columns with relatively large w/t ratios.

b. Ultimate Axial Load. By using the effective width concept discussed in Section II.C.1.d, a stub column specimen fails when the maximum edge stresses in the stiffened element reaches the yield stress of steel. The ultimate load carrying capacities of stub columns can be calculated by using Eq. (4.21).

$$P_u = A_e F_y \tag{4.21}$$

where

F_y = static or dynamic yield stress of steel

A_e = effective cross-sectional area of stub column for the maximum edge stress at F_y.

Equation (4.21) was used to calculate the failure loads of the specimens. In using Eq. (4.21), F_y values are listed in column (3) of Tables 4.11(a) and 4.11(b). For the calculation of computed ultimate loads, Table 4.11(a) uses static yield stress, while Table 4.11(b) uses static or dynamic yield stress, corresponding to the strain rate used in the test. The effective cross-sectional area of each stub column is listed in column (4) of Tables 4.11(a) and 4.11(b) by using the current AISI Automotive Design Manual and the appropriate yield stress. The

Table 4.11(a)

Comparison of Computed and Tested Failure Loads Based on the Effective Width Formulas in the 1986 AISI Automotive Steel Design Manual for Stub Columns with Stiffened Flanges
(35XF Sheet Steel)
(Based on Static Yield Stress)

Spec.	Strain Rate (in./in./sec.) (1)	w/t (2)	F_y (ksi) (3)	A_e ($in.^2$) (4)	$(P_u)_{comp}$ (kips) (5)	$(P_u)_{test}$ (kips) (6)	(6)/(5) (7)
1A1A	0.0001	27.15	29.83	1.2060	35.97	46.12	1.28
1A1B	0.0001	27.39	29.83	1.2060	35.97	44.89	1.25
1A2A	0.01	26.92	29.83	1.2010	35.82	50.02	1.40
1A2B	0.01	27.06	29.83	1.2010	35.82	49.29	1.38
1A3A	0.10	27.31	29.83	1.2009	35.82	53.54	1.49
1A3B	0.10	27.40	29.83	1.2009	35.82	54.37	1.52
1B1A	0.0001	38.93	29.83	1.5477	46.17	49.19	1.06
1B1B	0.0001	39.17	29.83	1.5480	46.18	53.54	1.16
1B2A	0.01	38.86	29.83	1.5412	45.97	56.28	1.22
1B2B	0.01	39.10	29.83	1.5463	46.13	57.01	1.23
1B3A	0.10	38.86	29.83	1.5463	46.13	64.78	1.40
1B3B	0.10	38.96	29.83	1.5440	46.06	60.87	1.32
1C1A	0.0001	52.69	29.83	1.8135	54.10	56.76	1.05
1C1B	0.0001	52.96	29.83	1.8122	54.06	56.52	1.05
1C2A	0.01	52.20	29.83	1.8122	54.06	61.02	1.13
1C2B	0.01	53.06	29.83	1.8147	54.13	64.58	1.19
1C3A	0.10	53.15	29.83	1.8164	54.18	73.96	1.36
1C3B	0.10	53.39	29.83	1.8130	54.08	69.27	1.28
Mean							1.265
Standard Deviation							0.139

Table 4.11(b)

Comparison of Computed and Tested Failure Loads Based on the Effective Width Formulas in the 1986 AISI Automotive Steel Design Manual for Stub Columns with Stiffened Flanges (35XF Sheet Steel) (Based on Dynamic Yield Stress)

Spec.	Strain Rate (in./in./sec.)	w/t	F_y (ksi)	A_e (in.^{2})	$(P_u)_{comp}$ (kips)	$(P_u)_{test}$ (kips)	(6)/(5)
	(1)	(2)	(3)	(4)	(5)	(6)	(7)
1A1A	0.0001	27.15	29.83	1.2060	35.97	46.12	1.28
1A1B	0.0001	27.39	29.83	1.2060	35.97	44.89	1.25
1A2A	0.01	26.92	31.92	1.2010	38.33	50.02	1.30
1A2B	0.01	27.06	31.92	1.2010	38.35	49.29	1.29
1A3A	0.10	27.31	34.06	1.2009	40.90	53.54	1.31
1A3B	0.10	27.40	34.06	1.2009	40.90	54.37	1.33
1B1A	0.0001	38.93	29.83	1.5477	46.17	49.19	1.06
1B1B	0.0001	39.17	29.83	1.5480	46.18	53.54	1.16
1B2A	0.01	38.86	31.92	1.5412	49.20	56.28	1.14
1B2B	0.01	39.10	31.92	1.5449	49.31	57.01	1.16
1B3A	0.10	38.86	34.06	1.5372	52.36	64.78	1.24
1B3B	0.10	38.96	34.06	1.5340	52.25	60.87	1.16
1C1A	0.0001	52.69	29.83	1.8135	54.10	56.76	1.05
1C1B	0.0001	52.96	29.83	1.8122	54.06	56.52	1.05
1C2A	0.01	52.20	31.92	1.7977	57.38	61.02	1.06
1C2B	0.01	53.06	31.92	1.8000	57.46	64.58	1.12
1C3A	0.10	53.15	34.06	1.7875	60.88	73.96	1.21
1C3B	0.10	53.39	34.06	1.7840	60.76	69.27	1.14
Mean							1.184
Standard Deviation							0.093

computed failure loads of stub columns, $(P_u)_{comp}$, are listed in column (5) of Tables 4.11(a) and 4.11(b). The tested failure loads of stub-column specimens are listed in column (6) of Tables 4.11(a) and 4.11(b). Comparisons of the computed and tested failure loads of stub columns are shown in column (7) of both tables. The mean values of $(P_u)_{test}/(P_u)_{comp}$ ratios and standard deviations are (1.265, 0.139) and (1.184, 0.093) for Tables 4.11(a) and 4.11(b), respectively. As expected, for specimens having the same w/t ratio, the tested ultimate load increases with strain rate. The tested to computed ultimate load ratios in Table 4.11(a) are higher than the corresponding values in Table 4.11(b). Figures 4.13 through 4.15 show graphically typical load-displacement curves for 1B sections under different strain rates. The computed critical local buckling and ultimate loads are marked in these figures for comparison with the tested ones.

Tables 4.12 and 4.13 were prepared to study the effect of strain rate on failure loads of box-shaped stub column specimens. Table 4.12 lists average failure loads obtained from Table 3.46. Each failure load value listed in this table is the average of two values obtained from similar tests. For the purpose of comparison, Table 4.13 shows the ratios of average failure loads obtained from the tests conducted at different strain rates. It is noted from Tables 4.12 and 4.13 that 1) the failure load increases with strain rate and 2) the ratio of dynamic to static failure loads increases with increasing w/t ratio. The percentage increase in failure loads is larger at higher strain rate as compared to the increase at lower strain rates.

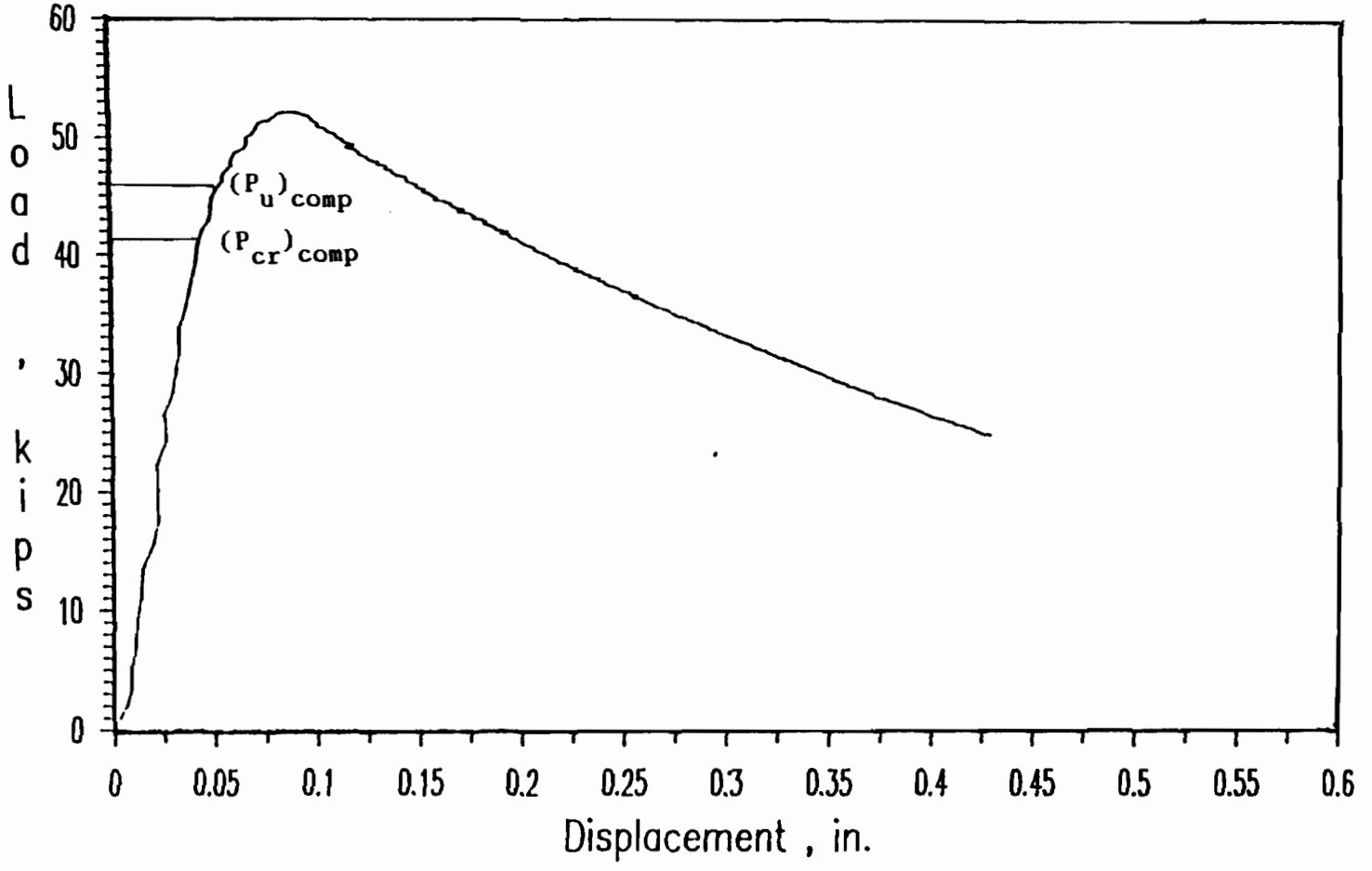

Fig. 4.13 Load-Displacement Curve for Box-Shaped Stub Column Specimen 1B1A

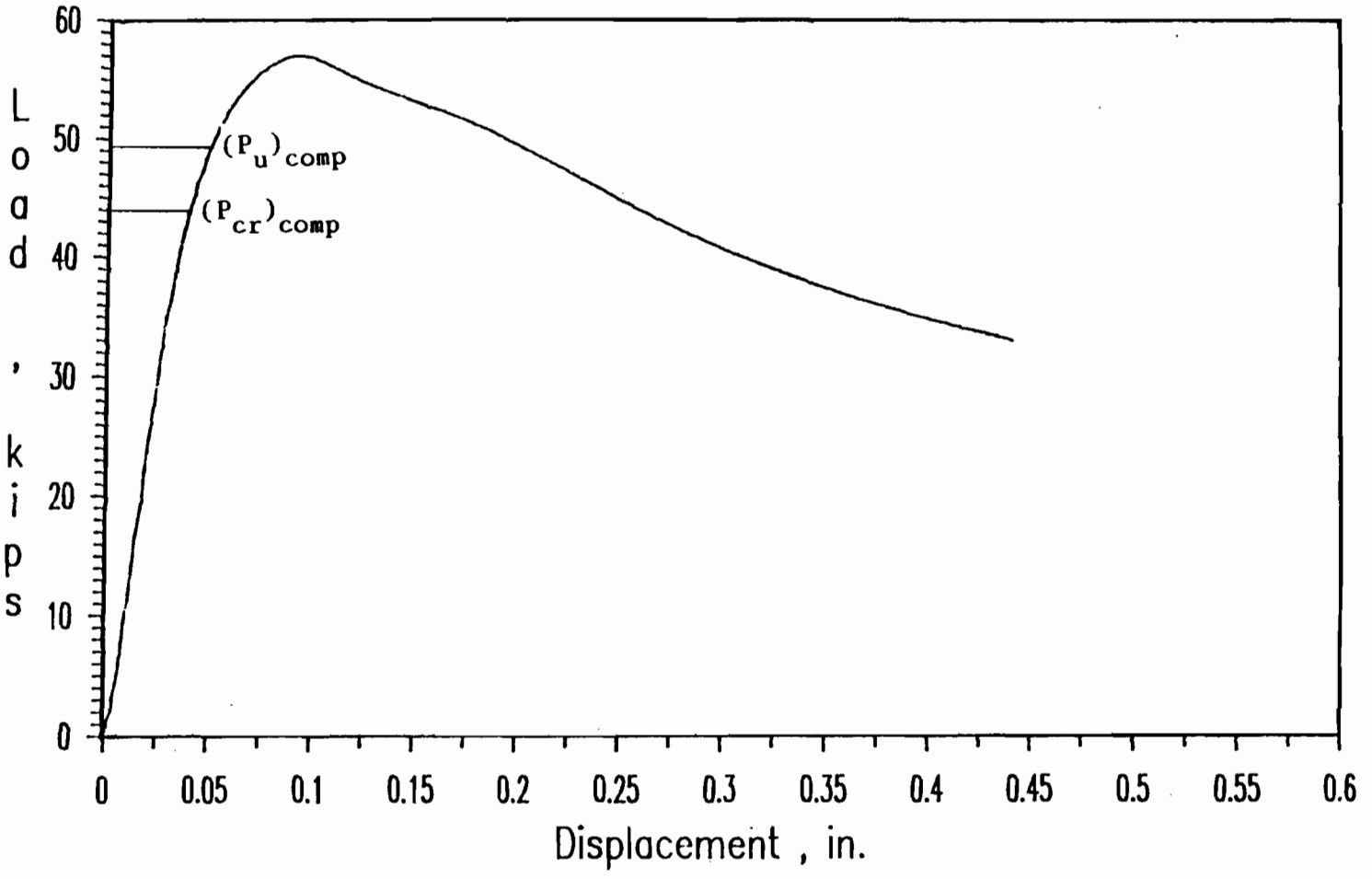

Fig. 4.14 Load-Displacement Curve for Box-Shaped Stub Column Specimen 1B2B

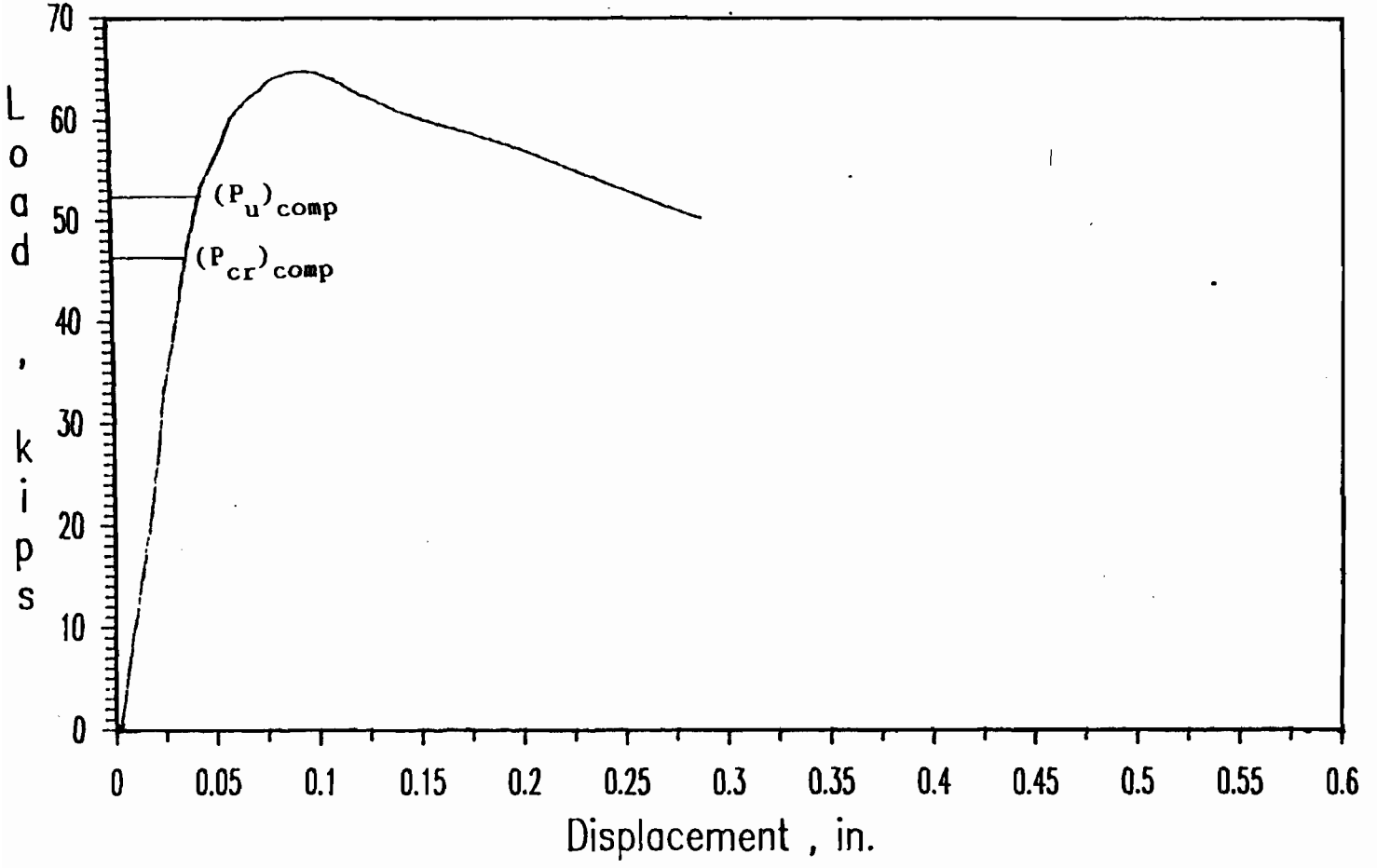

Fig. 4.15 Load-Displacement Curve for Box-Shaped Stub Column Specimen 1B3A

Table 4.12

Average Tested Failure Loads for Stub Column Specimens with Stiffened Flanges (35XF Sheet Steel)

Strain Rate	Failure Load, $(P_u)_{test}$, kips		
in./in./sec.	w/t		
	26.67	38.44	53.15
0.0001	45.50	51.36	56.64
0.01	49.65	56.64	62.80
0.1	53.95	62.82	71.48

Table 4.13

Ratios of Average Ultimate Loads for Stub Column Specimens Having Stiffened Flanges (35XF Sheet Steel)

w/t	$(P_u)_2/(P_u)_1$	$(P_u)_3/(P_u)_1$
29.67	1.09	1.18
38.44	1.10	1.22
53.15	1.11	1.26

Notes :

$(P_u)_1$= Average ultimate load for stub column specimens tested at strain rate of 0.0001 in./in./sec.

$(P_u)_2$= Average ultimate load for stub column specimens tested at strain rate of 0.01 in./in./sec.

$(P_u)_3$= Average ultimate load for stub column specimens tested at strain rate of 0.1 in./in./sec.

Figure 4.16 shows graphically the effect of strain rate on the failure loads of stub column spcimens. The horizontal axis represents logarithmic strain rate, while the vertical axis represents the ratio of dynamic to static failure loads. The static failure loads are corresponding to the tests performed at strain rate of 0.0001 in./in./sec.

3. Beam Tests for the Study of Unstiffened Elements. As mentioned in Chapter III, channel beams having small w/t ratios have been designed and fabricated to study the post-buckling strengths of unstiffened elements by using 35XF sheet steels. All the channel beams were subjected to two point loads at a distance of L/8 from end support as shown in Figs. 3.48 and 3.49. Lateral torsional buckling of channel beams was prevented by using lateral supports provided by aluminum angles connected to the compression flanges, as discussed in Chapter III. The webs of channel beam specimens were designed to be fully effective. The weight of the test specimen and the weight of the cross beam placed on the top of the specimen (approx. 70 lbs.) are small as compared to the ultimate loads and were neglected in the evaluation of test results. The tested tensile yield stress was used for computing yield moment (M_y) for all beam specimens studied in this investigation.

a. Critical Local Buckling Strength. The critical local buckling moments (M_{cr}) of channel beams can be computed by using Eq. (4.5). As discussed in Section IV.C.1.a, the critical local buckling stress (f_{cr}) can be computed by using Eq. (2.25) or Eq. (4.4), depending on the w/t ratio of the compression flange. In this phase of study, a value of 0.43

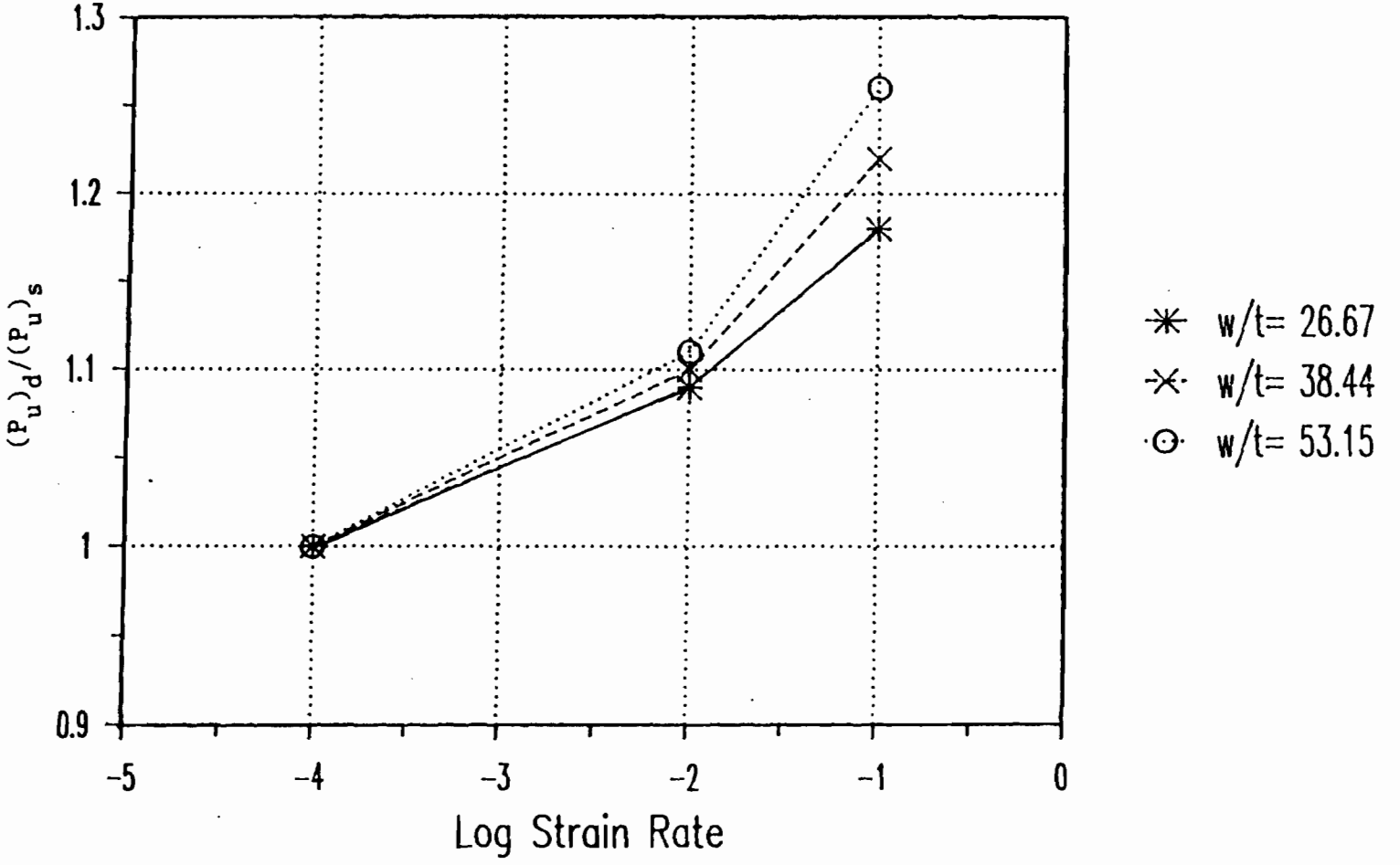

Fig. 4.16 Ratios of Dynamic to Static Average Ultimate Loads vs. Logarithmic Strain Rate for Box-Shaped Stub Columns

was used as the buckling coefficient for unstiffened flanges to calculate the critical local buckling stresses of compression flanges.

The computed critical local buckling moments of channel beams, listed in column (5) of Table 4.14, were calculated by using Eq. (4.5). The critical buckling local stresses were computed by using Eq. (4.4) for all channel beam tests. The tested critical local buckling moments listed in column (6) of the same table were determined from the product of bending arm (L/8) and one half of the critical local buckling loads $(P_{cr})/2$ as given in Eq. (4.6). The critical local buckling loads were determined from load-strain diagrams by using the modified strain reversal method. The span length of channel beams and other parameters (S_x, f_{cr}, P_{cr}) for each channel beam are given in Table 4.14. No local buckling was observed from load-strain diagrams for channel beams with small and medium w/t ratios. As shown in column (3) of Table 4.14, the tested critical local buckling load increases with strain rate.

A comparison of the tested and predicted critical local buckling moments is given in Table 4.14. Note that all tested critical local buckling moments are greater than the computed critical local buckling moments. This is because a value of 0.43 was used as the buckling coefficient for unstiffened compression flanges ignoring any effect of rotational edge restraint provided by the adjoining webs. The mean value of $(M_{cr})_{test}/(M_{cr})_{comp}$ ratios is equal to 1.405 with a standard deviation of 0.060.

Table 4.14

Comparison of Computed and Tested Critical Buckling Moments
Beam Specimens with Unstiffened Flanges (Based on k=0.43)
(35XF Sheet Steel)

Specimen	S_{xc} ($in.^3$) (1)	f_{cr} (ksi) (2)	$(P_{cr})_{test}$ (kips) (3)	L (in.) (4)	$(M_{cr})_{comp}$ (in.-kips) (5)	$(M_{cr})_{test}$ (in.-kips) (6)	(6)/(5) (7)
4A0A	0.384	28.22	N/A	37.00	10.84	N/A	N/A
4A1A	0.377	28.26	N/A	37.00	10.65	N/A	N/A
4A1B	0.382	28.26	N/A	37.00	10.79	N/A	N/A
4A2A	0.380	30.15	N/A	37.00	11.46	N/A	N/A
4A2B	0.377	30.23	N/A	37.00	11.40	N/A	N/A
4B0A	0.719	25.55	N/A	43.00	18.37	N/A	N/A
4B1A	0.717	25.53	N/A	43.00	18.30	N/A	N/A
4B1B	0.717	25.66	N/A	43.00	18.40	N/A	N/A
4B2A	0.717	27.22	N/A	43.00	19.52	N/A	N/A
4B2B	0.717	27.14	N/A	43.00	19.46	N/A	N/A
4C0A	1.153	21.64	8.22	65.00	24.95	33.39	1.338
4C1A	1.150	21.60	8.15	65.00	24.84	33.11	1.333
4C1B	1.148	21.64	8.63	65.00	24.84	35.06	1.411
4C2A	1.160	22.77	9.56	65.00	26.41	38.84	1.471
4C2B	1.153	22.82	9.52	65.00	26.31	38.67	1.470
Mean							1.405
Standard Deviation							0.060

b. Ultimate Flexural Strength. For channel beams having equal flanges, the ultimate section strengths of such flexural members can be calculated on the basis of initiation of yielding of the compression flanges in the effective section. The ultimate section strengths of all channel beams can be calculated by using Eq. (4.7).

As discussed earlier, the buckling coefficient of 0.43 was used in the 1986 AISI Automotive Design Manual to calculate the effective width of an unstiffened element. The computed ultimate moments of channel beams fabricated from 35XF sheet steels are given in Tables 4.15(a) and 4.15(b). The latter table uses static or dynamic yield stress depending on the strain rate used in the test, while the previous one uses static yield stress for all tests. The ultimate moments $(M_u)_{comp}$ listed in column (5) of both tables were calculated by using Eq. (4.7). Effective section modulus (S_e) was computed using the effective width formula for unstiffened elements adopted in the current AISI Automotive Design Manual along with the appropriate yield stress value. The computed values of effective section modulus for all channel beam tests are listed in column (1) of both tables (4.15(a) and 4.15(b)). The span lengths of channel beams are given in column (4) of these tables. The tested ultimate moments listed in column (6) of Tables 4.15(a) and 4.15(b) were determined from the product of the bending arms (L/8) and one half of the tested failure loads as given in Eq. (4.8). The tested failure load for each channel beam test was considered to be the maximum load the member can sustain during the test. The tested ultimate moments are compared with the computed ultimate moments in Tables 4.15(a) and 4.15(b).

Table 4.15(a)

Comparison of Computed and Tested Ultimate Moments
Beam Specimens with Unstiffened Flanges
(35XF Sheet Steel)
(Based on Static Yield Stress)

Specimen	S_e	F_y	$(P_u)_{test}$	L	$(M_y)_{comp}$	$(M_u)_{test}$	(6)/(5)
	($in.^3$)	(ksi)	(kips)	(in.)	(in.-kips)	(in.-kips)	
	(1)	(2)	(3)	(4)	(5)	(6)	(7)
4A0A	.3837	32.02	6.41	37.00	12.29	14.82	1.206
4A1A	.3772	32.02	7.15	37.00	12.08	16.53	1.369
4A1B	.3819	32.02	7.18	37.00	12.23	16.60	1.357
4A2A	.3801	32.02	7.53	37.00	12.17	17.41	1.430
4A2B	.3771	32.02	7.63	37.00	12.07	17.64	1.461
4B0A	.6788	32.02	9.77	43.00	21.73	26.26	1.208
4B1A	.6736	32.02	10.12	43.00	21.67	27.20	1.255
4B1B	.6772	32.02	9.87	43.00	21.78	26.52	1.218
4B2A	.6631	32.02	10.97	43.00	21.73	29.48	1.357
4B2B	.6613	32.02	10.98	43.00	21.67	29.51	1.361
4C0A	.9515	32.02	8.49	65.00	30.47	34.49	1.132
4C1A	.9428	32.02	8.83	65.00	30.35	35.87	1.182
4C1B	.9421	32.02	9.15	65.00	30.33	37.17	1.225
4C2A	.9311	32.02	10.23	65.00	30.62	41.56	1.357
4C2B	.9263	32.02	10.22	65.00	30.47	41.52	1.363
Mean							1.299
Standard Deviation							0.096

Table 4.15(b)

Comparison of Computed and Tested Ultimate Moments
Beam Specimens with Unstiffened Flanges
(35XF Sheet Steel)
(Based on Dynamic Yield Stress)

Specimen	S_e	F_y	$(P_u)_{test}$	L	$(M_y)_{comp}$	$(M_u)_{test}$	(6)/(5)
	($in.^3$)	(ksi)	(kips)	(in.)	(in.-kips)	(in.-kips)	
	(1)	(2)	(3)	(4)	(5)	(6)	(7)
4A0A	.3837	32.02	6.41	37.00	12.29	14.82	1.206
4A1A	.3772	32.87	7.15	37.00	12.40	16.53	1.333
4A1B	.3819	32.87	7.18	37.00	12.55	16.60	1.322
4A2A	.3801	36.40	7.53	37.00	13.83	17.41	1.259
4A2B	.3771	36.40	7.63	37.00	13.73	17.64	1.285
4B0A	.6788	32.02	9.77	43.00	21.73	26.26	1.208
4B1A	.6736	32.87	10.12	43.00	22.14	27.20	1.228
4B1B	.6772	32.87	9.87	43.00	22.26	26.52	1.191
4B2A	.6631	36.40	10.97	43.00	24.14	29.48	1.221
4B2B	.6613	36.40	10.98	43.00	24.07	29.51	1.226
4C0A	.9515	32.02	8.49	65.00	30.47	34.49	1.132
4C1A	.9428	32.87	8.83	65.00	30.99	35.87	1.157
4C1B	.9421	32.87	9.15	65.00	30.97	37.17	1.200
4C2A	.9311	36.40	10.23	65.00	33.89	41.56	1.226
4C2B	.9263	36.40	10.22	65.00	33.72	41.52	1.231
Mean							1.228
Standard Deviation							0.052

The mean value of $(M_u)_{test}/(M_u)_{comp}$ ratios and standard deviations are (1.299, 0.096) and (1.228, 0.052) for Tables 4.15(a) and 4.15(b), respectively.

As observed previously, the ratios of tested ultimate moments to the computed values are greater in Table 4.15(a) as compared to those ratios in Table 4.15(b), because the latter table took into account the effect of strain rate on yield stress. For specimens having the same dimensions, the tested ultimate load increases with the strain rate. Figures 4.17 through 4.19 show graphically typical moment-displacement curves for 4B sections under different strain rates. The computed critical local buckling and yield moments are marked in these figures for comparison with the tested ones.

Tables 4.16 and 4.17 were prepared to study the effect of strain rate on ultimate moments of channel beam specimens. Table 4.16 lists the average ultimate moments. Each ultimate load value listed in this table is the average of two values obtained from similar tests except that for the tests conducted at strain rate of 0.00001 in./in./sec. for which only one test was performed. For the purpose of comparison, Table 4.17 shows the ratios of ultimate moments. Each value listed in this table is the ratio of two ultimate moments for the specimens with the same dimensions but tested under different strain rates. It is observed from Tables 4.16 and 4.17 that 1) the failure load increases with strain rate and 2) the percentage increase of ultimate moments is larger at higher strain rate in most cases.

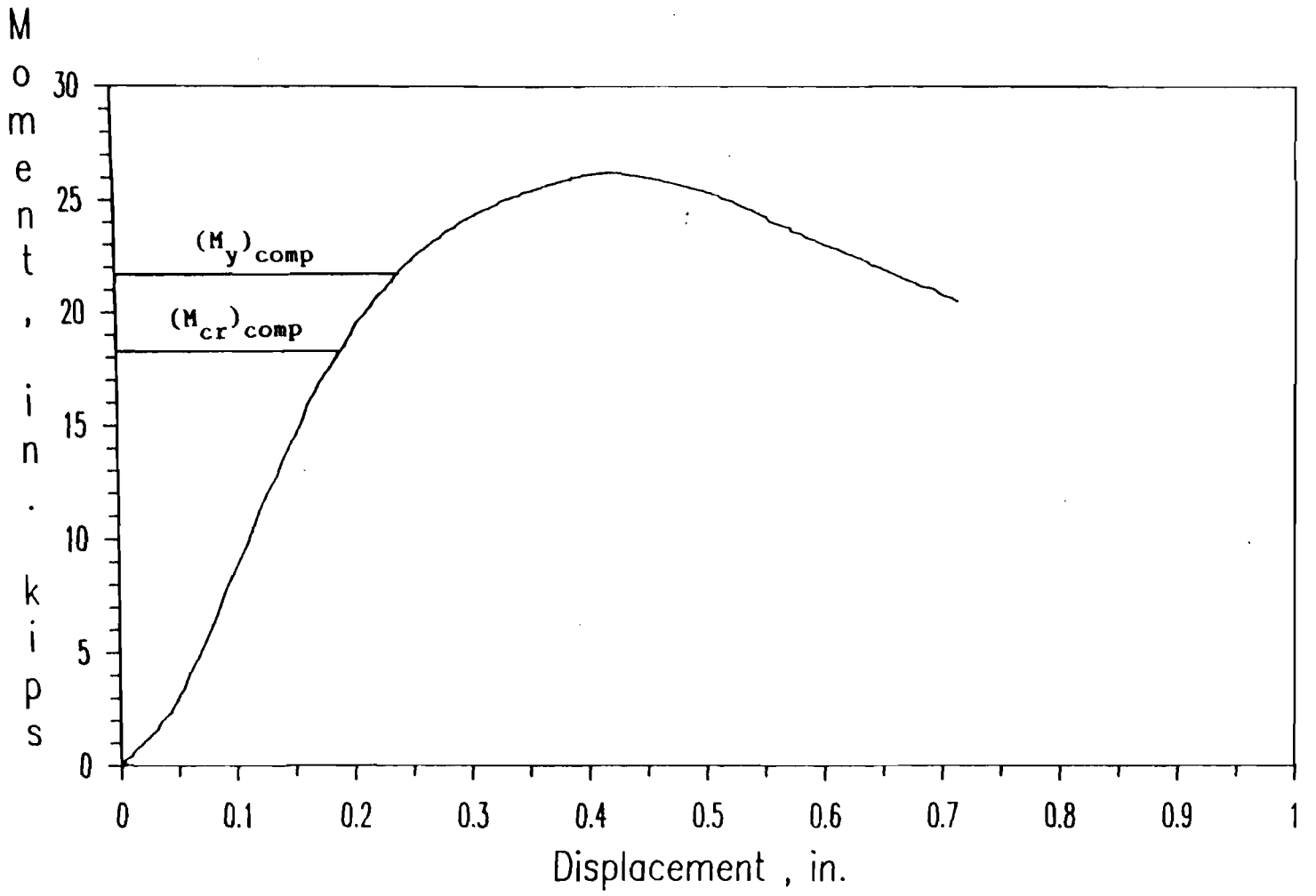

Fig. 4.17 Moment-Displacement Curve for Channel Beam Specimen 4B0A

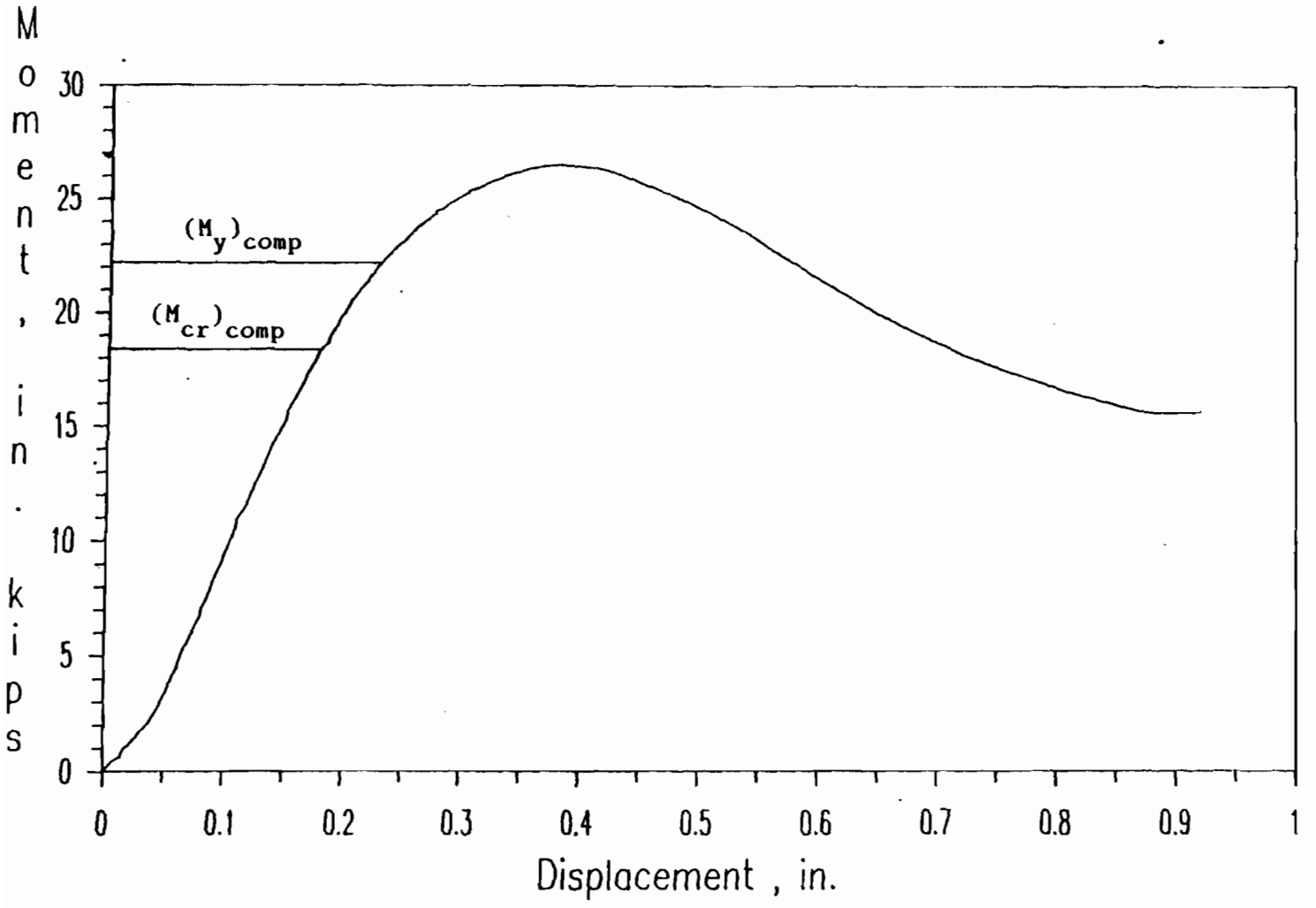

Fig. 4.18 Moment-Displacement Curve for Channel Beam Specimen 4B1B

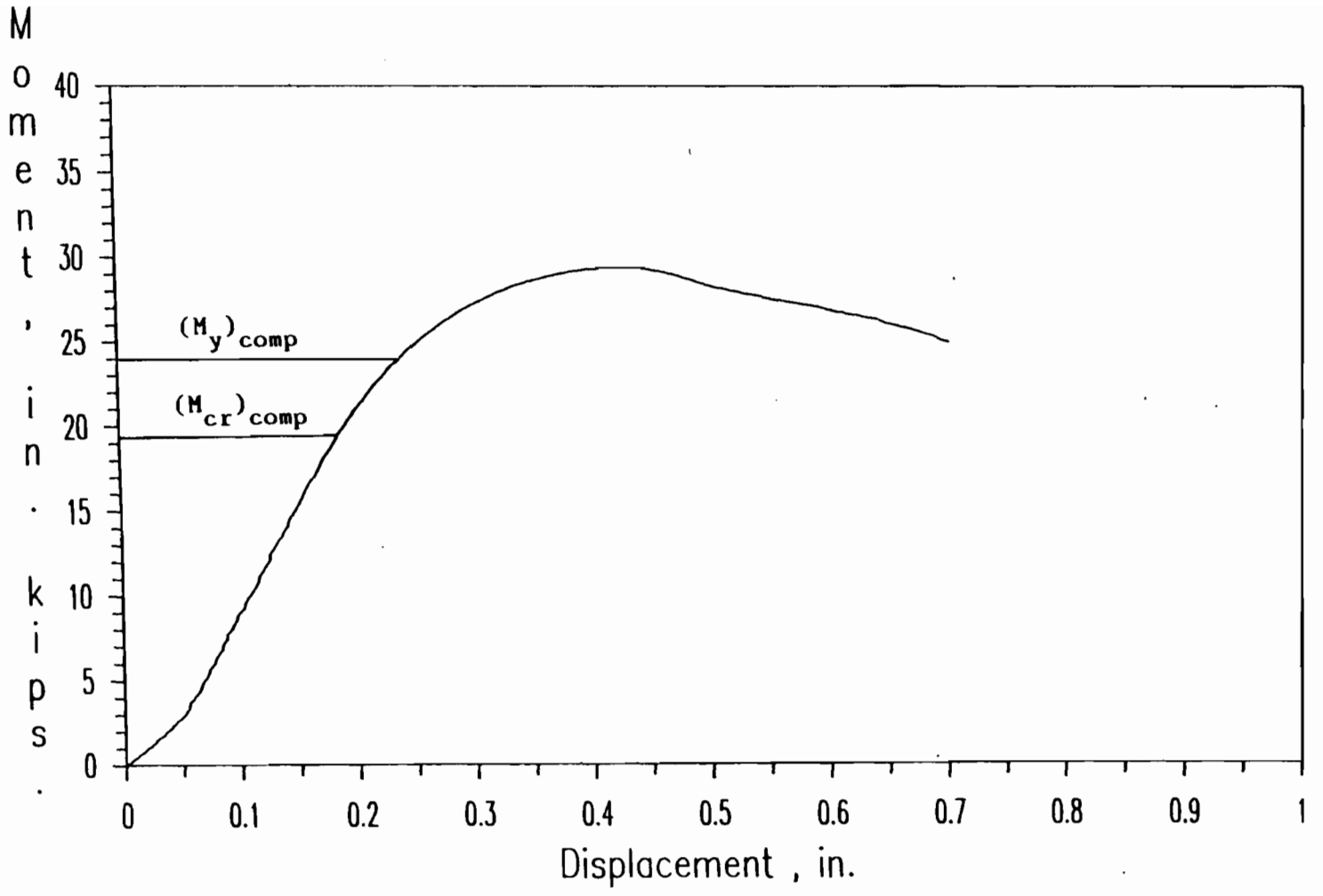

Fig. 4.19 Moment-Displacement Curve for Channel Beam Specimen 4B2B

Table 4.16

Average Tested Failure Moments for Channel Beam Specimens with Unstiffened Flanges (35XF Sheet Steel)

Strain Rate in./in./sec.	Failure Moment, $(M_u)_{test}$, in.-kips w/t		
	8.93	14.81	20.69
0.00001	14.82	26.26	34.49
0.0001	16.56	26.85	36.52
0.01	17.53	29.48	41.54

Table 4.17

Ratios of Average Ultimate Moments for Channel Beam Specimens Having Unstiffened Flanges (35XF Sheet Steel)

w/t	$(M_u)_0/(M_u)_1$	$(M_u)_2/(M_u)_1$
8.93	0.89	1.06
14.81	0.98	1.10
20.69	0.94	1.14

Notes :

$(M_u)_0$= Average ultimate moment for channel beam specimens tested at strain rate of 0.00001 in./in./sec.

$(M_u)_1$= Average ultimate moment for channel beam specimens tested at strain rate of 0.0001 in./in./sec.

$(M_u)_2$= Average ultimate moment for channel beam specimens tested at strain rate of 0.01 in./in./sec.

Figure 4.20 shows graphically the effect of strain rate on the ultimate moments of the channel beam specimens. The horizontal axis represents logarithmic strain rate while the vertical axis represents the ratio of dynamic to static ultimate moments. The tests performed at strain rate of 0.0001 in./in./sec. are considered to be the static loading conditions.

4. Stub Column Tests for the Study of Unstiffened Elements. I-shaped stub columns were designed and fabricated to study the post-buckling strengths of unstiffened elements under different strain rates by using 35XF steel. All the stub columns were subjected to uniform compression. Overall column buckling was prevented by the design of the stub columns. The thickness of the web in a stub column was twice the thickness of the unstiffened compression flange because the webs of stub columns were glued together. The tested compressive yield stress was used for the evaluation of all stub column specimens studied in this investigation.

a. Critical Local Buckling Load. The critical local buckling load of a stub-column specimen with unstiffened compression elements can be calculated using Eq. (4.20).

In Eq. (4.20), the critical local buckling stress of an unstiffened element can be calculated by using Eq. (2.25) or (4.4), depending on the w/t ratio of the unstiffened flange. A value of 0.43 was used as the buckling coefficient to calculate the critical local buckling stresses of unstiffened elements in this phase of study for using Eq. (4.4). The

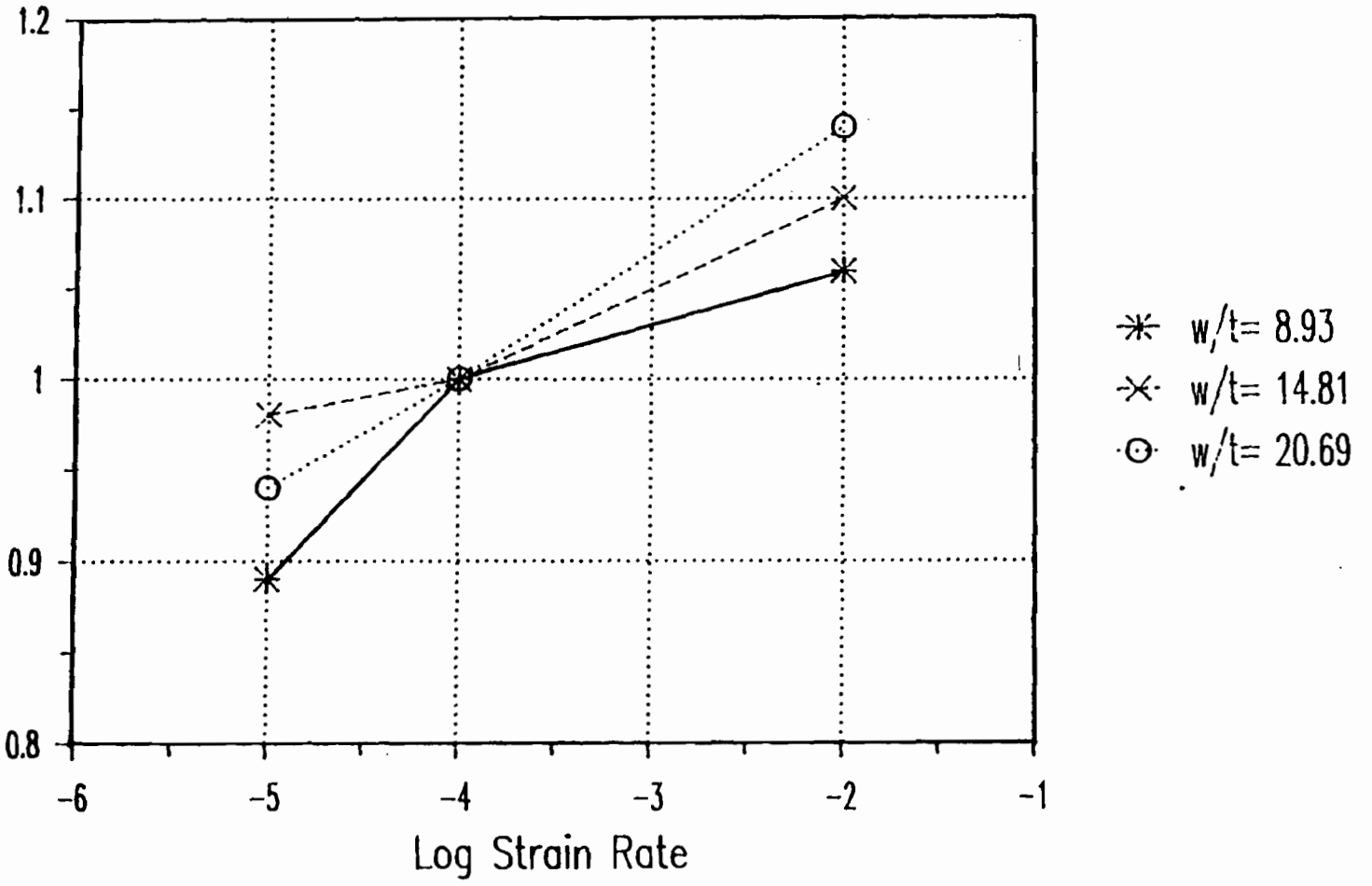

Fig. 4.20 Ratios of Dynamic to Static Average Ultimate Moments vs. Logarithmic Strain Rate for Channel Beam Specimens

total cross-sectional areas of stub columns are given in Table 3.48. The critical local buckling stress listed in column (1) of Table 4.18 for each stub column is the average value of four critical local buckling stresses of unstiffened flanges.

The computed and tested critical local buckling loads of specimens fabricated from 35XF steel are given in columns (2) and (3) of Table 4.18, respectively. The tested critical local buckling loads were determined from load-strain diagrams by using a modified strain reversal method. In Table 4.18, the tested critical local buckling load for each specimen is the average value of four tested critical local buckling loads determined from unstiffened flanges. The computed critical local buckling loads were determined from the product of the average critical local buckling stresses and the total cross-sectional areas. No critical local buckling was observed from the load-strain diagrams of I-shaped stub columns with small and medium w/t ratios. Note that the critical local buckling loads for stub columns with large w/t ratios tested in the present investigation were underestimated by using Eq (4.20). The mean values of $(P_{cr})_{test}/(P_{cr})_{comp}$ ratios and standard deviations are equal to 1.556 and 0.102, respectively. As shown in column (3) of Table 4.18, the tested critical local buckling load increases with the strain rate.

b. Ultimate Axial Load. From the concept of the effective width approach, stub-column specimens reach the ultimate axial load when the maximum edge stresses of the unstiffened elements reach yield stresses of the steels. The ultimate load carrying capacities (P_u) of the stub-column specimens can be calculated from Eq. (4.20).

Table 4.18

Comparison of Computed and Tested Critical Buckling Loads
Stub Columns with Unstiffened Flanges (Based on k=0.43)
(35XF Sheet Steel)

Specimen	$(f_{cr})_{comp}$ (ksi) (1)	$(P_{cr})_{comp}$ (kips) (2)	$(P_{cr})_{test}$ (kips) (3)	(3)/(2) (4)
2A1A	28.34	17.63	N/A	N/A
2A1B	28.30	17.79	N/A	N/A
2A2A	30.26	19.03	N/A	N/A
2A2B	30.20	18.95	N/A	N/A
2A3A	32.17	20.23	N/A	N/A
2A3B	32.16	20.11	N/A	N/A
2B1A	26.50	24.48	N/A	N/A
2B1B	26.47	24.31	N/A	N/A
2B2A	28.19	25.91	N/A	N/A
2B2B	28.21	26.00	N/A	N/A
2B3A	29.85	27.55	N/A	N/A
2B3B	29.80	27.50	N/A	N/A
2C0A	21.81	24.69	35.42	1.434
2C1A	21.71	24.59	36.44	1.482
2C1B	21.78	24.77	36.44	1.471
2C2A	22.78	25.85	40.40	1.563
2C2B	22.92	26.08	40.35	1.547
2C3A	23.70	26.87	46.95	1.747
2C3B	23.76	26.92	44.38	1.648
Mean				1.556
Standard Deviation				0.102

The computed and tested failure loads of stub columns were compared in Tables 4.19(a) and 4.19(b). Table 4.19(a) uses static yield stress, while Table 4.19(b) uses static or dynamic yield stress according to the strain rate used in the test. Equation (4.20) was used to compute the failure loads listed in column (5) of both tables using appropriate yield stresses. The yield stress values are listed in column (3) of the same tables. The effective cross-sectional areas computed by using the current AISI Automotive Design Manual are also given in Tables 4.19(a) and 4.19(b).

The tested ultimate loads of stub columns are listed in column (6) of Tables 4.19(a) and 4.19(b). Comparisons of the computed and tested failure loads are listed in column (7) of these tables. The mean values of $(P_u)_{test}/(P_u)_{comp}$ ratios are 1.417 and 1.334 with standard deviations of 0.136 and 0.070 for Tables 4.19(a) and 4.19(b) , respectively.

As shown in these tables, the ultimate load increases with strain rate. Because the latter table takes into account the effect of strain rate on yield stress, the ratios of tested to computed failure loads listed in Table 4.19(a) are greater than that given in Table 4.19(b). Figures 4.21 through 4.23 show graphically typical load-displacement curves for 2B sections under different strain rates. The computed critical local buckling and ultimate loads are marked in these figures for comparison with the tested ones.

Tables 4.20 and 4.21 were prepared to study the effect of strain rate on failure loads for I-shaped stub column specimens. Table 4.20 lists the average failure loads obtained from Table 3.48. Each failure load value

Table 4.19(a)

Comparison of Computed and Tested Failure Loads Based on the Effective Width Formulas in the 1986 AISI Automotive Steel Design Manual for Stub Columns with Unstiffened Flanges (35XF Sheet Steel) (Based on Static Yield Stress)

Spec.	Strain Rate (in./in./sec.) (1)	w/t (2)	F_y (ksi) (3)	A_e ($in.^2$) (4)	$(P_u)_{comp}$ (kips) (5)	$(P_u)_{test}$ (kips) (6)	(6)/(5) (7)
2A1A	0.0001	8.93	29.83	.6220	18.55	25.26	1.36
2A1B	0.0001	9.04	29.83	.6285	18.75	25.35	1.35
2A2A	0.01	8.93	29.83	.6288	18.76	26.04	1.39
2A2B	0.01	9.10	29.83	.6275	18.72	27.70	1.48
2A3A	0.10	8.93	29.83	.6288	18.76	31.41	1.67
2A3B	0.10	8.96	29.83	.6254	18.65	29.41	1.58
2B1A	0.0001	13.34	29.83	.9216	27.49	34.20	1.24
2B1B	0.0001	13.41	29.83	.9151	27.30	34.20	1.25
2B2A	0.01	13.40	29.83	.9160	27.32	36.30	1.33
2B2B	0.01	13.37	29.83	.9191	27.42	37.52	1.37
2B3A	0.10	13.34	29.83	.9208	27.47	41.67	1.52
2B3B	0.10	13.42	29.83	.9195	27.43	42.70	1.56
2C0A	0.00001	20.69	29.83	.9825	29.31	36.30	1.24
2C1A	0.0001	20.85	29.83	.9793	29.21	37.23	1.27
2C1B	0.0001	20.76	29.83	.9860	29.41	37.66	1.28
2C2A	0.01	20.97	29.83	.9785	29.19	41.28	1.41
2C2B	0.01	20.81	29.83	.9857	29.40	41.52	1.41
2C3A	0.10	20.93	29.83	.9787	29.19	47.92	1.64
2C3B	0.10	20.87	29.83	.9796	29.22	46.16	1.58
Mean							1.417
Standard Deviation							0.136

Table 4.19(b)

Comparison of Computed and Tested Failure Loads Based on the Effective Width Formulas in the 1986 AISI Automotive Steel Design Manual for Stub Columns with Unstiffened Flanges (35XF Sheet Steel) (Based on Dynamic Yield Stress)

Spec.	Strain Rate (in./in./sec.) (1)	w/t (2)	F_y (ksi) (3)	A_e ($in.^2$) (4)	$(P_u)_{comp}$ (kips) (5)	$(P_u)_{test}$ (kips) (6)	(6)/(5) (7)
2A1A	0.0001	8.93	29.83	.6220	18.55	25.26	1.36
2A1B	0.0001	9.04	29.83	.6285	18.75	25.35	1.35
2A2A	0.01	8.93	31.92	.6288	20.07	26.04	1.30
2A2B	0.01	9.10	31.92	.6275	20.03	27.70	1.38
2A3A	0.10	8.93	34.06	.6288	21.42	31.41	1.47
2A3B	0.10	8.96	34.06	.6254	21.30	29.41	1.38
2B1A	0.0001	13.34	29.83	.9216	27.49	34.20	1.24
2B1B	0.0001	13.41	29.83	.9151	27.30	34.20	1.25
2B2A	0.01	13.40	31.92	.9091	29.02	36.30	1.25
2B2B	0.01	13.37	31.92	.9122	29.12	37.52	1.29
2B3A	0.10	13.34	34.06	.9069	30.89	41.67	1.35
2B3B	0.10	13.42	34.06	.9049	30.82	42.70	1.38
2C0A	0.00001	20.69	29.77	.9828	29.26	36.30	1.24
2C1A	0.0001	20.85	29.83	.9793	29.21	37.23	1.27
2C1B	0.0001	20.76	29.83	.9859	29.41	37.66	1.28
2C2A	0.01	20.97	31.92	.9672	30.87	41.28	1.34
2C2B	0.01	20.81	31.92	.9745	31.11	41.52	1.33
2C3A	0.10	20.93	34.06	.9587	32.65	47.92	1.47
2C3B	0.10	20.87	34.06	.9637	32.82	46.16	1.41
Mean							1.334
Standard Deviation							0.070

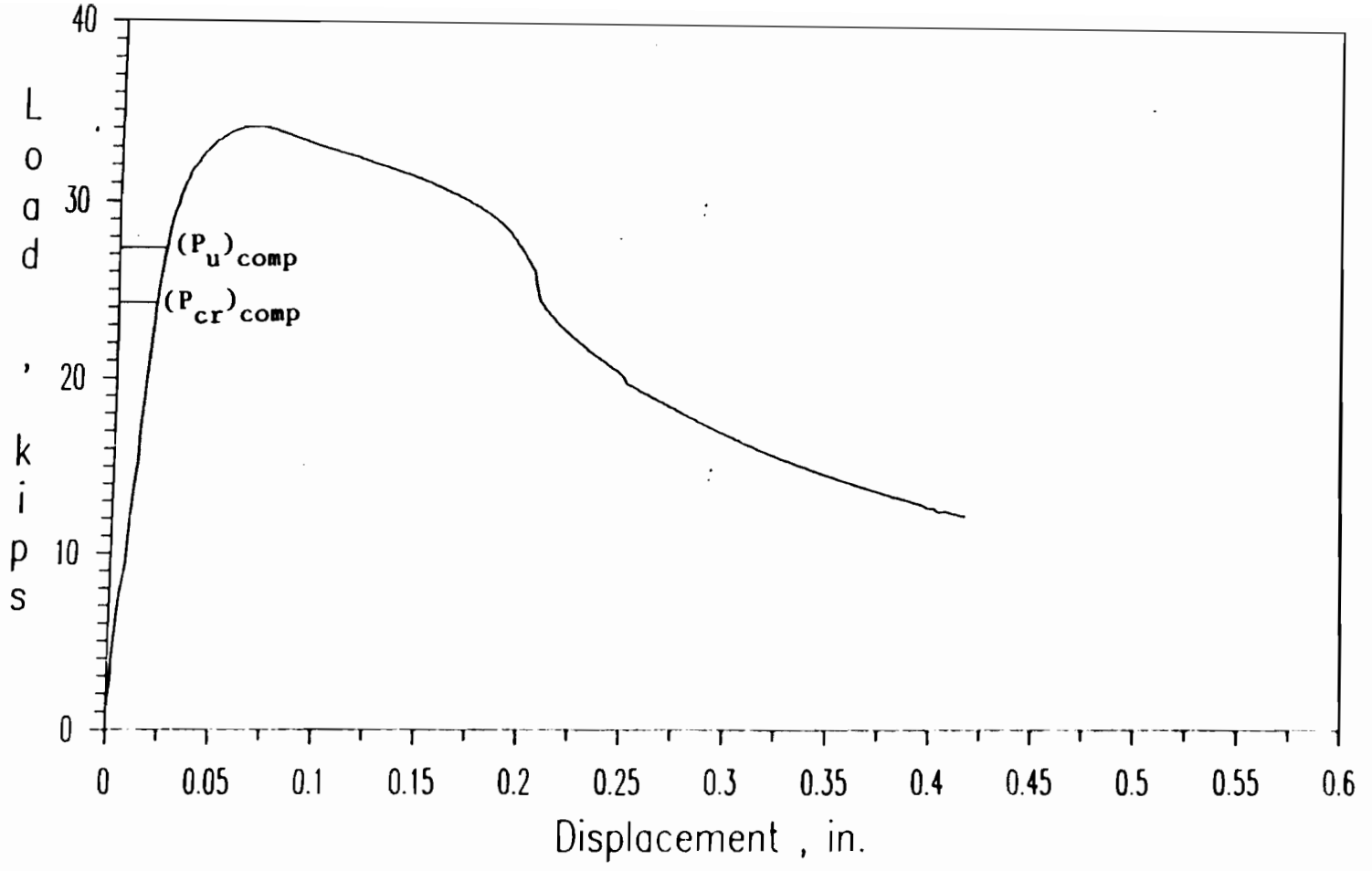

Fig. 4.21 Load-Displacement Curve for I-Shaped Stub Column

Specimen 2B1A

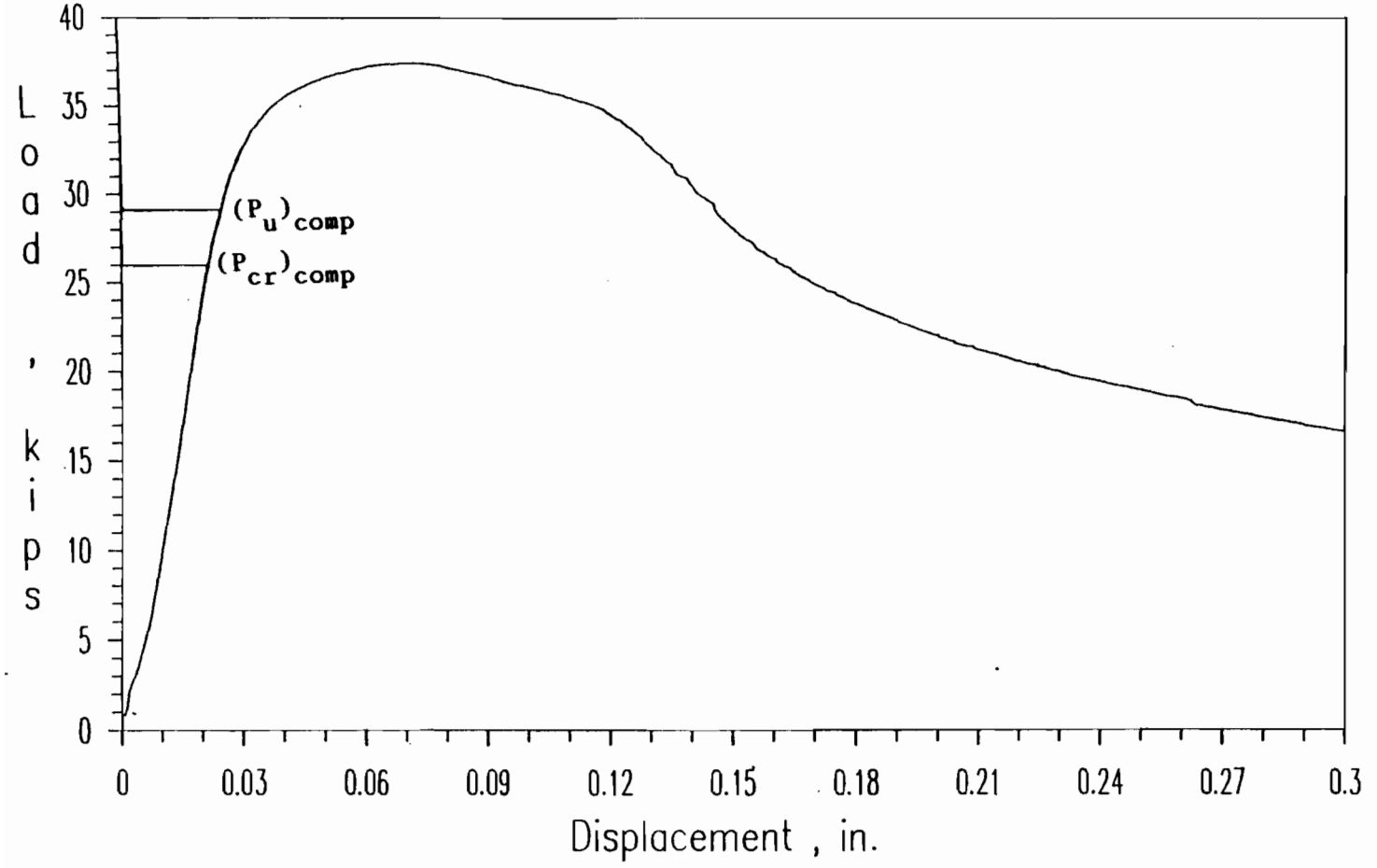

Fig. 4.22 Load-Displacement Curve for I-Shaped Stub Column Specimen 2B2B

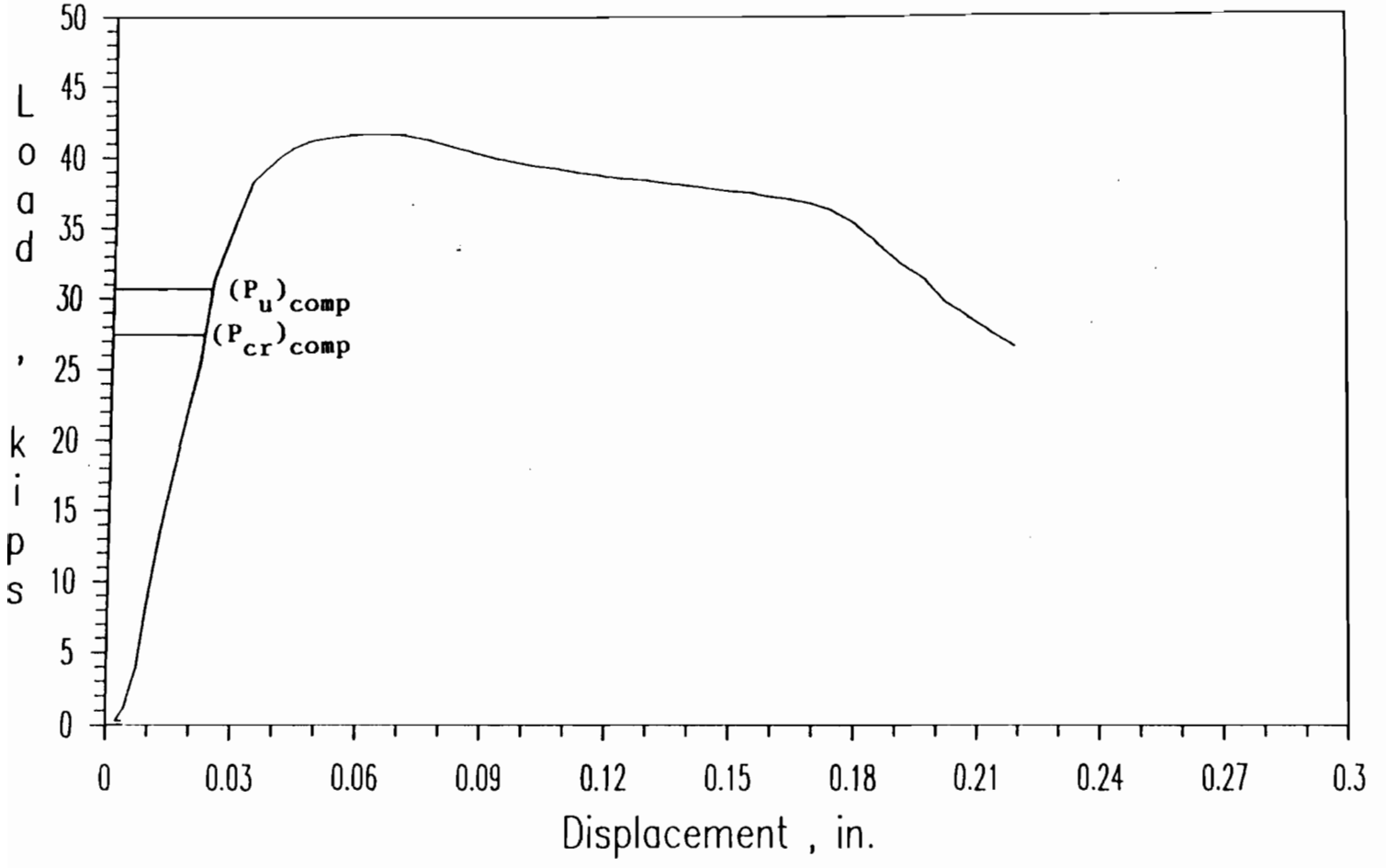

Fig. 4.23 Load-Displacement Curve for I-Shaped Stub Column

Specimen 2B3A

Table 4.20

Average Tested Failure Loads for I-Shaped Stub Column Specimens with Unstiffened Flanges (35XF Sheet Steel)

Strain Rate	Failure Load, $(P_u)_{test}$, kips		
in./in./sec.	w/t		
	8.93	13.34	20.69
0.0001	25.30	34.20	37.44
0.01	26.87	36.91	41.40
0.1	30.41	42.18	47.04

Table 4.21

Ratios of Ultimate Loads for I-Shaped Stub Column Specimens Having Unstiffened Flanges (35XF Sheet Steel)

w/t	$(P_u)_2/(P_u)_1$	$(P_u)_3/(P_u)_1$
8.93	1.06	1.20
13.34	1.08	1.23
20.69	1.11	1.26

Note :

$(P_u)_1$= Average ultimate load for I-shaped stub column specimens tested at strain rate of 0.0001 in./in./sec.

$(P_u)_2$= Average ultimate load for I-shaped stub column specimens tested at strain rate of 0.01 in./in./sec.

$(P_u)_3$= Average ultimate load for I-shaped stub column specimens tested at strain rate of 0.1 in./in./sec.

listed in this table is the average of two values obtained from similar tests. For the purpose of comparison, Table 4.21 shows the ratios of dynamic failure loads. Each value listed in this table is the ratio of two average failure loads for specimens having the same dimensions but tested under different strain rates. It is observed from Tables 4.20 and 4.21 that 1) the failure load increases with strain rate and 2) the ratio of dynamic to static failure loads increases with increasing w/t ratio. As observed previously, the percentage increase of failure load is larger at higher strain rates.

Similar to the previous figures, Fig. 4.24 shows the effect of strain rate on the failure loads of the I-shaped stub column specimens graphically. The tests performed at strain rate of 0.0001 in./in./sec. are considered to be the static loading conditions.

5. Deflection of Beam Specimens. As mentioned in Chapter III, the deflections at midspan of beam specimens (d in Fig. 4.25) were measured by two LVDTs located on both sides of hat and channel beam specimens as shown in Figs. 3.31 and 3.50. Tables 4.22 and 4.23 compare the computed and measured deflections under service moments for hat and channel beam specimens, respectively. The service moments were considered to be 60% of the computed yield moments and are listed in Table 4..6(b) for hat-beam specimens and in Table 4.15(b) for channel beam specimens. The measured deflection under service moment was obtained from the moment-deflection curve, while the computed value was calculated by using the following theoretical deflection equation with effective moment of inertia:

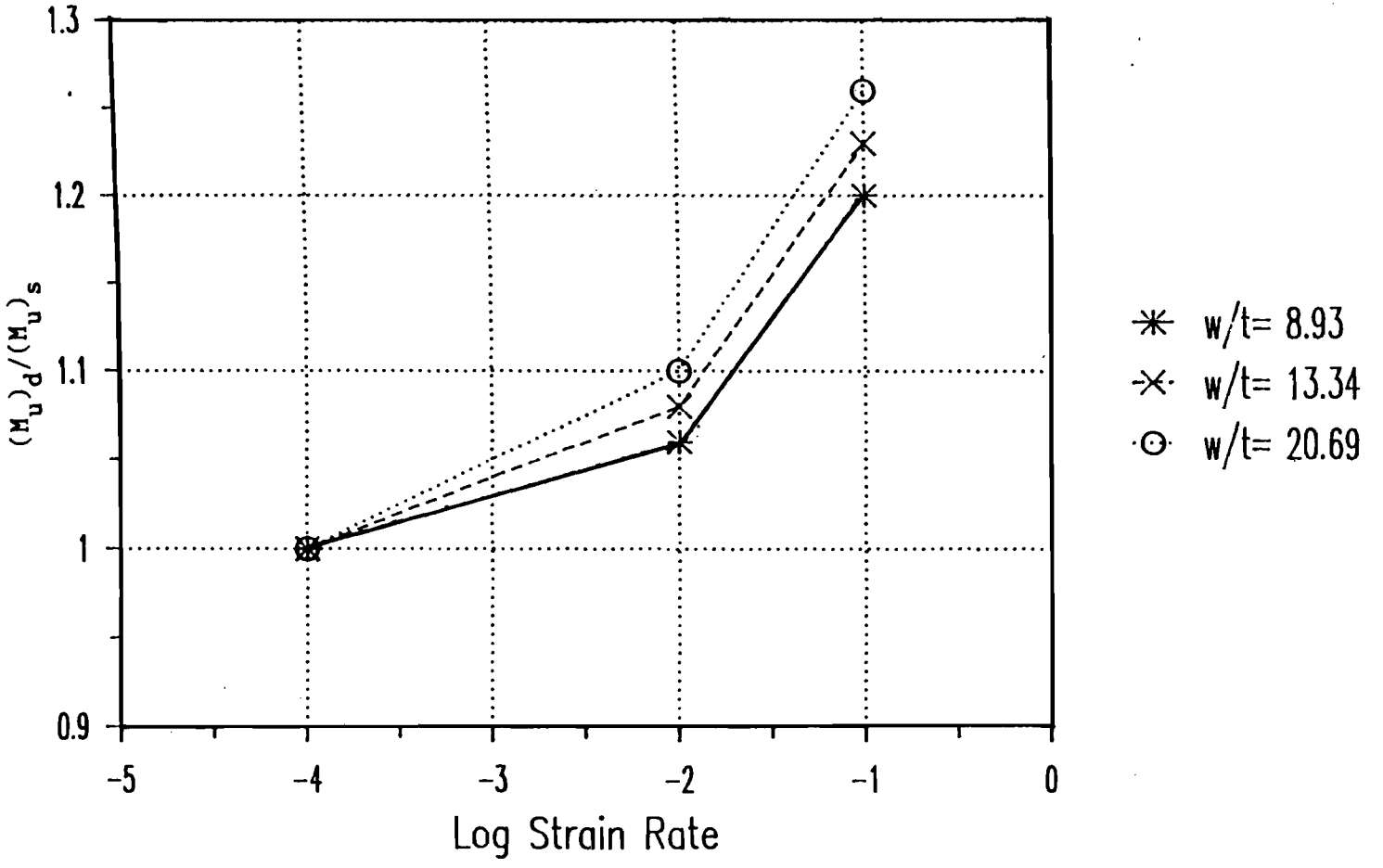

Fig. 4.24 Ratios of Dynamic to Static Average Ultimate Loads vs. Logarithmic Strain Rate for I-Shaped Stub Columns

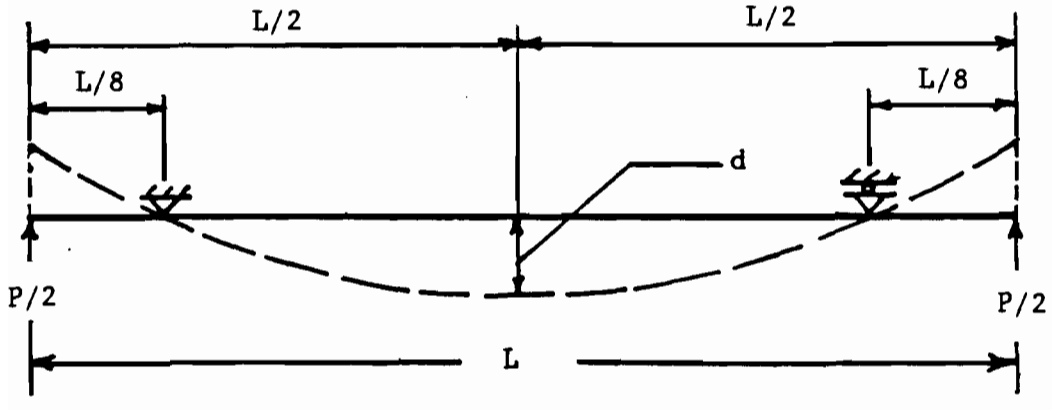

Fig. 4.25 Schematic Diagram for Beam Specimen Showing Midspan Deflection

Table 4.22

Deflections under Service Moments Based on Effective Sections for Hat-Beam Specimens with Stiffened Flanges (35XF Sheet Steel)

Specimen	$(M_s)_{test}$ (kips-in.) (1)	$(d)_{test}$ (in.) (2)	$(d)_{comp}$ (in.) (3)	$\frac{(2)}{(3)}$ (4)
3B1A	12.73	0.1213	0.1658	0.732
3B1B	12.40	0.1319	0.1661	0.794
3B2A	13.60	0.1350	0.1830	0.738
3B2B	13.72	0.1396	0.1827	0.764
3C0A	17.75	0.1518	0.2003	0.758
3C1A	18.32	0.1974	0.2037	0.969
3C1B	18.37	0.2002	0.2033	0.985
3C2A	20.60	0.1835	0.2329	0.788
3C2B	20.71	0.1727	0.2325	0.743
Mean				0.808
Standard Deviation				0.093

Table 4.23

Deflections under Service Moments Based on Effective Sections for Channel Beam Specimens with Unstiffened Flanges (35XF Sheet Steel)

Specimen	$(M_s)_{test}$ (kips-in.) (1)	$(d)_{test}$ (in.) (2)	$(d)_{comp}$ (in.) (3)	(2)/(3) (4)
4A0A	7.37	0.0639	0.0620	1.031
4A1A	7.44	0.0609	0.0641	0.950
4A1B	7.53	0.0715	0.0649	1.102
4A2A	8.30	0.0542	0.0708	0.765
4A2B	8.24	0.0471	0.0706	0.667
4B0A	13.04	0.0511	0.0635	0.805
4B1A	13.28	0.0491	0.0650	0.755
4B1B	13.36	0.0445	0.0649	0.701
4B2A	14.48	0.0588	0.0706	0.833
4B2B	14.44	0.0527	0.0707	0.745
4C0A	18.28	0.0929	0.1097	0.847
4C1A	18.59	0.0924	0.1126	0.821*
4C1B	18.58	0.0630	0.1127	0.559*
4C2A	20.33	0.0992	0.1227	0.808*
4C2B	20.23	0.0639	0.1232	0.519*
Mean				0.833
Standard Deviation				0.121

(*) This value was not considered in the calculation of mean and standard deviation because the LVDT which measured the midspan deflection was not functioning properly during the test.

$$d = \frac{9 M_s L^2}{128 E I_e} \qquad (4.22)$$

where

M_s = moment under service load

$= 0.6 (M_y)_{comp}$

L = span length of beam

E = modulus of elasticity

I_e = effective moment of inertia under service moment.

In the above expression, Eqs. 2.46 through 2.49 (Procedure II) were used to calculate the effective moment of inertia for hat beam specimens, while Procedure I was used to calculate the effective moment of inertia for channel beam specimens under service moments.

The computed and measured deflections under service moments are given in Tables 4.22 and 4.23 for hat and channel beam specimens, respectively. It is noted from these tables that most of the measured deflections were less than the computed values. It has been noted that the ratios of measured to computed deflections decrease with increasing strain rate for most of the cases which means that the deflections from the fast tests lag behind those from the slow tests at the same load level. The mean values of $(d)_{test}/(d)_{comp}$ ratios and standard deviations under service moments are equal to (0.808, 0.093) and (0.833, 0.121) for hat and channel beam specimens , respectively. Figure 4.26 shows graphically a typical moment-deflection curve for hat-beam specimens,

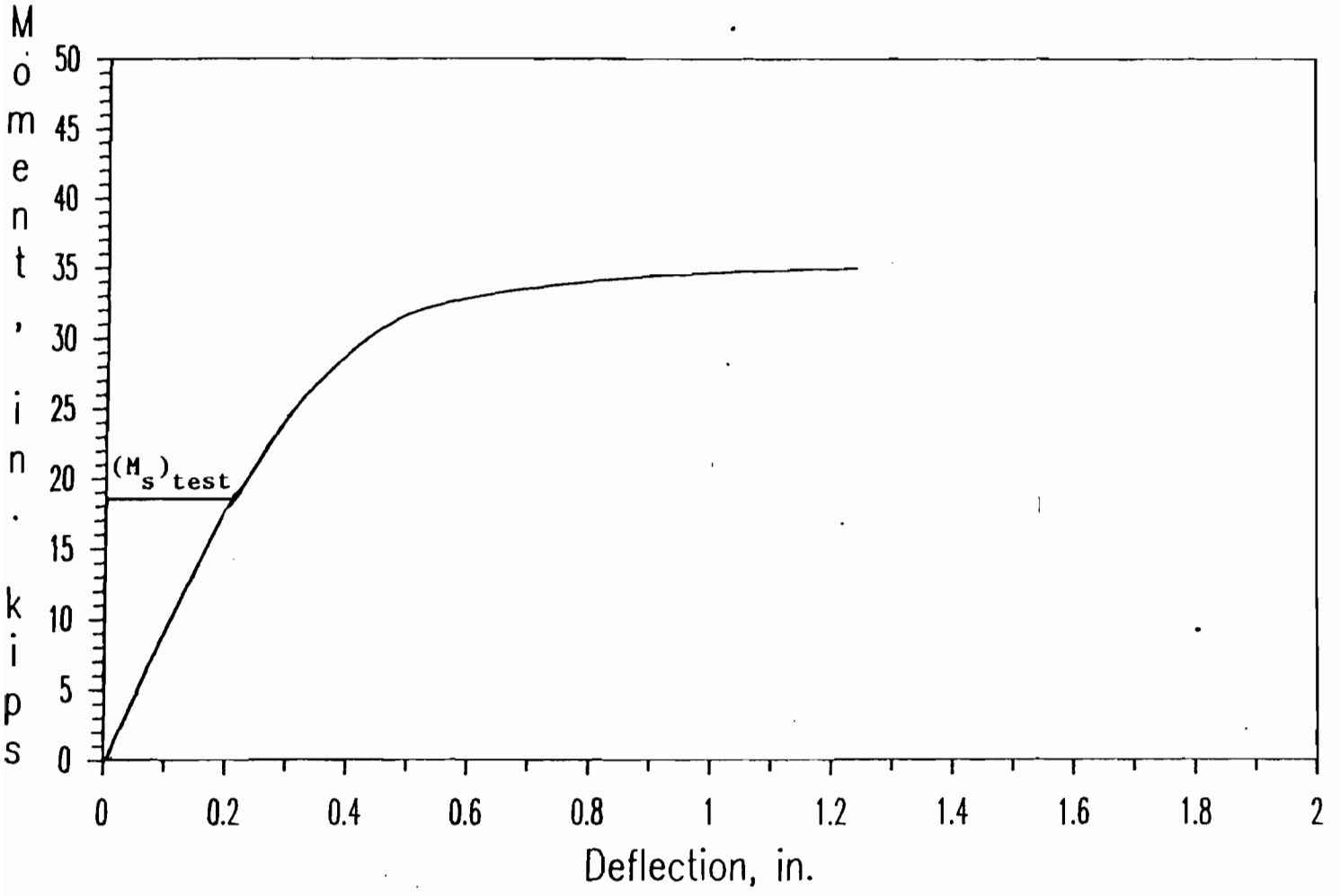

Fig. 4.26 Typical Moment-Deflection Curve for Hat-Beam Specimens

Specimen 3C1B

while Fig. 4.27 shows a typical moment-deflection curve for channel beam specimens.

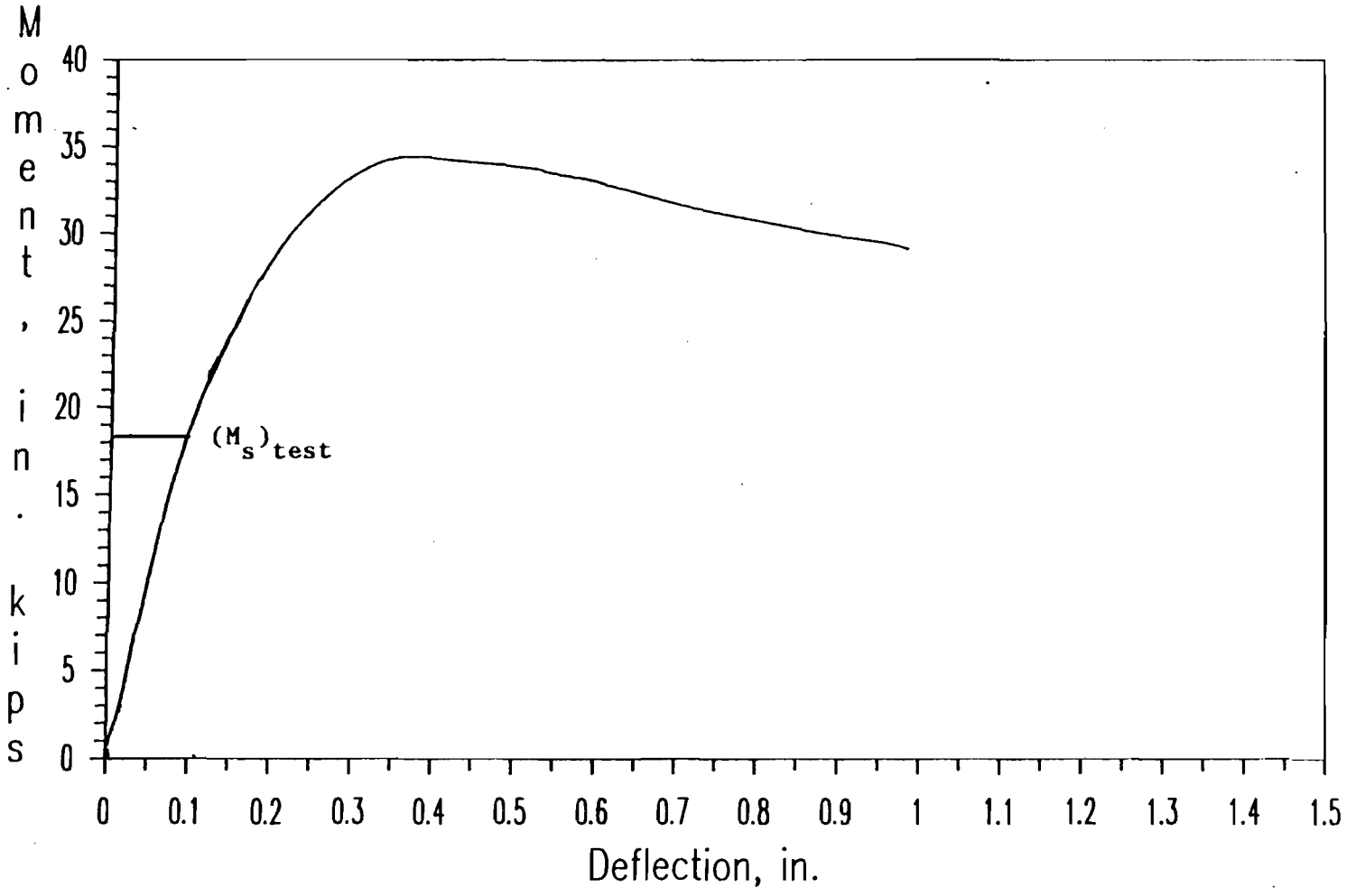

Fig. 4.27 Typical Moment-Deflection Curve for Channel Beam Specimens

Specimen 4C0A

V. CONCLUSIONS

A. GENERAL

This study dealt with the effect of strain rate on mechanical properties of sheet steels and the structural strengths of cold-formed steel members subjected to dynamic loads. Section V.B includes a summary of the research findings on the effect of strain rate on material properties of 35XF, 50XF, and 100XF sheet steels in tension as well as compression. Based on the available test data, Section V.C includes the conclusions drawn from the study of the effect of dynamic loads on structural strengths of cold-formed steel beams and stub columns fabricated from 35XF sheet steel.

B. MATERIALS

The findings of this investigation relative to material properties are:

1. Proportional limit, yield strength, and ultimate strength increase with increasing strain rate.

2. Yield strength is more sensitive to strain rate than ultimate strength.

3. The strain rate sensitivity value is not a constant. In most cases it increases with increasing strain rate.

4. The mechanical properties of sheet steels having low yield strengths are more sensitive to strain-rate effects.

5. A second degree polynomial is well fitted to the experimental data for both tension and compression and can be used to predict the yield and

ultimate strengths at high strain rates above the range of the strain rate used in the tests.

C. STRUCTURAL MEMBERS

The findings of this investigation relative to structural members are:

1. The critical local buckling strength, yield strength, and ultimate strength for most of the tests increased with increasing strain rates. The ultimate strengths showed larger increases at higher strain rates than at lower strain rates.

2. The effect of strain rate on member strength was found to be similar to those observed from the previous study of material properties as affected by different strain rates. However, ratios of dynamic to static ultimate strengths for beams and stub columns conducted in this study were found to be slightly higher than those for tensile or compressive material yield stresses.

3. The computed ultimate strength based on the AISI Automotive Design Manual, using static or dynamic yield stress, was found to be conservative for all beam and stub column tests. The mean and standard deviation values for the ratios of tested to computed ultimate strengths were improved by using the dynamic yield stresses rather than the static value for all cases studied in this investigation.

4. The computed midspan deflection under service moments are slightly larger than those measured from tests, except for two channel beams.

Future tests are suggested for a study of the effect of strain rate on structural strengths of cold-formed steel members fabricated from 35XF sheet steel using larger w/t ratios than those used in previous tests. Future tests are also suggested to investigate the effect of strain rate on member strengths using different sheet steels with various width-to-thickness ratios in order to obtain the needed information for determining the adequacy of the current effective width design formulas for members subjected to dynamic loads and to establish the required design recommendations.

BIBLIOGRAPHY

1. American Iron and Steel Institute, "Cost-Effective Weight Reduction with Sheet Steel", SG-631R.

2. American Iron and Steel Institute, "Sheet Steels: Automotive Problem Solvers", Cost-Effective Weight Reductions in Parts at 1980 AISI/SAE Exhibits, SG-932A.

3. American Iron and Steel Institute, "High Strength Sheet Steel Source Guide", SG-603D.

4. American Iron and Steel Institute, "The Materials Decision", SG-834.

5. Errera, S.J., "Automotive Structural Design Using the AISI Guide", SAE Tech. Paper Ser. 820021, February 22-26, 1982.

6. American Iron and Steel Institute, "Automotive Steels: They Still Do It Better", Cost Savings/Corrosion Protaction/Weight Reductions in Components seen at the 1982 AISI/SAE Exhibit, SG-937.

7. International Nickel Company, Inc., "A Cost/Weight Study of 1981-1982 Production Bumper Systems".

8. Levy, B.S., "Advances in Designing Ultra High Strength Steel Bumper Reinforcement Beams", SAE Tech. Paper Ser. 830399, February 28-March 4, 1983.

9. Vecchio, M.T., "Design Analysis and Behavior of Variety of As-Formed Mild and High Strength Sheet Materials in Large Deflection Bending", SAE Tech. Paper Ser. 830398, February 28-March 4, 1983.

10. American Iron and Steel Institute, "Guide for Preliminary Design of Sheet Steel Automotive Structural Components", 1981 Edition.

11. Yu, W.W., Santaputra, C., and Parks, M.B., "Design of Automotive Structural Components Using High Strength Sheet Steels", First Progress Report, Civil Engineering Study 83-1, University of Missouri- Rolla, January 1983.

12. Parks, M.B. and Yu, W.W., "Design of Automotive Structural Components Using High Strength Sheet Steels: Mechanical Properties of Materials", Second Progress Report, Civil Engineering Study 83-3, University of Missouri- Rolla, August 1983.

13. Santaputra, C. and Yu, W.W., "Design of Automotive Structural Components Using High Strength Sheet Steels: Strength of Beam

Webs", Third Progress Report, Civil Engineering Study 83-4, University of Missouri- Rolla, August 1983.

14. Parks, M.B. and Yu, W.W., "Design of Automotive Structural Components Using High Strength Sheet Steels: Strength of Curved Elements and Members Consisting of Curved Elements", Fourth Progress Report, Civil Engineering Study 83-5, University of Missouri- Rolla, August 1983.

15. Santaputra, C. and Yu, W.W., "Design of Automotive Structural Components Using High Strength Sheet Steels: Structural Behaviour of Beam Webs Subjected to Web Crippling and a Combination of Web Crippling and Bending", Fifth Progress Report, Civil Engineering Study 84-1, University of Missouri- Rolla, October 1984.

16. Parks, M.B. and Yu, W.W., "Design of Automotive Structural Components Using High Strength Sheet Steels: Status Report on the Study of Members Consisting of Flat and Curved Elements", Sixth Progress Report, Civil Engineering Study 84-2, University of Missouri- Rolla, October 1984.

17. Parks, M.B. and Yu, W.W., "Design of Automotive Structural Components Using High Strength Sheet Steels: Results and Evaluation of Stub Column Tests for Unstiffened Curved Elements", Seventh Progress Report, Civil Engineering Study 85-1, University of Missouri--Rolla, September 1985.

18. Santaputra, C. and Yu, W.W., "Design of Automotive Structural Components Using High Strength Sheet Steels: Web Crippling of Cold-Formed Steel Beams", Eighth Progress Report, Civil Engineering Study 86-1, University of Missouri- Rolla, August 1986.

19. Parks, M.B. and Yu, W.W., "Design of Automotive Structural Components Using High Strength Sheet Steels: Structural Behavior of Members Consisting of Flat and Curved Elements", Ninth Progress Report, Civil Engineering Study 87-2, University of Missouri-Rolla, June 1987.

20. Lin, S.H., Hsiao, L.E., Pan, C.L., and Yu, W.W., "Design of Automotive Structural Components Using High Strength Sheet Steels: Structural Strength of Cold-Formed Steel I-Beams and Hat Sections Subjected to Web Crippling Load", Tenth Progress Report, Civil Engineering Study 88-5, University of Missouri- Rolla, June 1988.

21. Pan, L.C., "Effective Design Widths of High Strength Cold-Formed Steel Members," Ph.D. Thesis, University of Missouri-Rolla, 1987.

22. American Iron and Steel Institute, "Automotive Steel Design Manual," 1986 Edition.

23. Kassar, M. and Yu, W.W., "Design of Automotive Structural Components Using High Strength Sheet Steels: The Effect of Strain Rate on Mechanical Properties of Sheet Steels", Eleventh Progress Report, Civil Engineering Study 89-2, University of Missouri- Rolla, January 1989.

24. Kassar, M. and Yu, W.W., "Design of Automotive Structural Components Using High Strength Sheet Steels: The Effect of Strain Rate on Compressive Mechanical Properties of Sheet Steels", Twelfth Progress Report, Civil Engineering Study 89-4, University of Missouri- Rolla, August 1989.

25. Kassar, M. and Yu, W.W., "Design of Automotive Structural Components Using High Strength Sheet Steels: Structural Strengths of Cold-Formed Steel Members under Dynamic Loads", Thirteenth Progress Report, Civil Engineering Study 90-1, University of Missouri- Rolla, March 1990.

26. Yu, W.W., Cold-Formed Steel Design, Wiley-Interscience, New York, 1985.

27. Hosford, W.F. and Caddel, R.M., Metal Forming-Mechanics and Metallurgy, Prentice Hall, Inc., N.J., 1983, 80-84.

28. Timoshenko, S., Strength of Materials-Part II, D. Van Nostrand Company, Inc., 1956, 400-428.

29. Malvern, L.E., Introduction to the Mechanics of a Continuous Medium, Prentice Hall , Inc., 1969, 327-333.

30. Juvinall, R.C., Stress, Strain and Strength, McGraw-Hill Book Company, New York, (1967), 96-100.

31. Follansbee, P.S., "High Strain Rate Compression Testing", Metals Handbook, American Society for Metals, Ninth Edition, Volume 8, 1985.

32. Lindholm, U.S., "Techniques in Metal Research", Vol. 5, Part 1, Wiley-Interscience, New York , 1971.

33. Zukas, J.A., Nicholas, T., Swift, H.F., Greszczuk, L.B., and Curran, D.R., Impact Dynamics, John Wiley & Sons, New York, 1982.

34. Staker, M.R., "High Strain Rate Testing," Metals Handbook, American Society for Metals, Ninth Edition, Volume 8, 1985.

35. Kumar, S., "Introduction," Mechanical Behavior of Materials Under Dynamic Loads, U.S. Lindholm (Ed.), Springer-Verlag, New York, 1968.

36. Norris, C.H., Hansen, R.J., Holley, M.J. Jr., Biggs, J.M., Namyet, S., and Minami, J.K., Structural Design for Dynamic Loads, McGraw-Hill Book Company, 1959.

37. Davis, E.A., "The Effect of the Speed of Streching and the Rate of Loading on the Yielding of Mild Steel," Journal of Applied Mechanics, ASME Transactions, Vol. 60,1938.

38. Winlock, J. and Leiter, R., "Some Factors Affecting the Plastic Deformation of Sheet and Strip Steel and Their Relation to the Deep Drawing Properties," American Society for Metals Transactions, Vol. 25, 1937.

39. Manjoine, M.J., "Influence of Rate of Strain and Temperature on Yield Stresses of Mild Steel," Journal of Applied Mechanics, ASME Transactions, 66, (1944).

40. Gillis, P.P., "Effect of Strain Rate on Flow Properties," Metals Handbook, American Society for Metals, Ninth Edition, Volume 8, 1985.

41. Chatfield, D.A. and Rote, R.R., "Strain Rate Effects on the Properties of High Strength, Low Alloy Steels," SAE Tech. Paper Ser. 740177, February 25-March 1, 1974.

42. Meyers, M.A., and Chawla, K.K., Mechanical Metallurgy: Principles and Applications, Prentice-Hall, Englewood Cliffs, N.J., 1984.

43. Alder, J.F., and Phillips, V.A., "The Effect of Strain Rate and Temperature on the Resistance of Aluminum, Copper, and Steel to Compression," Journal of the Institute of Metals, Vol 83, 1954-1955, pp. 80-86.

44. Cook, P.M., "True Stress-Strain Curves for Steel in Compression at High Temperature and Strain Rates, for Application to the Calculation of Load and Torque in Hot Rolling," Conference on The Properties of Materials at High Rates of Strain, Institute of Mechanical Engineers, 1957, pp. 86-97.

45. Davies, E.D.H., and Hunter, S.C., "The Dynamic Compression Testing of Solids by the Method of the Split Hopkinson Pressure Bar," J. Mech. Phys. Solids, Vol 11, 1963, pp. 155-172.

46. Holt, J.M., "The Effect of Strain Rate on the Tensile Properties of USS COR-TEN and USS TRI-TEN High-Strength Low-Alloy Steels",

United States Steel Corporation, Applied Research Center, Project Number 37.12-100(2), Pittsburgh, PA., 1962.

47. Watanabe, T., "Effect of Strain Rate on Yield Behavior of Cold-Rolled Sheet Steel," Transactions of the Iron and Steel Institute of Japan, Vol.22, 1982.

48. Peterson, D., Schwabe, J.E., and Fertis, D.G., "Strain Rate Effects in SA-106 Carbon Steel Pipe," Journal of Pressure Vessel Technology, ASME Transactions, Vol. 104, February, 1982.

49. Sachdev, A.K., and Wagonar, R.H., "Uniaxial Strain Hardening at Large Strain in Several Sheet Steels," Novel Techniques in Metal Deformation Testing, The Metallurgical Society of AIME, 1983.

50. Meyer, L.W., "Dynamic Tension Studies of Strength and Formability Characteristic of a High Alloyed Steel With Respect to Thermal Activation," Mechanical Properties at High Rate of Strain, Institute of Physics, London, No. 70, 1984.

51. Nagorka, M.S., "The Effect of Microstructure and Strain Rate on the Stage III Strain Hardening and Ductility of Dual-Phase Steels," Material Science and Engineering, 94, 1987, 183-193.

52. Albertini, C. and Montagnani, M., "Testing Techniques Based on the Split Hopkinson Bar," Mechanical Properties at High Rates of Strain, Institute of Physics, London, No.21, 1974.

53. Kassner, M.E., and Breithaupt, R.D., "The Yield Stress of Type 21-6-9 Stainless Steel Over a Wide Range of Strain Rate (10^{-5}-10^{4} s^{-1}) and Temperature," Mechanical Properties at High Rates of Strain, Institute of Physics, London, No.70, 1984.

54. Jones, A.H., Maiden, C.J., Green, S.J., and Chin, H., "Prediction of Elastic-Plastic Wave Profiles in Aluminum 1060-O under Uniaxial Strain Loading," Mechanical Behavior of Materials under Dynamic Loads, U.S. Lindholm (Ed.), Springer-Verlag, New York, 1968, 96-133.

55. Kanninen, M.F., Mukherjee, A.K., Rosenfield, A.R., and Hahn, G.T., "The Speed of Ductile-Crack Propagation and the Dynamics of Flow in Metals, Mechanical Behavior of Materials under Dynamic Loads, U.S. Lindholm (Ed.), Springer-Verlag, New York, 1968, 96-133.

56. Hockett, J.E., "Compression Testing at Constant True Strain Rates," Proc. ASTM, Vol 59, 1959, pp. 1309-1319.

57. Lindholm, U.S., and Yeakley, L.M., "High Strain-Rate Testing: Tension and Compression," Experimental Mechanics, Vol 8, 1968, pp. 1-9.

58. Lindholm, U.S. and Bessey, R.L., Technical Report AFML-TR-69-119, Air Force Materials Laboratory, Wright-Patterson Air Force Base, Ohio, 1969.

59. Lindholm, U.S., " Some Experiments With the Split Hopkinson Bar," J. Mech. Phys. Solids, Vol.12, 1964.

60. Maiden, C.J., and Green, S.J., "Compressive Strain Rate Tests on Six Selected Materials at Strain Rates From 10^{-3} to 10^{4} in./in./sec.", Transaction of the ASME, Sep. 1966.

61. Eleiche, A.M., Albertini, C. and Montagnani, M., " The Influence of Strain-Rate History on the Ambient Tensile Strength of AISI Type 316 Stainless Steel," Nuclear Engineering and Design, 1985.

62. Shirakashi, Takahiro and Usui, Eiji, "Effect of Temperature and Strain-Rate Upon Flow Stress of Metals in Compression," Bulletin of Japan Society of Precision Engineering, Vol.4, 1970.

63. Eleiche, A.M. and Campbell, J.D., Tech. Rep. ARML-TR-76-90 , Air Force Materials Laboratory, Wright-Patterson Air Force, 1976.

64. Wilson, M.L., Hawley, R.H. and Duffy, J., "Strain Rate and Strain Rate History Effects in Two Mild Steels", Brown University, Rep. NSF ENG 75-18532/8, 1979.

65. American Iron and Steel Institute, "Cold-Formed Steel Design Manual ," 1986 Edition.

66. Timoshenko, S. P. and Gere, J. M., Theory of Elastic Stability, 2nd Edition, New York: McGraw-Hill Book Company, Inc., 1961.

67. Bulson, P. S., The Stability of Flat Plates, New York: American Elsevier Publishing Company, Inc., 1969.

68. Saint Venant, "Discussion in Theorre de l'elasticte' des Corps Solides," by Clebsch, P.704, 1883.

69. Bleich, F. "Theorie .und Berechnung der eisernen Brcicken," Julius Springer, Berlin, 1924.

70. Bijlaard, P. P., "Theory of Plastic Stability of Thin Plates," Pubs. International Association for Bridge and Structural Engineering, Vol. VI, 1940-41.

71. Bijlaard, P. P., "Theory and Tests on the Plastic Stability of Plates and Shells," Journal of the Aeronautical Sciences, V. 16, PP529-541, 1949.

72. Ilyushin, A. A., "The Elastic-Plastic Stability of Plates," Translation in NACA Technical Memorandum 1188.

73. Stowell, E. Z., "A Unified Theory of Plastic Buckling of Columns and Plates," NACA Technical Note No. 1556, April 1948.

74. Von Karman, T., "Festigkeitsprobleme in Meschinenbau," Encyklpadie der Mathematischen, Vol. 4, 1910, P. 349.

75. Schnadel, G., "Die Uberschreitung der Knickgrenze bei dunnen Platlen," Proceedings of Third International Congress for Applied Mechanics, Stockholm, Vol. 3, 1930.

76. Cox, H. L., "The Buckling of Thin Plates in Compression," Technical Report of the Aeronautical Committee, 1933-34.

77. Marguerre, K., "Die Mittrangende Breite der Gedrukten Platte," Luftfahrtforschung, Vol. 14, 1937.

78. Levy, S., "Bending of Rectangular Plates with Large Deflections," NACA Technical Report 737, 1942, P.139.

79. Von Karman, T., Sechler, E. E., and Donnell, L. H., "The Strength of Thin Plates in Compression," Transactions, ASME, Vol. 54, APM54-5, 1932.

80. Winter, G., "Strength of Thin Steel Compression Flanges," Bulletin No. 35, Part 3, Cornell University, Engineering Experiment Station, Ithaca, N.Y., 1947.

81. Winter, G., "Performance of Thin Steel Compression Flanges," Preliminary Publication, 3rd Congress of the International Association for Bridge and Structural Engineering, 1948, P.137.

82. Winter, G., "Performance of Compression Plates as Parts of Structural Mambers," Bulletin No. 35, Cornell University, Engineering Experiment Station, Ithaca, N.Y., 1947.

83. Kalyanaraman, V., Pekoz, T., and Winter, G., "Analytical Study of Unstiffened Elements," Journal of Structural Division, ASCE, Vol. 104, No. ST9, September, 1978.

84. Kalyanaraman, V., Pekoz, T., and Winter, G., "Unstiffened Compression Elements," Journal of Structural Division, ASCE, Vol. 103, No. ST9, September 1977.

85. Kalyanaraman, V., "Local Buckling of Cold-Formed Steel Members," Journal of Structural Division, ASCE, Vol. 105, No. ST5, May 1979.

86. American Iron and Steel Institute, "Specification for the Design of Cold-Formed Steel Structural Members," 1968 Edition.

87. American Iron and Steel Institute, "Specification for the Design of Cold-Formed Steel Structural Members," 1980 Edition.

88. Pekoz, T., "Development of a Unified Approach to the Design of Cold-Formed Steel Members," Report SG86-4, AISI, Washington , D. C., May 1986.

89. Rawlings, B., "Response of Structures to Dynamic Loads," Mechanical Properties at High Rates of Strain, Institute of Physics, London, No.21, 1974.

90. Parkes, E. W.,"The Permanent Deformation of an Encastre Beam Struck Transversely at any Point in its Span," Proc. Inst. Civil Eng., July, 1958.

91. Ezra, A. A., "The Plastic Response of a Simply Supported Beam to an Impact Load at the Center," Proc. III U. S. Nat. Cong. Appl. Mech., 1958.

92. Duwez, P. E., Clark, D. S., and Bohnenblust, H. F., "The Behavior of Long Beams Under Impact Loading," J. Appl. Mech., Vol. 117, No. 1, March, 1950.

93. Bodner, S. R. and Symonds, P. S., "Experimental and Theoretical Investication of the Plastic Deformation of Cantilever Beams Subjected to Impulsive Loading," Journal of Applied Mechanics, Vol. 29, Dec.1962.

94. Rawlings, B., "The Dynamic Behavior of Steel in Pure Flexure," Proc. Royal Soc. Series A, Vol. 275, 1963.

95. Ting, T. C. T., "Large Deformation of a Rigid-Ideally-Plastic Cantilever Beam," J. Appl. Mech., June, 1965.

96. Bodner, S. R., "Deformation of Rate-Sensitive Structures under Impulsive Loading," Engineering Plasticity, Heyman and Leckie, Ed., Cambridge Univ. Press, 1968.

97. Symonds, P. S., Behavior of Materials Under Dynamic Loading, ASME, Huffington, N. J., Ed., 1965.

98. Jones, N., "Response of Structures to Dynamic Loading," Mechanical Properties at High Rates of Strain, Institute of Physics, London, No.47, 1979.

99. Aspden, R. J., and Campbell, J. D., "The Effect of Loading Rate on the Elasto-Plastic Flexure of Steel Beams," Proceedings of Royal Society of London, Vol. A290, 1966.

100. Jones, N., "Influence of Strain-Hardening and Strain-Rate Sensitivity on the Permanent Deformation of Impulsively Loaded Rigid-Plastic Beams," International Journal of Mechanical Sciences, Vol.9, 1967.

101. Culver, C. G., Zanoni, E. A., and Osgood, A. H., "Response of Thin-Walled Beams to Impact Loading," Proceedings of the First Specialty Conference on Cold-Formed Steel Structures, University of Missouri-Rolla, Aug. 1971.

102. Symonds, P. S. and Jones, N., "Impulsive Loading of Fully Clamped Beams with Finite Plastic Deflections and Strain-Rate Sensitivity," Int. J. Mech. Sci., Vol. 14, 1972.

103. Forrestal, M. J. and Sagartz, M. J., "Elastic-Plastic Response of 304 Stainless Steel Beams to Impulse Loads," Journal of Applied Mechanics, Vol. 45, September 1978.

104. Forrestal, M. J. and Wesenberg, D. L., "Elastic Plastic Response of Simply Supported 1018 Steel Beams to Impulse Loads," Journal of Applied Mechanics, Dec. 1977.

105. Meier, J. H., "On the Dynamic of Elastic Buckling," Journal of the Aeronautical Sciences, Vol. 12, 1945.

106. Hoff, N., "Dynamic Stability of Structures," Proceedings of an International Conference on Dynamic Stability of Structures, Northwestern University, Evanston, Illinois, October 1965.

107. Roberts, T. M., "The Response of Steel Struts to Impact Overload," PhD Thesis, University of Sheffield, 1972.

108. Culver, C. G. and Vaidya, N. R., "Impact Loading of Thin-Walled Columns," Proceedings of the First Specialty Conference on Cold-Formed Steel Structures, University of Missouri-Rolla, Aug. 1971.

109. Logue, J. M., "Experimental Study of Thin-Walled Columns Subjected to Impact Loading," Master Thesis, Carnegie-Mellon University, April, 1971.

110. Soden, P. D., Al-Hassani, S. T. S., and Johnson, W., "The Crumpling of Polyvinylchloride Tubes Under Static and Dynamic Axial Loads," Mechanical Properties at High Rates of Strain, Institute of Physics, London, No.21, 1974.

111. Wierzbicki, T., "Dynamic Crushing of Strain Rate Sensitive Box Columns," SAE Second International Conference on Vehicle Structural Mechanics, April 1977.

112. Ohkubo, Y., Akamatsu, T., and Shirasawa, K., "Mean Crushing Strength of Closed-Hat Section Members," SAE Paper No. 740040, 1974.

113. Wimmer, A., "Einfluss der Belastungsgeschwindigheit auf das Festigkeitsund Verformungsverhaten von Blechkonstruktionen am Beispiel von Kraftfahrzengen," ATZ 77, 1975.

114. Wierzbicki, T. and Abramowicz, W., "Crushing of Thin-Walled Strain-Rate Sensitive Structures," Dynamic and Crushing Analysis of Plastic Structures, Euromech Colloquium No. 121, August, 1979.

115. Abramowicz, W. and Jones, N., "Dynamic Axial Crushing of Square Tubes," Int. J. Impact Engng., Vol. 2, No. 2, 1984.

116. Galambos, T. V. (ed.), Guide to Stability Design Criteria for Metal structures, 4th Edition, New York: John Wiley & Sons, Inc.,1988.

117. Gerard, G., and H. Becker, Handbook of Structural Stability, Part I-Buckling of Flat Plates, NACA Technical Note 3781, July, 1957.

118. Winter, G., "Commentary on the 1968 Edition of the Specification for the Design of Cold-Formed Steel Structural Members," American Iron and Steel Institute, 1970 Ed.

119. Johnson, A. L. and Winter, G., "The Structural Performance of Austenitic Stainless Steel Members," Report No. 327, Cornell University, Nov., 1966.

120. Chajes, A., Britvec, S.J., and Winter, G., "Effects of Cold-Straining on Structural Sheet Steels," Journal of the Structural Division, proceedings of the American Society of Civil Engineers, Vol. 89, No. ST2, April, 1963.

121. Bleich, F., Buckling Strength of Metal Structures, New York: McGraw-Hill Book Company, 1952.

122. Reck, H. P., Pekoz, T., and Winter, G., "Inelastic Strength of Cold-Formed Steel Beams," Journal of Structural Division, ASCE Proceedings, vol. 101, Nov. 1975.

APPENDIX - NOTATION

The following symbols are used in this dissertation:

a	Length of plate
A	Actual tensile or compressive coupon area
	Constant
A_e	Effective cross-sectional area of stub columns
A_f	Tensile coupon area at fracture
A_o	Full tensile or compressive coupon area
A_t	Total cross-sectional area of stub columns
b	Effective width of a compression element
B	Constant
C	Constant
C_y	Compressive strain factor
d	Depth of the section
	Midspan deflection
D	Flexural rigidity of plate, $Et^3/12(1-\mu^2)$
	Constant
E	Modulus of elasticity of steel = 29,500 ksi
E_t	Tangent modulus of steel
f	Stress in the compression element
	Engineering stress
f_d	Compressive stress at the stiffened or unstifffend flange based on the effective section at service moment

f_{cr}	Critical local buckling stress
$(f_{cr})_E$	Elastic critical local buckling stress
$(f_{cr})_I$	Inelastic critical local buckling stress
f_{max}	Maximum edge stress of a compression element
f_x, f_y	Stress components in the x-y plane
F	Stress function
F_{pr}	Proportional limit
F_y	Yield strength
H	Thickness of the beam
I	Moment of inertia
I_e	Effective moment of inertia
k	Buckling coefficient
ℓ_o	Full tensile or compressive coupon gage length
ℓ	Deformed tensile or compressive coupon gage length
ℓ_f	Tensile coupon gage length at fracture
L	Span length
m	Number of half sine waves in x-direction
	Strain-rate sensitivity exponent
$\bar{n}$	Constant
M	Dynamic bending moment
M_0	Static collapse moment
M_{cr}	Critical local buckling moment
M_u	Ultimate moment
M_y	Yield moment

n	Number of half sine waves in y-direction
p	Constant
P	Coupon axial load
P_{cr}	Critical buckling load
P_y	Yield Load
P_u	Ultimate load
P_m	Mean crush force
q	Lateral uniform load
r	Ratio of the slopes of the elastic and plastic portions of the stress-strain curve
R	Dynamic correction factor
S_e	Elastic section modulus of the effective section
S_{xc}	Elastic section modulus of the full cross section relative to the compression flange
t	Thickness of plate
	Test time
v	Impact velocity
w	Width of plate
α	Constant
β	Constant
ϕ_s, ϕ_u	Stress reduction factors
ε	Engineering or true strain
$\dot{\varepsilon}$	Strain rate
λ, λ_d	Slenderness factors
η	Plasticity reduction factor

$\dot{\kappa}$	Curvature rate
ω	Deflection of plate perpendicular to surface
μ	Poisson's ratio
ν	Constant = $E/(r\ \sigma_0)$
ρ	Reduction factor
σ	True stress
	Dynamic yield stress
σ_0	Static yield stress
τ_{xy}	Shear stress component in the x-z and y-z planes